Synthesis of ZSM-5 zeolite from South African fly ash and its application as solid catalyst

By

Roland Missengue-Na-Moutoula

MSc Chemistry – University of the Western Cape

BSc (Honours) Chemistry – Université Marien Ngouabi

A thesis submitted in fulfilment of the requirements for the degree of Doctor of Philosophy in Chemistry in the Department of Chemistry, University of the Western Cape.

Supervisor: Prof. Leslie F. Petrik

Co-supervisors: Dr. Benoit Louis and Dr. Nicholas M. Musyoka

December 2016

ABSTRACT

Zeolites are widely used as environmentally friendly solid catalysts or catalyst supports in the refining and petrochemical industries. ZSM-5 zeolite is composed of a three-dimensional medium pore structure (openings of 5-5.5 Å) with high silica content, high temperature stability and strong acidity making it a well-known and an established catalyst for several petroleum derived chemical processes such as cracking, aromatic alkylation, disproportionation, Methanol-to-Gasoline, isomerisation, etc. Nowadays, the synthesis of ZSM-5 zeolite from silica, alumina sources and structure directing agents (templates) is well known. Its synthesis is possible from fly ash, which is a low cost source of both silica and alumina. Fly ash is an inorganic residue resulting from the combustion of coal in electricity generating plants, consisting mostly of SiO_2 and Al_2O_3. ZSM-5 zeolite has not been synthesised from South African coal fly ash and the literature reports that fly ash-based ZSM-5 zeolite was synthesised only with tetrapropylammonium (TPA^+) as structure directing agent and required an excessive amount of additional silica. The final ZSM-5 product was reported to still contain fly ash mineral phases after synthesis. This prevents the use of fly ash as a ZSM-5 zeolite precursor. Moreover, the synthesis of a high purity ZSM-5 zeolite from fly ash without additional silica has not been yet reported.

This study aimed to synthesise high purity ZSM-5 zeolite from South African coal fly ash without additional silica, and with tetrapropylammonium bromide (TPABr), 1,6-hexanediamine (HDA) or 1-propylamine (PA) as structure directing agent.

This aim was achieved by first optimising the synthesis of ZSM-5 zeolite from South African coal fly ash based on a formulation reported in the literature with fumed silica and TPABr as additional source of silica and structure directing agent respectively. Thereafter, the obtained optimum conditions were used to synthesise other fly ash-based ZSM-5 zeolite products by substituting TPABr with HDA or PA. Two routes of treating the as-received fly ash prior to the hydrothermal synthesis were applied in order to improve the quality of the final products or reduce the amount of the fumed silica that was used. The first route consisted of treating the as-received fly ash with concentrated H_2SO_4 in order to remove a certain amount of aluminium and increase the Si/Al in the acid treated fly ash solid residue but also remove some other elements such as Fe, Ca, Mg, and Ti which might have an undesirable effect on the product quality. The acid treated fly ash solid residue was used as ZSM-5 precursor with fumed silica as additional silica source and TPABr, HDA or PA as structure directing agent.

ABSTRACT

The ZSM-5 zeolite products that were synthesised from the as-received fly ash as well as from the H_2SO_4 treated fly ash were treated with oxalic acid solution in order to reduce the aluminium content in the final products. The second route consisted of fusing the as-received fly ash with NaOH and treating the powder fused fly ash extract with oxalic acid solution. The obtained fused and oxalic acid treated fly ash extracts were used as ZSM-5 precursors without additional fumed silica and with TPABr, HDA or PA as structure directing agent.

ZSM-5 zeolite was synthesised from the as-received South African coal fly ash not only with the commonly used structure directing agent TPABr but also with two other, lower cost structure directing agents, HDA and PA. The synthesis process did not generate any solid waste as fly ash was used as bulk, which could be a way of valorising South African coal fly ash. However, the final products contained some fly ash mineral phases such as mullite and quartz, and had poor physical and chemical properties compared to a commercial H-ZSM-5 zeolite. The treatment of the as-received fly ash with H_2SO_4 resulted in fly ash-based ZSM-5 zeolite products with better physical and chemical properties than those of ZSM-5 zeolite products that were synthesised from the as-received fly ash. Moreover, the post-synthesis treatment of the fly ash-based ZSM-5 zeolite products with oxalic acid resulted in an increase in the Si/Al ratio, offering a post-synthesis route to adjust the acidity of the catalysts. However, mullite and quartz phases were still present in the synthesised products. Alternatively, high purity ZSM-5 zeolite was synthesised from the fused and oxalic treated fly ash extracts without additional silica and with TPABr, HDA or PA as structure directing agent. Moreover, these synthesised fly ash-based ZSM-5 zeolite products had similar physical and chemical properties to the commercial H-ZSM-5 zeolite.

The synthesised fly ash-based ZSM-5 zeolite products were used as solid catalysts in the Methanol-to-Olefins (MTO) and Nazarov reactions. The ZSM-5 zeolite products that were synthesised from the H_2SO_4 treated fly ash as well as fused and oxalic treated fly ash were successfully used as solid catalysts in the MTO and Nazarov reactions. The ZSM-5 zeolite products that were synthesised from the H_2SO_4 treated fly ash presented a similar trend in MTO and Nazarov reactions depending on the structure directing agent that was used, and the ZSM-5 zeolite that was synthesised with HDA as structure directing agent had the highest MTO and Nazarov conversion. However these catalysts deactivated more quickly compared to the commercial H-ZSM-5 zeolite. On the other hand, the zeolites that were synthesised from the fused and oxalic acid treated fly ash had a high initial MTO conversion equivalent to

the commercial H-ZSM-5 zeolite. However, they deactivated after 5 h of time on stream due to diffusional constraints, because of their large crystal sizes.

This study developed novel routes in the synthesis of high value zeolites from fly ash. ZSM-5 zeolite was synthesised from fly ash with structure directing agents other that TPA^+ cation and had acceptable Brønsted acidity and high initial conversion in MTO and Nazarov reactions. This has not been yet reported in the literature. Moreover, for the first time a high purity ZSM-5 zeolite was synthesised from fly ash without additional silica and had similar properties to a commercial H-ZSM-5 zeolite. This constituted a breakthrough in the fly ash-based ZSM-5 zeolite synthesis procedure, which will promote the valorisation of fly ash through ZSM-5 synthesis due to avoiding the addition of silica source in the hydrothermal gel and preventing the presence of fly ash mineral phases in the final products. This study can have a significant economic and environmental impact in South Africa if the synthesis process is scaled up as it provides a potentially cheap and innovative way of using waste for making a high value green and acid catalyst, namely ZSM-5 zeolite that has several catalytic applications; and it promotes the valorisation of South African coal fly ash that is considered by many as waste material.

KEYWORDS

Coal fly ash

Acid leaching

Fusion

Oxalic acid

Tetrapropylammonium bromide

1,6-hexanediamine

1-propylamine

ZSM-5 zeolite

Methanol-to-Olefins (MTO) reaction

Nazarov cyclisation

DECLARATION

I declare that "Synthesis of ZSM-5 zeolite from South African fly ash and its application as solid catalyst" is my own work, that it has not been submitted for any degree or examination in any other university, and that all the resources I have used or quoted have been indicated and acknowledged by complete references.

Roland Missengue-Na-Moutoula December 2016

Signed……

ACKNOWLEDGEMENTS

First is to thank the Almighty God for the gift of life, strength and perseverance to carry out this research.

I am grateful to my main supervisor Prof Leslie Petrik, not only for the precious opportunity to complete my PhD in her research group, but also for her guidance, support, patience and encouragement in my academic and daily life. May the Almighty God bless you Prof. I cannot thank my co-supervisors Dr Benoit Louis (University of Strasbourg) and Dr Nicholas Musyoka (Council for Scientific and Industrial Research) enough for insightful contributions to my laboratory work and also for different kinds of opportunities during my PhD.

Special thanks go to Prof Patrice Pale, Mr Pit Losch, Ms Claire Bernardon and Mr Eric Wimmer, and to the rest of the Laboratoire de Synthèse, Réactivité Organiques et Catalyses (LASYROC) research group for their hospitality, constructive criticism that made my visit in Strasbourg fruitful.

I would like to thank Mrs Ilse Well, Mrs Vanessa Kellerman, Mr Rallston Richards and my colleagues at the Environmental and Nano Sciences (ENS) research group for their technical and administrative assistance, and interactions that made my research work comfortable.

I would like to thank Dr Edith Beukes (University of the Western Cape) for the assistance with the NMR analysis, Mr Adrian Josephs (University of the Western Cape) for the help in carrying out the SEM imaging and Mr Nicholas Laidler (University of Cape Town) for assisting with the XRD analysis.

I would like to thank Dr Ana Casanueva, Ms Naseema Sonday and Ms Aisha Mohamed Ali from the Technology Transfer Office (University of the Western Cape) for their assistance in patenting the novelty of this study.

I thank my family in Christ Jesus our Lord for their spiritual and emotional support.

My deepest gratitude goes to my uncle Mr Albert K. Mampassi, my sisters, family members and friends for always believing in me.

Lastly, I would like to thank the National Research Foundation (NRF) for financial support that made this study possible.

TABLE OF CONTENTS

LIST OF FIGURES

LIST OF TABLES

LIST OF TABLES

LIST OF ABBREVIATIONS

A	Analcime
AL	H_2SO_4 fly ash solid residue
ASTM	American Society for Testing Materials
ATR	Attenuation total reflection
BEs	Backscattered electrons
BET	Brunauer-Emmett-Teller
C_2	Selectivity toward ethylene
C_3	Selectivity toward propylene
CCPs	Coal combustion by-products
CS	Calsialic
EDS	Energy dispersive X-ray spectroscopy
FA	Fly ash
FCC	Fluid catalytic cracking
FCS	Ferricalsialic
FD	Framework density
FFAE	Fused fly ash extract
FT-IR	Fourier transform infrared
FID	Flame ionization detector
FID	Free-induction decay
FS	Ferrisialic
GC	Gas chromatography
H	Hematite
HA	High acid
HDA	1,6-hexanediamine
HP	High pozzolanic
HRTEM	High resolution transmission electron microscopy
I	Inert
ICDD	International Centre for Diffraction Data
ICP-AES	Inductively coupled plasma-atomic emission spectroscopy
ICP-OES	Inductively coupled plasma-optical emission spectroscopy
IUPAC	International Union of Pure and Applied Chemistry
IZA	International Zeolite Association

LIST OF ABBREVIATIONS

LA	Low acid
LOI	Loss on ignition
LP	Low pozzolanic
M	Mullite
MA	Medium acid
MAS-NMR	Magic angle spinning–nuclear magnetic resonance
MP	Medium pozzolanic
MTO	Methanol-to-Olefins
NMR	Nuclear magnetic resonance
OSDAs	Organic structure directing agents
P	Pozzolanic
PA	1-propylamine
Q	Quartz
RF	Radiofrequency
S	Sialic
SBUs	Secondary building units
SDA	Structure directing agent
SEs	Secondary electrons
SEI	Secondary electron imaging
SEM	Scanning electron microscopy
TEA^+	Tetraethylammonium cation
TEM	Transmission electron microscopy
TLC	Thin layer chromatography
TOS	Time on stream
TPA^+	Tetrapropylammonium cation
TPABr	Tetrapropylammonium bromide
XRD	X-ray diffraction
XRF	X-ray fluorescence
WHSV	Weight hourly space velocity
Z	ZSM-5 zeolite

ACADEMIC OUTPUTS OF RESEARCH REPORTED IN THIS THESIS

Patent in progress

Missengue, R.N.M., Petrik, F. "Conversion of South African coal fly ash into high purity ZSM-5 zeolite without additional silica source", Technology Transfer Office, University of the Western Cape.

Accepted paper

Missengue, R.N.M., Losch, P., Sedres, G., Musyoka, N.M., Fatoba, O.O., Louis, B., Pale, P., Petrik, L.F. (2016), "Transformation of South African coal fly ash into ZSM-5 zeolite and its application as an MTO catalyst", *Comptes Rendus Chimie*.

Drafted papers

Missengue, R.N.M., Losch, P., Musyoka, N.M., Louis, B., Pale, P., Petrik, L.F. "Conversion of South African coal fly ash into high purity zeolites ZSM-5 without an additional source of silica and their application as MTO-catalysts".

Missengue, R.N.M., Losch, P., Musyoka, N.M., Louis, B., Pale, P., Petrik, L.F. "Effect of the structure directing agent on the catalytic performance of South African coal fly ash-based zeolite ZSM-5".

Oral presentations

Missengue, R., Losch, P., Musyoka, N., Louis, B., Pale, P., Petrik, L. "South African coal fly ash-based zeolite ZSM-5 as solid catalyst", 26th Annual CATSA Conference, 15-18 November 2015, Kleinmond, Cape Town, South Africa.

Missengue, R., Losch, P., Musyoka, N., Louis, B., Pale, P., Petrik, L. "Characterisation of South African fly ash-based zeolite ZSM-5 for hydrogen storage", Materials-based hydrogen storage: Design, synthesis and characterisation of porous materials, Researcher Links South Africa-UK Workshop, 1-4 September 2015, Pretoria, South Africa.

Poster presentations

Missengue, R., Losch, P., Musyoka, N., Louis, B., Pale, P., Petrik, L. "Conversion of methanol to olefins over ZSM-5 zeolite synthesized from South African coal fly ash: Effect of a structure directing agent", 2nd Euro-Asia Conference 25-28 January 2015 Nice, France.

Missengue, R., Sedres, G., Losch, P., Bernardon, C., Musyoka, N., Fatoba, O.O., Louis, B., Pale, P., Petrik, L. "Valorisation of South African fly ash: extraction of metals and synthesis of zeolite ZSM-5 used as catalyst", WasteCon 2014 Conference, 6-10 October 2014, Somerset West, Cape Town, South Africa.

Missengue, R., Musyoka, N., Petrik, L. "Effect of acid pre-treatment on South African fly ash in the synthesis of zeolite ZSM-5", Spring meeting, BZA Conference, 9-11 April 2014, Glasgow, Scotland.

CHAPTER 1: GENERAL INTRODUCTION

1.1. Introduction

This chapter highlights the general introduction of the study and gives a brief overview of the research topic. It also presents the problem statement, motivation, hypothesis, novelty, aim and objectives, research questions, research approach, scope and delimitations of the study together with the thesis framework.

1.2. Background

Fly ash is an industrial by-product that is generated during the combustion of coal for energy production. The current annual production of coal fly ash worldwide is estimated to be around 500 million tonnes (Ahmaruzzaman, 2010). The low grade coal that is burnt in the South African coal-fired power plants, with a high inorganic content of up to 40 %, causes the production of a huge quantity of fly ash. In 2011, 36.22 million tonnes of fly ash was produced in South Africa and 94.5 % was disposed in ash dumps located near the coal-fired power stations (Eskom, 2011). The amount of fly ash generated from the combustion of coal is increasing at an alarming rate throughout the world and the disposal of such huge quantities of ash has become a pressing issue. Fly ash mainly consists of SiO_2, Al_2O_3 and Fe_2O_3, it also contains potentially toxic elements that condense from the flue gas and its large-scale storage is a source of significant environmental pollution (Ahmaruzzaman, 2010). Several studies have been undertaken on the use of fly ash. Fly ash is used to treat acid coal mine drainage (Petrik et al., 2003; Madzivire et al., 2010), to synthesise zeolites (Petrik et al., 2003; Musyoka et al., 2012; Chareonpanich et al., 2004; Kalyankar et al., 2011), and to produce construction materials (Ahmaruzzaman, 2010, Nyale et al., 2013). Fly ash has been used as low cost source of SiO_2, Al_2O_3 in the synthesis of zeolites. Alkaline hydrothermal process preceded by pectization or fusion of the raw material has been applied to synthesise zeolites (Somerset et al., 2004; Kuwahara et al., 2010, Musyoka et al., 2009; Musyoka et al., 2012, Muriithi, 2013). Musyoka et al., (2012) synthesised A, X and cancrinite zeolites from South African fly ash. Na-P1 Zeolite was also synthesised from South African fly ash (Musyoka et al., 2009). However, the synthesis of high silica content zeolites such as ZSM-5 zeolite from fly ash required an addition source of silica (Reanvattana, 2005). Chareonpanich et al., (2004) synthesised ZSM-5 zeolite using lignite fly ash and rice husk ash was used as additional source silica. Kalyankar et al., (2011) synthesised ZSM-5 zeolite using fly ash

obtained from an Indian thermal power station and silica sol was added as extra source of silica. The synthesis of ZSM-5 zeolite from fly ash without an additional source of silica has not yet been reported. However, the acidic or alkaline extraction of alumina or silica from fly ash that is reported in the literature (Guang-hui et al., 2010; Yao et al., 2014; Liu et al., 2012; Cheng-You et al., 2012; Lai-Shi et al., 2011; Panagiotopoulou et al., 2007) might be useful as means to change Si/Al ratios in the synthesis of ZSM-5 zeolite from fly ash without adding an additional Si source. ZSM-5 zeolite is conventionally synthesized using various types of organic structure-directing agents (templates). Tetrapropylammonium ion (TPA^+) was the first template that was reported to be able to induce ZSM-5 zeolite formation (Van Der Gaag et al., 1985; Petrik et al., 1995, Tuan et al., 2010; Martinez et al., 2011). However, Narayanan et al., (1995) reported synthesis of ZSM-5 zeolite without template. The range of the starting Si/Al ratios giving pure ZSM-5 zeolite increases in the following template order: alcohols<amines<TPABr. Besides the organic structure-directing agents, some ions such as Na^+, K^+, NO_3^- or SO_4^{2-} and the water content can influence the rate of formation and pore size distribution of ZSM-5 zeolite (Petrik, 2009). ZSM-5 zeolite is widely used as catalyst because of its properties: high silica content, high temperature stability and strong acidity (Lercher and Jentys, 2011; Triantafillidis et al., 1999; Bleken et al., 2012; Ramasamy and Wang, 2013, Varvarin et al., 2013; Sani-Souna-Sido et al., 2008), but the restriction of the pore size within it may induce some diffusional constraints when bulky reactants or products are used in catalytic applications (Song et al., 2000; Moliner, 2012). Today, with the necessity for the petrochemical industry to treat heavy feedstocks, the optimisation of the accessibility of zeolite-based catalysts for large molecules is important. The creation of a secondary pore system consisting of mesopores as well as micropores in zeolite crystals is a sufficient route to minimise the diffusion limitation and improve the catalyst efficiency. The synthesis of zeolites with mesopores as well as micropores is a more generally applied strategy to improve the molecular transport properties of zeolite. Mesopores can be created inside zeolite crystals by destructive or constructive synthesis strategies (Chal et al., 2011; Louis et al., 2010; Sazama et al., 2011; Petrik, 2009).

The present study will investigate different routes of synthesising ZSM-5 zeolite from South African coal fly ash with the addition of the smallest possible quantity of additional silica. It will also investigate a way of synthesising ZSM-5 zeolite from South African coal fly ash without an additional source of silica and with cheap templating agents to substitute costly

TPABr. The physico-chemical properties and catalytic efficiency of the synthesised fly ash-based ZSM-5 zeolite products will be compared to those of a commercial ZSM-5 zeolite.

1.3. Problem statement

The South African economy depends heavily on the energy produced during the combustion of coal. The rate of coal fly ash generated surpasses the rate of fly ash re-use significantly. A substantial amount of fly ash which is produced is still disposed in landfills and/or lagoons. This has become a serious environmental problem and the disposal of fly ash will soon be too costly. A considerable research effort needs to be undertaken on the use of coal fly ash in order to mitigate the increasing toxic threat to the environment related to its disposal. An economically sustainable solution to this issue should include utilisation of coal fly ash to synthesise valuable products such as zeolites in order to reduce land disposal. Fly ash – because of its composition – has been used as low cost raw material for the synthesis of various zeolites. The optimisation of the synthesis conditions in the production of pure phases of zeolites and the improvement of their properties are the keys for making South African fly ash-based zeolites competitive with expensive synthetic zeolites. However, fly ash typically has a Si/Al ratio of 1 – 2, thus is not suitable for making high silica zeolites such as ZSM-5 that requires a Si/Al about 10. ZSM-5 zeolite is one of the most useful acid catalysts in refining and petro-chemical industries. However, despite the importance of ZSM-5 zeolite in the catalytic industry, its synthesis from fly ash requires the addition of an important amount of silica source in order to adjust the Si/Al molar ratio to 10 or above. This limits the valorisation of fly ash for high value catalytic application and makes the scale up of the process unfeasible economically.

1.4. Motivation of the study

With the severe electricity crisis that South African experienced in 2008, with black outs all over the country and increasing energy demand, Eskom (South African national electricity supplier) required substantial funding and has started to build new coal fired power plants (Inglesi, 2010). This will lead to an increase of the rate of coal fly ash generation that already exceeds the rate of coal fly ash re-use. Moreover, with only 5 % of the current amount of coal fly ash being re-used (Petrik et al., 2003), the environmental issues related to its disposal will persist. Although South African coal fly ash has been used as feedstock in the synthesis of zeolites (Babajide et al., 2012; Musyoka et al., 2012), the small yield of the final product does

not promote the scaling up of the process. Furthermore, the synthesis of high silica content zeolites such as ZSM-5 zeolite from South African coal fly ash has not been reported yet and the synthesis process would require an important amount of an extra silica source because of the low Si/Al molar ratio of about 2 in South African coal fly ash (Musyoka, 2012). However, various scientific findings about extraction of silica and alumina from fly ash may be a foundation for the synthesis of ZSM-5 zeolite that requires a Si/Al molar ratio of above 10 (Liu et al., 2012; Panagiotopoulou et al., 2007; Baldyga et al., 2012; Awizar et al., 2013; Van der Gaag, 1987). Moreover, the synthesised ZSM-5 zeolite may be used as catalyst in the Methanol-to-Olefins (MTO) conversion. The success of the dealumination of fly ash feedstock may lead to an industrial transformation of South African coal to light olefins using a coal fly ash-based ZSM-5 zeolite (Van Dijk et al., 1983; Bleken et al., 2012), instead of merely burning the coal for energy generation.

1.5. Hypothesis

The extraction of silica and alumina from fly ash can be a foundation for an innovative synthesis of high purity ZSM-5 zeolite from coal fly ash without addition of an extra silica source.

1.6. Novelty of the study

Despite the availability of huge amounts of coal fly ash in South Africa and several investigations in converting South African coal fly ash into high purity zeolites, the country continues importing important amounts of zeolites. Moreover, only low and intermediate silica zeolites have been synthesised from South African fly ash. This could be because the synthesis of high silica content zeolites such as ZSM-5 zeolite from fly ash requires the addition of a huge amount of silica and the synthesis of ZSM-5 zeolite from fly ash without an additional source of silica has not yet been reported in the literature. Therefore, this current study suggests an innovative way of synthesising ZSM-5 zeolite from South African coal fly ash without an additional source of silica. It also suggests the use of cheap templates such as 1-propylamine in combination with fly ash extracts for ZSM-5 synthesis. The success of this study will bring more value to South African coal fly ash and open a window of industrialising the synthesised fly ash-based ZSM-5 zeolite for catalytic hydrocarbon processing.

1.7. Aim and objectives

The aim of this study is to synthesise high purity ZSM-5 zeolite from South African fly ash without an additional source of silica and use the synthesised fly ash-based ZSM-5 zeolite as catalysts in the Methanol-to-Olefins (MTO) and Nazarov reactions.

The main objectives of this study include:

- Obtaining the chemical composition of Arnot fly ash in order to monitor and adjust the Si/Al molar ratio by adding fumed silica in the hydrothermal gel.
- Determining the optimal conditions for the synthesis of ZSM-5 zeolite after acid pre-treatment of fly ash with concentrated sulphuric acid or fusion with sodium hydroxide.
- Investigating an innovative way of synthesising ZSM-5 zeolite from fly ash without an additional source of silica.
- Comparing the physico-chemical properties of the fly ash-based ZSM-5 zeolite to that of a commercial ZSM-5 zeolite.
- Comparing the catalytic efficiency of the fly ash-based ZSM-5 zeolite to that of a commercial ZSM-5 zeolite for MTO and Nazarov reactions.

1.8. Research questions

To achieve the aim and objectives mentioned above, this study seeks to find answers to the following research questions:

- What is the smallest amount of silica source (fumed silica) that can be added in the synthesis of ZSM-5 zeolite from fly ash?
- What is the effect of acid pre-treatment of fly ash on the hydrothermal gel composition and properties of the synthesised fly ash-based ZSM-5 zeolite?
- Can a high purity ZSM-5 zeolite be synthesised from fly ash extracts after fusion with NaOH?
- What is the effect of the structure directing agent (tetrapropylammonium bromide, 1,6-hexanediamine or 1-propylamine) on the properties of the synthesised fly ash-based ZSM-5 zeolite?
- Can the fly ash-based ZSM-5 zeolite compete with a commercial in the Methanol-to-Olefins (MTO) conversion and Nazarov cyclisation of 1-phenyl-2-ethylpropenone?

- Can oxalic acid post-synthesis treatment of the fly ash-based ZSM-5 zeolite improve their catalytic efficiency?

1.9. Research approach

To answer the research questions mentioned above, a wide literature review on the research topic was carried for the better understanding of previous studies and finding a suitable methodology to achieve the research objectives. Several characterisations and experiments were carried out. This included, the characterisation of the raw fly ash using X-ray fluorescence (XRF), X-ray diffraction (XRD), scanning electron microscopy (SEM), ^{27}Al nuclear magnetic resonance (^{27}Al NMR) and Fourier transform infrared (FT-IR). Thereafter, fly ash (FA) was treated with concentrated sulphuric acid (H_2SO_4) (95-99 %) in order to remove as much aluminium as possible from fly ash, so as to increase the Si/Al ratio in the H_2SO_4 fly ash solid residue (AL) and reduce the addition of an extra silica source (fumed silica) in the hydrothermal gel. Alternatively, FA was fused with sodium hydroxide (NaOH). The fused fly ash was mixed with deionised water and the fused fly ash extract (FFAE) was precipitated by the addition of concentrated H_2SO_4 (95-99 %) dropwise until a pH of about 10. FFAE was also treated with a saturated oxalic solution in order to reduce the percentage of impurities in the extract prior to the hydrothermal synthesis. FA, AL or FFAE were used as starting source of Si and Al in the synthesis of ZSM-5 zeolite with tetrapropylammonium bromide (TPABr), 1,6-hexanediamine (HDA) or 1-propylamine (PA) as structure directing agent (SDA). Fumed silica was added as extra silica source to adjust the Si/Al ratios in the case of FA and AL hydrothermal gels. Zeolite products obtained from FA and AL hydrothermal gels were treated with a saturated oxalic acid solution in order to remove undesirable extra-framework cations that could affect their catalytic efficiency. FFAE extracts were used to synthesise ZSM-5 zeolite without an additional silica source in the hydrothermal gels. The physico-chemical properties of the fly ash-based ZSM-5 zeolite were compared to that of a commercial H-ZSM-5 zeolite obtained from Zeolyst. The synthesised zeolites as well as the commercial ZSM-5 were characterised using X-ray fluorescence (XRF), X-ray diffraction (XRD), scanning electron microscopy (SEM), ^{27}Al nuclear magnetic resonance (^{27}Al NMR), Fourier transform infrared (FT-IR) and N_2 adsorption. The Brønsted acidity of all the zeolites was determined using the H/D exchange isotope technique and ^{1}H NMR. The catalytic efficiency of the selected zeolites was compared for the Methanol-to-Olefins (MTO) conversion and Nazarov cyclisation of 1-phenyl-2-

ethylpropenone. Gas chromatography (GC) and ^{1}H NMR were used to characterise the reagents and final products of the MTO conversion and Nazarov cyclisation, and the conversion and selectivity toward the targeted products were compared.

1.10. Scope and delimitations of the study

Among the types of South African coal fly ash, Arnot coal fly ash was chosen as starting material of this study based on its important amorphous phase content. Due to time and cost constraints, this study only investigated the synthesis of ZSM-5 zeolite; which choice was motivated by the importance of ZSM-5 zeolite in the catalytic industry and the fact that its synthesis from fly ash without an additional silica source had not yet been reported. The synthesis of ZSM-5 zeolite commonly requires the addition of an organic structure directing agent and there are several organic structure directing agents used in the synthesis of ZSM-5 zeolite. However, in this study the effect of only three organic structure directing agents (tetrapropylammonium bromide, 1,6-hexanediamine and 1-propylamine) on the physico-chemical properties of the fly ash-based ZSM-5 zeolite was investigated. From the multitude of catalytic reactions in which ZSM-5 zeolite is used as heterogeneous catalyst, its activity in only Methanol-to-Olefins (MTO) conversion and Nazarov cyclisation of 1-phenyl-2-ethylpropenone were investigated in the current study.

1.11. Thesis structure

This thesis is composed of eight chapters in the following sequence including this one, which presented the general introduction of the study:

CHAPTER 2: LITERATURE REVIEW

Chapter 2 gives an insight of the background of the study and presents general literature on coal fly ash, zeolites and their applications. Different ways of synthesising ZSM-5 zeolite from fly ash are highlighted in this study. Previous work on extracting silica and alumina from fly ash that can be a foundation for the synthesis of ZSM-5 zeolite without an additional silica source are also presented. The characterisation techniques of fly ash, zeolites and catalytic products are reviewed. The literature review ends with a critical evaluation of the state of the art and highlights the issues this study addresses.

CHAPTER 3: EXPERIMENTAL AND ANALYTICAL TECHNIQUES

This chapter details the sampling and storage conditions of the raw fly ash and lists of chemicals and equipment used in this study. It also highlights the methodological approaches used to synthesis ZSM-5 zeolite from South African coal fly ash. The two catalytic reactions (Methanol-to-Olefins conversion and Nazarov cyclisation) are detailed just before the methods for using different analytical techniques used in this study are presented.

CHAPTER 4: CHARACTERISATION OF ZSM-5 ZEOLITE SYNTHESISED FROM COAL FLY ASH

This chapter presents and discusses the characterisation of the raw fly ash feedstock and fly ash-based ZSM-5 zeolite synthesised from the as-received fly ash.

CHAPTER 5: CHARACTERISATION OF ZSM-5 ZEOLITE SYNTHESISED FROM ACID TREATED COAL FLY ASH

The results of characterisation of the acid treated feedstock and of ZSM-5 zeolite synthesised from acid treated fly ash are detailed and discussed in this chapter.

CHAPTER 6: CHARACTERISATION OF ZSM-5 ZEOLITE SYNTHESISED FROM FUSED FLY ASH EXTRACT WITHOUT AN ADDITIONAL SOURCE OF SILICA

This chapter highlights the results of characterisation of the fused fly ash extracts as well as ZSM-5 zeolite synthesised from fused fly ash extracts without an additional source of silica.

CHAPTER 7: APPLICATION OF FLY ASH-BASED ZSM-5 ZEOLITE AS SOLID CATALYST

The comparison of the activity, conversion and selectivity of some ZSM-5 products are presented for the catalytic reactions (Methanol-to-Olefins conversion and Nazarov cyclisation) in this chapter.

CHAPTER 8: CONCLUSIONS AND RECOMMENDATIONS

This chapter draws the conclusions of this thesis by summarising the relevant findings made including the novelty of the study. Lastly, it outlines recommended future work based on the results obtained in this study.

CHAPTER 2: LITERATURE REVIEW

2.1. Introduction

This chapter gives an overview of coal fly ash. Applications of coal fly ash are also highlighted. Thereafter, it gives insight into the significance and literature on zeolites in general and on ZSM-5 zeolite in particular. Different characterisation techniques used to determine the properties of coal fly ash and zeolites are also presented.

2.2. Coal fly ash

Coal fly ash is a waste generated from coal combustion during the production of electricity. Table 2.1 gives different coal-fired power plants in South Africa and the capacity of electricity they generate.

Table 2.1: South African coal-fired power plants.

Power Plant	Province	Date commissioned	Capacity (Megawatt)	Status
Arnot	Mpumalanga	1975	2100	Operational
Bloemfontein	Free State		102	Operational
Camden	Mpumalanga	1967	1600	Operational
Duvha	Mpumalanga	1980	3600	Operational
Grootvlei	Mpumalanga	1969	1200	Operational
Hendrina	Mpumalanga	1970	2000	Operational
Kelvin	Gauteng	1957	600	Operational
Kendal	Mpumalanga	1988	4116	Operational
Komati	Mpumalanga	1961	1000	Operational
Kriel	Mpumalanga	1976	3000	Operational
Kusile	Mpumalanga	Projected	4800	Under construction
Lethabo	Free State	1985	3708	Operational
Majuba	Mpumalanga	1996	4110	Operational
Matimba	Limpopo		3990	Operational
Malta	Mpumalanga	1983	3600	Operational
Medupi	Limpopo	Projected	4800	Under construction
Pretoria West	Gauteng	1952	180	Operational
Rooiwal	Gauteng	1963	300	Operational
Tutuka	Mpumalanga	1985	3654	Operational

According to Eskom, (2011) South African coal-fired power plants generate more than 36.22 Mt/annum of fly ash with only 4.5 % being reused and the rest being disposed in fly ash dams or heaps. The chemical composition of fly ash reveals the presence of toxic elements such as Hg, U, Y, V and Sr. The colour of coal fly ash varies from tan to black, depending on the amount of unburned carbon in the ash. Fly ash is an aluminosilicate material with small spherical particles (20-80 μm in size) and a high surface area (Gitari et

al., 2003; Styszko-Grochowiak et al., 2004). It is abrasive, alkaline and refractory in nature (Madzivire, 2009). Fly ash causes water and air contamination due to its alkalinity and the presence of toxic elements. It also causes a huge disposal problem because of the large volumes and the leaching potential (Akinyemi et al., 2011). Because of the environmental problems associated with fly ash disposal, much research has been carried out on the subject worldwide. Fly ash is used as a low-cost adsorbent for the removal of organic compounds, water treatment, light weight aggregate, mine back fill, road sub-base and zeolite synthesis (Ahmaruzzaman, 2010).

2.2.1. Formation

The combustion of coal generates by-products that are named coal combustion by-products (CCPs) and are composed of non-combustible inorganic residues and incompletely combusted organics, depending on the nature of the mineral matter and physico-chemical alterations that occur during the combustion process (Querol et al., 2002; Speight, 2005). CCPs are wet bottom boiler slag, dry bottom ash, fly ash and flue gas desulphurization materials (Figure 2.1) (Scheetz and Earle, 1998; Kalyoncu, 2001).

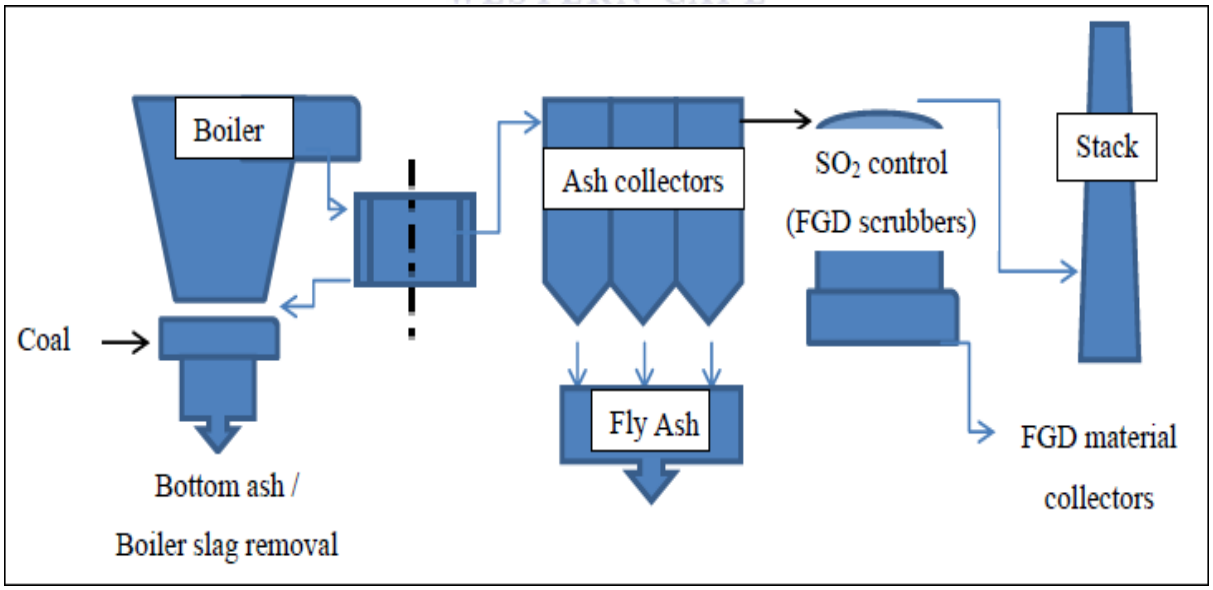

Figure 2.1: Schematic for CCPs collection (Musyoka, 2012).

The mechanism of formation of coal fly ash depends on the combustion conditions and parameters such as coal chemical composition, intrinsic reactivity, content of volatiles and ash content, particle size, porosity, mineral matter properties (Crelling et al., 2010). Fly ash consists of inorganic materials present in the coal that have been fused during coal combustion, solidified while suspended in the exhaust gases and collected by electrostatic precipitators (Mackiewicz and Ferguson, 2005). The inorganic materials undergo physico-chemical transformations during the thermal process (1400-1700 °C), fuse and cool rapidly to form ashes (Chung and Smith, 2000). A small part of ash falls to the bottom of the boiler and is termed bottom ash. The main part is instead dragged up by the exhausted gas stream, cools quickly and solidifies in the form of small, vitreous, spherical particles that are termed fly ash (Vassileva and Vassilev, 2002; Mackiewicz and Ferguson, 2005). The physical transformations of the inorganic materials during the thermal process include:

- Coalescence of individual mineral grains within a char particle,
- Shedding of the ash particles from the surface of chars,
- Incomplete coalescence due to disintegration of the char,
- Convective transport of ash from the char surface during de-volatilization,
- Fragmentation of the inorganic mineral particles,
- Formation of cenospheres,
- Vaporization and subsequent condensation of the inorganic components upon gas cooling (Miller and Tillman, 2008).

2.2.2. Physico-chemical properties

Fly ash consists predominantly of fine, spherical glassy particles (Figure 2.2) (Ahmaruzzaman, 2010). It is an alumina-silicate with particle size between 20-80 μm (Gitari et al., 2003; Styszko-Grochowiak et al., 2004). The mineralogical phase composition of coal shows the presence of minerals such as quartz, illite, aluminosilicate clay minerals and pyrite. After combustion, the obtained fly ash is dominated by aluminosilicate glass and crystalline phases formed during the cooling (mullite, magnetite, hematite) and quartz that did not melt or react during the combustion (Chung and Smith, 2000). According to Petrik et al., (2003) the major elements in South African fly ash are Si, Al, Fe, Ca, K, Na, Mg and Ti, and the most common minerals are quartz (SiO_2), mullite ($Al_6Si_2O_{13}$), hematite (Fe_2O_3), anhydrite

($CaSO_4$), lime (CaO), periclase (MgO) and unburned carbon. In addition, fly ash contains traces of toxic elements such as Zn, Pb, Cu, Cd, Sb, Hg, Ni, Y, V, Th, Ge, Ce and U.

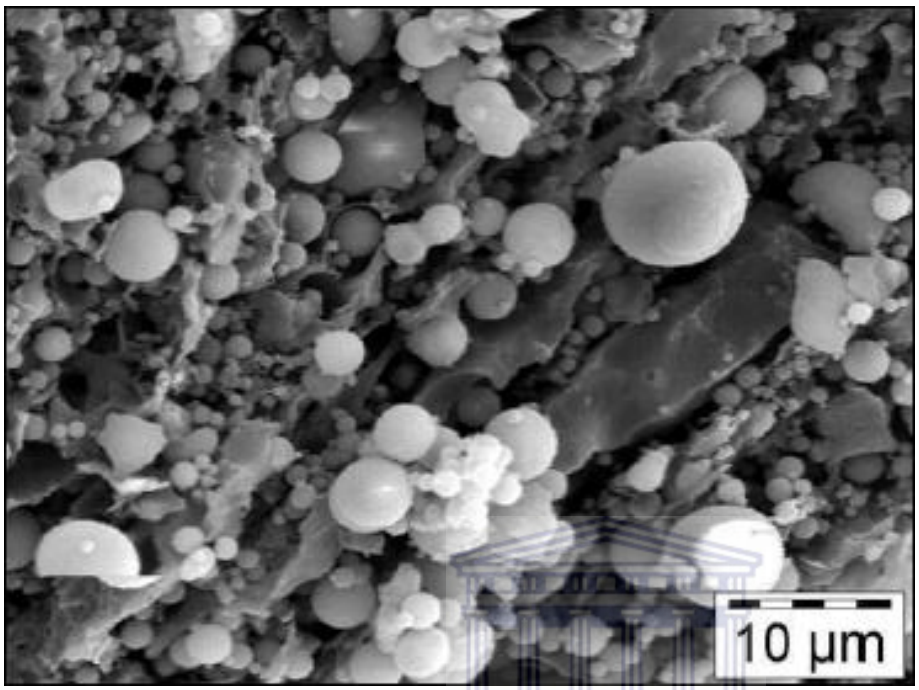

Figure 2.2: SEM imagine of fly ash particles (Musyoka, 2012).

2.2.3. Classification

American Society for Testing Materials standard (ASTM C618-93) is a specification that classifies coal fly ash and natural pozzolan for their cementitious or pozzolanic properties. It categorizes coal fly ash in two main classes named class F and class C. Class F is generated by combusting anthracite or bituminous coal while class C comes from the combustion of sub-bituminous or lignite coal (Joshi and Lohtia, 1997). Table 2.2 gives the chemical requirements for fly ash to be used in Portland cement concrete as per ASTM C618-93.

Table 2.2: Requirements for fly ash in Portland cement concrete (Joshi and Lohtia, 1997).

Requirements	Mineral admixture class	
	F	C
$SiO_2+Al_2O_3+Fe_2O_3$, min %	70	50
SO_3, max %	5	5
Moisture content, max %	3	3
Loss on ignition, max %	6	6
Na_2O, max %	1.5	1.5

It has been reported that class F fly ashes contain about 5 % CaO while the CaO percentage of class C fly ashes ranges between 10 % and 35 % (Koukouzas et al., 2007; Ahmaruzzaman, 2010). Joshi and Lohtia, (1997) reported that quartz, mullite and hematite are the major crystalline phases in class F fly ashes and the crystalline phases in class C are mainly anhydride, tricalcium aluminate, lime, quartz, periclase, mullite, merwinite and ferrite. South African coal fly ashes belong to class F category (Babajide et al., 2012; Madzivire et al., 2011; Musyoka et al., 2012; Somerset et al., 2004). Vassilev and Vassileva, (2007) introduced a new way for the classification of coal fly ashes based on their origin, mineral phases and chemical composition. The chemical classification system is based on the contents, common geochemical associations and correlations of ash-forming elements in fly ashes (Figure 2.3A). This approach divides fly ashes into four types: Sialic (high and medium acids), calsialic and ferrisialic (medium and low acids), and ferricalsialic (low acid). The mineral phase classification system depends on the contents, associations, correlations and properties of species in fly ashes (Figure 2.3B). This approach gives four phase-mineral fly ash types: Pozzolanic (high and medium pozzolanic properties), inert and active (medium and low pozzolanic properties), and mixed (low pozzolanic property).

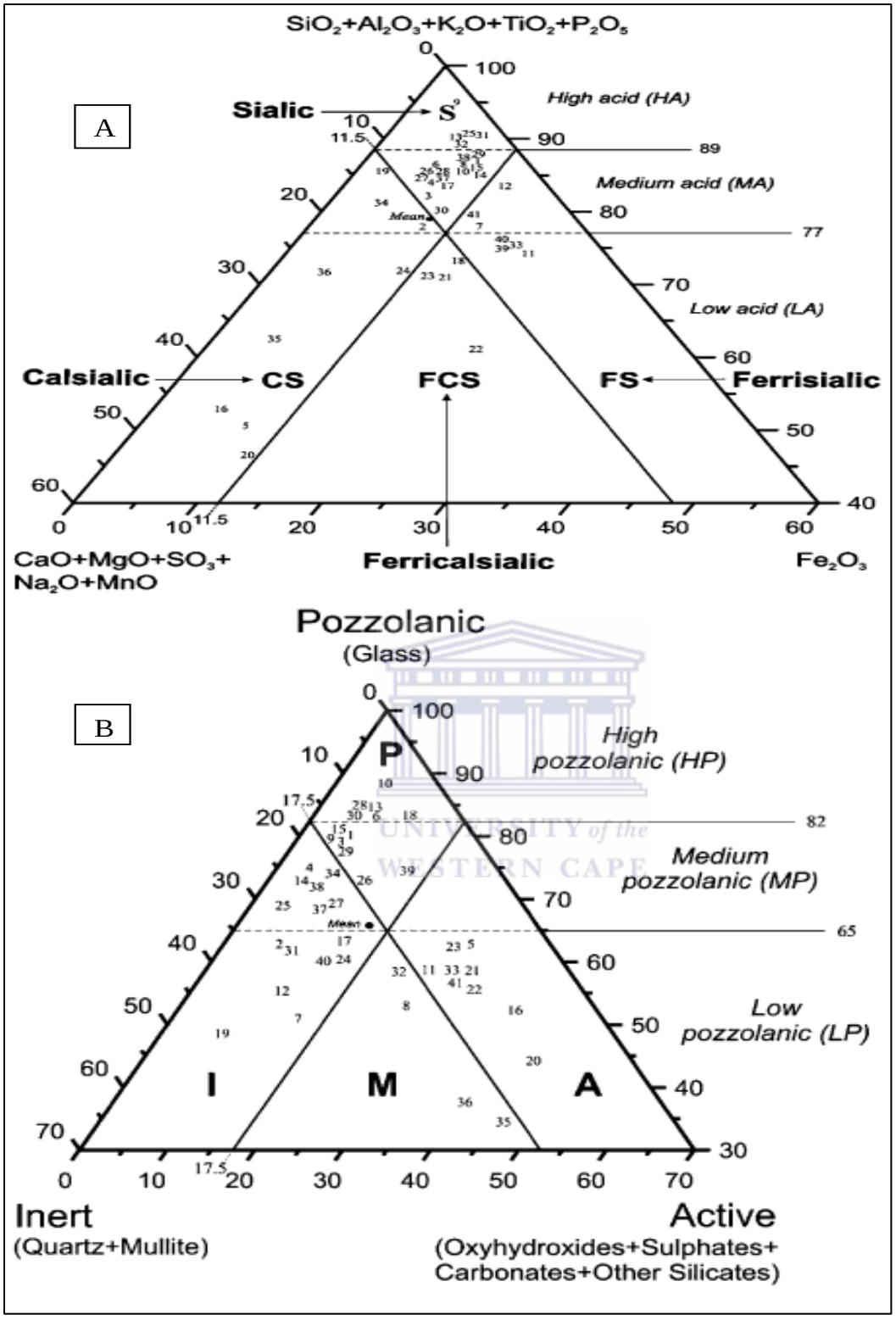

Figure 2.3: Chemical (A) and phase-mineral (B) classifications of fly ashes (S=sialic, CS=calsialic, FCS=ferricalsialic, FS=ferrisialic, HA=high acid, MA=medium acid, LA=low acid, P=pozzolanic, I=inert, A=active, HP=high pozzolanic, MP=medium pozzolanic, LP=low pozzolanic, M=medium) (Vassilev and Vassileva, 2007).

2.2.4. Impact on the environment

Coal-fired power plants consume coal in the production of electricity and generate a large amount of solid by-products mainly fly ash and bottom ash (Molina and Poole, 2004; Ye et al., 2008). Fly ash, the major residue generated during the combustion of pulverized coal, causes several environmental and health problems (Gottlieb et al., 2010). In South Africa, 94.5 % of the fly ash produced is disposed in ash dams and dumps that are situated near the coal-fired power plants (Eskom, 2011). The disposal of that huge amount of fly ash is a source of contamination of ground water due to leaching of toxic elements that are contained in it, that cause air pollution and land degradation (Adriano et al., 1980; Eary et al., 1990). Fly ash toxic elements (Pb, Hg, Cd, Ba, Th, Ge, Ce, U...) could leach into water, subsequently contaminating underground aquifers and surface waters, and pose a serious threat to aquatic species that live in those waters. Some toxins travel via the air as fine particles. They follow various routes and make their way into the human body. They can injure all of the major organ systems causing cancer, heart damage, lung disease, respiratory distress, kidney disease, reproductive problems, gastrointestinal illness, birth defects, impaired cognitive deficits and developmental delays and behavioural problems (Gottlieb et al., 2010).

2.2.5. Uses of fly ash

As mentioned, poor management of fly ash causes severe environmental and health problems, so research on comprehensive utilization of fly ash is necessary. Wang and Wu (2006) have reported that fly ash can have many applications in different sectors. Figure 2.4 summarises the possible applications of fly ash based on its physico-chemical properties. Coal fly ash has been used in the treatment of acid mine drainage (Petrik et al., 2003; Madzivire et al., 2011; Gitari et al., 2003), synthesis of zeolites (Musyoka et al., 2012; Somerset et al., 2004; Babajide et al., 2012; Mainganye et al., 2013; Chareonpanich et al., 2004), in backfilling of mine voids (Skousen et al., 2000), synthesis of geopolymers (Nyale et al., 2013; Skvara et al., 2005). It has been reported that fly ash can also be used in agriculture as an amendment in soil because of its physical properties (texture, water holding capacity, bulk density and pH) and because it contains almost all essential plant nutrients (Gupta et al., 2012). Fly ash is used in wastewater treatment to remove organic matters, colour and heavy metals (Viraraghavan, 1993). Lai-shi et al., (2011) and Liu et al., (2012) extracted alumina from coal fly ash using sulphuric acid. Groppo and Honaker (2009) reported that magnetite had been

recovered from coal fly ash using dense-medium separators. Shcherban et al., (1995) extracted aluminium, iron and silica from coal ash. Fly ash has a pozzolanic property (it can react with calcium hydroxide at ordinary temperature to form compounds possessing cementitious properties); this allows its use as cheap construction material, saves the fuel used in cement production and reduces CO_2 emissions from lime calcination (Foner et al., 1999). Fly ash has been used as an adsorbent for the removal of SO_2 and NOx from flue gases (Al-Shawabkeh et al., 1995; Davini, 1996; Lu and Do, 1991). Despite the large number of applications, coal fly ash continues to be a major environmental and health problem in South Africa. Therefore, more research is necessary to find beneficial routes to use fly ash. The current study focuses on the synthesis of ZSM-5 zeolite using South African fly ash as source of silica and alumina. ZSM-5 zeolite finds application in industrial and fine chemistry as a catalyst in cracking reactions of hydrocarbons and synthesis of hydrocarbons from alcohols.

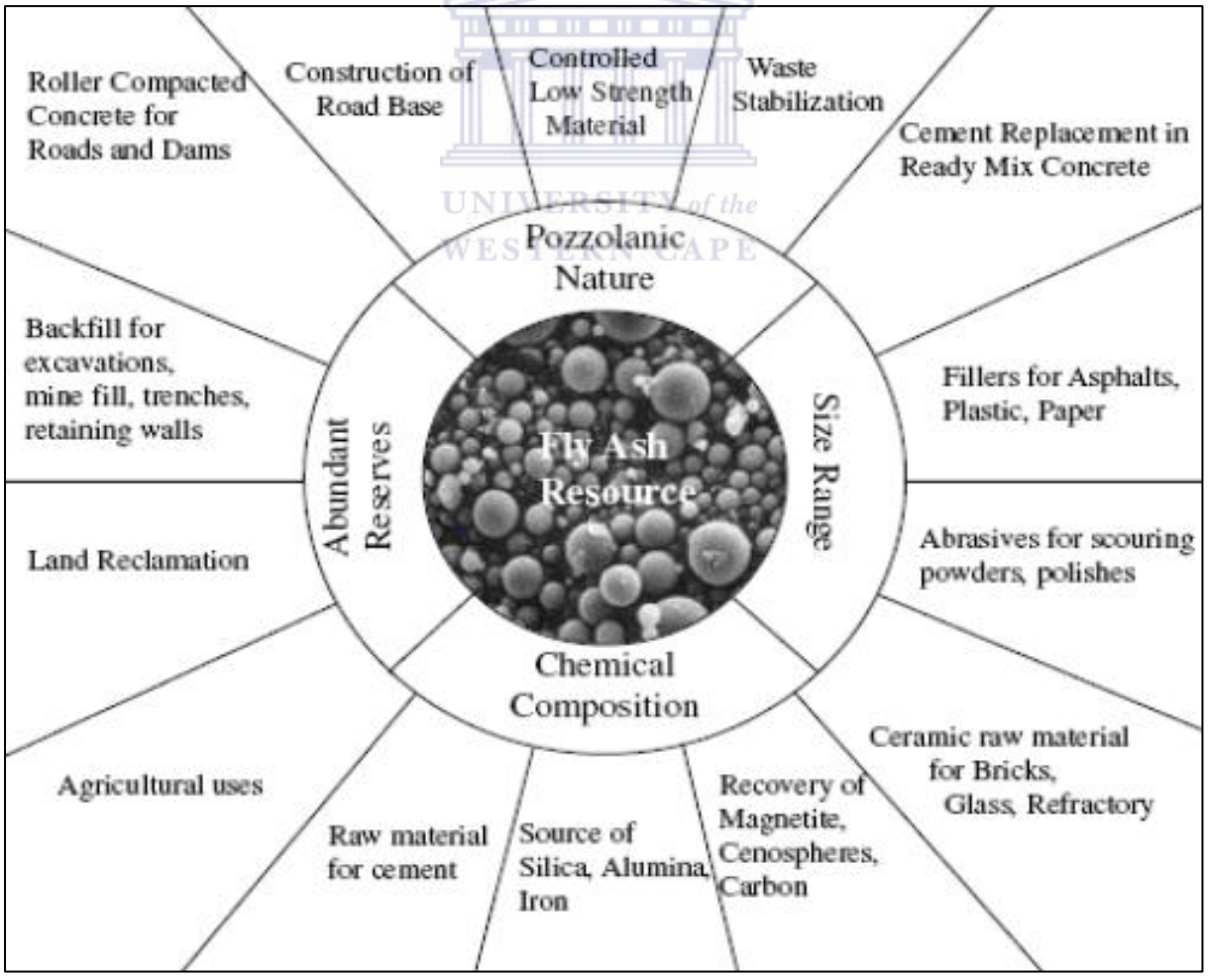

Figure 2.4: Summary of possible applications of fly ash (Wang and Wu, 2006).

2.3. Zeolites

Zeolites are highly porous crystalline hydrated aluminosilicates that are made of tetrahedrally-connected three dimensional frameworks and extra-framework charge balancing alkali and alkaline earths, with O:(Al+Si) ratio of 2. Zeolites belong to the mineral family that covers feldspars and felspathoids (Chester and Derouane, 2009). The zeolite frameworks contain cages and channels that are one-, two-, or three-dimensionally connected and the pores can accommodate molecules of up to 1 nm in size (Wright and Lozinska, 2011). The name zeolite derives from two Greek terms: *zeo* for boil and *lithos* for stone, so zeolite means boiling stone (Chester and Derouane, 2009). Zeolites are widely used as ion exchangers, adsorbents and catalysts.

2.3.1. History

The first zeolite to be discovered was stilbite in 1756 by a Swedish mineralogist A.F. Cronstedt. The crystals exhibited intumescence when they were heated in a blowpipe flame and Cronstedt called the mineral "zeolite" that means the boiling stone (Chester and Derouane, 2009). Between 1777 and 1800, different authors described the properties of zeolites such as adsorption, reversible cation exchange and dehydration. In 1862, St. Claire Deville reported the first hydrothermal synthesis of a zeolite called levynite (Flanigen et al., 2010). Friedel (1896) and Grandjean (1910) reported that dehydrated zeolites have open frameworks. They discovered that dehydrated zeolites adsorbed various liquids (alcohol, benzene and chloroform) and gases (ammonia, air and hydrogen) respectively. Weigel and Steinhoff (1925) observed the first molecular selectivity within the zeolites. They noted that dehydrated chabazite adsorbed water, methanol, ethanol and formic acid but not acetone nor benzene. Taylor (1930) described the first single crystal structure of analcite ($NaAlSi_2O_6.H_2O$). Barrer (1945) presented the first classification of zeolites based on their molecular size. A number of commercially significant zeolites, types A, X and Y were discovered between 1949 and 1954 and were first used in drying of refrigerant gas and natural gas. In 1959, zeolite Y was marketed as an isomerization catalyst. Between 1962 and 1969, Mobil Oil used the synthetic X zeolite as a hydrocarbon cracking catalyst (Flanigen et al., 2010). The first inclusion of organic molecules as templating agents during the zeolite synthesis was reported by Barrer and Denny. They synthesized high silica zeolites beta and ZSM-5 using tetra-ammonium cations. In the late 1960s, Mobil Oil started using quaternary ammonium cations for the synthesis of zeolites, type's beta, ZSM-12, ZSM-5 and ZSM-11

(Cejka et al., 2007). Union Carbide introduced zeolites for ion-exchange separations in 1977 (Flanigen et al., 2010). Figure 2.5 presents the chronological discovery of novel synthetic zeolites. If the first synthetic zeolites were prepared using chemical reactants, nowadays any source of silica and alumina can be used as feedstock of the zeolite synthesis. Kuwahara et al., (2010) synthesised zeolites, types A and X from blast furnace slag that contained 34.58 % of SiO_2 and 14.78 % of Al_2O_3. Musyoka et al., (2012) synthesised P, A, X and cancrinite zeolites from South African fly ash with 51.52 % of SiO_2 and 27.52 % of Al_2O_3. Atta et al., (2007) converted kaolin clay that contained 47.30 % of SiO_2 and 36.80 % into X and Y zeolites.

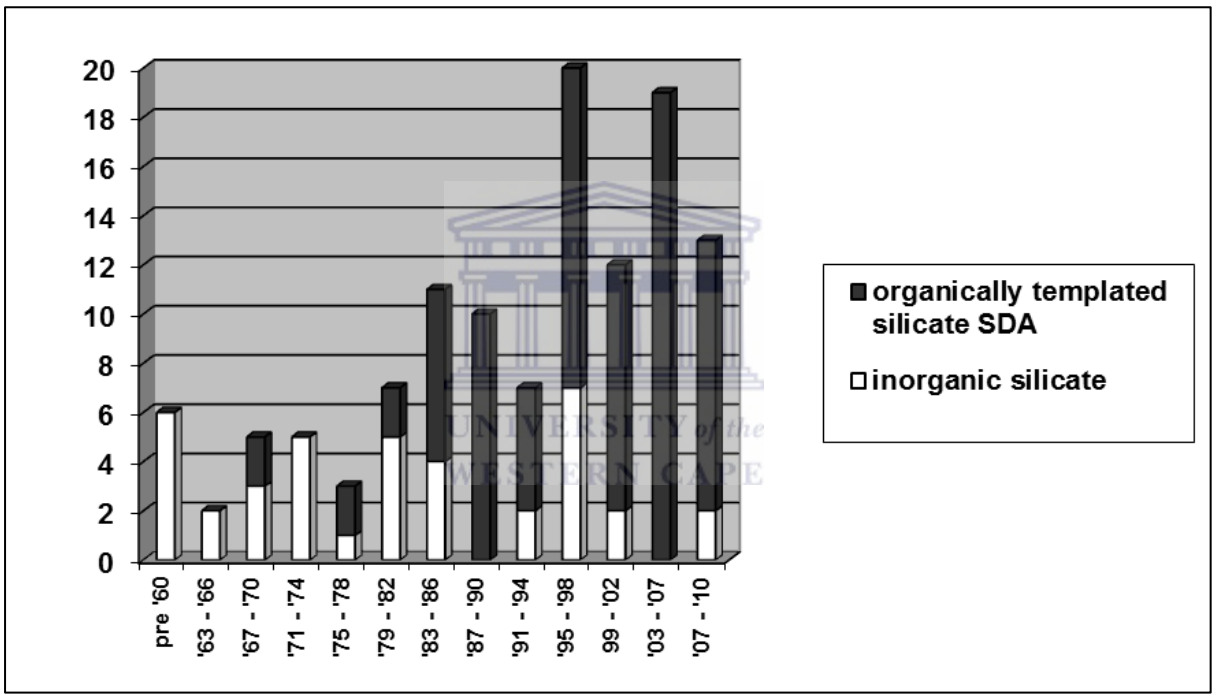

Figure 2.5: Chronological discovery of novel synthetic zeolitic silicates (Wright and Lozinska, 2011).

2.3.2. Fundamentals of zeolite structure

Zeolites are aluminosilicate materials with tetrahedrally-connected framework structures (AlO_4 and SiO_4 tetrahedra). Conceptually, they may consist of pure silica frameworks or with Si (+IV) being substituted by Al (+III) (Figure 2.6). The +3 charge brought by Al imparts negative charges to the framework, which are charge compensated with extra-framework cations to keep the structure neutral (Wright and Lozinska, 2011). According to Lowenstein's

rule, Al-O-Al linkages are not possible in the zeolite structure because of electrostatic repulsions between the negative charges (Zhao et al., 1997).

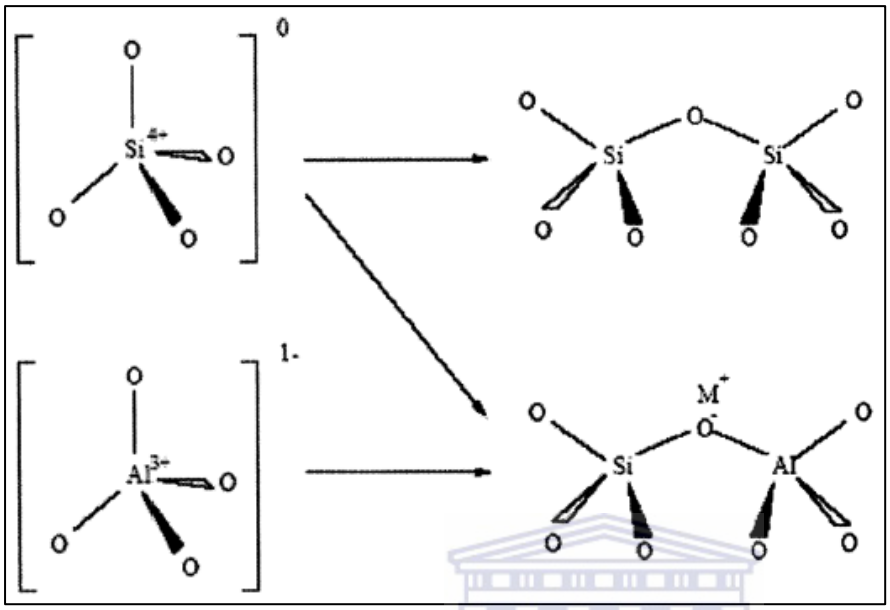

Figure 2.6: Primary building blocks of zeolites (Musyoka, 2012).

An empirical formula for a zeolite is

$$M^{n+}_{x/n} Al_x Si_{1-x} O_2 . yH_2O$$ **(Equation 2.1)**

With x=0 to 0.5, M^{n+}= compensating exchangeable cation, y= number of water molecules. M^{n+} can mainly be alkali, alkali earth metal cations or alkylammonium cations, which can also be replaced by almost any inorganic cation or a proton during post-synthetic modifications (Wright and Lozinska, 2011). Al^{3+} can also be replaced by other three or four valence state ions such as B, Ga, Fe, Ge, Ti, etc. (Chester and Derouane, 2009). Silicate and aluminate tetrahedra are primary building units (PBUs) but the zeolite frameworks can also be considered in terms of limitless secondary building units (SBUs) that are made of linked PBUs (Figure 2.7). The corners of the polyhedra represent tetrahedral atoms (Wright and Lozinska, 2011).

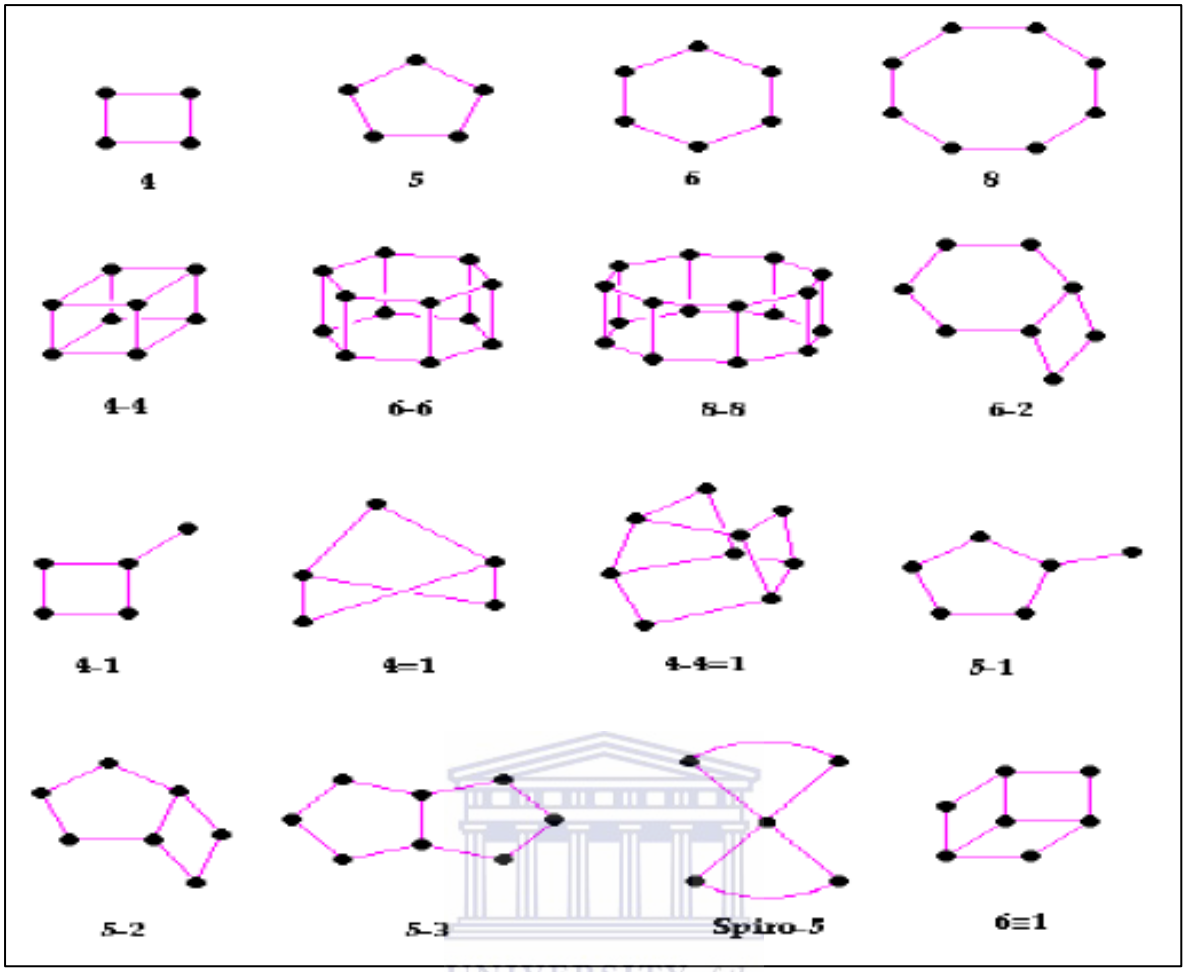

Figure 2.7: Secondary building units (Meier et al., 1996; Nagy et al., 1998).

The same building units as shown in Figure 2.8 can give different zeolitic structures such as A zeolite, sodalite or X/Y zeolite with different pore diameters, cages or channels (Masoudian et al., 2013).

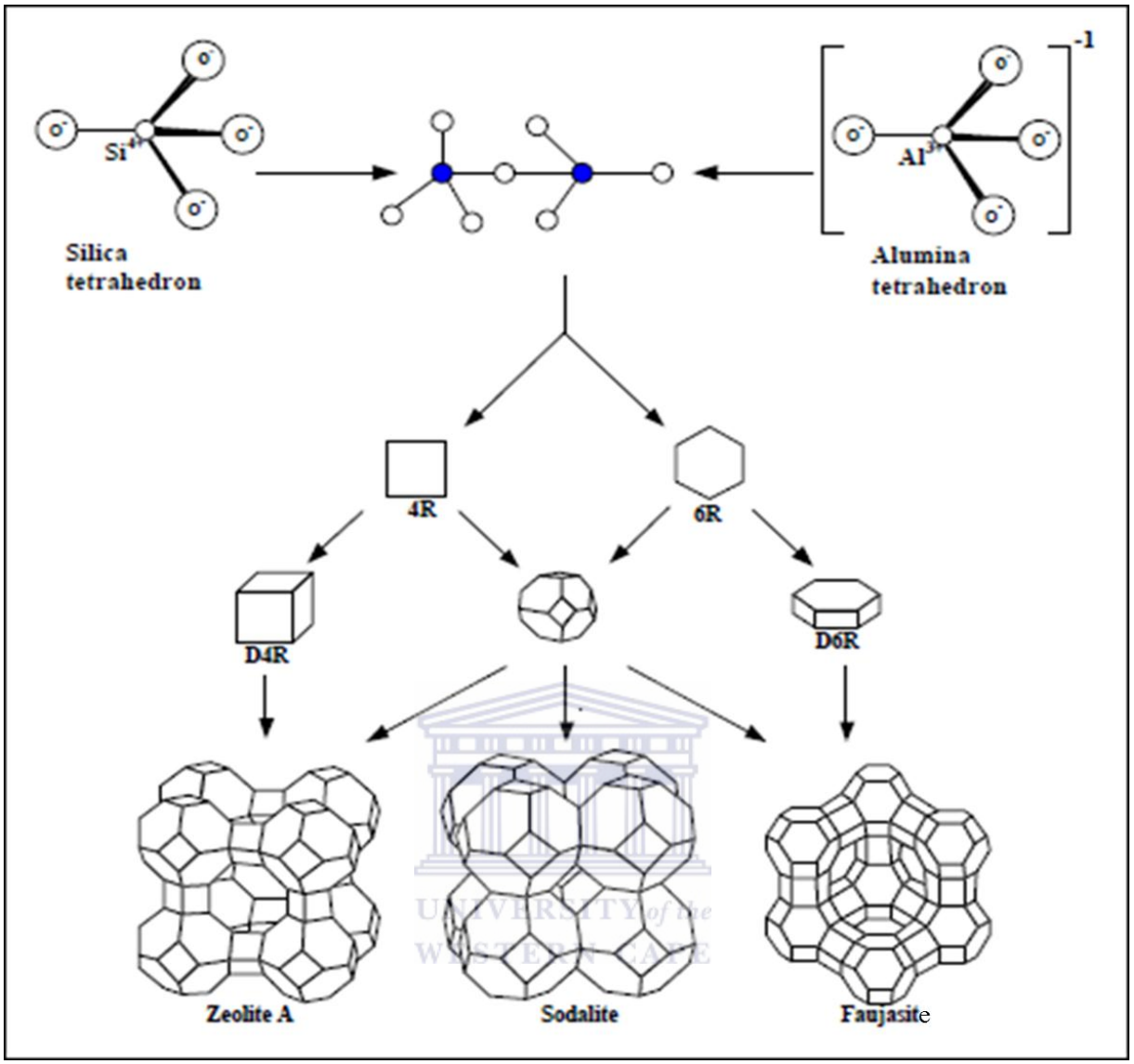

Figure 2.8: Different types of zeolites obtained from sodalite unit (Masoudian et al., 2013).

2.3.3. Properties

The presence of extra framework cations, usually hydrated, gives zeolites an ion exchanging ability; which varies from one structure to another. For many low silica content zeolites such as A, X or chabazite a complete ion exchange is possible (Wright and Lozinska, 2011). When they are protonated, zeolites exhibit acidic properties with the presence of Brønsted acid sites, which can be transformed into Lewis acid sites by losing a water molecule (Figure 2.9).

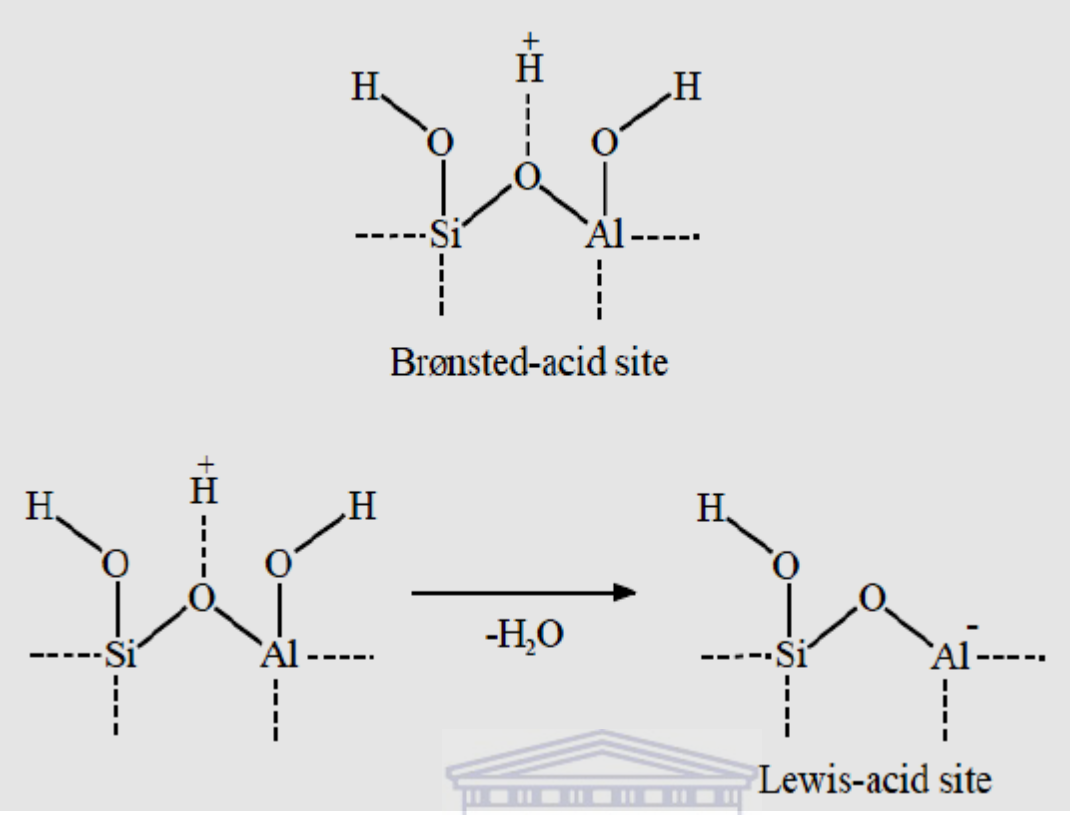

Figure 2.9: Schematic for Brønsted and Lewis acid sites (Barzetti et al., 1996).

Zeolites can be subjected to reversible hydration (Kirov and Filizova, 2012). The dehydration reduces the coordination of cations, which move to achieve a better coordination with framework oxygen atoms and so lower the overall energy (Wright and Lozinska, 2011). The movement of cations through the framework gives the zeolites electrical conductivity (Breck, 1974; Nagy et al., 1998). The pore architecture is interconnected, with cages and channels of different size and shape, fronted by SiO_4 and AlO_4^-. This gives zeolites their unique and inherent ability to selectively adsorb molecules based on shape and size; for this reason, zeolites are referred to as "molecular sieves" (Davis, 2002).

2.3.4. Formation

Zeolites can occur naturally or are synthesised in the laboratory. Nowadays, over 40 naturally occurring zeolites and over 140 synthetic zeolites have been identified (Amber et al., 2013). The number of synthetic zeolites increases constantly, particularly after the discovery of aluminophosphate zeolites by Wilson et al., (1982).

2.3.4.1. Natural formation

Natural zeolites are mostly found in regions of former or present magmatic activity. Their formation required high temperature and the presence of water. Natural zeolites can be formed by one of the following routes (Chester and Derouane, 2009):

- Crystals resulting from hydrothermal or hot-spring activity involving reactions between solutions and basaltic lava flows.
- Deposits formed from volcanic sediments in closed alkaline and saline lake systems.
- Similar formations from open freshwater lake or groundwater systems acting on volcanic sediments.
- Deposits formed from volcanic materials in alkaline solids.
- Deposits resulting from hydrothermal or low-temperature alteration of marine sediments.
- Formation which are the result of low-grade burial metamorphism.

These reactions occur in open systems and depend on variables such pressure, temperature and time (Chester and Derouane, 2009). Eight zeolites (analcime, chabazite, clinoptilolite, erionite, heulandite, laumontite, mordenite and phillipsite) commonly make up the major part of the zeolitic materials in sedimentary rocks (Hay and Sheppard, 2001). Naturally occurring zeolites are mostly contaminated to varying degrees by other minerals.

2.3.4.2. Synthetic formation

The understanding of the formation of natural zeolites inspired the laboratory synthesis of zeolites that evolved by duplicating the conditions under which natural zeolites were formed. However, time is the condition that cannot be duplicated in the laboratory because it covers 1000 years or more in nature (Chester and Derouane, 2009). Zeolites can be synthesised under hydrothermal conditions, with temperatures between 45 °C and 200 °C, in the presence of organic and/or inorganic cations and a mineralising agent (Belviso et al., 2009; Moliner, 2011; Musyoka, 2012). Table 2.3 presents the general routes by which zeolites can be synthesised. The complex chemical processes involved in the synthesis of zeolites are called zeolitization (Hay and Sheppard, 2001).

Table 2.3: Zeolite preparation process (Chester and Derouane, 2009).

Synthesis process	Reactants	Products
Hydrogel	Reactive oxides, soluble silicates, soluble aluminates, caustic	High purity powders, gel preform, zeolite in gel matrix
Clay conversion	Raw kaolin, metakaolin, calcined kaolin, soluble silicate, caustic sodium, chloride	Low to high purity powder, binderless, preform zeolite in clay, derived matrix
Others	Natural SiO_2, acid treated clay, amorphous mineral, volcanic glass, caustic, $Al_2O_3.3H_2O$	Low to high purity powder, zeolite on ceramic support. Binderless preforms.

Several mechanisms of zeolitization have been suggested since the discovery of the first synthetic zeolite in a laboratory. The first possible zeolitization mechanism was proposed by Barrer et al. (1959). Porous aluminosilicates are formed from secondary buildings units, as rings of polyhedral, but not from additions of individual Al or Si tetrahedra. Many years later, it was suggested that these mechanisms are based on the transformation of the initial reactants in amorphous form towards a crystalline microporous product, by means of solution-mediated crystallization or solid transformation (Figure 2.10) (Moliner, 2011). But the exact crystallisation mechanism of zeolites is still not well defined (Cubillas and Anderson, 2010).

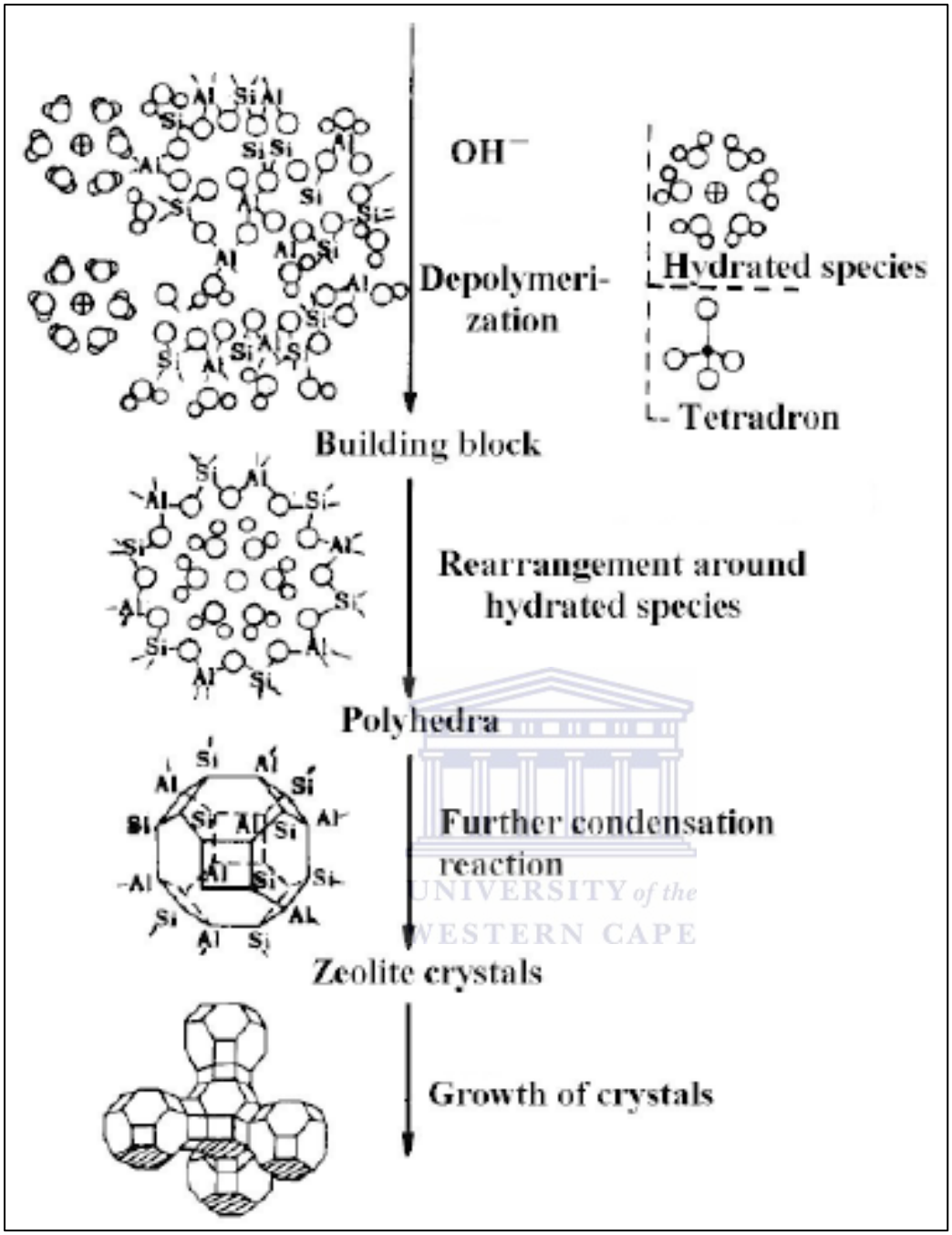

Figure 2.10: Schematic illustration of the solution-mediated crystallisation (Chester and Derouane, 2009).

The complexity of the mechanisms of zeolite formations is due to the plethora of chemical reactions, equilibria and solubility variations that take place during the crystallisation process (Byrappa and Yoshimura, 2001). The synthesis of zeolites involves three steps which are: Induction, nucleation and crystal growth (Figure 2.11).

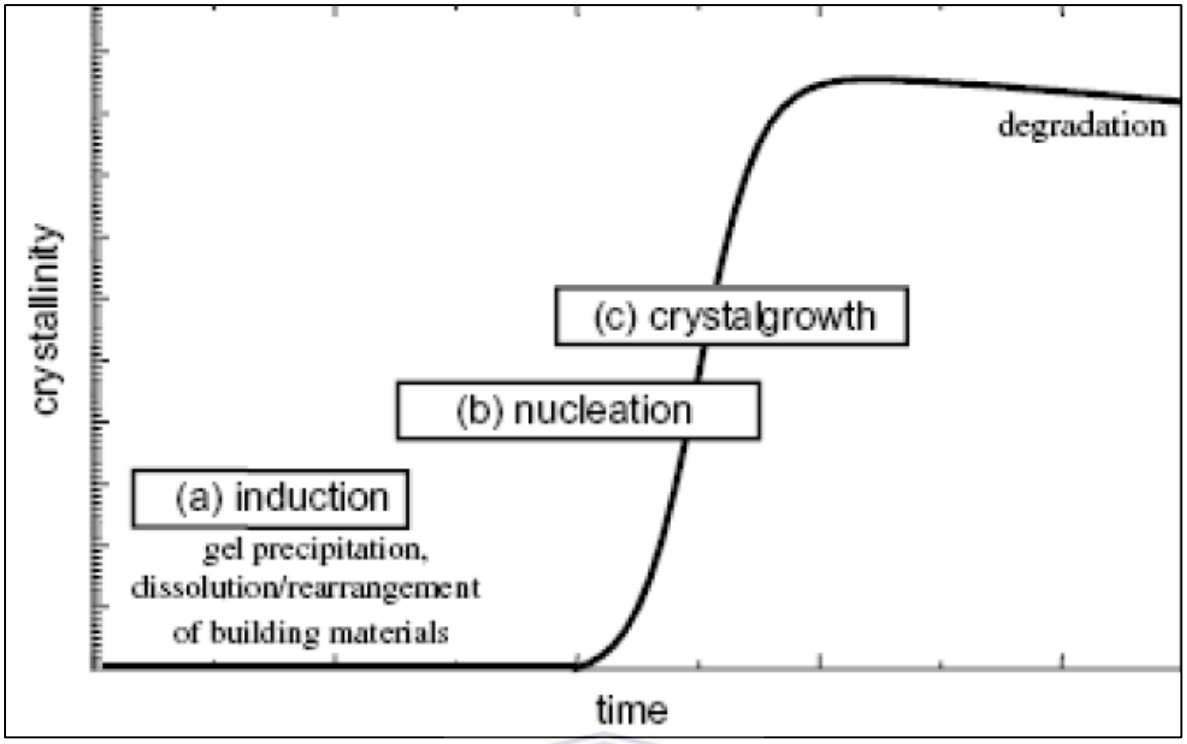

Figure 2.11: Steps involved in the zeolite formation (Herrmann et al., 2005).

- Induction: this initial stage involves gel precipitation, dissolution and/or rearrangement of building materials (Herrmann et al., 2005).
- Nucleation: it is the process by which the atoms and molecules of a reactant phase rearrange into a cluster of the product phase, which is large enough to have the ability to grow irreversibly to a macroscopically larger size (Cubillas and Anderson, 2010).
- Crystal growth: it is the process in which nuclei grow either by addition or condensation towards full grown crystals (Byrappa and Yoshimura, 2001).
- Degradation: synthetic zeolites are metastable structures that may, under certain conditions be transformed into other thermodynamically more stable types of zeolites, following the Ostwald's law of successive transformation (Hay and Sheppard, 2001).

It is well known that super-saturation is the driving force of crystal growth kinetics. The super-saturation of a particular zeolite depends on the variables involved in the synthesis such as temperature, alkalinity, and chemical composition of the reactant mixtures and cooling profile of the final product (Lewis et al., 2014). These variables do not necessarily lead to the targeted zeolite because nucleation appears to be kinetically rather than thermodynamically

determined and controlled. The kinetic variables are the treatment of reactants prior to the crystallisation, their chemical and physical nature (Chester and Derouane, 2009).

2.3.4.3. Principal chemical variables affecting the zeolite synthesis

One of the most important factors that affect the synthesis of zeolites is the chemical composition of the slurry (or gel or solution) from which crystals will grow. There is a wide range of inorganic and organic components that are used to govern the outcome of the crystallisation (Figure 2.12). They play an important role in many steps of the zeolite synthesis (induction, nucleation and crystal growth) (Derouane et al., 1992).

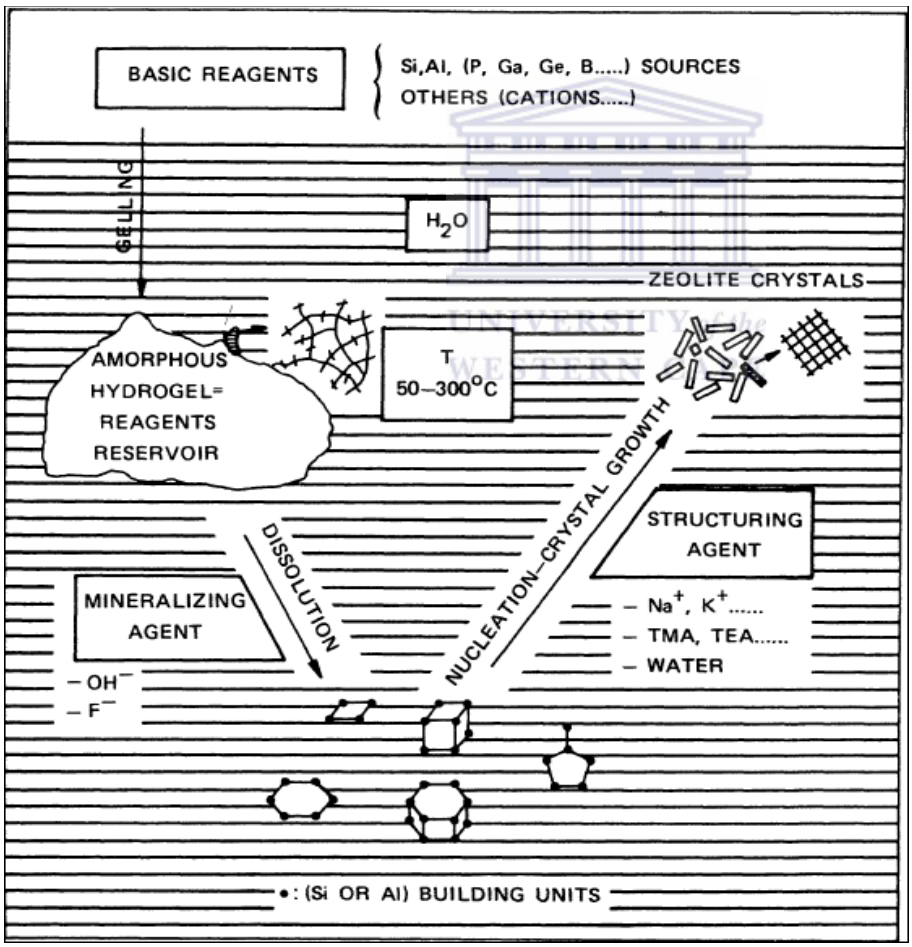

Figure 2.12: Simplified zeolite synthesis scheme (Marcilly, 1986).

a. Silicon and aluminium sources

The primary building units of zeolites are made of silicon, aluminium and oxygen (Wright and Lozinska, 2011). The composition and purity of the source of silicon and aluminium is one of the properties that govern the purity and properties of the synthesised zeolites (Robson, 2001). Silica and alumina chemical sources have the advantage of producing pure zeolite phases with high catalytic efficiency (Losch et al., 2015; Losch et al., 2016; Htun et al., 2012). However, those silica and alumina chemical sources are expensive (Georgiev et al., 2009). Thus, fly ash, clays materials, naturals, municipal solid waste and industrial slags have been used as cheaper sources of silicon and aluminium in zeolite synthesis (Georgiev et al., 2009, Musyoka et al., 2012; Musyoka et al., 2014, Kuwahara et al., 2010, Chareonpanich et al., 2004)

b. Solvent

Water is the most used solvent in the synthesis of zeolites. It helps the mineralizing agent to dissolve species that are needed for the crystallisation and can also act as template (Guth et al., 1999). Some studies have been carried out using organic solvents such as ethylene glycol, propanol, ethanolamine or ethylendiamine in the synthesis of sodalite structure (Bibby and Dale, 1985; Braunbarth et al., 1996; Braunbarth et al., 1997). It has been reported that ionic liquids (imidazolium) were used as both solvent and organic directing agent in the synthesis of zeolites (Cooper et al., 2004)

c. Mineralizing agent

The mineralizing agent is the chemical specie that dissolves and precipitates the silicate and aluminosilicate species among others in the synthesis gel. It acts as catalyst in the zeolite synthesis, where it is consumed during the dissolution of species and recovered during the crystallisation (Guth et al., 1999). It plays an important role in the pre-nucleation (induction) stage (Derouane et al., 1992). The hydroxyl anion (OH^-) is the most used mineralizing agent. It increases the solubility of silicon and aluminium sources and directs the formation of soluble silicate ion $\left[Si(OH)_{4-n}O_n^{n-}\right]$ and aluminate ion $\left[Al(OH)_4^-\right]$ (Moliner, 2011). The hydroxyl anion usually directs the synthesis of aluminium rich zeolites (Milton, 1959). When the synthesis is carried out in the presence of the organic structure directing agents (OSDAs),

at high temperature and pH, OH^- can cause thermal stability problems to the OSDAs, as the quaternary ammonium cations can suffer Hoffman degradation (Moliner, 2011). The use of fluoride anion (F^-) as mineralizing agent was the breakthrough to prevent the degradation of OSDAs, as the zeolite synthesis through the fluoride route can be performed at near neutral pH. This fluoride synthesis route was first described by Flanigen and Patton in 1978 and it favours the synthesis of silicon rich zeolites (Flanigen and Patton, 1978).

d. Structure directing agent

The synthesis of zeolites, types A, Y, X and many natural zeolites utilise inorganic cations such as Na^+, K^+, Ca^{2+}, Mg^{2+}, etc. as structure directing agents. These zeolites tend to have relatively high aluminium content, which is charge compensated with such cations thus their pore space contains many of the above exchangeable cations (Wright and Lozinska, 2011). The introduction of quaternary ammonium cations such as tetraethylammonium (TEA^+) and tetrapropylammonium (TPA^+) cations as organic structure directing agents (OSDAs) in the zeolite synthesis, allowed the preparation of new zeolite phases such as Beta and ZSM-5. This introduces new zeolite growth mechanisms (Moliner, 2011). The quaternary ammonium cations can be bulky, so fewer can be included in the zeolite pores than would be the case for inorganic cations. This lowers the density of framework negative charge and consequently lowers the aluminium content. Therefore, zeolites templated by large OSDAs generally have high silicon content (Wright and Lozinska, 2011).

The various ways in which tetrahedral groups (AlO_4 and SiO_4 tetrahedra) are linked by the common shared oxygen atom to form poly-nuclear complexes leads to the structural complexity of zeolites and a very wide diversity of zeolites and zeolite-like materials (Chester and Derouane, 2009). The tetrahedral groups (primary building units) are connected through their common shared oxygen atoms to form a wide range of secondary building units; which are interconnected to form polyhedra. The polyhedra are connected to form the infinitely extended frameworks of various specific zeolites (Wright and Lozinska, 2011). The framework density (FD) that is the number of tetrahedrally coordinated atoms per nm^3 is one of the criteria used to establish the identity of zeolite frameworks (Chester and Derouane, 2009).

Kirov and Filizova, (2012) investigated the influence of structure directing agents (Na^+, K^+, Ca^{2+}, Mg^{2+}, TEA^+, TPA^+ and water) in the zeolitization process. In aqueous solutions, a

cation hydrates by orienting the water dipoles and forming hydration shells that manly depend on the ionic radius and charge of the cations. The state of cations governs their behaviour in ion transport through zeolite channels. The water molecules and cations in channels and cavities interact with each other and with the oxygen of the aluminosilicate framework. Table 2.4 gives the number of water molecules and framework oxygen atoms surrounding Na^{+}, Ca^{2+}, K^{+} and Mg^{2+} in some zeolite structures.

Table 2.4: Number of water molecules and framework oxygen atoms surrounding some extra framework cations in zeolite structures (Kirov and Filizova, 2012).

Zeolite	Na^+		Ca^{2+}		K^+		Mg^{2+}	
	H_2O	O	H_2O	O	H_2O	O	H_2O	O
Analcime (Na) – Wairakite (Ca)	2	4	2	4	-	-	-	-
Natrolite (Na) – Scoletite (Ca)	2	4	3	4	-	-	-	-
Laumontite	-	-	3	4	-	-	-	-
Amicite	3	3	3	4	-	-	-	-
Gismondite	-	-	4	2	-	-	-	-
Heulandite	6	2	5	3	-	-	-	-
Stilbite	3	2	7	0	-	-	-	-
Chabasite	-	-	5	0	-	-	-	-
Offretite	-	-	6	0	0	6	5	0
Clinoptilolite	-	-	-	-	3(1)	6	6	0
Ferrierite	-	-	-	-	-	-	6	0
Phillipsite	-	-	-	-	4	4	-	-

As shown in Table 2.4, Ca^{2+}, Na^+ and Mg^{2+} are highly hydrated and they have more water molecules than oxygen atoms in their surroundings or are only coordinated by water molecules. These hydrated cations are located in large channels in which water molecules distribute their cationic charges to AlO_4^- tetrahedrons that are not directly in contact with cations. This governs the stability of large channels. High temperature causes the decrease of water molecules surrounding the cations, which have a close contact with AlO_4^- tetrahedrons and influence their number and distribution. There is a correlation between the charge of the cations and the number of AlO_4^- tetrahedrons that are close to them (Figure 2.13) (Kirov and Filizova, 2012).

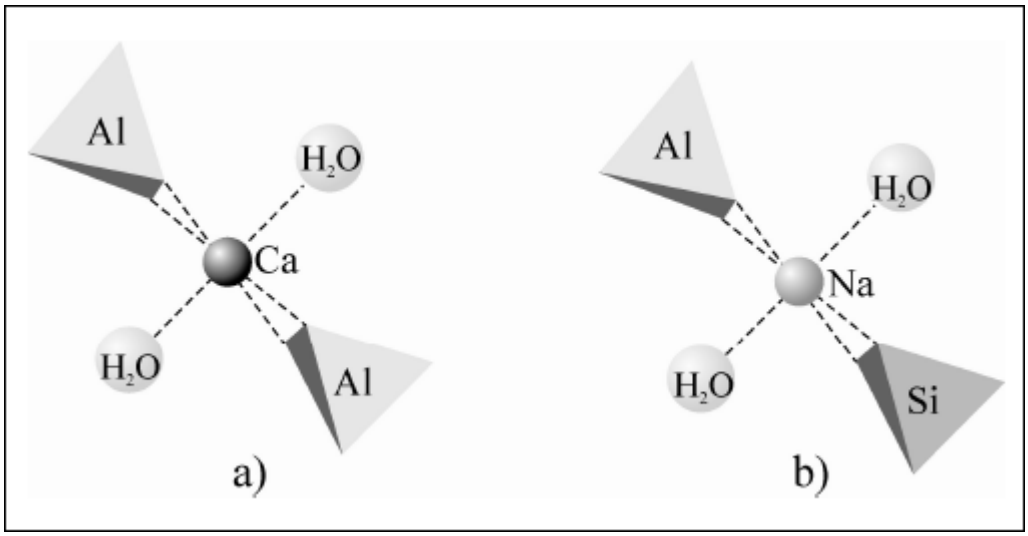

Figure 2.13: Coordination of (a) Ca^{2+} and (b) N^{a+} (Takeuchi et al., 1979).

The position of extra framework cations has been extensively investigated and Figure 2.14 presents different sites where these cations can be found in A and X zeolites. These include sites in the D6Rs of X zeolite (sites I and I'), in sodalite cages (II and II') and in the super-cages (III) (Wright and Lozinska, 2011).

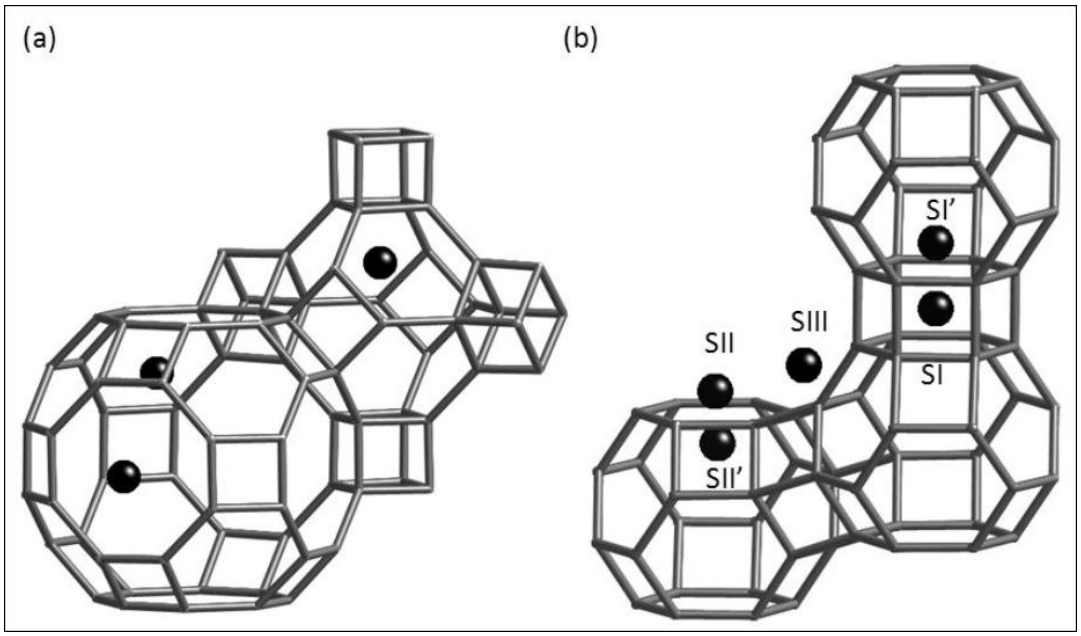

Figure 2.14: Extra framework cation sites in A zeolite (a) and X zeolite (b) (Wright and Lozinska, 2011).

2.3.4.4. Post-synthetic modifications of zeolite structure

Zeolites are used in different applications such as catalysts, adsorbents and ion exchangers. However, prior to their application their post-synthetic treatments are needed – starting from the routine drying and detemplating to a wide spectrum of treatments – in order to tailor their properties for improvement of conventional or realization of emerging applications. The post-synthetic treatments can include the introduction, dislodgement or replacement of framework atoms or charge balancing cations; detemplation and functionalization by inorganic and organic species; introduction of auxiliary porosity (Valtchev et al., 2013; Yan et al., 2003). The introduction of another atom (T) than Si in the zeolite structure requires its compatibility with TO_4 tetrahedra-related framework. The incorporation of elements with high or low oxidation states comes with charges that will need to be balanced. Table 2.5 gives the most common elements that can perform the isomorphic substitution of Si in the tetrahedral zeolite framework (Moliner, 2011). Trivalent ions such as Ga^{3+}, Fe^{3+} or B^{3+} can substitute Al^{3+} in the zeolite frameworks and change their acidic properties. Bayense et al., (1993) reported the introduction of Ga^{3+} in dealuminated H-ZSM-5 and H-Y zeolites. Besides the introduction of charges in the zeolite structures, these elements also affect the size and shape of pores as well as the relative framework stability (Moliner, 2011).

Table 2.5: Elements that can substitute Si in the tetrahedral zeolite framework (Moliner, 2011).

Oxidation state	II	III	IV	V
Elements	Be	Al	Ge	P
	Zn	B	Sn	
	Mg	Ga	Ti	

Dislodgement and replacement of framework atoms produce various effects due to their introduction on the zeolites properties (Valtchev et al., 2013). Kitaev et al., (2013) modified the acid characteristics of H-ZSM-5 zeolite with appearance of superacid centers by sequentially loading Ti and S into the zeolite structure through a treatment with titanium tetrachloride and sulfuryl chloride. Maier et al., (2011) reported a dealuminination and

modification of acidity of BEA zeolite via steaming treatment. Zhang et al., (2014) reported the transformation of Na-ZSM-5 to H-ZSM-5 through treatment with oxalic acid followed by calcination at 550 ℃ for 4 h that was used as support for preparation of TiO_2/H-ZSM-5 composite photocatalyst.

Zeolites are widely used as catalysts, but the restriction of their pore size may induce some diffusional constraints when bulky reactants are used in catalytic applications (Moliner, 2012). The synthesis of zeolites with mesopores as well as micropores is a more generally applied strategy to improve the molecular transport properties of zeolite. Mesopores can be created inside zeolite crystals by destructive or constructive synthesis strategies (Chal et al., 2011; Louis et al., 2010). It has been reported that the alteration of acidic properties of zeolites as well as the introduction of auxiliary porosity can be performed by dealumination via calcination, steaming or acid leaching and desilication via alkaline leaching (Chal et al., 2011). Bjørgen et al., (2008) decreased the Si/Al of ZSM-5 zeolite, synthesised from Ludox LS and $Al(OH)_3$, from 46 to 39 with an increase in BET surface area from 313 m^2/g to 372 m^2/g by treating the catalyst with 0.05 M NaOH solution, and they reported an increase in MTO conversion from 86 % to 89 % with an improved lifetime of the catalyst. The introduction of organic compounds within the pores or in the framework of zeolites allows tailoring of their physicochemical properties extending their shape-selectivity properties due to the different nature of the organic functional groups (Moliner, 2012). Metals such as Cu, Ag, Fe, etc. have been loaded into various zeolites in order to take advantage of both catalytic and shape-selectivity properties of the loaded metals and zeolites, respectively (Chassaing et al., 2007; Dong et al., 2009).

2.3.4.5. Synthesis of zeolites from coal fly ash

Fly ash has been used as the starting material for the synthesis of zeolites because of its abundance of amorphous aluminosilicate glass (Holler and Wirsching, 1985). Nowadays, the synthesis of fly ash-based zeolites has been increasing. Several methods have been suggested, which differ from one another in alkaline solution, molarity of alkaline agents, solution/solid ratio, time, temperature and type of incubation (Belviso et al., 2009). The processes typically used to synthesise zeolites from fly ash are:

- The hydrothermal process was proposed by Holler and Wirsching (1985). It had been reported that zeolites, types X, A, P, L ZSM-18, sodalite, erionite and analcime were synthesised using the hydrothermal process without the fly ash being activated. The activation consists in dissolving silica and alumina from fly ash through alkaline treatment (Chigondo, et al., 2013; Vadapalli et al., 2010; Adamczyk et al., 2005; Moutsatsou et al., 2008). It should be noted that the zeolites typically synthesised from the as-received fly ash were mixed with some non-reacted minerals such as quartz and mullite found in the fly ash (Musyoka, 2012).
- Hydrothermal process with fusion treatment was proposed by Shigemoto et al., (1993). The introduction of the fusion step enhanced the zeolite formation and reduced the percentage of unreacted parent mineral phases in the final product (Ojha et al., 2004; Musyoka, 2012). The fusion consists of mixing fly ash with sodium hydroxide. The mixture is heated at a temperature ranging between 450 °C and 650 °C and the time ranges between 1 h and 3 h (Klamrassamee et al., 2010; Musyoka, 2012; Ruen-ngam and Rungsuk, 2009). An acid treatment can be performed prior to the fusion step in order to dealuminate the fly ash, and remove iron and other metals to a certain extent (Ojha et al., 2004). Purer zeolite phases are synthesised when amorphous Si and Al are extracted from fused fly ash by water and used as starting materials (Musyoka, 2012). The synthesis of high silica content zeolites such as ZSM-5 zeolite generally requires an addition of source of silica. Reanvattana (2005) reported the synthesis of high purity ZSM-5 zeolite from alkaline fly ash extract that contained Si and Al. Silica extracted from rice husk ash was added to increase the Si/Al ratio.

2.3.4.6. Extraction of silica and alumina from fly ash for the zeolite synthesis

Several applications of fly ash are the result of its high silicon and aluminium content (Wang and Wu, 2006). With the decreases of bauxite as resource and the increasing aluminium demand, extraction of aluminium from fly ash has become an important research topic (Guang-hui et al., 2010; Yao et al., 2014; Liu et al., 2012; Cheng-You et al., 2012; Lai-Shi et al., 2011). Moreover, if aluminium can be extracted from fly ash the silica content would not need to be augmented for high silica zeolites to form. The technologies of alumina extraction from fly ash are classified into acidic, alkali and acid-alkali methods (Guang-Hui et al., 2010). The stability of aluminium in the mullite mineral phase leads to the use of power-

consuming processes such as roasting or sintering in order to extract alumina from fly ash (Yao et al., 2014; Liu et al., 2012). Sodium hydroxide has been used to remove amorphous silica from fly ash prior to the extraction of alumina (Zhu et al., 2013). According to Panagiotopoulou et al., (2007), 20 % of Si and Al were extracted from fly ash using 10 M of sodium hydroxide solution for 24 h. Several studies have been conducted using fusion of fly ash with sodium hydroxide as a pre-treatment step in the synthesis of high purity zeolites (Musyoka, 2012; Moreno et al., 2002). It was reported by Baldyga et al. (2012) that silica precipitates in an aqueous solution at a pH of 9.3. Awizar et al. (2013) summarised the extraction of silica from the rice husk ash as follows:

$$SiO_2(Ash) + 2NaOH \rightarrow Na_2SiO_3 + H_2O \quad \textbf{(Equation 2.2)}$$

$$Na_2SiO_3 + H_2SO_4 \rightarrow SiO_2 + Na_2SO_4 + H_2O \quad \textbf{(Equation 2.3)}$$

Scientific advances made in the extraction of silica and alumina can rationalise the synthesis of zeolites without extra sources of silica or alumina, which informs the primary aim of this study.

2.3.5. Classification

The classification of zeolites has been made based on their morphological characteristics, crystal structure, chemical composition, effective pore diameter, etc. (Jacob, 1998). Zeolites can be classified based on their macroscopic crystalline habit (Table 2.6). The fibrous zeolites form needles or fibrous aggregates. The platy or lamellar zeolites are characterised by their cleavage and lamellar habit. The cubic or robust zeolites are characterised by their 4- and 6-rings and present sorptive properties (Szostak and Stepto, 1998).

Table 2.6: Classification of natural zeolites based on their morphological characteristics (Szostak and Stepto, 1998).

Fibrous zeolites	Platy or lamellar zeolites	Cubic or robust zeolites
natrolite, solecite, mesolite, thomsonite, edingtonite	heulandite, brewsterite, mordenite, wellsite, phillipsite	faujasite, chabazite, gmelinite, levyne

The classification of zeolites according to their chemical composition is based on their Si/Al ratio (Table 2.7). The Si/Al ratio is an important characteristic of zeolites. It is inversely proportional to the ion exchange capacity and directly proportional to the thermal stability (Ramesh et al., 2011)

Table 2.7: Classification of zeolites based on their chemical composition (Jacob, 1998).

Class	Si/Al ratio	Examples
Low silica zeolites	1-1.5	A, X
Intermediate silica zeolites	2-5	erionite, chabazite, clinoptilolite, mordenite, L, Y, omega.
High silica zeolites	10-several thousands	ZSM-5, ZSM-11, EU-1, EU-2, beta, mordenite, erionite, Y
Silica molecular sieves	Several thousands to infinity	silicalite

Zeolites can be classified according to their pore openings (Table 2.8). Zeolites with 8-membered rings are considered as small pore zeolites; with free pore diameters of 3 to 4.5 Å.

Medium pore zeolites have 10-membered rings and free pore diameters of 4.5 to 6 Å. Zeolites with 12-membered rings or more are considered as large pore zeolites. They have a free pore diameter of 8 Å or more (Ramesh et al., 2011; Wright and Lozinska, 2011).

Table 2.8: Classification of zeolites based on their pore openings (Jacob, 1998).

8-membered ring (small pore)	10-membered (medium pore)	12-membered ring (large pore)
linde A, ZK-5, chabazite, bikitaire, gismondine, etc.	heulandite, ZSM-5, EU-1, EU-2, ZSM-11, etc.	faujasite, mordenite, beta, omega, etc.

Several criteria have been used to classify zeolites. But the International Union of Pure and Applied Chemistry (IUPAC) commission on the zeolite nomenclature and the International Zeolite Association (IZA) Structure commission have set rules and designations consisting of the use of a three capital letter code (mnemonic codes) to classify the zeolites (Table 2.9) (Auerbach et al., 2003). Zeolites can also be described based on the framework density (FD), and the maximum FD for zeolites goes up to 21 T-atoms per 1000 $Å^3$ (Baerlocher et al., 2007).

Table 2.9: IUPAC mnemonic codes of zeolites and their framework density (FD) (Meier and Baerlocher, 1999).

Structure type code	Type material	Isotypes	FD
ABW	Li-A (BW)	BePO-ABW, ZnAsO-ABW	17.6
AFI	AlPO-5	SSZ-24, CoAPO-5, SAPO-5	16.9
ANA	Analcime	Leucite, Wairakite, AlPO-24	19.2
BEA	Beta	Tschernichite, Borosilicate-BEA	15.3
CAN	Cancrinite	Tiptopite, basic CAN, ECR-5	16.9
CHA	Chabazite	AlPO-34, MeAPO-47, Phi	15.1
ERI	Erionite	AlPO-17, LZ220	16.1
FAU	Faujasite	X, Y, SAPO-37, ZnPO-X	13.3
GIS	Gismondine	Garronite, Na-P, MAPO-43	16.4
HEU	Heulandite	Clinoptilolite, LZ219	17.5
LTA	Linde type A	SAPO-42, ZK-4, GaPO-LTA	14.2
MEL	ZSM-11	Silicalite-2, Borolite-D, TS-2	17.4
MFI	ZSM-5	Silicalite-1, Borolite-C, TS-1	18.4
SOD	Sodalite	Tugtupite, basic SOD, AlPO-20	16.7

2.3.6. Applications

The potential applications of zeolites vary as a function of their properties. Around 300,000 tons of synthetic zeolites are being used annually as catalysts and adsorbents. In addition, 250,000 tons of natural zeolites are being used annually in waste water treatment, or for soil improvement and as animal feed additive (Jha and Singh, 2011; Yilmaz and Muller, 2009). This wide applicability of zeolites is due to the following factors:

- Ion exchange capacity and adsorption.

- The presence or variety of their active sites (Brønsted and Lewis acid sites, basic sites, redox-active sites) that have different physicochemical properties and act independently or cooperatively for catalysing multi-functional processes.
- Their shape selectivity that can affect positively the selectivity, rate and stability of the reactions and allow them to be considered as a network of "nanoreactors" (Byrappa and Yoshimura, 2001). It has been four decades since the introduction of the shape-selective character of zeolites into industrial applications.

2.3.6.1. Ion exchange

Ion exchange capacity is an important zeolite property that allows many industrial applications. It has been found that Na-A zeolite is effective as filler in detergents. It is used as a water softener agent by ion exchanging Na^{+} with Ca^{2+} and Mg^{2+} in the input water (Jha and Singh, 2011). The removal of heavy metals from a solution is a necessary process in soil chemistry and hydrometallurgy in addition to the treatment of industrial wastewaters. Many factors affect the removal of heavy metals such as pH, ionic strength, initial metal ion concentration, etc. (Ismail et al., 2013). Zeolites with high cation exchange capacity (up to 500 meq/100 g) such as zeolites, types P, A, faujasite, chabazite, herschelite, etc. have been used for decontamination of sludge, industrial effluents and other waste water by removing heavy metals such as Pb^{2+}, Cd^{2+}, Cu^{2+}, Zn^{2+} (Scott et al., 2001). Ismail et al., (2013) reported that 99.99 % of Pb^{2+} and 95.68 % of Zn^{2+} could be removed from aqueous solution using LTA zeolite. Hg and Pb were removed from wastewater using fly ash-based zeolite containing sodalite, faujasite and linde A phases (Somerset et al., 2007). Zeolites are also used in the treatment of radioactive waste. Eisler, (2012) reported the removal of Fukushima radiocontaminants (Cs, Sr and Ba) from drinking water using a synthetic A4 zeolite and a natural zeolite, mordenite.

2.3.6.2. Adsorption

The rigid structure and the presence of cages and channels give zeolites high adsorption/desorption characteristics without any effect on their lattice structure (Jha and Singh, 2011). Zeolites can be used in adsorption of both gas and liquid phases (Roland and Kleinschmit, 2005). They have potential applications as additives in soils, for heavy metal adsorption, as carrier of pesticides, herbicides and fungicides. They are also used as additives

in animal feeds to act as detoxifying agents. Zeolites are used as molecular sieves to absorb water molecules from gas streams or to trap SO_2 and NH_3 from water or gaseous emissions. Zeolites have also been used in animals sheds for adsorbing hydrogen sulphides, ammonia and subsequent odour control in the surrounding environment (Jha and Singh, 2011). It has been reported that A and X zeolites were used in removal of dye and methylene blue from waste water (Chunfeng et al., 2009).

2.3.6.3. Catalysis

Heterogeneous catalysis is one of the key elements in the chemical industry because of the important role it plays in many chemical processes (Yilmaz and Muller, 2009). The presence of Brønsted acid sites and some properties such as thermal stability, porosity, ion exchange capacity and ability to be modified by isomorphous replacement of Al with Fe, B, Ga or Ti has led zeolites to act as a green replacement for mineral acids in catalysis (Bekkum et al., 1991; Nagy et al., 1998). Zeolites have the advantages of not being corrosive and are easily recovered from the reaction mixture unlike conventional catalysts ($AlCl_3$, $ZnCl_2$, H_2SO_4, etc.) that were firstly used (Byrappa and Yoshimura, 2001). Moreover, the presence of Brønsted and Lewis acidity as well as their shape and size selectivity ability is the key driver for their use in many industrial processes. The shape selectivity allows the product selectivity away from the equilibrium mixture (Yilmaz and Muller, 2009; Roland and Kleinschmit, 2005). While a large number of zeolite structures are known, only a few are currently applied as catalysts. This includes faujasite, mordenite, beta, ZSM-5, ferrierite and ZSM-22 (Lercher and Jentys, 2011). However, the application of zeolites as catalysts accounts for an estimated 27 % of the world zeolite market on a value basis. In chemical and petrochemical industries some examples of zeolite-catalysed processes that are currently in operation include hydroxylation, alkylation, oximation, epoxidation, methanol-to-gasoline, fluid catalytic cracking (Yilmaz and Muller, 2009; Millini, 2011). There are many emerging applications of zeolites in a series of fields linked to cleaner energy technologies and energy savings (Gilson et al., 2011). Fluid catalytic cracking (FCC) catalysts constitute more than 95 % of zeolite catalyst consumption, mainly Y and ZSM-5 zeolites (Hudec, 2011).

2.4. Zeolite ZSM-5

ZSM-5 zeolite is composed of a three-dimensional medium pore structure (openings of 5-5.5 Å) with high silica content, high temperature stability and strong acidity making it a well-known and an established catalyst for several petroleum derived chemical processes such as cracking, aromatic alkylation and acylation, disproportionation, methanol to gasoline, isomerisation, etc. (Ohrman, 2005; Yilmaz and Muller, 2009; Millini, 2011; Yilmaz and Muller, 2009).

2.4.1. Fundamentals

The structure of ZSM-5 zeolite is built up from the 5-5-1 secondary building units (SBUs), SBUs are of pentasil structures which join to form chains. These chains link together to form sheets and the ZSM-5 zeolite structure is obtained when these sheets link across a centre of inversion, with the structure directing agent (SDA) at the channel intersections and tetrapropylammonium cation (TPA^+) is the most commonly used SDA (Figure 2.15) (Wright and Lozinska, 2011, Bonilla et al., 2004).

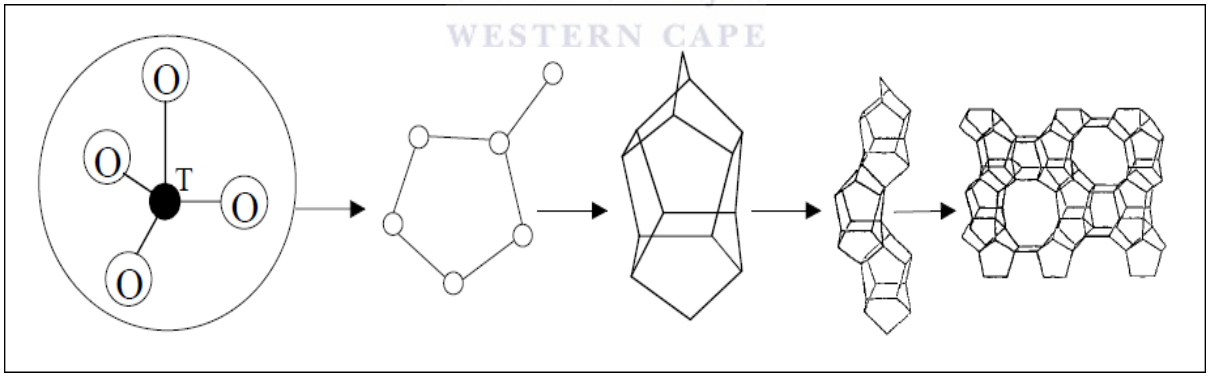

Figure 2.15: Three dimensional structure of ZSM-5 zeolite (Devadas, 2006).

ZSM-5 zeolite is a member of the MFI structure type with 10 membered ring pore windows and a Si/Al ratio that ranges between 10 and several thousand (Jacob, 1998). It has two pore systems: straight channels of elliptical shape (5.3 Å x 5.6 Å) in the b-direction and sinusoidal channels of almost circular cross-section (5.1 Å x 5.5 Å) in the a-direction. MFI crystals usually have a coffin shape, which is a result of a fast growth in a c-direction (Figure 2.16)

(Ohrman, 2005). However, Petrik et al., (1995) reported that the shape of ZSM-5 zeolite crystals can easily be altered by changing some synthesis parameters such as the template type, sodium or potassium content, water content and aluminium source.

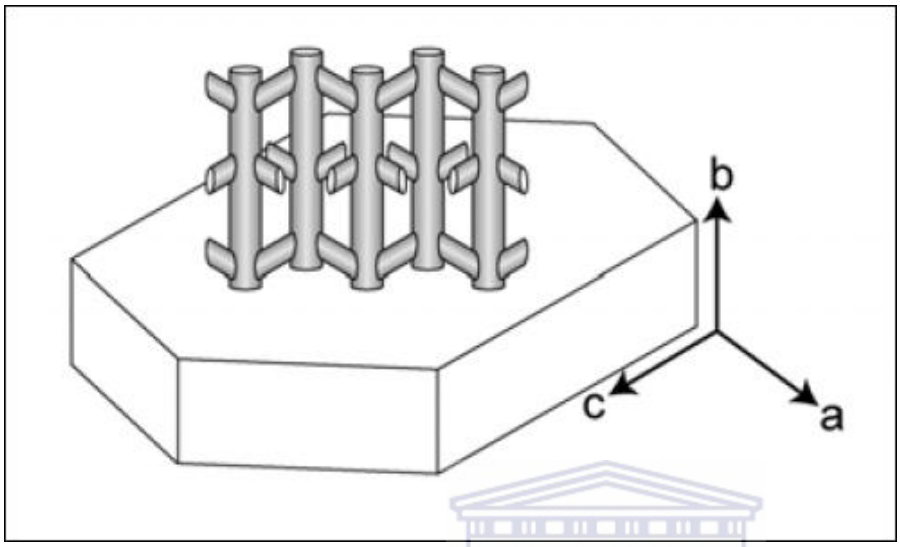

Figure 2.16: Illustration of the channel system of MFI (Ohrman, 2005).

The three dimensional pore structure together with the high thermal stability and high acid strength that derive from the Si/Al ratio makes ZSM-5 zeolite a highly active and shape selective catalyst (Wright and Lozinska, 2011). The unit cell of ZSM-5 zeolite contains 96 T-atoms with the maximum of 8 Al atoms (Si/Al≥11) and 192 O-atoms. The void volume of ZSM-5 zeolite is 0.17 mL/g (Van der Gaag, 1987).

2.4.2. Synthesis

In general, ZSM-5 zeolite is synthesized from a hydrothermal solution containing Al and Si sources and an organic structure directing agent (OSDA) also called template (Van der Gaag, 1987). Tetrapropylammonium cation (TPA^+) is a common template used in the synthesis of ZSM-5 zeolite (Narayanan et al., 1995; Bonilla et al., 2004). Table 2.10 lists other organic molecules that induce the ZSM-5 formation.

Table 2.10: Organic structure directing agents reported for the synthesis of ZSM-5 zeolite (Van der Gaag, 1987).

Tetrapropylammonium halide	Methylquinuclidine
Tetraethylammonium halide	Morpholine
Tripropylamine	Ethylenediamine
Dipropylamine	Diethylenetetraamine
Propylamine	Triethylenetriamine
1,6-diaminohexane	Dipropylenetriamine
1,6-hexanediol	Dihexamethylenetriamine
1,5-diaminopentane	Di-n-butylamine
Ethanolamine	Ethanol
Propanolamine	Ethanol+ammonia
Pentaerythritol	Glycerol

The template promotes the formation of the desired building blocks in the hydrothermal gel and acts as a hydrophobic pore filler to prevent dissolution and recrystallization of already formed crystals. The size of templates that give pure ZSM-5 zeolite increase as follows: alcohols < amines < tetrapropylammonium halide (Van der Gaag, 1987). However, it was reported that ZSM-5 zeolite could be synthesized without any organic structure directing agent (Narayanan et al., 1995). Other parameters that influence the crystallization as well as the morphology of ZSM-5 zeolite are Al content, template/silica ratio, water content, nature of the cations present, alkalinity, degree of polymerization of the silica and the hydrothermal synthesis conditions (Petrik et al., 1995; Petrik, 2009; Bleken et al., 2012; Wang et al., 2008).

It has been reported that ZSM-5 zeolite can be synthesized from fly ash. However, a source of silica needs to be added in order adjust the Si/Al ratio (Chareonpanich et al., 2004; Kalyankar et al., 2011; Reanvattana, 2005). Chareonpanich et al., (2004) synthesised ZSM-5 zeolite from Thailand lignite fly ash (with 39.6 % of SiO_2 and 24.3 % of Al_2O_3) with TPABr as organic structure directing agent. Different amounts of SiO_2 extracted from rice husk ash

were added to adjust the Si/Al molar ratio to 20, 40, 60, 80, 100 or 200. The prepared aluminosilicate gels underwent hydrothermal synthesis at 150, 180 or 210 °C for 4 h. It was reported that 43 % phase purity of ZSM-5 zeolite was synthesised and 20 % of Al_2O_3 in fly ash was not involved in the synthesis of ZSM-5 zeolite. However, the synthesis of high purity ZSM-5 zeolite from fly ash without addition of a source of silica has not been reported yet. Hence, that is one of the objectives this study is aiming to meet.

2.4.3. Applications

ZSM-5 zeolite is one of the most used zeolites as acid heterogeneous catalyst in industrial processes (Lercher and Jentys, 2011). ZSM-5 zeolite is the main catalytic route to increase the octane number of gasoline in a fluid catalytic cracking (FCC) unit and it has been adopted in a large number of commercial units since the initial reports in 1983 (Triantafillidis et al., 1999). ZSM-5 zeolite has been used to convert alcohols into hydrocarbons (Bleken et al., 2012; Ramasamy and Wang, 2013, Varvarin et al., 2013). In South Africa, the Methanol-to-Olefins (MTO) conversion process can be exploited at an industrial scale and adds more value to coal and coal fly ash, as methanol can be synthesized from coal (Van Dijk et al., 1983) and ZSM-5 zeolite from coal fly ash (Chareonpanich et al., 2004). ZSM-5 zeolite has also been used to convert arylvinylketones to indanones via Nazarov cyclization (Figure 2.17) (Sani-Souna-Sido et al., 2008). Indanones are important bioactive molecules that exhibit a biological activity against cancer cells and Alzheimer's disease (Oliverio et al., 2014).

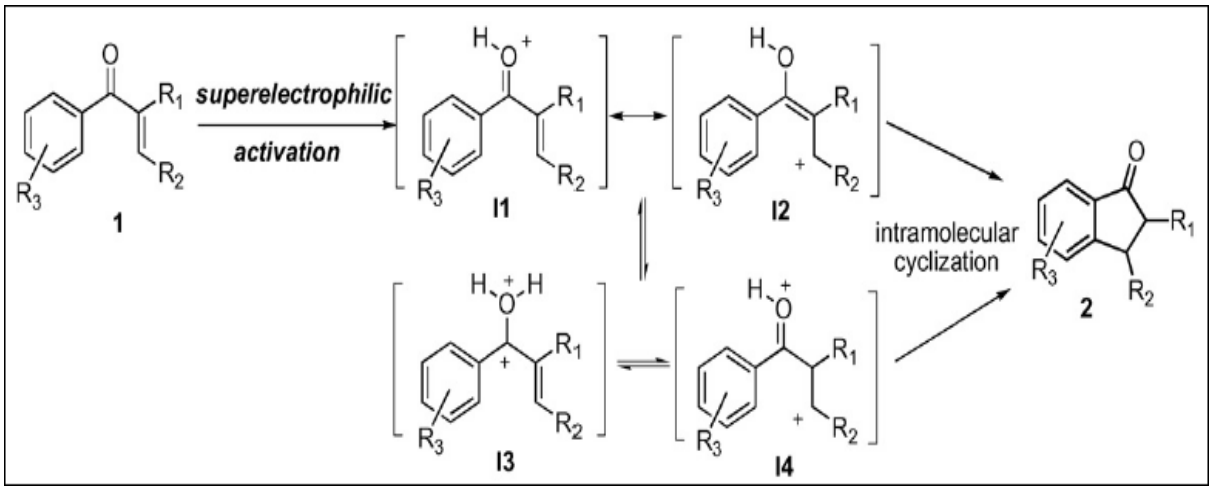

Figure 2.17: Intramolecular cyclisation of arylvinylketones via Nazarov reaction (Sani-Souna-Sido et al., 2008).

Boltz et al., (2014) reported that aromatic chlorination could be performed over ZSM-5 zeolite materials with different morphologies. The use of ZSM-5 zeolite as heterogeneous catalyst has been limited by the formation of coke, which causes its deactivation. Hence, it is necessary to tune it by some post-synthesis modifications such as loading metals to inhibit the deposition of carbon (Inaba et al., 2006) and creating a hierarchical pore system to optimize the accessibility of large molecules and improve the ZSM-5 zeolite efficiency (Louis et al., 2010). Moreover, metals have been loaded into ZSM-5 zeolite for specific applications such as NO_x decomposition (Ohman et al., 2002; Pieterse et al., 2007). Petrik et al., (1995) reported that the catalytic activity of ZSM-5 zeolite could be affected by the change of their crystal morphology.

2.5. Characterisation of fly ash, zeolites and catalytic products

This section presents some literature details of different techniques that were used to characterise the as-received fly ash, fly ash extracts, synthesis zeolites as well as the gas and liquid products used or to be obtained in this study. This is for a better understanding of the sampling requirements and operation of the equipment.

2.5.1. X-ray diffraction spectroscopy

X-ray diffraction (XRD) is an important tool in the identification and characterisation of zeolites at different stages (synthesis, post-synthesis modification and catalysis) (Cundy and Cox, 2005). The crystal structure is described by associating lattice points with a group of atoms within the unit cell known as the basis. The lattice points of a given crystal structure define an infinite number of families of parallel planes. Each family is defined by the set of Miller indices hkl. If X-rays of wavelength, λ, strike those planes at an angle, Θ (Figure 2.19), constructive interference will occur when the path difference between the diffracted (or reflected) waves from each plane is equal to an integral number, n, of wave length (Equation2.4) (Byrappa and Yoshimura, 2001).

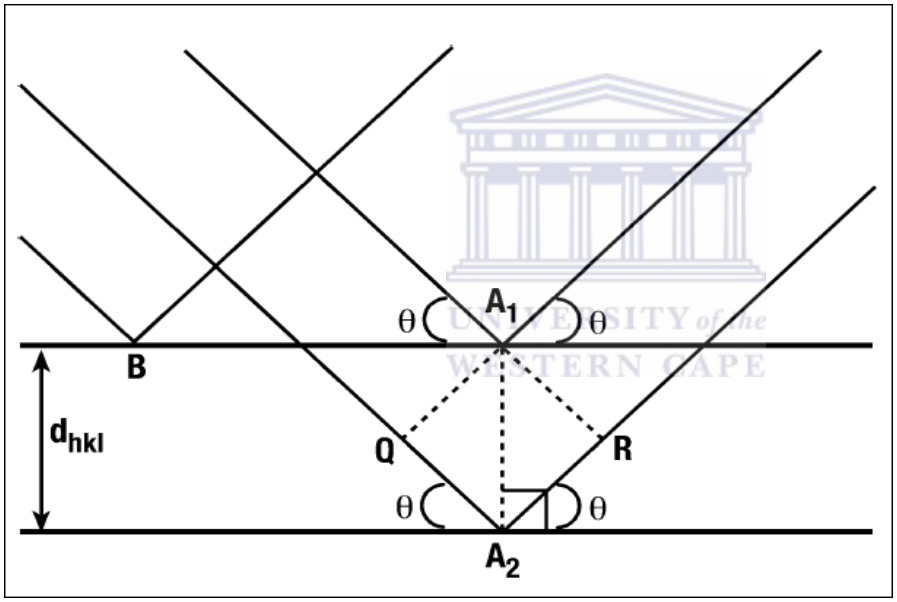

Figure 2.18: Illustration of diffraction from two parallel planes (Byrappa and Yoshimura, 2001).

$n\lambda = 2d\sin\theta$ **(Equation 2.4)**

The diffraction of X-rays occurs within a given crystal from the hkl families of planes. Zeolite samples can be prepared mainly in the form of polycrystalline powders, with a crystal size between 0.1 and 10 μm. In zeolite powder samples, there are millions of crystallites that are randomly oriented with respect to the beam, with a ring of diffracted intensity at an angle

2Θ. Most modern laboratory powder diffractometers use Bragg-Brentano geometry, in which the detector moves along a single dimension and records intensity for each 2Θ angle (Pecharsky, 2005). The peak widths and shapes of a powder diffraction pattern are influenced by the crystallite size, strain and instrumental broadening. The Scherrer equation relates diffraction peak width to the average crystallite dimension (Equation 2.5) (Byrappa and Yoshimura, 2001).

$$\beta_s(2\theta) = \frac{K\lambda}{T\cos\theta} \quad \textbf{(Equation 2.5)}$$

With β_s the crystallite size contribution to the integral peak width in radians, K a crystal shape constant near unity, T the average thickness of the crystal in a direction normal to the diffraction plane hkl. ZSM-5 zeolite can be identified by its characteristic XRD patterns (Figure 2.19).

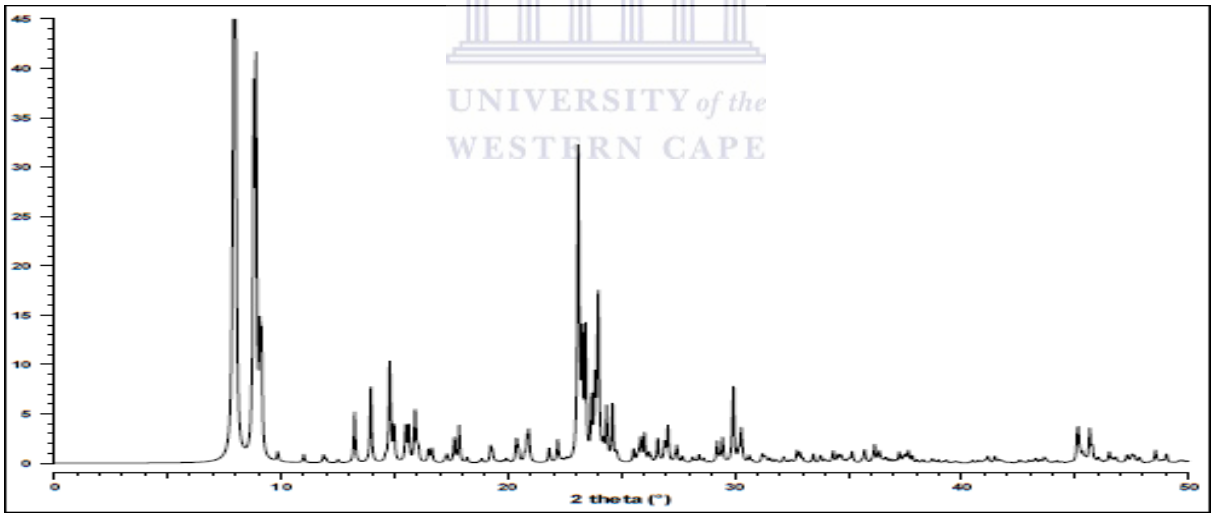

Figure 2.19: XRD patterns of calcined ZSM-5 zeolite (Treacy and Higgins, 2001).

2.5.2. Electron microscopy and imaging

Imaging techniques have been a fundamental analytical tool of solid and liquid samples for years, presenting specific aspects of a material's microstructure such as the particle shape and size, morphology, etc. (Byrappa and Yoshimura, 2001). The use of electrons as microscope illumination source was introduced by Knoll and Ruska in the early 1930s to study material

characteristics by overcoming the limitations set by the wavelength of light (~ 400 nm) that was used earlier in optical microscopy (Williams and Carter, 1996). Secondary electron imaging (SEI) is used in scanning electron microscopy (SEM) to provide very useful information about zeolite particles that can be relatively large (~ 1 µm). However, the zeolite unit cell is better characterized by transmission electron microscopy (TEM) (Terasaki and Ohuna, 1995).

2.5.2.1. Scanning electron microscopy

Secondary electrons (SEs) are low energy electrons that are generated from the top few nanometers of the material's surface after interaction with the incident electron beam. They are generally emitted in scanning electron microscopy (SEM), producing images that have a three-dimensional nature and giving crystallite topography such as overall crystal size/shape, general surface roughness, etc. (Terasaki and Ohuna, 1995). Zeolites are not electrically conductive in SEM. The sample needs to be in contact with a conductive surface such as the SEM stub, carbon paint or carbon tape for a better image and highly extensive sample preparation is generally not required. The characterization of zeolite crystals requires low accelerating voltages (<~ 5 kV) that minimize the creation of backscattered electrons (BEs) (Byrappa and Yoshimura, 2001).

2.5.2.2. Transmission electron microscopy

Unlike for SEM, zeolite crystals are too agglomerated to directly image in the TEM without an extensive sample preparation. The zeolite powder may need to be transferred into a non-interacting solvent such as isopropyl alcohol, ethanol, etc. to create a dilute suspension, which is dropwise deposited on a standard holey carbon-coated TEM grid (Csencsits and Gronsky, 1988). The holey carbon gives enough electrical conductivity to prevent the specimen from building up electrical charge during the TEM characterization (Goodhew, 1972). High resolution TEM (HRTEM) imaging shows critical pore structures, lattice planes and atomic arrangement within materials. However, it has to be conducted with extreme caution to prevent electron beams from damaging the zeolite microstructure. In general, the electron beam damage occurs more rapidly in zeolites that have higher water content, low silica content or low levels of rare earth additions (Byrappa and Yoshimura, 2001).

2.5.3. Infrared spectroscopy

Infrared spectroscopy is one of the most widely used techniques in zeolites chemistry and catalysis. There are several sampling techniques in IR spectroscopy: KBr water technique, attenuation total reflection (ATR), diffuse reflectance, photo-acoustic Fourier transformed infrared (FTIR) and time-resolved FTIR. It is divided into three categories depending on the instrumental designed:

- Near-IR (>3000 cm^{-1}): gives information on adsorbed species such as water, organic molecules and small gas molecules, etc. in zeolite cavities or channels.
- Mid-IR (4000 – 400 cm^{-1}): provides information on surface OH groups, adsorbed molecules and framework vibrations.
- Far-IR (< 300 cm^{-1}): gives information on framework oxygen atoms and charge-balancing cations in zeolite structures (Byrappa and Yoshimura, 2001).

The framework vibrations of zeolites range between 1400 and 300 cm^{-1} (Flanigen, 1976). The zeolitic vibrational spectra are usually complex due to the influence of other factors such as the existence and nature of charge-balancing cations, the degree of hydration and the Si/Al ratio. The increase in Al in the framework leads to the shifting of some bands towards lower wavenumbers due to the longer Al-O (1.75 Å) bond compared to Si-O bond (1.62 Å) (Byrappa and Yoshimura, 2001). The vibrations of TO_4 tetrahedra are divided into internal and external vibrations; which represent the vibrations in the tetrahedral building units and between them (double rings and pore openings) (Auerbach et al., 2003). Table 2.11 gives IR data of zeolites containing 5-membered rings.

Table 2.11: IR data of zeolites containing 5-membered rings (Auerbach et al., 2003).

Zeolite types	Asymmetrical stretch		Symmetrical stretch		Double ring	T-O bend
	External	Internal	External	Internal		
Silicate	1225 (sh)	1093 (s)	790 (w)	-	550 (m)	450 (s)
ZSM-5	1225 (sh)	1093 (s)	790 (w)	-	550 (m)	450 (s)
Boralite	1228 (sh)	1096 (s)	800 (w)	-	550 (m)	450 (s)
ZSM-11	1225 (sh)	1093 (s)	790 (w)	-	550 (m)	450 (s)
Mordernite	1223 (sh)	1045 (s)	800 (w)	720 (w)	580, 560 (w)	450 (s)
Ferrierite	1218 (sh)	1060 (s)	780 (w)	695 (w)	563 (w)	455 (s)
Epistilbite	1175 (sh)	1050 (s)	795 (w)	690 (w)	563 (w)	455 (s)
Dachiardite	1210 (sh)	1050 (s)	775 (w)	670 (w)	558 (w)	440 (s)
Bikitaite	1105 (sh)	968 (s)	782 (w)	680 (w)	-	460 (s)
ZSM-39	-	1090 (s)	790 (w)	-	-	460 (s)
ZSM-34	-	1060 (s)	785 (w)	-	635, 580, 550 (w)	465 (s)
ZSM-35	1232 (sh)	1070 (s)	790 (w)	-	590 (m)	460 (s)

Sh=shoulder, s=strong, w=weak.

2.5.4. X-ray fluorescence spectroscopy

The X-ray fluorescence spectroscopy (XRF) is an analytical technique giving the elemental composition of the matter. The interaction of an X-ray with the electrons of the sample atoms creates fluorescent spectra that identify and quantify the bulk elemental composition of solid samples (Bekkum et al., 1991). It is useful for both qualitative and quantitative elemental analysis (Somerset et al., 2004) and is widely used for the determination of both major and trace elements in a wide variety of geological materials (Potts and Webb, 1992). The main

principle of X-ray fluorescence (XRF) spectroscopy is that when atoms are irradiated with X-rays, they emit secondary X-rays (fluorescent radiation). The wavelength and energy of the fluorescent radiation is specific for each element and their concentration can be calculated using the intensity of their fluorescent radiation. There are two methods of the sample preparation namely pressed and loose powder methods. For powders that are difficult to press into pellets, a mixing with a binder is required to avoid fine powder particles to fall off or scatter from the pellet surface. The loose powder method requires the reproducibility of the sample preparation to be checked. Moreover, a special attention needs to be paid because the sensitivity of some light elements decreases during the measurement and can affect the accuracy of the machine. A blank measurement also needs to be performed in order to monitor any impurity in the sample (Takahashi, 2015).

2.5.5. Inductively coupled plasma-atomic emission spectroscopy

Inductively coupled plasma-atomic emission spectroscopy (ICP-AES), also referred to as inductively coupled plasma-optical emission spectroscopy (ICP-OES) is a powerful tool for the quantification of metals in a variety of different sample matrices (Hou and Jones, 2000). Liquid samples (acidified water or solids digested into aqueous forms) are analysed by ICP-AES. The sample solution is acidified up to 2-3 % in HNO_3 to prevent adsorption of metals onto polypropylene sample bottle or onto instrument tubing or glassware prior to introduction into the plasma. Nebulizers are used to convert the liquid sample into an aerosol. Only very fine droplets (~ 8 µm) are suitable for injection into the plasma. Larger droplets are removed from the aerosol in the spray chamber (Hou and Jones, 2000). High temperatures (6727 °C to 9727 °C) are required to produce a strong atomic emission from all chemical elements. These temperatures are obtained when inert-gas plasma is generated. The aerosol droplets are converted into salt particles in the hot area of the plasma. These salt particles are split into individual molecules that subsequently fall apart to atoms and ions. The energy that is transferred to the atoms and ions promotes their excitation. When they return to their ground state or to lower excitation states they emit electromagnetic radiation in the ultra-violet/visible range of the spectrum. Each excited element emits specific wavelengths and simultaneous detection makes it possible to measure all elements at the same time (Kollander, 2011). Every step in the ICP-OES analysis can contain an error that may affect the accuracy and reproducibility of the results. The sample matrix may also cause errors

during the preparation step or interferences during measurements. However, the sample preparation is the main source of errors during measurement. The sample preparation includes dilution, acid digestion, extraction, etc. depending on the nature of the sample. Moreover, the quality of the results can be determined by the use of control samples with known compositions (Welna et al., 2011).

2.5.6. N_2 Brunauer-Emmett-Teller

The surface area is a crucial parameter for optimising the use of porous materials in numerous applications. The N_2 adsorption and Brunauer-Emmett-Teller (BET) method is widely used for the evaluation of surface areas of micro- and mesoporous adsorbents (Cejka et al., 2007). The gas adsorption allows probing of the entire surface including irregularities and pore interiors. The International Union of Pure and Applied Chemistry (IUPAC) proposed the classification of pores by their internal pore width:

- Micropore: pore of internal width less than 2 nm;
- Mesopore: pore of internal width between 2 and 50 nm;
- Macropore: pore of internal width greater than 50 nm (Lowell et al., 2004).

Macropores can be considered as nearly flat surfaces; hence their sorption behaviour is distinct from that of micro- and mesopores. The interactions between fluid molecules and the pore walls dominate the sorption behaviour in the micropores. In mesopores, the sorption behaviour does not depend only on the fluid-wall attractions, but also on the attractive interaction between fluid molecules (Lowell et al., 2004). Langmuir, (1918) described the kinetic behaviour of the adsorption process. He postulated that at equilibrium, the rate of adsorption and the rate of desorption were equal, with heat of adsorption being constant. There are six sorption isotherms that describe the type of pores in the adsorbent (Figure 2.20). The amount of gas adsorbed depends on the temperature and relative pressure (P/P^o) (Cejka et al., 2007):

- The type I isotherm or pseudo-“Langmuir”: the steep slope represents high uptakes at low relative pressure, which is characteristic of micropores. The plateau is due to essentially zero external area.
- Type II isotherm: the rounded knee indicates the location of monolayer formation. The low slope in the middle of the isotherm indicates the formation the first few

multilayers. The absence of the hysteresis indicates adsorption-desorption from a non-porous surface.

- Type III isotherm: the absence of the knee indicates that the attractive adsorbate-adsorbent interactions are relatively weak.
- Type IV: the most characteristic feature of this isotherm is the presence of hysteresis loop, which is associated with the occurrence of pore condensation and is typical for mesoporous materials.
- Type V isotherm: there is a presence of hysteresis. However, the absence of the knee indicates weak attractive interactions between the adsorbent and the adsorbate.
- Type VI isotherm: this is a special case, which represents stepwise multilayer adsorption on a uniform, non-porous surface (Lowell et al., 2004).

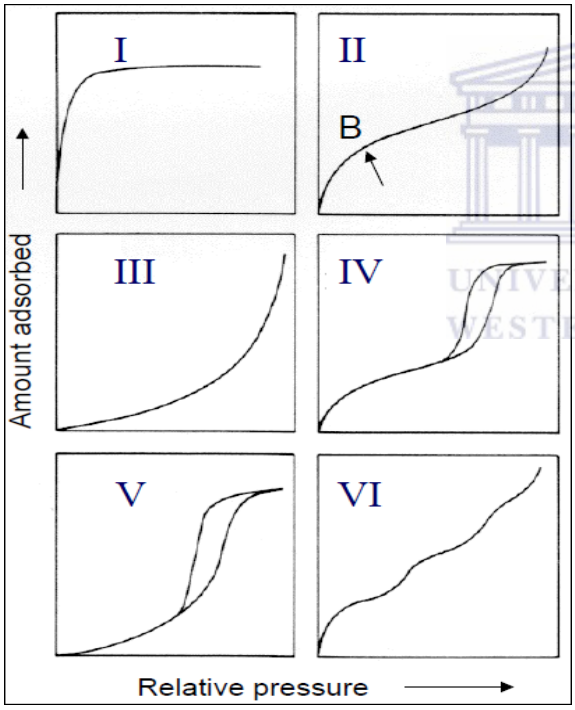

Figure 2.20: IUPAC classification of sorption isotherms (Lowell et al., 2004).

In the case of ZSM-5 zeolite, a significant surface area is insured by detemplating the zeolite and ion-exchanging it through treatment with NH_4NO_3, oxalic acid, etc., followed by calcination (Losch et al., 2016, Zhang et al., 2014). The BET surface area of ZSM-5 zeolite may vary from one sample to another one depending on the synthesis and/or the post-synthesis conditions. Bjøgen et al., (2008) synthesised H-ZSM-5 zeolite from Ludox LS,

$Al(OH)_3$ and tetrapropylammonium cation with a BET surface area of 313 m^2/g. They increased that BET surface area to 419 m^2g by treatment of the sample with 0.2 M of NaOH solution. Sang et al., (2004) varied the BET surface area from 293.6 to 312.1 m^2/g by varying the type of structure directing agent in the hydrothermal gel. Lu et al., (2003) reported that a commercial H-ZSM-5 zeolite from the catalytic factory of Nankai University had a BET surface area of 388.5 m^2/g with 303.1 m^2/g of micropore area and 85.4 m^2/g mesopores area.

2.5.7. Nuclear magnetic resonance

Nuclear magnetic resonance (NMR) is a widely applied analytical method to deliver structure data. It is complementary to infrared and chromatography methods in the case of liquid-state NMR, to X-ray diffraction and infrared in the case of solid-state NMR. This section details the liquid-state and solid-state NMR.

2.5.7.1. Liquid-state nuclear magnetic resonance

The first application of nuclear magnetic resonance spectroscopy to a biological sample was reported by Jacobson et al., (1954) on the effect of hydration of deoxyribonucleic acid. After that the field of NMR underwent a revolution, with the award of the 1991 Nobel Prize for chemistry to Richard Ernst (Bagguley, 1992). The NMR phenomenon occurs as a result of the quantum mechanical property of spin. Note that common biological nuclei such as ^{12}C or ^{16}O have a nuclear spin (I) equal to zero (0) and therefore do not give NMR spectra. Table 2.12 gives some typical nuclei of interest in NMR with their nuclear spin and NMR frequency (MHz). In a magnetic field, there are (2I+1) possible orientations given by the value of the magnetic quantum number (m_I) for a nucleus of spin I. The energies are quantized, with the two possible values of m_I ($\pm 1/2$) and the external field (Jacobsen, 2007).

Table 2.12: Magnetic properties of some NMR nuclei.

Isotope	Spin	NMR frequency at a field (T) of 2.3488
^{1}H	1/2	100.000
^{13}C	1/2	25.144
^{15}N	1/2	10.133
^{17}O	5/2	13.557
^{19}F	1/2	94.077
^{35}Cl	3/2	9.798

The NMR absorption is a consequence of transitions between the energy levels stimulated by applied radiofrequency (RF) radiation. In a RF single pulse experiment, the detected signal called free-induction decay (FID) is recorded and Fourier transformation is performed to get the NMR frequency spectrum (Figure 2.21) (Keeler, 2010).

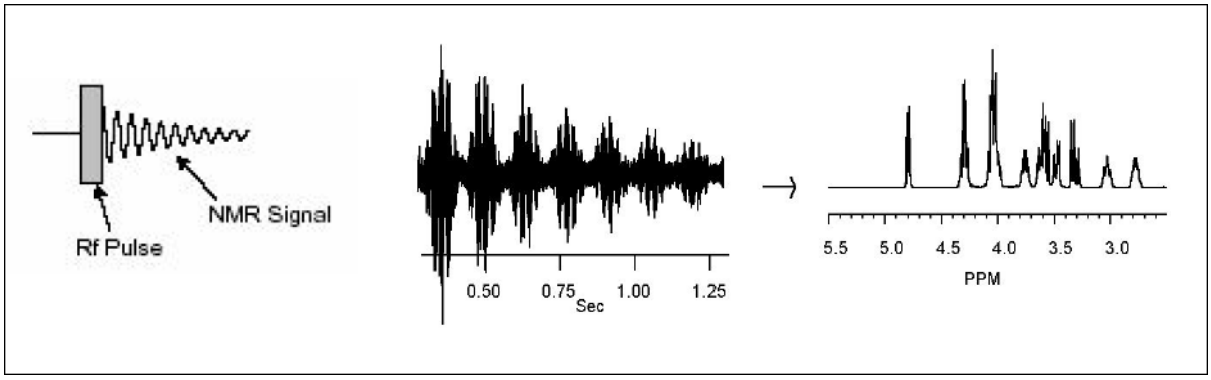

Figure 2.21: Illustration of the RF pulse followed by FID and NMR frequency spectra.

The NMR samples are prepared by dissolving an analyte in deuterium lock solvents ($CDCl_3$, C_6D_6, acetone-d_6, DMSO-d_6, CD_2Cl_2, CD_3CN, Pur-d_5, etc.). One to 20 g of the sample is generally sufficient for acquiring a NMR spectrum. A standard 5 mm NMR tube needs to be filled to a depth of 4 cm for optimum results, which represents 0.6 to 0.7 mL of deuteriated solvent (Jacobsen, 2007).

2.5.7.2. Solid-state nuclear magnetic resonance

The mechanisms responsible for the broadening of solid-state NMR signals and their characteristic line shape function are based on the dominant nuclear interactions that occur in the solids and are described by the total Hamiltonian equation (Equation 2.6).

$$H = H_{II} + H_{IS} + H_{csa} + H_q \quad \textbf{(Equation 2.6)}$$

With H_{II}, H_{IS}, H_{csa} and H_q, denoting the homonuclear and heteronuclear dipole-dipole interaction, the anisotropic chemical shielding and quadrupolar interaction, respectively (Harris, 1986). Solid-state NMR techniques are used for the characterization of zeolites because of their high sensitivity for chemical bonds in resonating nuclei, such as framework atoms, extra-framework species, surface sites and adsorbate complexes in zeolites. Many atoms found in zeolites have isotopes (^{1}H, ^{27}Al, ^{29}Si, ^{31}P, etc.) with a nuclear spin that renders them NMR-active (Byrappa and Yoshimura, 2001). There are many NMR techniques for characterization of solid powdered samples and the magic angle spinning – nuclear magnetic resonance (MAS-NMR) is the most important technique of high resolution solid-state NMR spectroscopy for zeolite investigation (Byrappa and Yoshimura, 2001). MAS-NMR is the standard technique for improving the resolution in solid-state NMR spectroscopy, where the sample is rapidly rotated around an axis inclined (54.736°) with respect to the external magnetic field (Figure 2.22). The MAS rate increases as the rotor diameter decreases (Ashbrook et al., 2014).

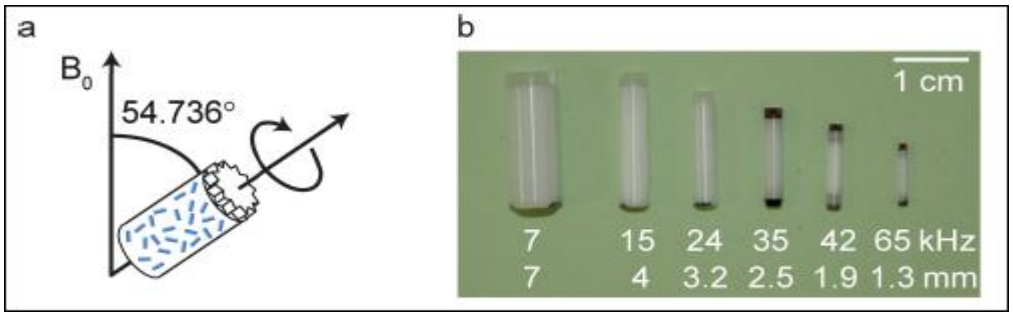

Figure 2.22: a) Scheme of the MAS-NMR technique based on the rapid rotation of sample around an axis (54.736°), b) rotors with various outer diameters and their maximum MAS (Ashbrook et al., 2014).

a. ^{29}Si MAS NMR spectroscopy

The basic units of zeolite framework are TO_4 (Q^4), with silicon atoms at the central T-positions. When aluminium atoms are incorporated in the second coordination sphere of the silicon atoms at T-positions, the SiO_4 (Q^4) are characterized by up to five different environments denoted as Si(nAl) (with n=0, 1, 2, 3 and 4), which cause the chemical shifts of Si(nAl) (Figure 2.23). Terminal hydroxyl groups bound to silicon atoms cause Q^3 (Si(3Si,1OH)) and Q^2 (Si(2Si,2OH)) signals depending on the number of OH groups bound to the silicon atom at T-position (Byrappa and Yoshimura, 2001).

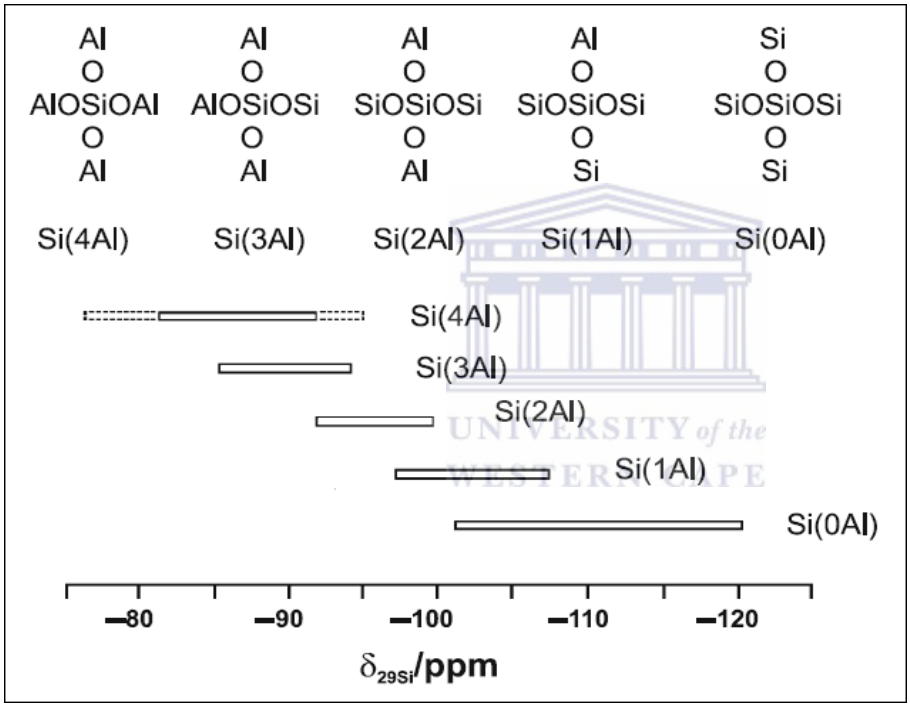

Figure 2.23: ^{29}Si chemical shift values of Si(nAl) units in zeolites (Byrappa and Yoshimura, 2001).

The framework n_{si}/n_{Al} ratio of zeolites can be calculated as follows:

$$n_{Si}/n_{Al} = \sum_{n=0}^{4} I_{Si(nAl)} / \sum_{n=0}^{4} 0.25 * n * I_{Si(nAl)} \quad \textbf{(Equation 2.7)}$$

With $I_{Si(nAl)}$, the intensity of the Si(nAl) signal (Byrappa and Yoshimura, 2001).

b. ^{27}Al NMR spectroscopy

According to Loewenstein's rule, the formation of Al-O-Al bondings in the zeolite framework is forbidden (Zhao et al., 1997); therefore, exclusively Al(4Si) units exist and the ^{27}Al NMR spectra of tetrahedrally coordinated framework aluminium (Al^{VI}) in zeolites consist of a single signal in the chemical shift range of 55-70 ppm. Extra-framework aluminium species in hydrated zeolites are octahedrally coordinated (Al^{VI}) causing a narrow signal at 0 ppm. If the extra-framework aluminium species are in the form of polymeric aluminium oxide in zeolite cages or pores, quadrupolar line broadening may occur owing to distortions of the octahedral symmetry of the AlO_6 units and broad ^{27}Al MAS NMR signals at 30-50 ppm may be the results of aluminium species in a disturbed tetrahedral coordination ($Al^{IV'}$) or penta-coordinated species (Byrappa and Yoshimura, 2001). When the zeolite undergoes calcination followed by rehydration and dealumination through steaming, signals appeared at 60 ppm and 0 ppm due to tetrahedrally coordinated framework species (Al^{IV}) and octahedrally coordinated framework species (Al^{VI}) (Jiao et al., 2006).

c. Characterization of acid sites and base sites

Solid-state NMR spectroscopy is a suitable method for characterizing Brønsted acid sites of zeolites (Hunger, 1997). Their behaviour in heterogeneously catalysed reactions depends on the nature, chemical properties and accessibility of their surface sites, such as OH groups acting as Brønsted acid sites (Byrappa and Yoshimura, 2001). Pfiefer et al., (1991) described the use of ^{1}H NMR for determining the number, strength and accessibility of acidic protons in zeolites. Brønsted acid sites in dehydrated zeolites are caused by bridging OH groups (SiOHAl) formed at Si-O-Al bridges in the local structure of negatively charged framework aluminium atoms. The aptitude to protonate strongly basic probe molecules or to form hydrogen bonds to these molecules is used to distinguish between acidic and non-acidic surface OH groups (Byrappa and Yoshimura, 2001). The H/D exchange has also been used for determining the strength of Brønsted acid sites (Farneth and Gorte, 1995; Huang et al., 2007; Boltz et al., 2012). Louis et al., (2004) determined the Brønsted acid density of zeolites, types MOR, MFI, SAPO, EMT, BEA and HUSY by exchanging H-zeolite to D-zeolite using D_2O and back exchanging D-zeolite to H-zeolite using H_2O. The obtained partially exchanged water H_xOD_y composed by H_2O, HDO and D_2O was used to determine the amount of protonated and deuterated acids using NMR technique and calculate the acid

site density. The detailed ^{1}H NMR shift values of unperturbed SiOHAl groups in large units such as of zeolites, types X and Y or of H-ZSM-5 and H-mordenite depends on the framework n_{Si}/n_{Al} ratio and cover a range of chemical shifts from 0 to 16 ppm (Hunger, 1997). Unlike Brønsted acid sites, Lewis acid sites and base sites in zeolites are difficult to investigate in a direct manner such as by solid-state ^{27}Al or ^{17}O NMR spectroscopy. Probe molecules are used for determining Lewis acid sites and base sites. However, there is no correlation between the NMR shifts of probe molecules coordinated at Lewis acid sites and the strength of these surface sites and some of the probe molecules are used for evaluating both Brønsted and Lewis acid sites (Byrappa and Yoshimura, 2001).

2.5.8. Gas chromatography

Gas chromatography (GC) – specifically gas-liquid chromatography – is a powerful and widely used tool for the separation, identification and quantitation of volatilised components in a complex mixture. It has developed since its introduction by James and co-workers in 1952 (Grob and Barry, 2004). The GC is mainly composed of a sample injection port, column and detector. A sample is vaporised and injected onto the head of a thermally controlled column. The sample is transported through the column by the flow of inert gaseous mobile phase (often helium, nitrogen, argon or carbon dioxide). The column contains a liquid stationary phase that is adsorbed onto the surface of an inert solid. The sample components interact with the stationary phase and their retention time strongly depends on their respective polarity and boiling point (Jennings, 2012).

2.6. Chapter summary

In summary, this chapter shows that South African economy largely depends on the production of electricity via combustion of coal, which generates a large amount of coal fly ash. Fly ash is considered by many as a waste causing water and air contamination due to its alkalinity and the presence of toxic elements. Only a portion of South African fly ash has been used in the construction industry and the rest is being dumped in the field causing several environmental problems. Moreover, more research related to the reuse of coal fly ash such as treatment of acid mine drainage and synthesis of geopolymers and zeolites is emerging. The chronological discovery of zeolites is highlighted in this chapter. Zeolites can be synthesised using different sources of silicon and aluminium. Several grades of low and

intermediate silica zeolites such as zeolites A, Y, sodalite or cancrinite have been synthesised from coal fly ash because of high silico and aluminium content; with some zeolites such as A and Y zeolites having promising industrial applications. However, the use of fly ash as feedstock in the synthesis of a high silica zeolite such as ZSM-5 requires the addition of extra silica and South African fly ash has not yet been used as feedstock in the synthesis of ZSM-5. This could be due to its low Si/Al ratio of about 2, while high silica zeolites require the Si/Al ratio to be higher than 10 in the hydrothermal gel. Yet the final products still contained some unreacted fly ash mineral phases. The synthesis of ZSM-5 zeolite from coal fly ash without an additional silica source has not yet been reported. On the other hand, the synthesis of ZSM-5 zeolite also usually requires the use of organic structure directing agents (OSDAs) with tetrapropylammonium cation (TPA^+) being the most used. Several other OSDAs such as propylamine; 1,6-diaminohexane; 1,6-hexanediol; 1,5-diaminopentane; ethanolamine; propanolamine; etc. that have been used in the synthesis of ZSM-5 zeolite. However, the literature only reported the use of TPA^+ in the synthesis of ZSM-5 from fly ash. Therefore, an important number of studies can still be carried out in the conversion of South African coal fly ash into ZSM-5 zeolite, with the synthesis fly ash-based ZSM-5 zeolite without an addition of extra silica source being the most challenging. This is motivated by the fact that ZSM-5 has many applications in the catalytic industry. On the other hand, studies have been carried out in the recovery of aluminium and silicon from fly ash, which this current study is aiming to exploit in the synthesis of high purity ZSM-5 zeolite from South African fly ash without an additional silica source. This chapter also highlights different techniques used to characterised fly ash and zeolites.

This chapter helps to find gaps in the synthesis of ZSM-5 from South African coal fly ash and its applications. Three OSDAs namely tetrapropylammonium bromide; 1,6-hexanediamine and 1-propylamine will be used to direct the formation of the ZSM-5 structure in order to investigate the substitution of tetrapropylammonium bromide with cheap OSDAs, hence promoting a cheap way of synthesising high purity ZSM-5 zeolite from South African coal fly ash. ZSM-5 will also be synthesised from coal fly ash extract without the addition of extra silica or alumina source.

CHAPTER 3: EXPERIMENTAL AND ANALYTICAL TECHNIQUES

3.1. Introduction

This chapter details the materials and chemicals used in this study. It also highlights different experimental procedures used to achieve the objectives of this project. The characterisation techniques are also presented in this chapter. The experimental approach overview that is presented in Figure 3.1 summarises the research approach that was used to address research questions of the study as set out in Chapter 1.

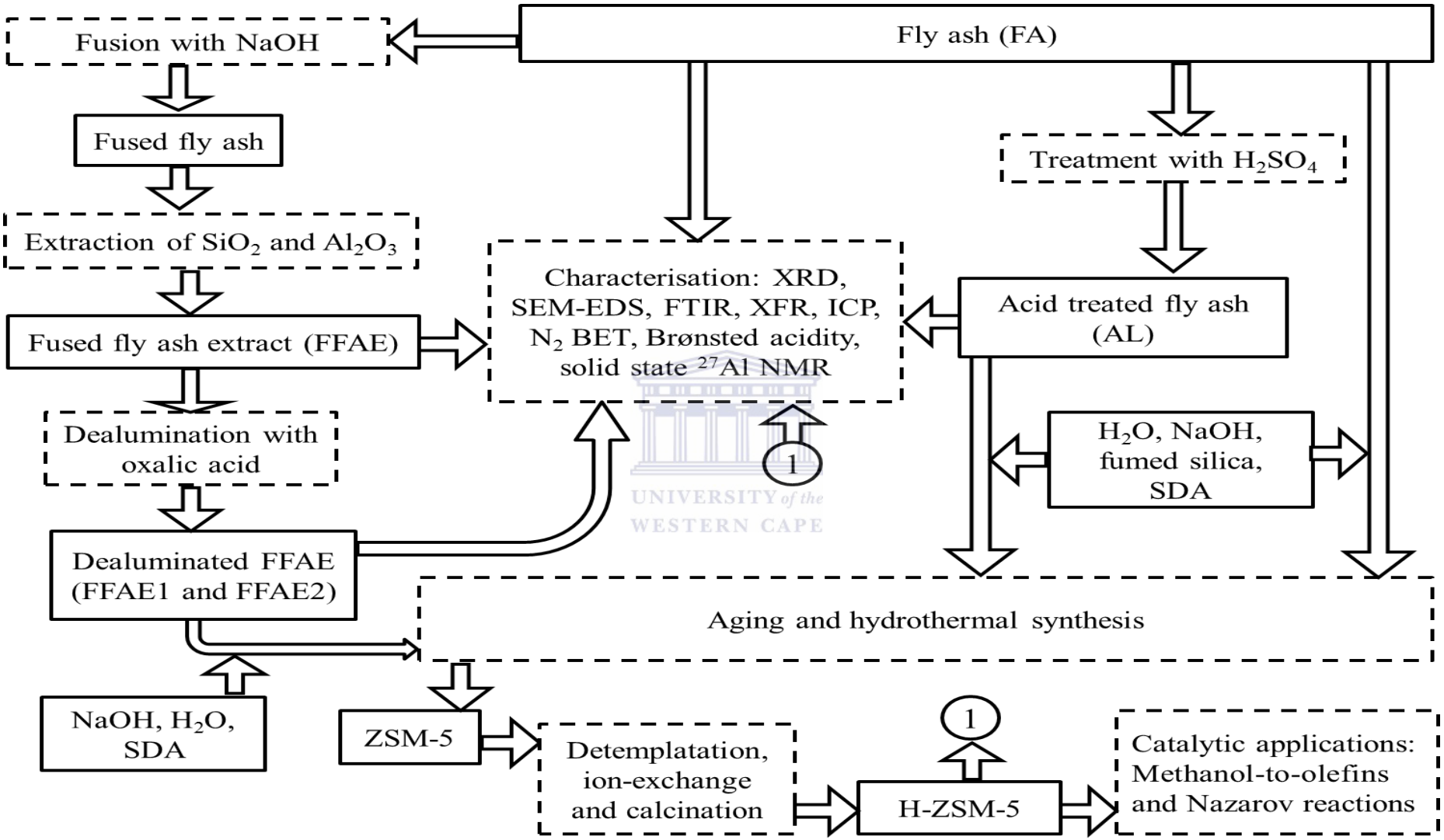

Figure 3.1: Experimental approach (SDA = structure directing agent).

3.2. Materials and chemicals

This section presents the sampling and storage of the raw material (coal fly ash) used as precursor of ZSM-5 zeolite as well as the list of chemicals and equipment used in this study.

3.2.1. Sampling and storage of coal fly ash

The coal fly ash used in this study was collected from ash hoppers at Arnot coal-fired power plant in the Province of Mpumalanga (South Africa) (Figure 3.2).

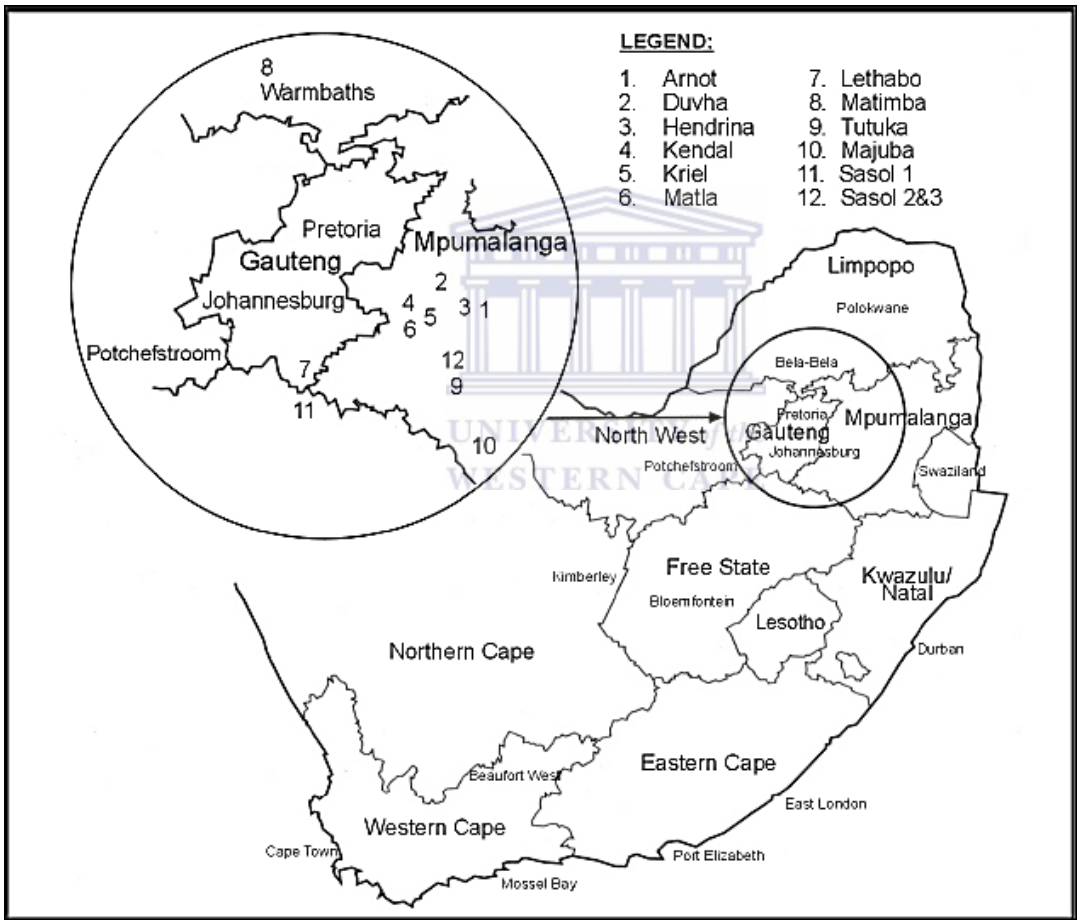

Figure 3.2: Location of coal-fired thermal power plants in South Africa (Kruger, 2003).

The coal fly ash sample was kept in a sealed plastic bag and stored in a dark place to prevent any alteration of its composition, which could affect the synthesis conditions of the fly ash-based zeolites.

3.2.2. Chemicals

The list of chemicals used in this study is presented in Table 3.1.

Table 3.1: List of chemicals used in this study.

Chemical	Source	Purity
Sulphuric acid (H_2SO_4)	Merck Chemicals	95-99 %
Sodium hydroxide (NaOH)	Kimix Chemicals	97 %
Fumed silica	Sigma-Aldrich	99.8 %
Tetrapropylammonium bromide	Sigma-Aldrich	98 %
1,6-hexanediamine	Kimix Chemicals	99.5 %
1-propylamine	Merck Chemicals	99 %
Ammonium nitrate (NH_4NO_3)	Sigma-Aldrich	≥98 %
Oxalic acid	Kimix Chemicals	≥99 %
1-phenyl-1-butanone	Sigma-Aldrich	98 %
Morpholine	Merck Chemicals	≥99.5 %
Formaldehyde	Avocado	37 %
Glacial acetic acid	Sigma-Aldrich	≥99.85 %
Sodium bicarbonate ($NaHCO_3$)	Sigma-Aldrich	≥99.7 %
Ethyl acetate	Sigma-Aldrich	99.8 %
Hydrochloric acid	Merck Chemicals	37 %
Sodium chloride	Sigma-Aldrich	≥99 %
Anhydrous magnesium sulphate ($MgSO_4$)	Sigma-Aldrich	≥97 %
Chloroform	Sigma-Aldrich	99.9 %
Chloroform-d	Sigma-Aldrich	100 %, 99.96 atom % D
Cyclohexane	Sigma-Aldrich	99.5 %
Hexamethylbenzene	Sigma-Aldrich	99 %
Chlorobenzene	Sigma-Aldrich	99.8 %
Dichloromethane	Sigma-Aldrich	≥99.8 %
Heavy water (D_2O)	Sigma-Aldrich	100 %, 99.99 atom % D
Trifluoroacetic anhydride	Sigma-Aldrich	≥99 %
Hydrofluoric acid	Merck Chemicals	48 %
Nitric acid	Merck Chemicals	65 %
H-ZSM-5	Zeolyst	/

3.2.3. Equipment

The list of equipment used in this study is presented in Table 3.2.

Table 3.2: List of equipment used in this study.

Equipment	Model and specifications
30 mL and 100 mL Teflon lined stainless autoclaves	Parr bomb
Laboratory oven	Scientific Series 2000 (Maximum T=250 °C)
Tube furnace	Labofurn (Maximum T=1000 °C)
Laboratory furnace	Thermo Scientific (Maximum T=1000 °C)
Hot plate	Lab Smart MS-H-Pro (Maximum T=340 °C)
Methanol-to-Olefins set up	/
H/D isotope exchange set up	/
Manual pelletizer	Dickie and Stockler

3.3. Methodology

The different methods used to synthesise ZSM-5 zeolite from South African coal fly ash as well as their catalytic testing are detailed in this section. This section also presents the equipment used during the synthesis and catalytic applications.

3.3.1. Synthesis of ZSM-5 zeolite from South African coal fly ash

ZSM-5 zeolite was synthesised from as-received coal fly ash (FA) or fly ash solid residue (AL) after acid leaching with concentrated H_2SO_4 (95-99 %) or fused fly ash solid extracts

(FFAEs) (Figure 3.1). Three types of templates were used as structure directing agents (SDA): tetrapropylammonium bromide (TPABr), 1,6-hexanediamine (HDA) or 1-propylamine (PA)

3.3.1.1. Synthesis of ZSM-5 zeolite from as-received coal fly ash (FA)

FA (0.75, 1 or 1.25 g) was used to synthesise ZSM-5 zeolite using the synthesis conditions detailed in Table 3.3. FA was mixed with a given amount of fumed silica (0.25, 0.5 or 0.75 g) in 15 or 20 mL of deionised water. Then sodium hydroxide (0.25, 0.375 or 0.5 g) was added to the mixture while stirring. Finally, TPABr (1, 1.375 or 1.5 g) was added to the mixture. After aging, the final mixture was poured in a Teflon lined stainless steel autoclave, which was put in a pre-heated oven at 120, 140 or 160 °C for 12, 24, 48 or 72 h. Thereafter, the Teflon lined stainless steel autoclave was allowed to cool down. The synthesised product was filtered, washed with deionised water and dried in an oven at 70 °C. The dried product was detemplated in a furnace at 550 °C for 3 h in air with a ramping temperature of 15 °C/min to burn off TPABr. After cooling down, the product was washed with deionised water and dried in an oven at 70 °C.

Table 3.3: Experimental conditions for the synthesis of ZSM-5 zeolite from coal fly ash.

Sample	Variable parameters		Fixed parameters
	FA (g)	Fumed silica (g)	
FA0	1.25	0.25	TPABr (1 g), NaOH (0.25 g), H_2O (15 mL), Aging
FA1	1.00	0.50	(room temperature, 2 h), hydrothermal synthesis
FA2	0.75	0.75	(160 °C, 72 h)
	NaOH (g)		
FA2	0.250		FA (0.75 g), fumed silica (0.75 g), TPABr (1 g),
FA3	0.375		H_2O (15 mL), Aging (room temperature, 2 h),
FA4	0.500		hydrothermal synthesis (160 °C, 72 h)
	TPABr (g)		
FA2	1.000		FA (0.75 g), fumed silica (0.75 g), NaOH (0.25 g),
FA5	1.375		H_2O (15 mL), Aging (room temperature, 2 h),
FA6	1.500		hydrothermal synthesis (160 °C, 72 h)
	H_2O (mL)		
FA2	15		FA (0.75 g), fumed silica (0.75 g), TPABr (1 g),
FA7	20		NaOH (0.25 g), Aging (room temperature, 2 h),
			hydrothermal synthesis (160 °C, 72 h)
	Aging		
	Temperature (°C)	Time (h)	
FA2	Room	2	FA (0.75 g), fumed silica (0.75 g), TPABr (1 g),
FA8		6	NaOH (0.25 g), hydrothermal synthesis (160 °C,
FA9		12	72 h)
FA10	60	2	
	Hydrothermal synthesis		
	Temperature (°C)	Time (h)	
FA2	160	72	FA (0.75 g), fumed silica (0.75 g), TPABr (1 g),
FA11		48	NaOH (0.25 g), Aging (room temperature, 2 h),
FA12		24	
FA13		12	
FA14	140	72	
FA15	120		

The effect of each variable parameter is discussed in Chapter 4, Section 4.3.

The influence of the structure directing agent (SDA) on the properties of ZSM-5 zeolite synthesised from South African fly ash was investigated by substituting tetrapropylammonium bromide (TPABr) by 1,6-hexanediamine (HDA) or 1-propylamine (PA) using suitable conditions that were obtained after varying all the synthesis parameters (see Table 3.3): FA (0.75 g), fumed silica (0.75 g), SDA (TPABr, HDA or PA) (1 g), NaOH (0.25 g), deionised water (20 mL), aging (room temperature, 2 h) and hydrothermal synthesis (160 °C, 72 h). The molar regime of hydrothermal gels is presented in Table 3.4. The synthesised products were filtered, washed with deionised water and dried in an oven at 70 °C. They were then detemplated at 550 °C for 3 h in air with a ramping temperature of 15 °C/min, washed with deionised water and dried in an oven at 70 °C.

Table 3.4: Code name of synthesised zeolites and their molar regime.

Code name	Molar regime
FA-TPABr	Si(4.8), Al(1.0), Na(1.5), H_2O(267.6), TPABr(0.7)
FA-HDA	Si(4.8), Al(1.0), Na(1.5), H_2O(267.6), HDA(2.1)
FA-PA	Si(4.8), Al(1.0), Na(1.5), H_2O(267.6), PA(4.1)

The detemplated products in their Na-form Na-FA-TPABr, Na-FA-HDA and Na-FA-PA were transformed to their H-form by ion-exchange with 0.5 M ammonium nitrate (NH_4NO_3) as proposed by Narayanan et al., (1995). In this case, Na-FA-TPABr, Na-FA-HDA or Na-FA-PA was ion-exchanged with 0.5 M NH_4NO_3 solution at a ratio of zeolite/NH_4NO_3 of 1:10 at 80 °C for 1 h. The mixture was filtered and the treatment was repeated 4 times with a fresh aliquot of NH_4NO_3 each time. The solid products (NH_4-FA-TPABr, NH_4-FA-HDA and NH_4-FA-PA) obtained after filtration were dried overnight at 70 °C and calcined in air at 550 °C with a ramping rate of 15 °C/min and a holding time of 3 h to drive off NH_3 and produce the H-form of the products (H-FA-TPABr, H-FA-HDA and H-FA-PA).

A post-synthesis oxalic acid treatment of H-FA-TPABr, H-FA-HDA and H-FA-PA was carried out by treatment with aqueous saturated solution of oxalic acid using the method that was used by Sazama et al., (2011). H-FA-TPABr, H-FA-HDA and H-FA-PA were treated

with an aqueous saturated solution of oxalic acid at ratio of 1:10, at 80 °C for 6 h under reflux conditions. The obtained products were washed with deionised water and calcined at 550 °C for 3 h in air in order to burn off the remaining oxalic acid. The characterisation of the oxalic acid treated products (H-FA-TPABr-OA, H-FA-HDA-OA and H-FA-PA-OA) are discussed in chapter 4, section 4.4.

3.3.1.2. Synthesis of ZSM-5 zeolite from the fly ash solid residue after acid leaching

The aim of the acid leaching of fly ash was to remove a certain amount of aluminium in order to increase the Si/Al ratio of the starting fly ash material as well as to remove other elements such as Ca, Fe, Mg from the fly ash (FA) feedstock, which might affect the synthesis of ZSM-5 zeolite and its catalytic activity. The acid leaching method adopted in this study was proposed by Lai-shi et al., (2011). FA (100 g) was mixed with 500 mL of concentrated sulphuric acid (95-99 %) in a 1000 mL round-bottom flask (Figure 3.3). The round-bottom flask was placed in a pre-heated silicon oil batch at 200 °C for 2 h under reflux conditions. Thereafter, the mixture was allowed to cool down and the solid to settle. Most of the supernatant was then removed and the remaining slurry was mixed with 180 mL of deionised water in a 500 mL beaker. The mixture was heated at 85 °C while stirring for 30 min, filtered while hot and the FA residue was washed three (3) times with 100 mL of boiling deionised water. The acid treated FA solid residue obtained, called AL, was dried at 80 °C overnight in an oven and used in the following synthesis step. The elemental composition of FA and AL was determined by XRF and the analysis was replicated 4 times.

Figure 3.3: Set up of the acid leaching of coal fly ash.

The H_2SO_4 treated fly ash solid residue (AL) was used as starting material in the synthesis of ZSM-5 zeolite. AL (0.75 g) was mixed with 0.75 g of fumed silica in 20 mL of deionised water. Pearls of sodium hydroxide (0.25 g) were added to the mixture while stirring. Thereafter, 1 g of the structure directing agent (TPABr, HDA or PA) was added (Table 3.5). After aging, the final mixture was poured in a Teflon lined stainless steel autoclave, which underwent hydrothermal synthesis in a pre-heated oven at 160 °C for 72 h as specified in Table 3.5. Thereafter, the Teflon lined stainless steel autoclave was allowed to cool down. The synthesised product was filtered, washed with deionised water and dried in an oven at 70 °C. The dried product was detemplated at 550 °C for 3 h in air with a ramping temperature of 15 °C/min to burn off the structure directing agent (TPABr, HDA or PA). The product was washed with deionised water and dried in an oven at 70 °C.

Table 3.5: Synthesis conditions using H_2SO_4 treated fly ash solid residue (AL) and molar regime of the hydrothermal gel.

Code name	Variable parameters (g)			fixed parameters	Molar regime
	TPABr	HDA	PA		
AL-TPABr	1	-	-	AL (0.75 g), fumed silica (0.75 g), NaOH (0.25 g),	Si(5.8), Al(1.0), Na(1.9), H_2O(338.8), TPABr(1.0)
AL-HDA	-	1	-	H_2O (20 mL), Aging (room temperature, 2 h),	Si(5.8), Al(1.0), Na(1.9), H_2O(338.8), HDA(2.6)
AL-PA	-	-	1	hydrothermal synthesis (160 °C, 72 h)	Si(5.8), Al(1.0), Na(1.9), H_2O(338.8), PA(5.2)

The synthesised and detemplated products in their Na-form (Na-AL-TPABr, Na-AL-HDA and Na-AL-PA) were ion-exchanged 4 times with 0.5 M ammonium nitrate (NH_4NO_3) at a ratio of 1:10, at 80 °C for 1 h under reflux conditions. The solid product (NH_4-AL-TPABr, NH_4-AL-HDA and NH_4-AL-PA) obtained after filtration was dried overnight at 70 °C and calcined at 550 °C in air with a ramping temperature of 15 °C/min for 3 h to drive off NH_3 and produce H-form of the products (H-AL-TPABr, H-AL-HDA and H-AL-PA).

The post-synthesis oxalic acid treatment of the synthesised products in their H-form (H-AL-TPABr, H-AL-HDA and H-AL-PA) was carried out as that detailed in Section 3.3.1.1. The results of the characterisation of the oxalic acid treated products (H-AL-TPABr-OA, H-AL-HDA-OA and H-AL-PA-OA) are discussed in Chapter 5.

3.3.1.3. Synthesis of ZSM-5 zeolite from fused coal fly ash extract

FA was fused as was suggested by Hollmann et al., (1999). FA (50 g) was ground up with 60 g of NaOH. The dry mixture was fused at 550 °C for 1.5 h. The obtained fused sample was mixed with 500 mL of deionised water for 2 h and filtered. Concentrated sulphuric acid (95-99 %) was then added dropwise to the filtrate while stirring to precipitate silica as suggested by Baldyga et al., (2012). A white precipitate named fused fly ash extract (FFAE) was formed at a pH of 10. FFAE was filtered, washed with deionised water and dried overnight at 70 °C. FFAE (10 g) was mixed with 100 mL of saturated oxalic acid solution at 80 °C for 6 h under reflux conditions. The obtained extract, called FFAE1, was dried overnight at 70 °C. FFAE1 (5 g) was then again mixed with 50 mL of a fresh saturated oxalic solution at 80 °C for 6 h under reflux conditions. The obtained extract, called FFAE2, was also dried overnight at 70 °C.

FFAE1 and FFAE2 were washed with deionised water and dried at 70 °C. FFAE, FFAE1 or FFAE2 (2 g) was then mixed with 0.4 g of NaOH in 50 mL of deionised water. Thereafter, 1.5 g of SDA (TPABr, HDA or PA) was added to the mixture (Table 3.6). The obtained mixture underwent aging (30 min, room temperature) and hydrothermal crystallisation (72 h, 160 °C). The synthesised products were detemplated and transformed into their H-form (H-FFAE-TPABr, H-FFAE1-TPABr, H-FFAE2-TPABr, H-FFAE1-HDA and H-FFAE1-PA) using ammonium nitrate as was presented in section 3.3.1.1. The characterisation of H-FFAE-TPABr, H-FFAE1-TPABr, H-FFAE2-TPABr, H-FFAE1-HDA and H-FFAE1-PA is discussed in Chapter 6.

Table 3.6: Synthesis condition for ZSM-5 zeolite from the fused fly ash extracts.

Code name	Variable parameters (g)						Molar regime
	FFAE	FFAE1	FFAE2	TPABr	HDA	PA	
FFAE-TPABr	2	-	-	1.5	-	-	Si(10), Al(1), Na(50), H_2O(3473), TPABr(4)
FFAE1-TPABr	-	2	-	1.5	-	-	Si(36), Al(1), Na(27), H_2O(5556), TPABr(7)
FFAE2-TPABr	-	-	2	1.5	-	-	Si(87), Al(1), Na(56), H_2O(13890), TPABr(14)
FFAAE1-HDA	-	2	-	-	1.5	-	Si(36), Al(1), Na(27), H_2O(5556), HDA(20)
FFAE1-PA	-	2	-	-	-	1.5	Si(36), Al(1), Na(27), H_2O(5556), PA(38)

The fixed parameters were: NaOH (0.4 g), H_2O (50 mL), Aging (30 min, room temperature), Hydrothermal synthesis (72 h, 160 °C)

3.3.2. Total digestion of solid samples

The fused fly ash extracts (FFAE. FFAE1 and FFAE2) were digested in order to determine their chemical composition using ICP. The total digestion method used in this study was adopted from the one used by Missengue et al., (2015). A sample of a fused fly ash extract (0.25 g) was mixed with 2 mL of a concentrated hydrofluoric acid (HF), 5 mL of aqua regia (HNO_3/HCl, 1:3) in a digestion vessel that was placed in a pre-heated oven at 250 °C for 2 h. Thereafter, the mixture was allowed to cool and the excess HF in the digestate was neutralised by adding 25 mL of saturated boric acid (H_3BO_3) solution. The digestate was filtered through a 45-µm pore filter paper; and the effluent diluted to 50 mL with deionised water. The chemical composition of each sample was determined using ICP-OES analyser. The atomic percentage of each element in each sample was then calculated.

3.3.3. Catalytic testing

The fly ash-based ZSM-5 zeolite products that were synthesised from the H_2SO_4 treated fly ash (H-AL-TPABr, H-AL-HDA, H-AL-PA, H-AL-TPABr-OA, H-AL-HDA-OA and H-AL-PA-OA) as well as those synthesised from the fused fly ash extracts (H-FFAE1-TPABr, H-FFAE2-TPABr, H-FFAE1-HDA and H-FFAE1-PA) were used as heterogeneous catalysts in the MTO and Nazarov reactions with the commercial H-ZSM-5 that was characterised above as reference. This section details the procedure of the two reactions.

3.3.3.1. Methanol-to-Olefins conversion

The Methanol-to-Olefins (MTO) reaction adopted in this study was proposed by Bleken et al., (2012). The zeolite H-ZSM-5 sample (H-AL-TPABr, H-AL-HDA, H-AL-PA, H-AL-TPABr-OA, H-AL-HDA-OA, H-AL-PA-OA, H-FFAE1-TPABr, H-FFAE2-TPABr, H-FFAE1-HDA, H-FFAE1-PA or the commercial H-ZSM-5) (60 mg) was placed in a fixed bed quartz reactor and heated at 450 °C in air with a heating rate of 15 °C/min. After desorbing water from the catalyst for 1 h, the reactor was connected to a container containing methanol, kept at 0 °C. Methanol was carried to the reactor by a constant N_2 flow (20 mL/min) to achieve the weight hourly space velocity (WHSV) of 1.12 g_{MeOH}/ g_{cat}* 1 / h (Figure 3.4). A gas product (1 mL) was sampled with a gas tight syringe at the sampling point every hour up to 24 h and analysed using a Hewlett Packard 5890 Gas Chromatograph (GC) equipped with a PONA column and a flame ionization detector (FID). The percentages of MTO conversion

and the selectivity of propylene/ethylene were determined while considering methanol and dimethyl ether (intermediate product) as reactants (Equation 3.2, Equation 3.3).

Equation 3.1: Conversion of methanol to hydrocarbons.

$$2CH_3OH \underset{+H_2O}{\overset{-H_2O}{\rightleftharpoons}} CH_3OCH_3 \xrightarrow[MTO]{-H_2O} \text{Light olefins (ethylene and propylene)} \xrightarrow[MTG]{-H_2O} \text{Aromatic hydrocarbons}$$

$$X = \frac{n(MeOH)_{in} - \left[n(MeOH)_{out} + 2 * n(DME)\right]}{n(MeOH)_{in}} * 100\% \quad \textbf{(Equation 3.2)}$$

$$S = \frac{\sum x * n(CxHy)}{n(MeOH)_{in} - \left[n(MeOH)_{out} + 2 * n(DME)\right]} * 100\% \quad \textbf{(Equation 3.3)}$$

With $\sum$ being applied for the calculation of the selectivity towards light olefins (C_2-C_4) fraction.

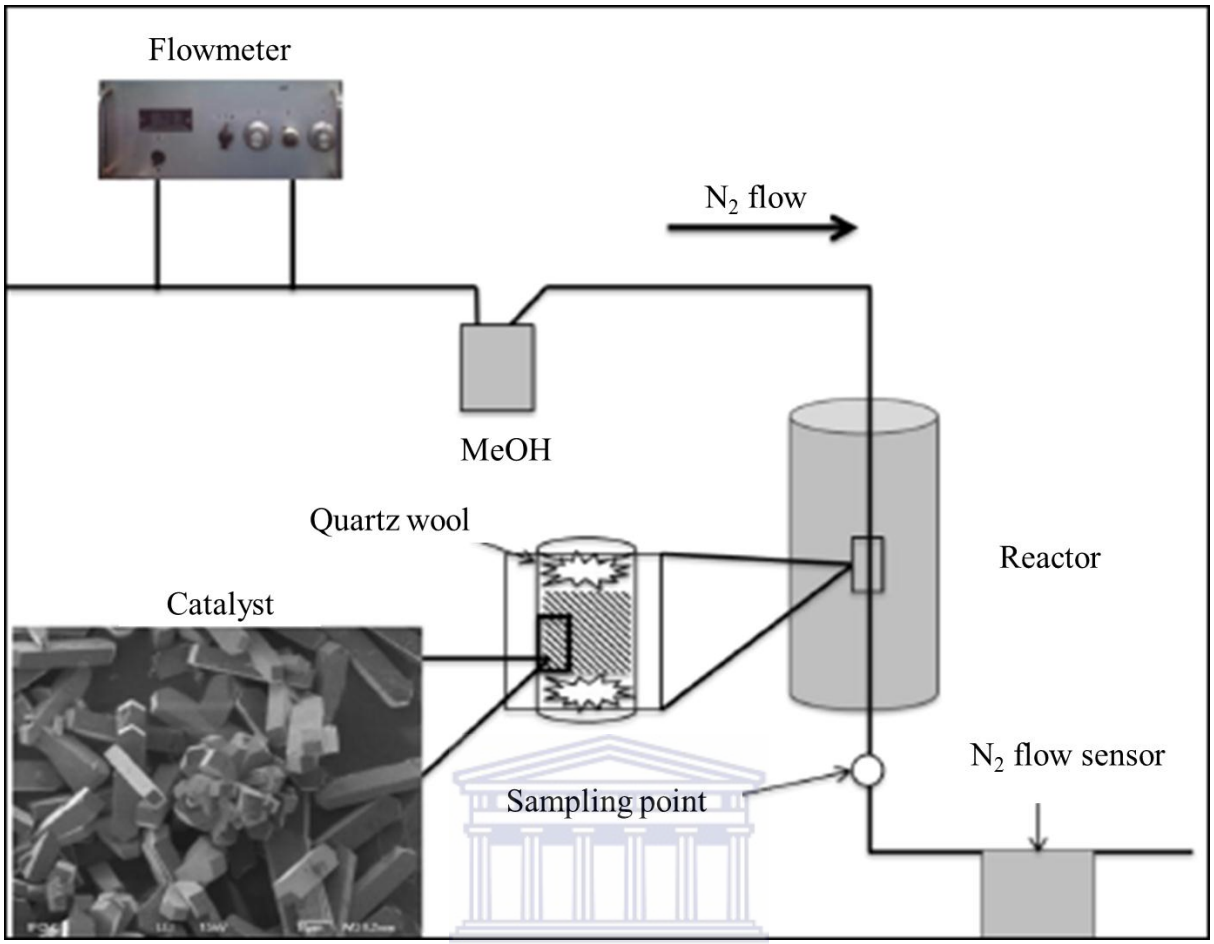

Figure 3.4: Set up for the Methanol-to-Olefins (MTO) conversion (Boltz and Louis, 2013).

3.3.3.2. Nazarov cyclisation of 1-phenyl-2-ethylpropenone

The Nazarov cyclisation adopted in this study was proposed by Sani-Souna-Sido et al., (2008). 1-phenyl-2-ethylpropenone was used as precursor for the synthesis of 2-ethylindan-1-one. The first part of this section presents the synthesis of the precursor 1-phenyl-2-ethylpropenone from 1-phenylbutan-1-one and formaldehyde (Equation 3.4). The second part of the section highlights the Nazarov cyclisation of 1-phenyl-2-ethylpropenone (Equation 3.5) over H-AL-TPABr-OA, H-AL-HDA-OA and H-AL-PA-OA that were synthesised as detailed in Section 3.3.1.2.

a. Synthesis of the precursor arylvinylkenone (1-phenyl-2-ethylpropenone)

The synthesis of the precursor 1-phenyl-2-ethylpropenone was performed using Manich condensation as proposed by Rodrigues et al., (2003). 1-phenylbutan-1-one (1.45 mL)

and 0.43 mL of morpholine were mixed in 20 mL of glacial acetic acid. The mixture was heated at 125 °C under reflux conditions (Figure 3.5). Formaldehyde (5 mL) was added dropwise over several hours. After the reaction was complete, it was cooled down.

The reaction was complete after 48 h and was monitored by analysing the components in a drop of the reaction mixture every 12 h using a silica thin layer chromatography (TLC) plate with a mixture of cyclohexane/ethyl acetate (90:10) as eluent (mobile phase). The mixture to be analysed was spotted near the bottom of the TLC plate. After the spot had dried, the plate was placed in a developing chamber containing the eluent at a level below the spot. The eluent slowly rose up the TLC plate by capillary action carrying with it the components present in the reaction mixture based on their affinity to the eluent. Thereafter, the plate was removed from the developing chamber and dried before observing the level of different components on it under UV light in order to distinguish between the final product and the reagent. 1-phenylbutan-1-one was used as blank for the TLC analysis.

Afterwards, the glacial acetic acid was evaporated from the final mixture under reduced pressure at 40 °C using a rotary evaporator and the residual product was diluted in 50 mL of ethyl acetate. The obtained solution was washed successively with 50 mL of 5 % of an aqueous solution of $NaHCO_3$, followed by 50 mL of 10 % of HCl, 50 mL of water and 50 mL saturated NaCl. At each washing step, the organic phase was separated from the aqueous phase by decantation. The organic phase obtained after the last washing with a saturated NaCl solution was dried with anhydrous $MgSO_4$ and the solvent was evaporated off under reduced pressure at 40 °C using a rotary evaporator. Thereafter, the final product in the crude extract was separated from the residual reagent 1-phenylbutan-1-one using column chromatography with silica sandwiched between two layers of sand as stationary phase. The crude extract was diluted in 100 mL of cyclohexane/ethyl acetate mixture (90:10) used as mobile phase. The mixture was introduced at the top of the column and was allowed to pass through the column. Different fractions (about 10 mL each) of the mixture were collected separately in test tubes at the bottom of the column. A drop of each fraction was analysed by TLC as detailed above. All the mixture fractions that showed only a single spot of the final product were mixed together. Afterwards, the solvent (cyclohexane/ethyl acetate) was evaporated off under reduced pressure at 40 °C using a rotary evaporator. A portion of the final product (10 µL) was diluted in 0.5 mL of chloroform-d and analysed by ^1H NMR. The rest of the final product was used as precursor in the Nazarov cyclisation as detailed in the section below.

Figure 3.5: Set up for the synthesis of the precursor 1-phenyl-2-ethylpropenone.

Equation 3.4: (A) Equation of synthesis of the precursor 1-phenyl-2-ethylpropene and (B) its mechanism.

(A)

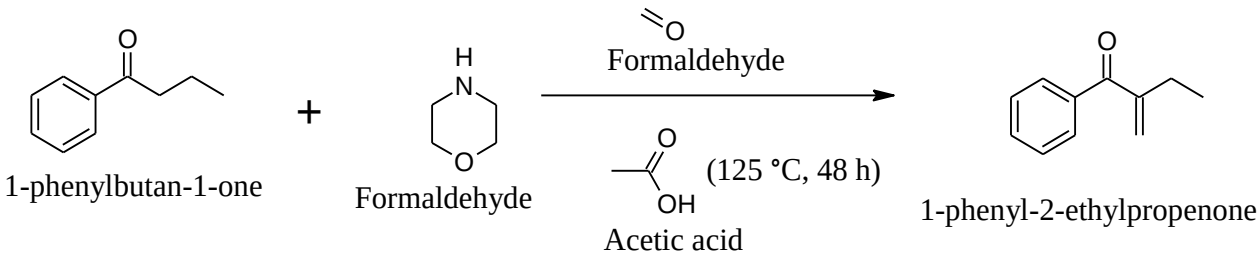

(B)

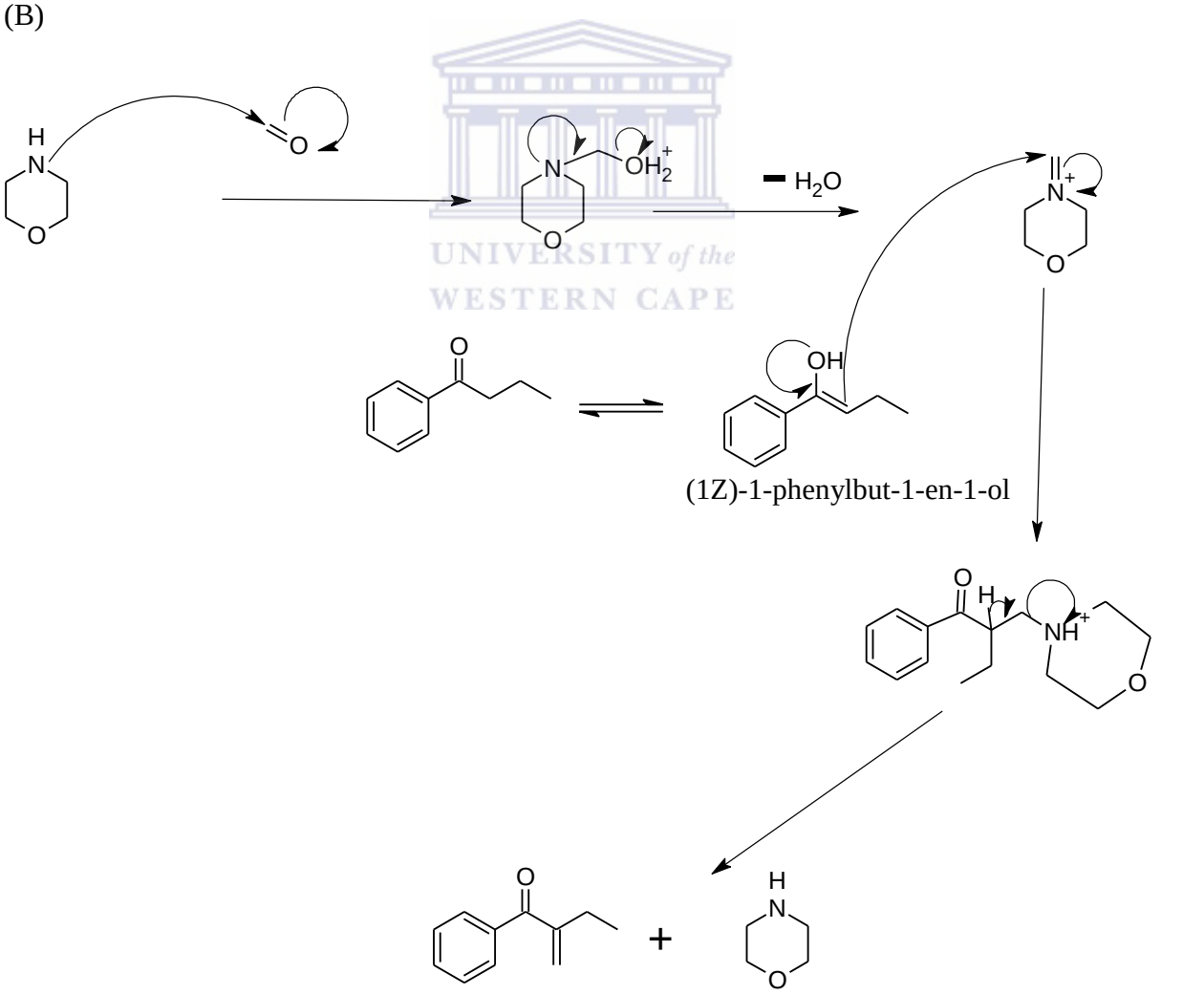

b. Synthesis of 2-ethylindan-1-one through Nazarov cyclisation of 1-phenyl-2-ethylpropenone

The synthesis conditions of 2-ethylindan-1-one used in this section were proposed by Sani-Souna-Sido et al., (2008) (Equation 3.5). The precursor (1-phenyl-2-ethylpropene) synthesised as shown above (16 mg) was mixed with 200 mg of ZSM-5 zeolite sample, 1 mL of chlorobenzene and 2.7 mg of hexamethyl benzene (internal standard) in a sealed pressure tube (Figure 3.6). The mixture was stirred at 130 °C for 16 h. A blank made of 16 mg of the synthesised precursor, 1 mL of chlorobenzene and 2.7 mg of hexamethyl benzene was also stirred at 130 °C for 16 h. After cooling down, 5 mL of methanol was added and the resulting mixture was stirred for 1 h at 80 °C. Thereafter, the solution was filtered and poured into a round bottom flask. The solvent in the flask was evaporated under reduced pressure at 40 °C using a rotary evaporator. The final product was dissolved in 0.5 mL of chloroform-d and analysed by ^{1}H NMR. Equation 3.5 shows the mechanism of formation of 2-ethylindan-1-one from 1-phenyl-2-ethylpropenone.

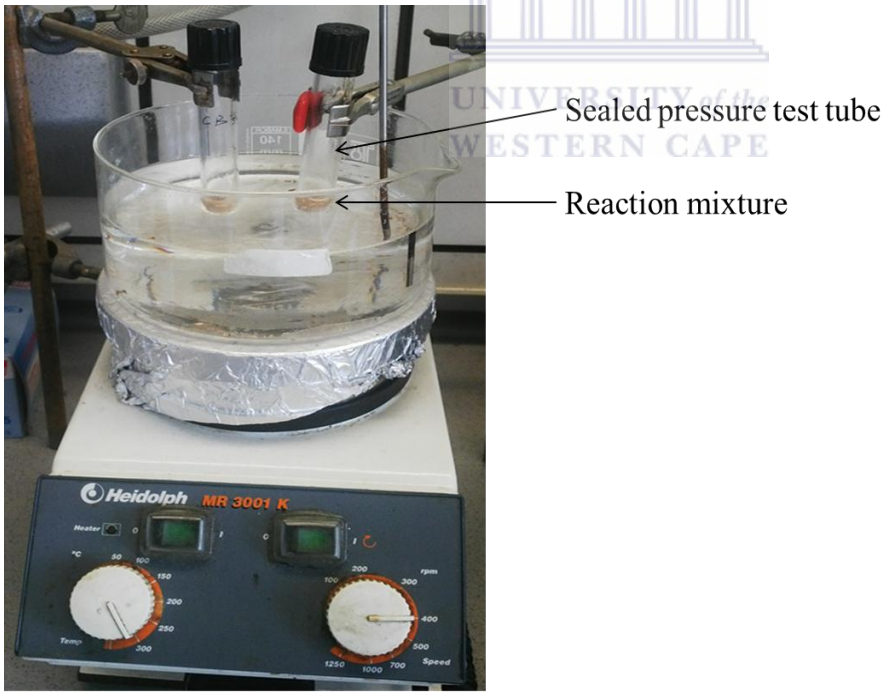

Figure 3.6: Set up for Nazarov cyclisation.

Equation 3.5: (A) Nazarov cyclisation and (B) mechanism of formation of 2-ethylindan-1-one or the by-product chloro(2-ethyl-3-phenylben-3-en-1-yl)benzene.

(A)

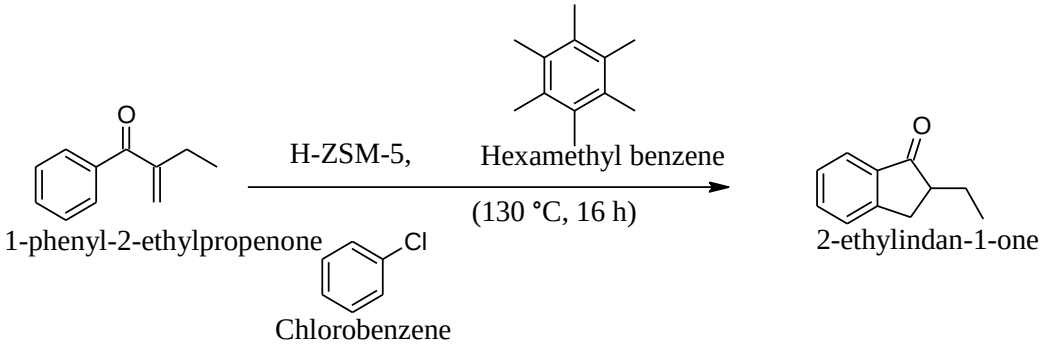

(B)

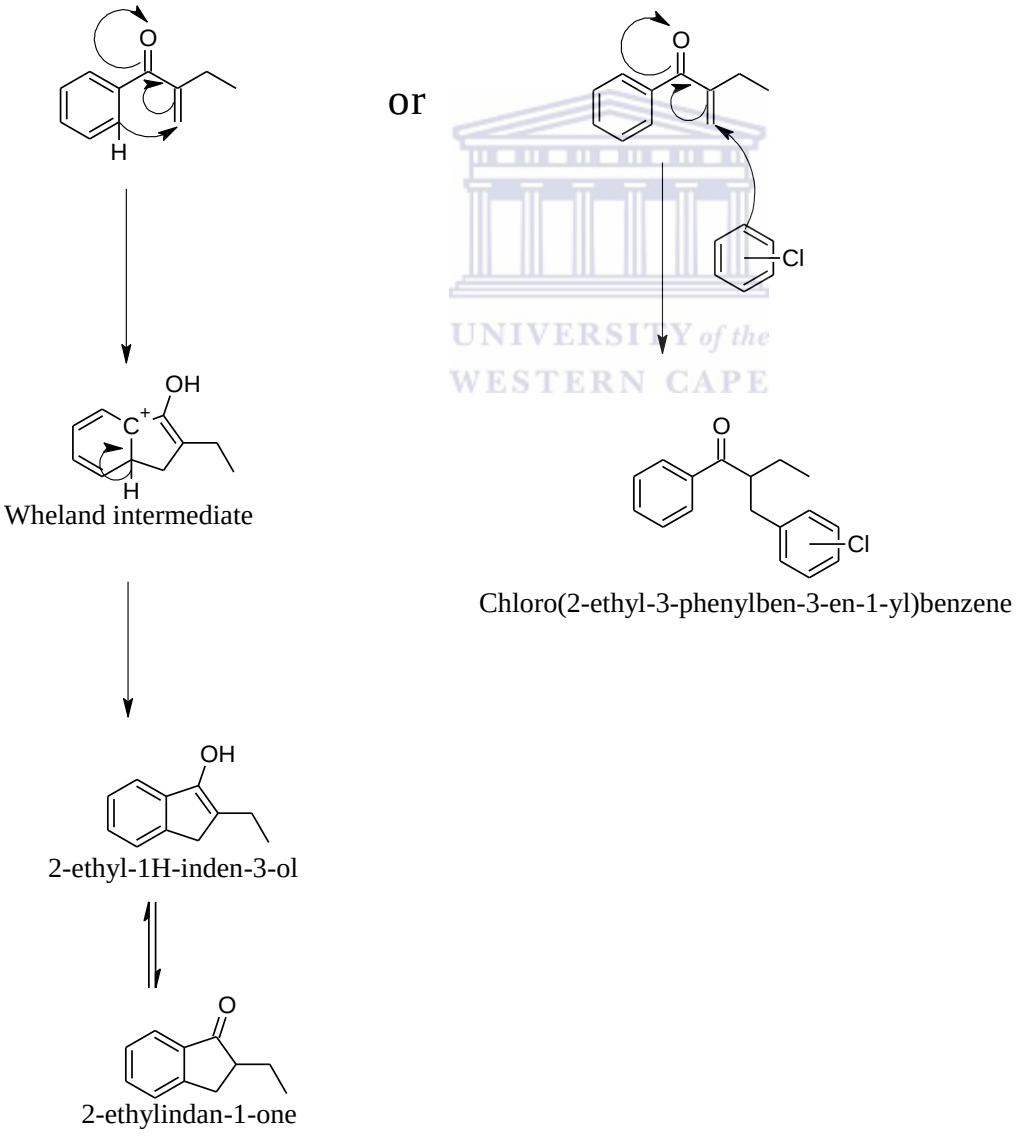

3.4. Characterisation techniques

This section details the different techniques used to characterise the fly ash, synthesised fly ash-based ZSM-5 zeolite samples as well as the products and reagents for Methanol-to-Olefins (MTO) and Nazarov reactions.

3.4.1. X-ray diffraction spectroscopy analysis

The mineralogical characterisation of as-received coal fly ash, treated coal fly ashes and synthesised zeolites was conducted using a Philips X-pert pro MPD X-ray diffractometer with Cu-K radiation at 40 kV and 40 mA. The sample was ground to a fine powder and packed into a rectangular polypropylene holder which was clipped into the X-ray diffraction (XRD) instrument. The analysis was performed between 4° and 60° 2Θ. The different mineral phases were identified using Highscore Xpert software, comparing the collected patterns with the standard patterns from the powder diffraction database supplied by International Centre for Diffraction Data (ICDD).

3.4.2. Scanning electron microscopy-energy dispersive spectroscopy

The morphology and particle size of as-received coal fly ash, treated coal fly ashes and synthesised zeolites were investigated with a Hitachi X-650 Scanning Electron Micro-analyser equipped with a CDU-lead detector at 25 kV, a tungsten filament and an energy spectroscopy (EDS) system for chemical analysis. The current and illumination were 5 kV and 0.1 mrad respectively. The samples were prepared by placing a carbon adhesive tape onto an aluminium stub. A small amount of each sample was applied onto the carbon adhesive tape. The samples were then coated with carbon in an Emitech K950X carbon evaporator for 6 sec to make them conductive. Then, the samples were introduced into the analyser and scanning electron micrographs of each sample were captured. The elemental composition of some samples was determined via the EDS system.

3.4.3. Fourier transform infrared spectroscopy

Fourier transform infrared (FTIR) spectroscopy was used to monitor the structural changes induced during the pre-synthesis, synthesis and post-synthesis treatments of ZSM-5 zeolite from coal fly ash. Approximately 15 mg of each sample was placed on the Attenuated Total

Reflectance (ATR) sample holder of Perkin Elmer spectrum 100 FT-IR spectrometer. Gentle force was applied to the sample and infrared (IR) spectra were collected within a range of 4000 – 400 cm^{-1} to identify structural configuration and provide information about the structure of the sample. Before data collection, baselines were corrected for background noise which was subtracted from the spectra.

3.4.4. X-ray fluorescence spectroscopy analysis

X-ray Fluorescence (XRF) was used to determine the elemental composition of the as-received fly ash and acid treated fly ash. Loss on ignition (LOI) was determined by heating approximately 2 g of each sample in a muffle furnace at 900 °C for 4 h. However, the percentage of LOI was not reported and the elemental composition of all the samples was determined on a dry weight basis.

For the major element analysis, each sample was dried at 110 °C overnight and was prepared as follows: 0.65 g of a sample and 5.60 g of a flux (consisting of 66.67 % $Li_2B_4O_7$, 32.83 % $LiBO_2$ and 0.50 % LiBr) were mixed, and the mixture was fused to a glass bead. The oxides of the major elements namely SiO_2, Al_2O_3, Fe_2O_3, CaO, TiO_2, MgO, K_2O, P_2O_5, MnO and Cr_2O_3 of each sample were determined using a Philips PW 1480 X-ray spectrometer. The spectrometer was fitted with a chromium tube, five analysing crystals namely LIF 200, LIF 220, GE, PE and PX and the detectors being a combination gas-flow proportional counter and a scintillation detector. The gas-flow proportional counter uses P10 gas, which is a mixture of argon and methane at 9:1 ratio. The analysis was conducted four times using a fresh fly ash sample each time.

3.4.5. Inductively coupled plasma-optical emission spectroscopy

The inductively coupled plasma-optical emission spectroscopy (ICP-OES) was used to determine the elemental composition of digested samples (see section 3.3.2). The digested samples were filtered using a micro-membrane filter of 0.45 μm to remove suspended particles. Then, they were diluted in 2 % HNO_3 aqueous solution at the ratio (V/V) of 1:10 or 1:100, depending on the concentration of elements to be analysed. The samples were analysed using Varian 710-ES ICP-OES instrument, which was calibrated using standards of each analysed element and the analysis was conducted in triplicate.

3.4.6. Acid site titration using the H/D exchange isotope technique

The acidity of the synthesised zeolites was determined following the method proposed by Louis et al. (2004). The ZSM-5 zeolite sample (200 mg) was activated under N_2 flow (60 mL/min) at 450 °C for 1 h to desorb water with a heating rate of 15 °C/min. The temperature was lowered to 200 °C; thereafter D_2O was passed through and absorbed by the respective sample for 1 h under a N_2 flow (Figure 3.7). Dry N_2 flow then swept the excess of D_2O from the sample for 1 h (Equation 3.6). The titration of O-D sites was performed by back-exchanging deuterium (D) present on the surface of the zeolite with hydrogen (H), H_2O saturated N_2 stream was passed through and absorbed by the sample for 1 h (Equation 3.7). H_xOD_y composed of H_2O, D_2O and HDO was collected in a cold U-tube trap at -78 °C and weighed.

$$Zeolite(OH) \xrightarrow{D_2O(excess)} Zeolite(OD) + H_2O + HDO + D_2O \quad \textbf{(Equation 3.6)}$$

$$Zeolite(OD) \xrightarrow{H_2O(excess)} Zeolite(OH) + H_2O + HDO + D_2O \quad \textbf{(Equation 3.7)}$$

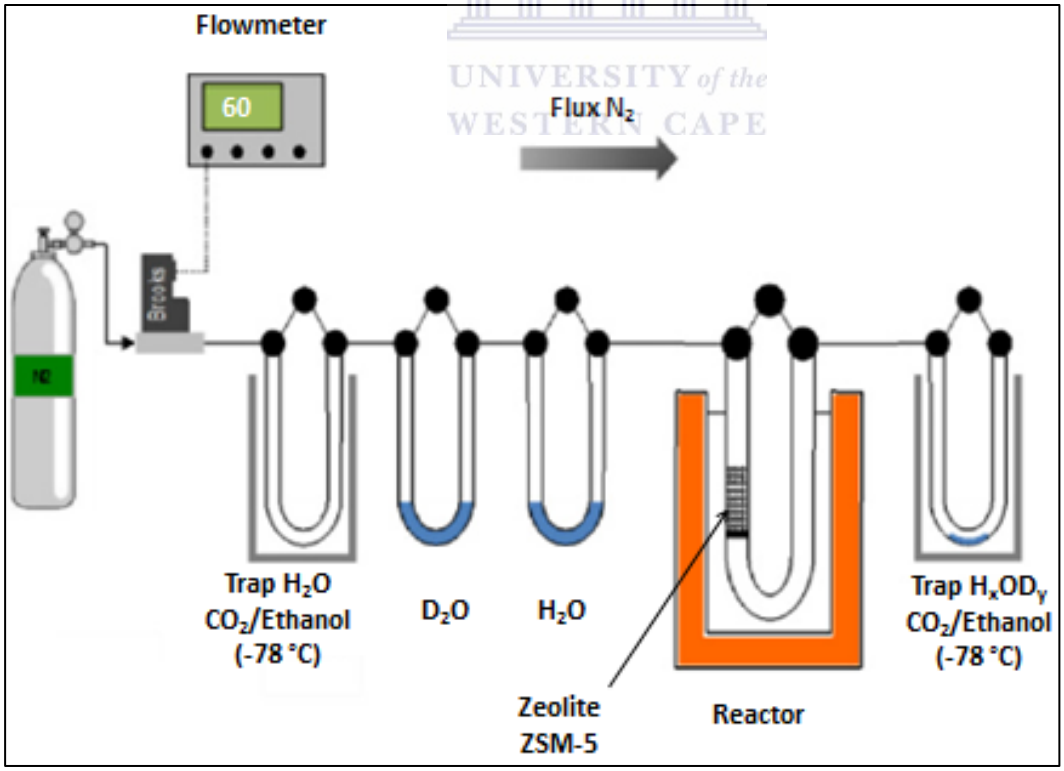

Figure 3.7: Set up for the acid site titration using the H/D exchange isotope technique (Boltz et al., 2012).

The collected H_xOD_y was mixed with 0.6 mL of trifluoroacetic anhydride in a NMR tube (Equation 3.8). A few drops of $CHCl_3/CDCl_3$ (ratio 10:1) were added. A reference solution was made of the mixture of H_2O (40 µL) and D_2O (10 µL) in 0.6 mL of trifluoroacetic anhydride, with a few drops of $CHCl_3/CDCl_3$ (ratio 10:1) added. The prepared NMR tubes were analysed using Bruker UltraShield 300 MHz/54 mm spectrometer for proton nuclear magnetic resonance (^{1}H NMR). The acid site density was then calculated based on the H/D ratio measured and the mass of H_xOD_y collected.

$$H_xOD_y \xrightarrow{(CF_3CO)_2O(excess)} xCF_3COOH + yCF_3COOD \quad \textbf{(Equation 3.8)}$$

The number of acid site per gram of zeolite was calculated as follows:

$$n(H_2O) = \frac{I(H) * n(CHCl_3)}{2} \quad \text{And} \quad n(D_2O) = \frac{I(H) * n(CDCl_3)}{2}$$

With $I =$ NMR peak integration

$$\begin{cases} \dfrac{n(H_2O)}{n(D_2O)} = \dfrac{x}{y}(1) \\ x + y = 2(2) \end{cases} \Rightarrow y = \left[2 * \frac{n(D_2O)}{n(H_2O)}\right] / \left[1 + \frac{n(D_2O)}{n(H_2O)}\right]; x = 2 - y$$

$$n(H_xOD_y) = \frac{m(H_xOD_y)}{M(H_xOD_y)}$$

With $m(H_xOD_y) =$ mass of the sample collected from the U-tube

$$M(H_xOD_y) = (1 * x + 2 * y + 16) g/mol$$

$$n(D) = \frac{n(H_xOD_y)}{y} \quad \text{And} \quad \frac{n(H^+)}{m(zeolite)} = \frac{n(D)}{m(zeolite)}(mol/g)$$

$n(H^+) =$ Number of acid sites in the zeolite.

3.4.7. N_2 Brunauer-Emmett-Teller

The BET surface area of the synthesised zeolites was determined using Micromeritics ASAP 2020 instrument. Approximately 500 mg of the sample was dried over night at 90 °C. Then it was put in a sample tube and inserted in the BET instrument, where it was first degassed successively at 90 °C for 2 h and 400 °C for 4 h in order to remove moisture adsorbed inside the porous network. The BET analysis was performed at 77.41 K with N_2 as adsorptive using Micromeritics ASAP 2020 Surface Area and Porosity Analyzer.

3.4.8. Nuclear magnetic resonance spectroscopy

The nuclear magnetic resonance (NMR) spectroscopy was used to determine the number of Brønsted acid sites of the synthesised fly ash-based ZSM-5 zeolite products and to monitor the intramolecular cyclisation of 1-phenyl-2-ethylpropenone into an indanone. The samples used to determine the number of Brønsted acid sites were prepared as mentioned in Section 3.4.6 and they were analysed using Bruker UltraShield 300 MHz/54 mm spectrometer for proton nuclear magnetic resonance (^{1}H NMR). Nazarov cyclisation of 1-phenyl-2-ethylpropenone into 2-ethylindan-1-one was monitored by ^{1}H NMR and the samples were prepared as shown in Section 3.3.3.2. The prepared samples were analysed using Bruker UltraShield 300 MHz/54 mm spectrometer.

The solid state NMR (^{27}Al NMR) was also used to determine the coordination of aluminium in the fly ash-based ZSM-5 zeolite products. Approximately 50 mg of the sample was compressed in a NMR rotor that had an inner diameter of 7 mm. The rotor was closed and inserted in the NMR instrument. The analysis was performed using Bruker UltraShield 600 MHz/54 mm spectrometer.

3.4.9. Gas chromatography

The products of the MTO reaction were analysed by gas chromatography (GC). The MTO samples (1 mL) collected at the sampling point were analysed using Hewlett Packard 5890 Gas Chromatograph (HP 5890 GC) that was equipped with a 50 m capillary column (PONA) and a flame ionization detector (FID). The instrument was programmed as follows: Temperature in the injector (300 °C), He flux (17 psi). The running of the sample was programmed as follows: 40 °C for 7 min, increase the temperature to 270 °C with the ramping temperature of 20 °C/min and leave the temperature stable at 270 °C for 5 min. The temperature in the detector was 270 °C.

CHAPTER 4: CHARACTERISATION OF ZSM-5 ZEOLITE SYNTHESISED FROM THE AS-RECEIVED FLY ASH

4.1. Introduction

This chapter presents the physical and chemical properties of the as-received fly ash that was obtained from Arnot power plant station (South Africa) and used as starting material for the synthesis of ZSM-5 zeolite. The XRD, SEM, FTIR and XRF data of the as-received fly ash are presented as baseline. The hydrothermal gel of the zeolites that are characterised in this chapter was made of the as-received fly ash, tetrapropylammonium bromide, fumed silica, sodium hydroxide and deionised water; and their synthesis conditions were detailed in Table 3.3. The effect of the physical and chemical parameters of the synthesis process on the quality of the final products was monitored using XRD analysis. Lastly, this chapter compares the physical and chemical properties of ZSM-5 zeolite synthesised from the as-received fly ash with either tetrapropylammonium bromide, 1,6-hexandiamine or 1-propylamine as structure directing agent using XRD, SEM, FTIR, BET, Brønsted acidity and ^{27}Al NMR analyses.

4.2. Characteristics of the as-received fly ash

The results of the characterisation of the as-received fly ash (FA) are discussed in this section. Figure 4.1 presents the XRD pattern of FA.

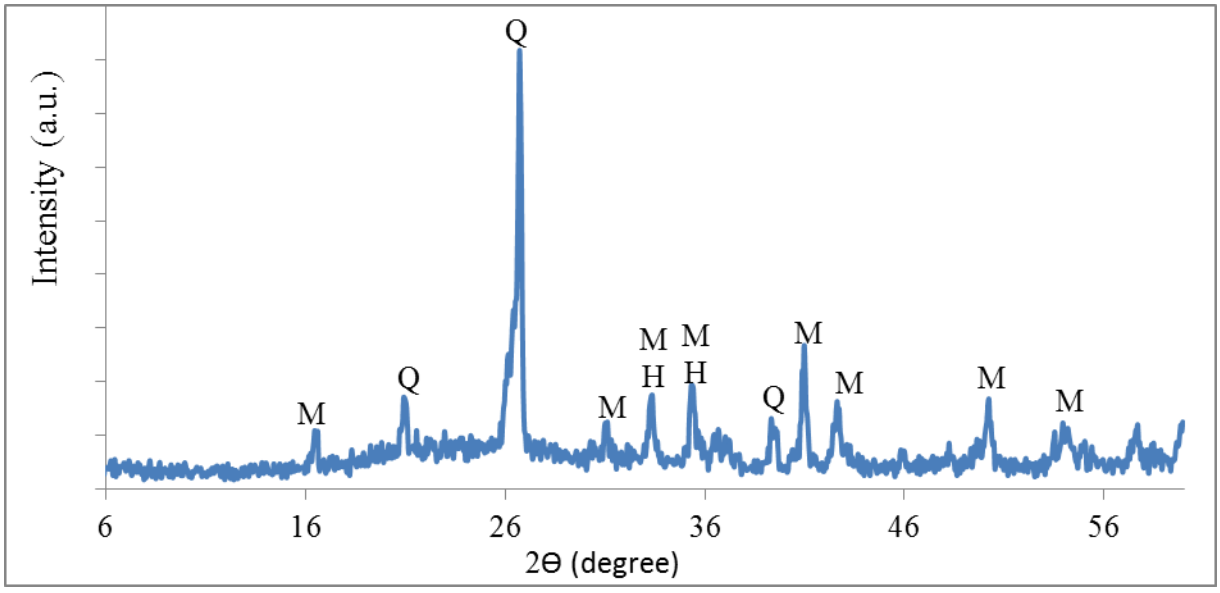

Figure 4.1: XRD pattern of the as-received fly ash (FA) from Arnot power plant (M=mullite; Q=quartz; H=hematite).

Figure 4.1 showed that the major mineral phases found in fly ash (FA) were mullite (M), quartz (Q) and hematite (H). The hump that was observed between 18 and 33° 2Θ characterised the amorphous phase of FA. Musyoka, (2012) also reported that FA from Arnot power plant was made of mullite, quartz, hematite and amorphous phases.

Figure 4.2 shows the SEM micrograph of FA.

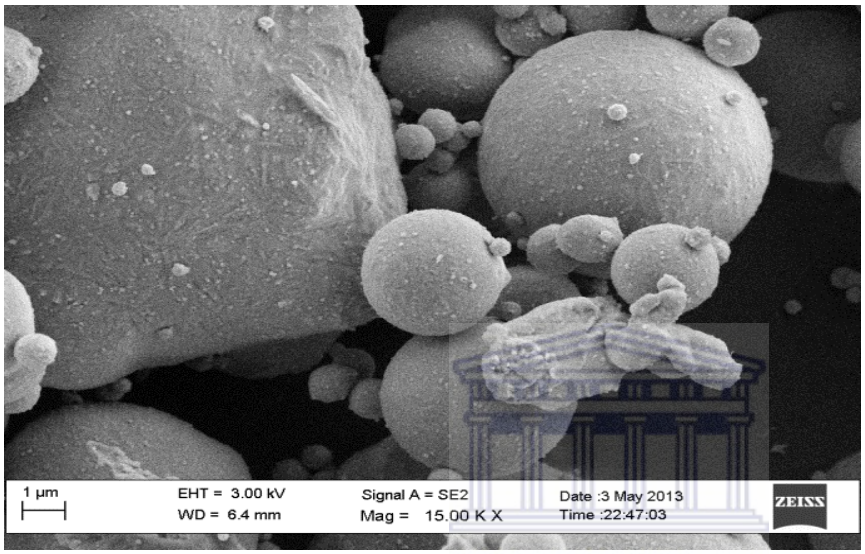

Figure 4.2: SEM micrograph of the as-received fly ash (FA) from Arnot power plant station (South Africa).

Figure 4.2 showed that FA particles were generally smooth and spherical in shape. Vassilev and Vassileva, (2007) stated that SEM analysis is one of the techniques that are recommended and mostly used for physical characterisation of FA. FA particles are smooth and spherical because of the glass phase that covers their surface (Querol et al., 2002) and their morphology depends on the heating and cooling processes in the pulverised coal boiler (Inada et al., 2005; Shao et al., 1997). Ahmaruzzaman, (2010) reported that fly ash particles are predominantly spherical in shape that is in agreement with the FA image presented in Figure 4.2.

Figure 4.3 summarises the structural analysis of FA obtained via FTIR.

Figure 4.3: FTIR spectrum of the as-received fly ash (FA).

The FTIR spectrum of FA showed two bands at 451 and 555 cm^{-1} that could be assigned to Si-O-Si symmetric bend and Al-O stretch for mullite. The band at 800 cm^{-1} could be attributed to a glassy-amorphous phase. The band at 919 could be attributed to the Al-O stretch (AlO_4) in-plane. The intense band at 1099 cm^{-1} could be assigned to Si-O asymmetric stretch for mullite, glass phase and quartz. The shoulder that appeared at 1415 cm^{-1} could be attributed to the carbonate. The band at 1876 cm^{-1} could be associated with presence of potassium phosphate (Voll et al., 2002; Abou Rida et al., 2014; Miller and Wilkins, 1952).

It is important to remember that ZSM-5 zeolite is a high silica zeolite with a Si/Al molar ratio above 10 (Jacob, 1998). Therefore, it is necessary to investigate the elemental composition of the starting material fly ash (FA) in order to know if there is a need to adjust the Si/Al molar ratio in the hydrothermal gel by the addition of a silica source. Table 4.1 gives the percentage of the major elements contained in FA on dry basis without LOI. The analysis was repeated four times as detailed in Section 3.4.4.

Table 4.1: Elemental composition of Arnot coal FA (n=4).

Major elements	Fly ash sample (%)				Average (%)
SiO_2	59.08	58.63	58.35	59.02	58.77±0.34
Al_2O_3	27.99	27.83	27.69	28.04	27.89±0.16
Fe_2O_3	5.09	4.98	4.96	5.03	5.01±0.06
CaO	4.04	3.94	3.94	4.04	3.99±0.06
TiO_2	1.65	1.64	1.63	1.66	1.65±0.01
MgO	1.20	1.20	1.19	1.19	1.20±0.01
K_2O	0.65	0.66	0.66	0.65	0.65±0.01
P_2O_5	0.37	0.35	0.35	0.40	0.37±0.02
MnO	0.04	0.04	0.04	0.04	0.04±0.00
Cr_2O_3	0.04	0.03	0.03	0.03	0.03±0.01
Total	100.14	99.31	98.83	100.11	99.60±0.64
Si/Al	1.86	1.86	1.86	1.86	1.86

The XRF analysis was repeated four times using a fresh fly ash sample each time and the small standard deviation of the average of each oxide percentage indicated the fly ash sample used in this study was homogenous. Table 4.1 presented the percentage of oxides of major element on dry basis without LOI to avoid significant errors that can be caused by the presence of moisture in the sample structure. It could be seen that SiO_2 and Al_2O_3 were the two main oxides in the as-received FA and together represented 86.66 % of its total elemental content. It could also be observed that the oxides of divalent elements such Ca, Mg and Mn were present at minor level, while oxides of monovalent elements were at trace level. Querol et al., (2002) reported that fly ash is used as starting material in the synthesis of zeolites such as faujasite, sodalite, etc., because of its compositional resemblance to some volcanic material, precursor of natural zeolites. However, FA was not suitable for the synthesis of ZSM-5 zeolite because of its low Si/Al molar ratio which was found to be 1.86, while ZSM-5 zeolite required a Si/Al molar ratio above 10.

4.3. Effect of synthesis conditions on the quality of ZSM-5 zeolite synthesised from as-received fly ash with tetrapropylammonium bromide as structure directing agent

The synthesis of ZSM-5 from fly ash required an addition of silica sources. In the present study, fumed silica was added to the hydrothermal gel as additional silica source to increase

the Si/Al molar ratio. Several chemical and physical parameters namely the amount of FA, fumed silica, NAOH, TPABr and H_2O, aging (time and temperature) and hydrothermal crystallisation (time and temperature) were also varied subsequently in order to establish their effect on the product quality as set out in Table 3.3. Qualitative XRD analysis was used to monitor the synthesis of zeolite ZSM-5 from the as-received fly ash with tetrapropylammonium bromide (TPABr) as structure directing agent (SDA), by investigating the mineralogical transformations that occur during the synthesis process. All the fly ash-based ZSM-5 zeolite products analysed in this section were in their Na-form. The use of TPABr at this stage of the synthesis was motivated by the fact that TPA^+ is the most commonly used SDA in the synthesis of ZSM-5 zeolite (Wright and Lozinska, 2011).

4.3.1. Effect of the Si/Al molar ratio by varying the amount of fly ash and fumed silica

Figure 4.4 shows the mineral phases present in the as-received fly ash (FA) and mineralogical changes that were induced by the variation of the amount of fly ash and fumed silica in the hydrothermal gel. The synthesis conditions of FA0, FA1 and FA2 were described in Table 3.3. FA (1.25, 1 or 0.75 g) and fumed silica (0.25, 0.5 or 0.75 g) were mixed to obtain the FA/fumed silica mass ratio of 1.25:0.25; 1.00:0.50 or 0.75:0.75 in FA0, FA1 or FA2 respectively. Other parameters were kept constant: tetrapropylammonium bromide (1 g), NaOH (0.25 g), H_2O (15 mL), aging (room temperature, 2 h) and hydrothermal synthesis (160 °C, 72 h).

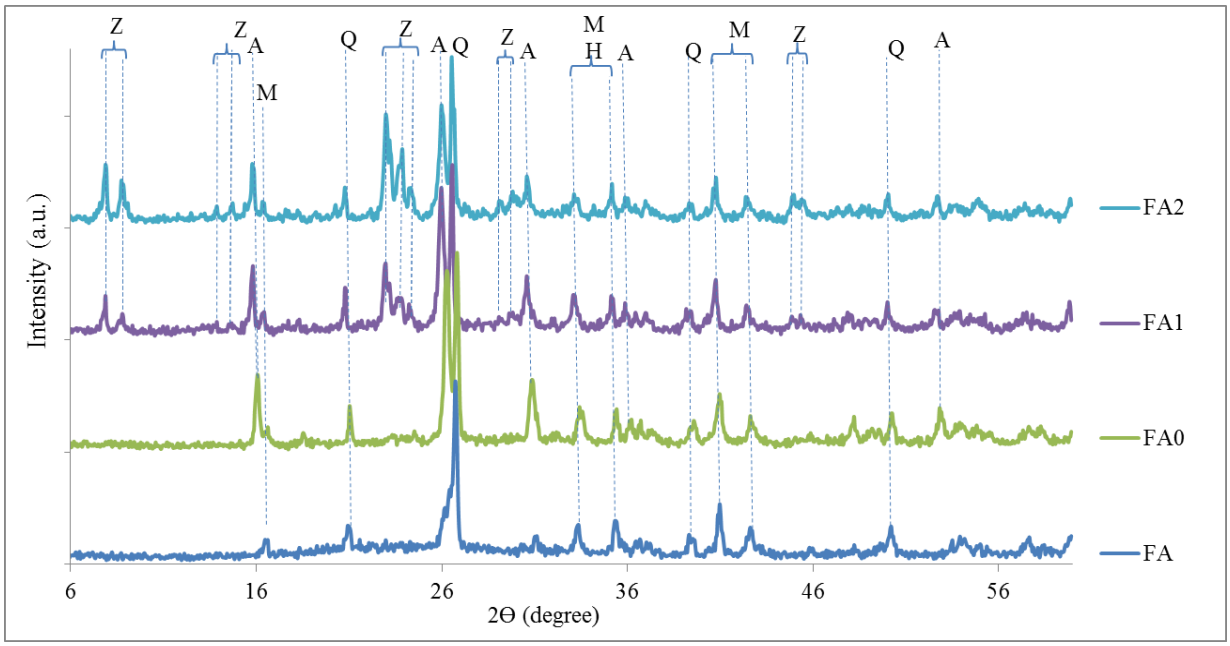

Figure 4.4: Effect of the FA/fumed silica ratio on the XRD patterns of the fly ash-based ZSM-5 zeolite samples FA0 (1.25:0.25), FA1 (1.00:0.50) and FA2 (0.75:0.75) (Z= ZSM-5 zeolite; A=analcime; M=mullite; Q=quartz; H=hematite).

The major mineral phases found in fly ash (FA) were mullite (M), quartz (Q) and hematite (H). The XRD patterns of FA0 showed the presence of mullite, quartz and hematite phases in the final product which did not contain a desired ZSM-5 zeolite phase, but the intensity of mullite peaks at 16.5 and 40° 2Θ decreased. There was the appearance of characteristic peaks of an analcime phase at 16, 26.5, 30.5, 35.5 and 53° 2Θ that decreased in intensity with the increase in the amount of fumed silica in the starting hydrothermal gel. The XRD patterns of FA1 and FA2 showed the appearance of peaks characteristic of zeolite ZSM-5 at 7.7, 8.9, 13.8, 14.6, 15.8, 23, 23.9, 24.4, 29, 29.7, 44.9 and 45.4° 2Θ. The intensity of zeolite ZSM-5 peaks increased from FA1 to FA2. The FA/fumed silica mass ratio used in this section resulted in a Si/Al molar ratio of 2.39, 3.29 and 4.80 in FA0, FA1 and FA2 respectively. ZSM-5 zeolite could be synthesised only at a Si/Al molar ratio at or above 3.2; however, quartz and mullite phases from fly ash were not fully converted and analcime which is a denser phase framework co-crystallised. The peaks of ZSM-5 zeolite obtained for FA1 and FA2 were similar to those of the ZSM-5 zeolite presented in the collection of simulated XRD powder patterns for zeolites (Treacy and Higgins, 2001). However, the presence of mullite, quartz and hematite mineral phases in FA1 and FA2 patterns led to the conclusion that not all the silicon and aluminium present in the hydrothermal gel was involved in the synthesis of ZSM-5 zeolite. It was deemed that the masses of the raw materials used should describe the

synthesis conditions of ZSM-5 zeolite from bulk fly ash better than the molar ratio of the different building elements such as silicon and aluminium in the hydrothermal gel. Furthermore, the Si/Al molar ratio of 3.29 and 4.80 in FA1 and FA2 respectively was actually too low to synthesise ZSM-5 zeolite if all the silicon and aluminium in FA had been involved in the synthesis, as ZSM-5 zeolite is a high silica zeolite and requires a Si/Al molar ratio above 10 (Jacob, 1998). Chareonpanich et al., (2004) synthesised ZSM-5 zeolite from Thailand lignite fly ash and silica extracted from rice husk ash as detailed in Section 2.4.2. However, their final product was a mixture of ZSM-5 and P zeolites with some non-identified peaks from the feedstock. Therefore, the addition of fumed silica in the current study was useful to compensate the unreacted silicon present in FA. Thus the most suitable FA/fumed silica mass ratio was considered to be 0.75:0.75 because of the increase in ZSM-5 product crystallinity. However, the participation of FA in the making of zeolite will be discussed in Section 4.4.3 and Section 4.4.5.

4.3.2. Effect of the amount of sodium hydroxide (NaOH)

Figure 4.5 presents the XRD patterns of the products FA2, FA3 and FA4 obtained by varying the mass of NaOH (0.25, 0.375 and 0.50 g) in the hydrothermal gel respectively. The amount of NaOH was varied to try to enhance the dissolution and mineralisation of the refractory quartz and mullite phases. Other parameters were kept constant: fly ash (0.75 g), fumed silica (0.75 g), tetrapropylammonium bromide (TPABr) (1 g), H_2O (15 mL), aging (room temperature, 2 h) and hydrothermal synthesis (160 °C, 72 h).

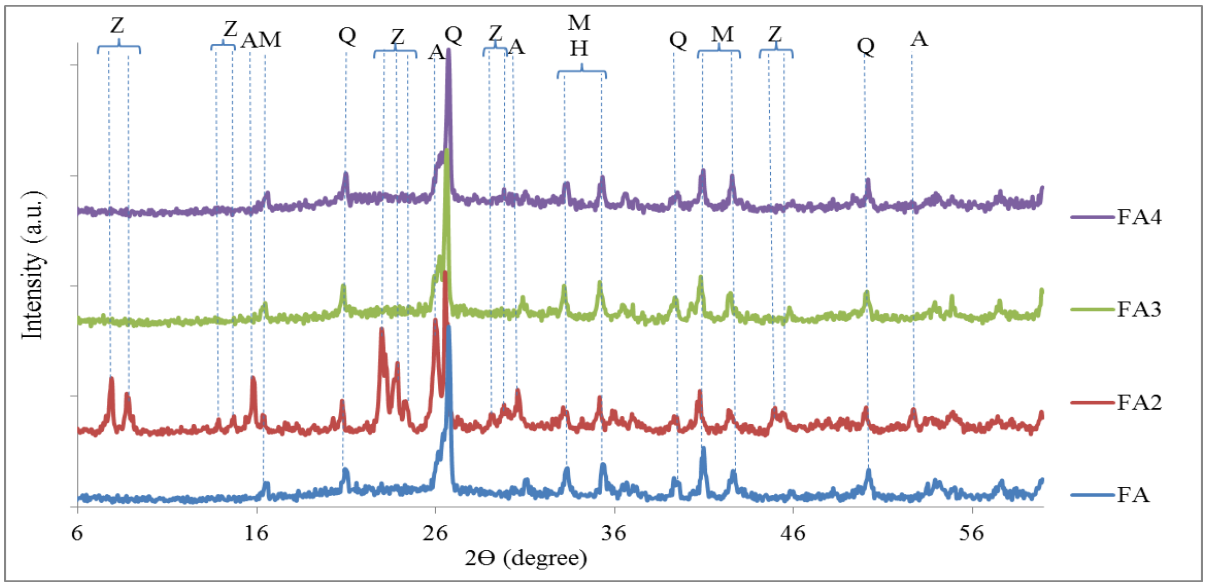

Figure 4.5: Effect of NaOH content on the XRD patterns of fly ash-based ZSM-5 zeolite samples FA2 (0.25 g), FA3 (0.375 g) and FA4 (0.50 g) (Z= ZSM-5 zeolite; A=analcime; M=mullite; Q=quartz; H=hematite).

Figure 4.5 showed that the characteristic peaks of ZSM-5 zeolite at 7.7, 8.9, 13.8, 14.6, 15.8, 23, 23.9, 24.4, 29, 29.7, 44.9 and 45.4° 2Θ were observed only for FA2. FA3 and FA4 presented the same patterns as FA with mullite, quartz and hematite as major mineral phases. However, it could be seen that the increase in the amount of the mineralising agent (NaOH) in the aluminosilicate gel prevented the formation of ZSM-5 zeolite. According to Moliner, (2011), the hydroxyl anion (OH^-) is the most used mineralising agent, as it increases the solubility of silicate or aluminosilicate species among others; however, it also affects the stability of organic structure directing agents at certain concentrations in the gel causing Hoffman degradation. Thus an excess of NaOH above 0.25 g was not advantageous to synthesise the targeted ZSM-5 zeolite.

4.3.3. Effect of the amount of tetrapropylammonium bromide (TPABr)

Figure 4.6 presents the XRD patterns of FA, FA2, FA5 and FA6. The synthesis conditions of FA2, FA5 and FA6 are detailed in Table 3.3. The amount of TPABr in FA2, FA5 or FA6 hydrothermal gel was 1.000, 1.375 or 1.500 g respectively. The TPABr content was varied to enhance the product quality. Other parameters remained constant: fly ash (0.75 g), fumed silica (0.75 g), NaOH (0.25 g), H_2O (15 mL), aging (room temperature, 2 h) and hydrothermal synthesis (160 °C, 72 h).

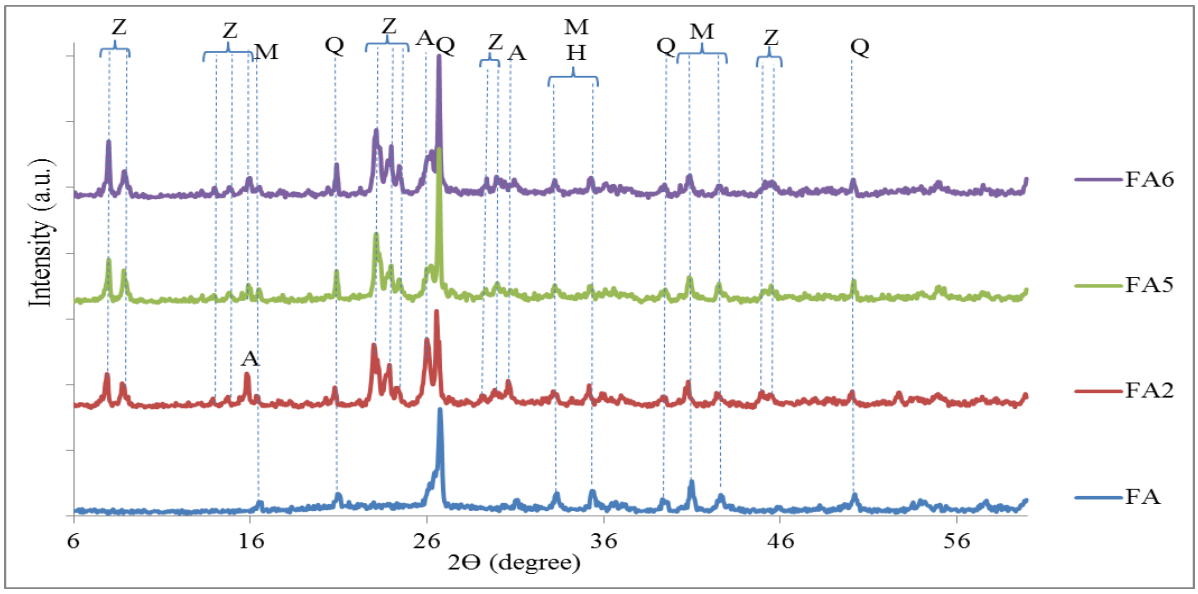

Figure 4.6: Effect of TPABr content on the XRD patterns of the synthesised ZSM-5 zeolite samples FA2 (1.000 g), FA5 (1.375 g) and FA6 (1.500 g) (Z= ZSM-5 zeolite; A=analcime; M=mullite; Q=quartz; H=hematite).

Figure 4.6 compared the XRD patterns of FA, FA2, FA5 and FA6 showing the mineralogical changes induced by the variation of the amount of TPABr in the starting aluminosilicate gel. FA2, FA5 and FA6 presented the characteristics peaks of ZSM-5 zeolite at 7.7, 8.9, 13.8, 14.6, 15.8, 23, 23.9, 24.4, 29, 29.7, 44.9 and 45.4° 2Θ. However, it could be observed that analcime peaks present in FA2 at 16, 26.5 and 30.5° 2Θ disappeared in FA5 and FA6. Furthermore, the characteristic quartz peaks from the fly ash were still present in FA5 and FA6 at 20.9 and 26.8° 2Θ. Moreover, characteristic ZSM-5 peaks of FA5 and FA6 increased in intensity and decreased in linewidth at 7.7, 8.9° 2Θ. According to Drzajet at., (2011), the decrease in linewidth may be due to aluminium enrichment in the edge of the crystals, which leads to the possible change in unit cell, decrease of aluminium per unit cell and an increase in crystallinity. The optimum amount of TPABr in the formulated hydrothermal gel was deemed to be 1.5 g as less analcime co-crystallised and the product purity was enhanced.

4.3.4. Effect of water content

Figure 4.7 presents XRD patterns of FA, FA2 and FA7 and shows the mineralogical changes induced by varying the water content in the starting aluminosilicate gel. The synthesis conditions of FA2 and FA7 are detailed in Table 3.3. Water content was varied to further enhance the product quality without needing to add TPABr which is expensive. The volume of water used in the aluminosilicate gel was 15 or 20 mL for FA2 or FA7. Other

parameters remained constant: fly ash (0.75 g), fumed silica (0.75 g), tetrapropylammonium bromide (1 g), NaOH (0.25 g), aging (room temperature, 2 h) and hydrothermal synthesis (160 °C, 72 h).

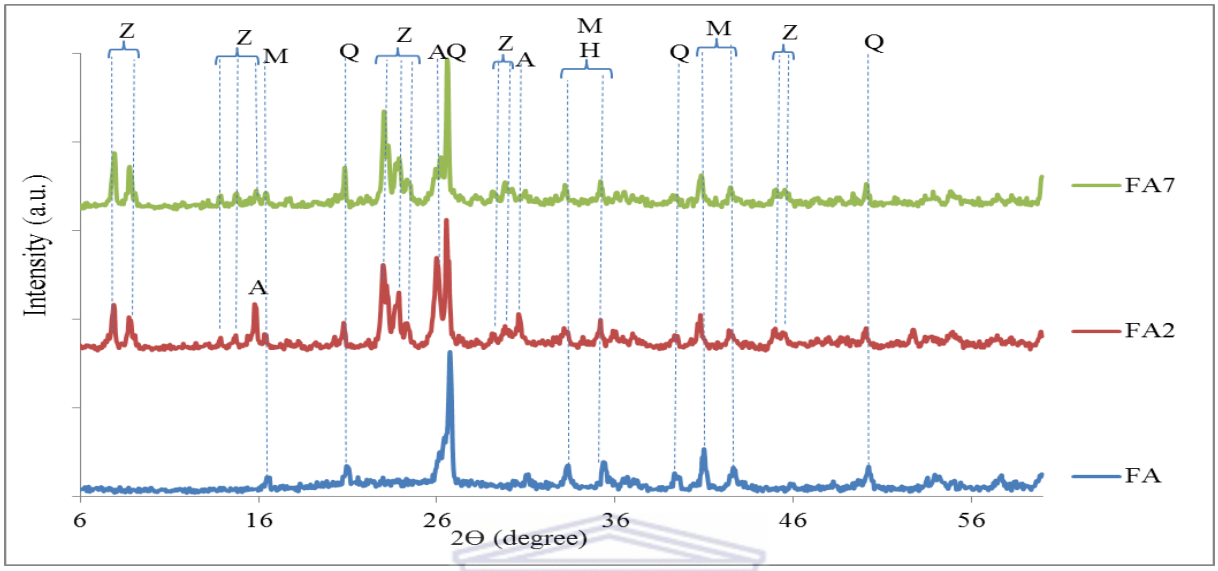

Figure 4.7: Effect of water content on the XRD patterns of the synthesised ZSM-5 zeolite samples FA2 (15 mL) and FA7 (20 mL) (Z= ZSM-5 zeolite; A=analcime; M=mullite; Q=quartz; H=hematite).

Figure 4.7 showed that the increase in water in the formulation produced the same effect as the increase in TPABr (Figure 4.6) with the disappearance of the analcime peaks at 16, 26.5 and 30.5° 2Θ and the decrease in linewidth of ZSM-5 peaks at 7.7, 8.9 and 23° 2Θ. Water content was varied to see if it was possible to enhance the product quality without needing to add more TPABr which is expensive. Hence, it could be concluded that the increase in water content also contributed to the increase of the zeolite purity; as was reported by Guth et al., (1999) that water helps the mineralizing agent to dissolve silicon and aluminium needed for the zeolite crystallisation and can also act as template. Kirov and Filizova, (2012) also reported that water molecules play an important role in the synthesis of zeolites by interacting with extra-framework cations and the framework oxygen bound to aluminium, and stabilising larger channels and cavities of the zeolite structures. So the increase in water content in the hydrothermal gel had a positive effect on the product quality and there was no need to add more TPABr in the hydrothermal gel. The optimum volume of water in the hydrothermal gel was deemed to be 20 mL.

4.3.5. Parameter variation during the aging step

This section presents the effect of the aging time and temperature of the hydrothermal gel on the mineralogical phase purity of fly ash-based ZSM-5 zeolite samples.

4.3.5.1. Effect of the aging time

Figure 4.8 presents the XRD patterns of FA and ZSM-5 zeolite samples FA2, FA8 and FA9 which were obtained when the aging time was 2, 6 or 12 h respectively. The pre-synthesis aging time was varied to investigate whether longer times would enhance the dissolution of quartz and mullite. The rest of the parameters remained constant: fly ash (0.75 g), fumed silica (0.75 g), tetrapropylammonium bromide (1 g), NaOH (0.25 g), volume of water (15 mL), aging temperature (room temperature) and hydrothermal synthesis (160 °C, 72 h).

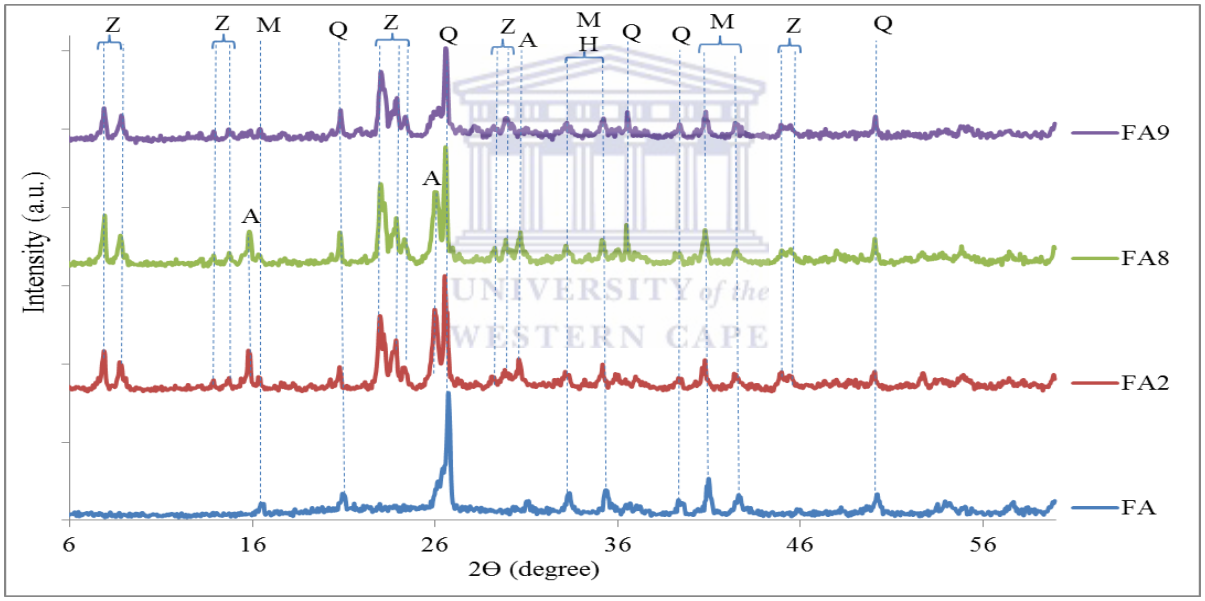

Figure 4.8: Effect the aging time on the XRD patterns of the synthesised zeolites FA2 (2 h), FA8 (6 h) and FA9 (12 h) (Z=ZSM-5 zeolite; A=analcime; M=mullite; Q=quartz; H=hematite).

It could be observed that ZSM-5 zeolite was synthesised after extending the aging time prior to synthesis for 2 h (FA2), 6 h (FA8) or 12 h (FA9) (Figure 4.8). Mullite, quartz and hematite mineral phases were present in both starting material (FA) and final products (FA2, FA8 and FA9). The increase in the aging time induced the progressive disappearance of the peaks that characterised the analcime phase at 16, 26.5, 30.5, 35.5 and 53° 2Θ, but did not affect the

quartz and mullite impurities. Increasing the aging time improved the product phase purity since less analcime formed and the most suitable aging time was 12 h.

4.3.5.2. Effect of the aging temperature

Figure 4.9 presents the XRD patterns of FA, FA2 and FA10, showing the mineralogical changes induced by the variation of the aging temperature in order to try to reduce the quartz phase. FA2 and FA10 were synthesised after aging the aluminosilicate gel either at room temperature (20 °C) or at 60 °C respectively and the rest of the parameters remained constant: fly ash (0.75 g), fumed silica (0.75 g), tetrapropylammonium bromide (1 g), NaOH (0.25 g), volume of water (15 mL), aging time (2 h) and hydrothermal synthesis (160 °C, 72 h).

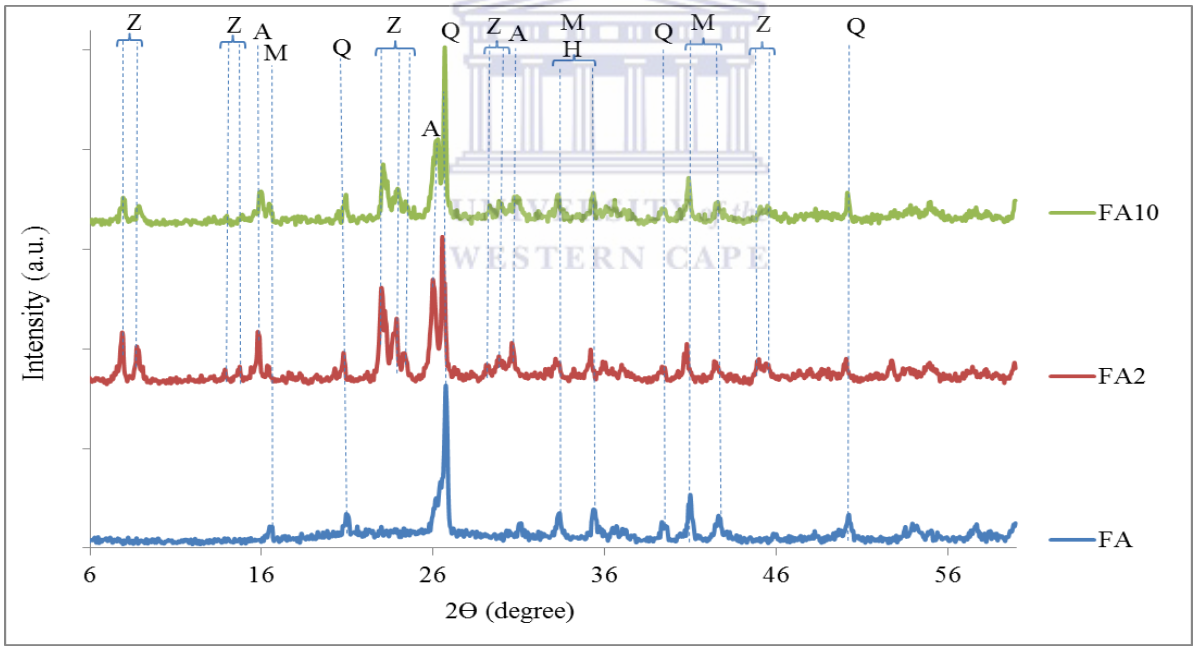

Figure 4.9: Effect of the aging temperature on the XRD patterns of fly ash-based zeolites FA2 (20 °C) and FA10 (60 °C) (Z=ZSM-5 zeolite; A=analcime; M=mullite; Q=quartz; H=hematite).

Figure 4.9 showed that ZSM-5 zeolite could be synthesised after aging of the aluminosilicate gel at room temperature as well as at 60 °C. The increase in the aging temperature was accompanied by the decrease of the intensity of peaks that characterized analcime at 16, 26.5, 30.5° 2Θ and ZSM-5 zeolite at 7.7, 8.9, 13.8, 14.6, 15.8, 23, 23.9, 24.4, 44.9 and 45.4° 2Θ,

but quartz impurities remained, hence an increase in aging temperature was not deemed beneficial to the product quality and the most suitable aging temperature was considered to be room temperature (20 °C).

4.3.6. Parameter variation during the hydrothermal synthesis

This section presents the effect of the hydrothermal synthesis time and temperature on the fly ash-based ZSM-5 zeolite product.

4.3.6.1. Effect of the hydrothermal synthesis time

Figure 4.10 presents the XRD patterns of FA, FA2, FA11, FA12 and FA13. The time of hydrothermal synthesis of FA2, FA11, FA12 or FA13 was 72, 48, 24 or 12 h which were varied in order to reduce phase impurities. The rest of the parameters were kept constant: fly ash (0.75 g), fumed silica (0.75 g), tetrapropylammonium bromide (1 g), NaOH (0.25 g), volume of water (15 mL), aging (room temperature, 2 h) and hydrothermal synthesis temperature (160 °C).

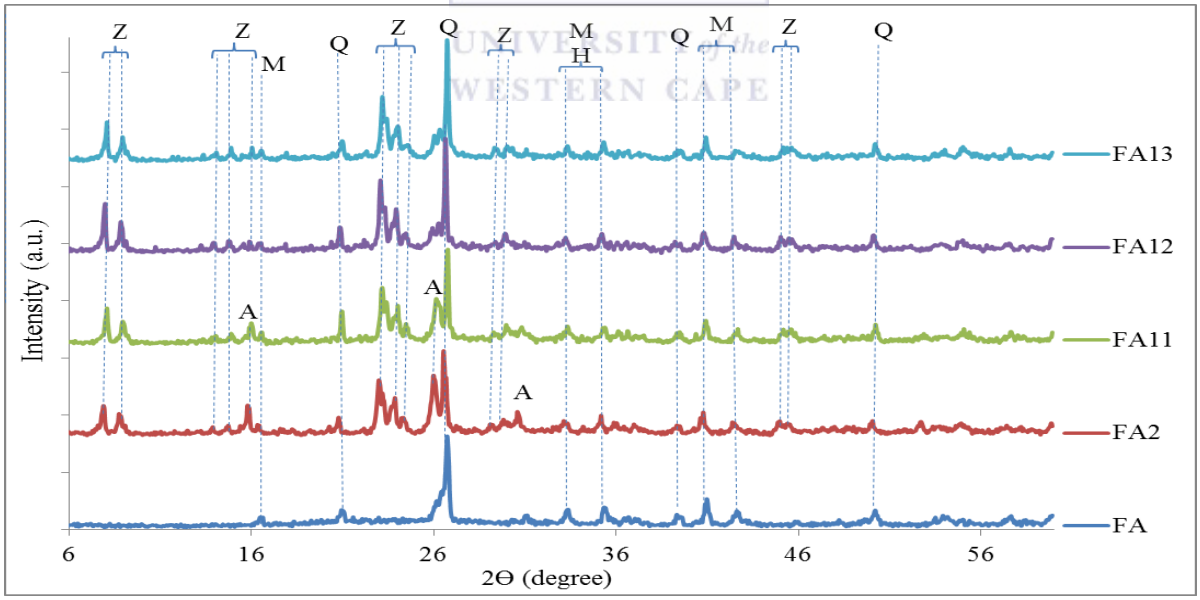

Figure 4.10: Effect of the hydrothermal synthesis time on the XRD patterns of synthesised zeolites FA2 (72 h), FA11 (48 h), FA12 (24 h) and FA13 (12 h) (Z=ZSM-5 zeolite; A=analcime; M=mullite; Q=quartz; H=hematite).

Figure 4.10 showed that ZSM-5 zeolite with the characteristic peaks at 7.7, 8.9, 13.8, 14.6, 15.8, 23, 23.9, 24.4, 29, 29.7, 44.9 and 45.4° 2Θ was synthesised from the synthesis conditions applied for FA2, FA11, FA12 or FA13. Quartz, mullite and hematite phases were still present after the synthesis indicating that not all the Si and Al in the feedstock was involved in the synthesis of ZSM-5 zeolite. The analcime phase (16, 26.5, 30.5, 35.5 and 53° 2Θ) gradually increased with the increase in hydrothermal synthesis time, hence longer synthesis times promoted denser phases to form by Ostwald ripening. The increase in hydrothermal synthesis time was also accompanied with the decrease in intensity of characteristic ZSM-5 zeolite peaks at 7.7, 8.9, 23, 23.9 and 24.4° 2Θ as well as a characteristic peak of quartz at 26.5° 2Θ. Thus, the most suitable hydrothermal synthesis time was deemed to be between 12 and 24 h.

4.3.6.2. Effect of the hydrothermal synthesis temperature

Figure 4.11 presents the XRD patterns of FA2, FA14 and FA15. The synthesis conditions of FA2, FA14 and FA15 are presented in Table 3.3. The hydrothermal synthesis temperature of FA2, FA14 or FA15 was 160 °C, 140 °C or 120 °C respectively in order to further reduce the input energy, while other parameters remained constant: fly ash (0.75 g), fumed silica (0.75 g), tetrapropylammonium bromide (1 g), NaOH (0.25 g), volume of water (15 mL), aging (room temperature, 2 h) and hydrothermal synthesis time (72 h).

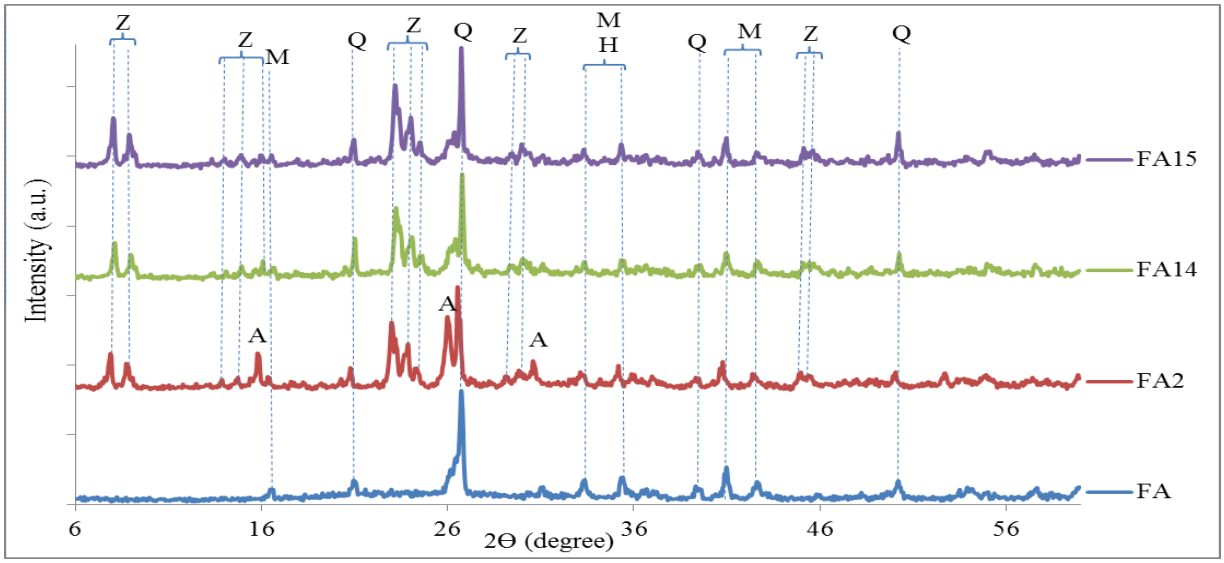

Figure 4.11: Effect of the hydrothermal synthesis temperature on the XRD patterns of the synthesised zeolites FA2 (160 °C), FA14 (140 °C) and FA15 (120 °C) (Z=ZSM-5 zeolite; A=analcime; M=mullite; Q=quartz; H=hematite).

A decrease in the hydrothermal synthesis temperature induced the same effect as was observed for a decrease in the hydrothermal synthesis time with the disappearance of the characteristic peaks of analcime and the increase in intensity of characteristic peaks of ZSM-5 zeolite and quartz. Thus reducing the synthesis temperature resulted in a ZSM-5 phase quality improvement and lower input energy. The most suitable hydrothermal synthesis temperature was deemed to be 120 °C.

4.3.7. Suitable conditions for the synthesis of ZSM-5 zeolite from the as-received fly ash

The variation of the chemical parameters (fly ash, fumed silica, NaOH, TPABr and water) involved in the synthesis of ZSM-5 zeolite from the as-received fly ash (FA) (Table 3.3) allowed plotting the ternary diagrams below using Origin Pro 8 software. Figure 4.12 presents the ternary diagrams of the mole fractions of the different chemical species involved in the synthesis of ZSM-5 zeolite from FA. Figure 4.13 presents the ternary diagrams of the mass fraction of the raw materials and chemicals used in the synthesis.

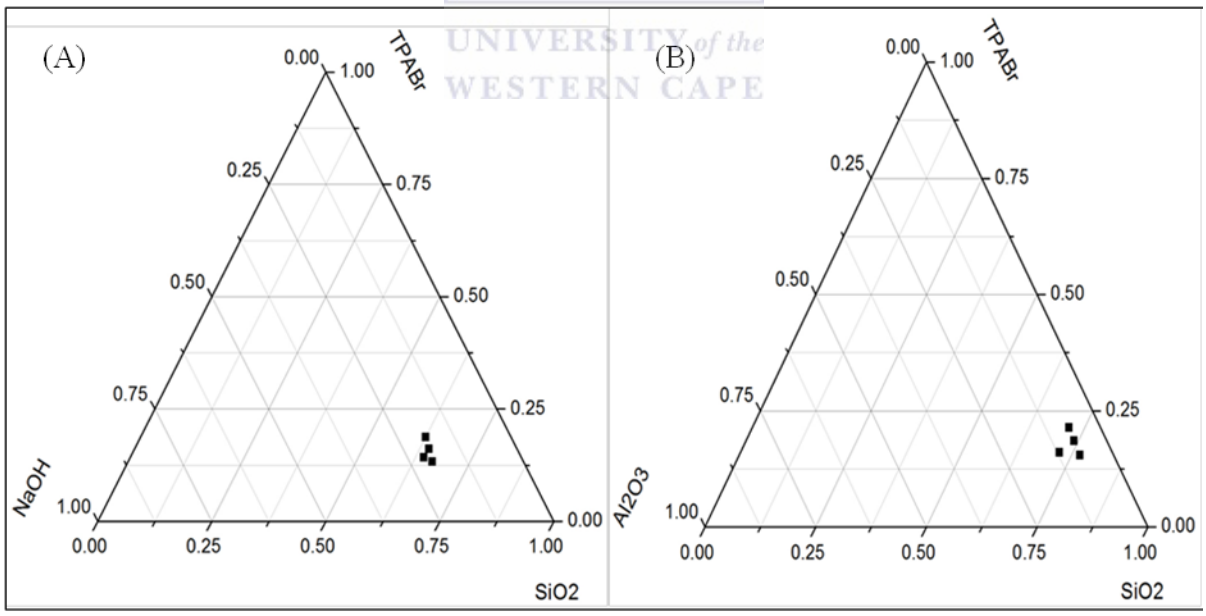

Figure 4.12: Mole fraction ternary diagrams of NaOH, SiO_2 and TPABr (A) and Al_2O_3, SiO_2 and TPABr (B) that were involved in the synthesis of ZSM-5 zeolite from FA, V(H2O)=15 mL.

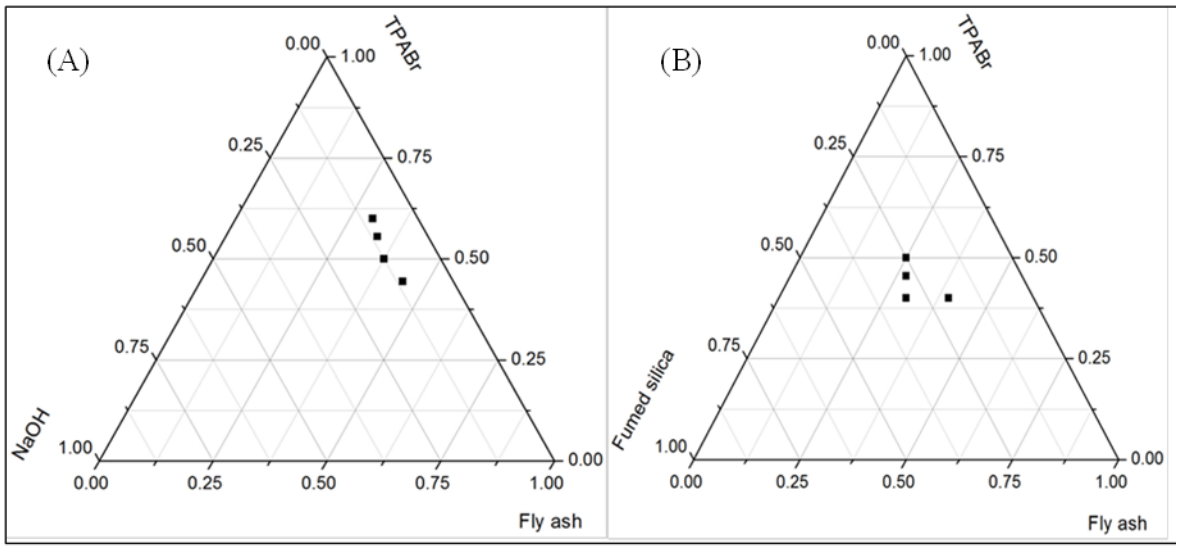

Figure 4.13: Mass fraction ternary diagram of NaOH, fly ash and TPABr (A) and fumed silica, fly ash and TPABr (B) that were used in the synthesis of ZSM-5 zeolite from FA, V(H2O)=15 mL.

Figures 4.12 and 4.13 summarised chemical conditions in which ZSM-5 zeolite was synthesised from FA. Figure 4.12 (A and B) presented the mole fractions of SiO_2, NaOH, Al_2O_3 and TPABr that led to the synthesis of ZSM-5 zeolite from the aging and hydrothermal crystallisation conditions applied in this study. Looking at the XRD results presented in the sections above, it could be observed that in addition to ZSM-5 zeolite phase the final products contained quartz, mullite and hematite phases of the starting material (FA). Thus not all the silica and alumina present in FA were involved in the synthesis of ZSM-5 zeolite, as quartz is made of SiO_2 and mullite is made of SiO_2 and Al_2O_3 (Elmas et al., 2013). The amount of the mineralizing agent (NaOH) that was used in the synthesis conditions presented in Table 3.3 was not able to dissolve all the SiO_2 and Al_2O_3 contained in FA. It was possible for some of the available SiO_2 and Al_2O_3 to be sequestrated in the FA quartz and mullite and did not participate in the reaction. These fractions of SiO_2 and Al_2O_3 should not be taken into consideration while plotting ternary diagrams. Hence, it was not proper to present these synthesis conditions in terms of molar regime as was summarised in Figure 4.12. The synthesis conditions were better represented by the ternary diagrams of mass fractions in Figure 4.13, as this gave the range for ZSM-5 formation in term of masses of actual raw materials and chemicals used.

Besides the fact that not all the SiO_2 or Al_2O_3 present in FA was involved in the synthesis of ZSM-5 zeolite, the Si/Al molar ratio of 1.86 in FA was too low for the synthesis of ZSM-5 zeolite that is a high silica zeolite. Therefore, an extra source of SiO_2 (fumed silica) was needed to adjust the Si/Al molar ratio. The most suitable synthesis conditions were: 0.75 g of FA, 0.75 g of fumed silica, 0.25 g of NaOH, 1.5 g of TPABr, 20 mL of deionised , aging (12 h and 20 °C) and hydrothermal synthesis (24 h and 120 °C). On the one hand, the increase in TPABr, deionised water content and aging time led to the disappearance of the analcime phase and improvement of the ZSM-5 product quality. On the other hand, the decrease in the hydrothermal synthesis time and temperature also improved the quality of the product. It is possible that mainly the fumed silica dissolution resulted in ZSM-5 phase formation as it appeared that the FA was mostly not well mineralised but as quantification of the mineral phases was not done this was difficult to assess.

4.4. Effect of the structure directing agent on the properties of ZSM-5 zeolite synthesised from the as-received fly ash

The ZSM-5 zeolite products discussed in this section were synthesised as follows: 0.75 g of as-received fly ash (FA), 0.75 g fumed silica, 0.25 g of NaOH, 1 g of TPABr and 20 mL of de-ionised water. However, the time and temperature of the hydrothermal synthesis were kept to 72 h and 160 °C respectively for Chapter 4, Chapter 5 and Chapter 6 of this study in order to compare the properties of all the synthesised zeolite products on the same basis as that commonly used in the literature. Furthermore, tetrapropylammonium bromide (TPABr) was substituted by 1,6-hexanediamine (HDA) or 1-propylamine (PA) in the hydrothermal gel in order to investigate the effect of the structure directing agent on the chemical and physical properties of the fly ash-based ZSM-5 zeolite samples as well as their catalytic applications. It was noteworthy to mention that 1 g of each structure directing agent (TPABr, HDA or PA) corresponded to different numbers of moles as was shown in the molar regime of FA-TPABr, FA-HDA and FA-PA (Table 3.4). The synthesised zeolites samples (FA-TPABr, FA-HDA and FA-PA) were subsequently transformed to their H-form using a NH_4NO_3 solution and treated with a saturated oxalic acid solution as detailed in Section 3.3.1.1. The properties of the acid oxalic treated ZSM-5 products H-FA-TPABr-OA, H-FA-HDA-OA and H-FA-PA-OA were compared using XRD, SEM, FTIR, Brønsted acidity and ^{27}Al NMR analyses. The post-synthesis treatment of fly ash-based ZSM-5 zeolite products (H-FA-TPABr, H-FA-HDA and H-FA-PA) with oxalic acid was motivated by the fact that Yan et al., (2003) reported the

transformation of H-Y zeolite into USY zeolite using different concentrations of oxalic acid solution, which extracted a certain amount of Al and enhanced the catalytic efficiency of the obtained zeolite.

4.4.1. Mineralogical study of the oxalic acid treated zeolite products H-FA-TPABr-OA, H-FA-HDA-OA and H-FA-PA-OA by X-ray Diffraction

Figure 4.14 presents the results of the qualitative XRD analysis of FA, the oxalic acid treated fly ash-based zeolite ZSM-5 products H-FA-TPABr-OA, H-FA-HDA-OA and H-FA-PA-OA compared to a commercial H-ZSM-5 zeolite (Com-ZSM-5). The revised synthesis conditions of FA-TPABr, FA-HDA and FA-PA were: 0.75 g of FA, 0.75 g fumed silica, 0.25 g of NaOH, 1 g of the structure directing agent (TPABr, HDA or PA), 20 mL of deionised water, aging (6 h, room temperature) and hydrothermal synthesis (72 h, 160 °C). After the synthesis, FA-TPABr, FA-HDA and FA-PA were transformed to their H-form by treating them with 0.5 M of NH_4NO_3 solution four times followed by calcination and treated with a saturated oxalic acid solution followed by calcination as detailed in Section 3.3.1.1. The calcination of oxalic acid treated ZSM-5 zeolite products H-FA-TPABr-OA, H-FA-HDA-OA and H-FA-PA-OA was performed in order to remove the remaining oxalic acid in their framework. It was noteworthy that the use of 1 g TPABr, HDA or PA corresponded to different moles used in the molar regime of FA-TPABr, FA-HDA and FA-PA as shown (Table 3.4).

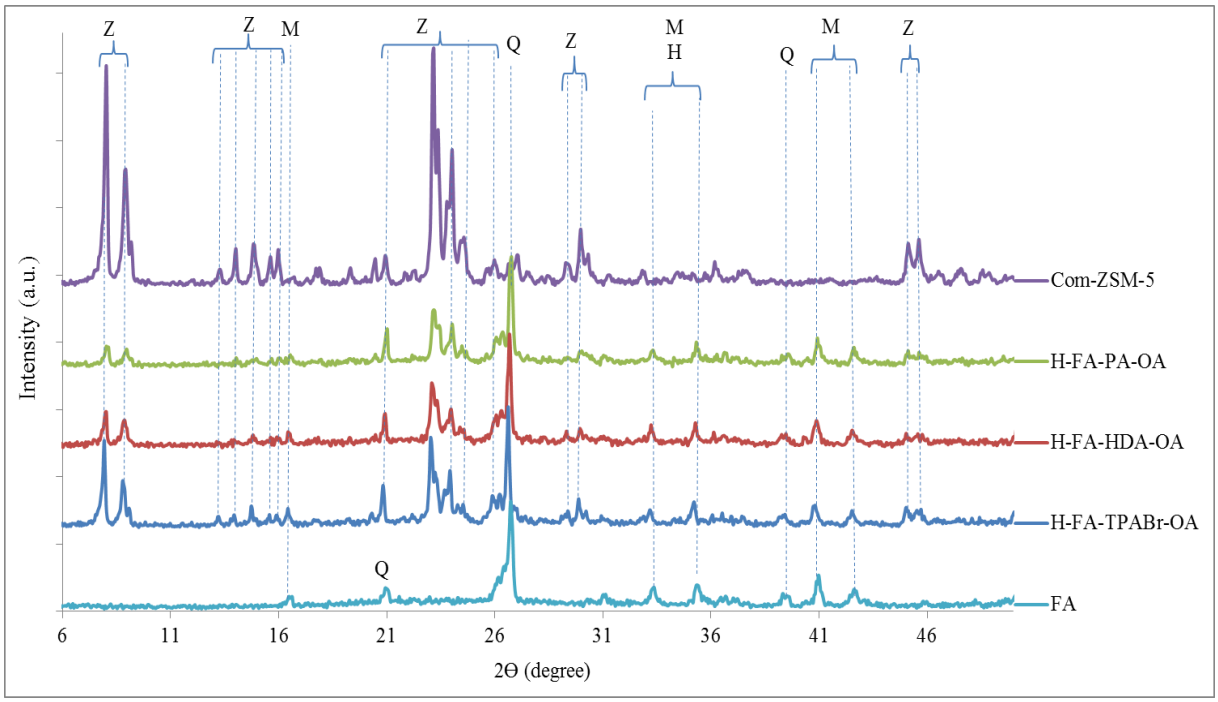

Figure 4.14: Comparison of XRD patterns of FA, oxalic acid treated zeolites H-FA-TPABr-OA, H-FA-HDA-OA and H-FA-PA-OA, with a commercial H-ZSM-5 (Com-ZSM-5) as reference (Z=ZSM-5 zeolite, M=mullite, Q=quartz, H=hematite).

Figure 4.14 showed that FA was mainly composed of mullite, quartz, hematite and amorphous phases as previously discussed in section 4.2, Figure 4.1. The XRD patterns of the oxalic acid treated ZSM-5 zeolite products H-FA-TPABr-OA, H-FA-HDA-OA and H-FA-PA-OA showed the presence of the characteristic peaks of ZSM-5 zeolite at 7.7, 8.9, 12.5, 13.8, 14.6, 14.9, 15.8, 21.2, 23, 23.9, 24.4, 25.6, 29, 29.7, 44.9 and 45.4° 2Θ as confirmed by the XRD patterns of the commercial ZSM-5 zeolite and the collection of simulated XRD powder patterns for zeolites (Treacy and Higgins, 2001). The characteristic peaks of mullite, quartz and hematite phases of FA could be seen in H-FA-TPABr-OA, H-FA-HDA-OA and H-FA-PA-OA. It was noteworthy that the use of the revised synthesis formulation of FA-TPABr, FA-HDA and FA-PA according to the most suitable parameters discussed in section 4.3.7 led to the disappearance of the dense analcime phase in the final ZSM-5 products (H-FA-TPABr-OA, H-FA-HDA-OA and H-FA-PA-OA).

Querol et al., (2002) reported that the conversion efficiency of fly ash into zeolites depends on the content of non-reactive phases such as hematite and the resistant aluminium-silicate phases such as mullite and quartz. The dissolution rate of Al- and Si-bearing phases is: glass>quartz>mullite. In addition, the complex composition of FA makes it difficult to monitor the effect of each of its components in the synthesis of ZSM-5 zeolite, and this in

agreement with Vassilev et al., (2003), who stated that the complex composition of bulk FA limits its potential utilisation in many fields because of the difficulty to relate an observed effect or result to a particular component. Chareonpanich et al., (2004) reported the synthesis ZSM-5 zeolite mixed with P zeolite and some unidentified mineral phases using a fly ash which was mainly amorphous in nature and silica extracted from rice husk ash as detailed in section 2.4.2.

Figure 4.15 presents the calculated ZSM-5 relative XRD crystallinity of the acid oxalic treated zeolite ZSM-5 products H-FA-TPABr-OA, H-FA-HDA-OA and H-FA-PA-OA with a commercial H-ZSM-5 as a reference. The calculation of the ZSM-5 relative XRD crystallinity was adopted from the formulation suggested by Nicolaides, (1999):

$$Relative\_XRD\_crystallinity = \frac{\sum peak\_intensities\_of\_ZSM5\_in\_the\_sample}{\sum peak\_intensities\_of\_the\_reference} * 100$$

(Equation 4.1)

OriginPro 8 software was used to measure the ZSM-5 peak intensities at 7.7, 8.9, 21.2, 23, 23.9, 29.7, 44.9 and 45.4 ° 2Ɵ.

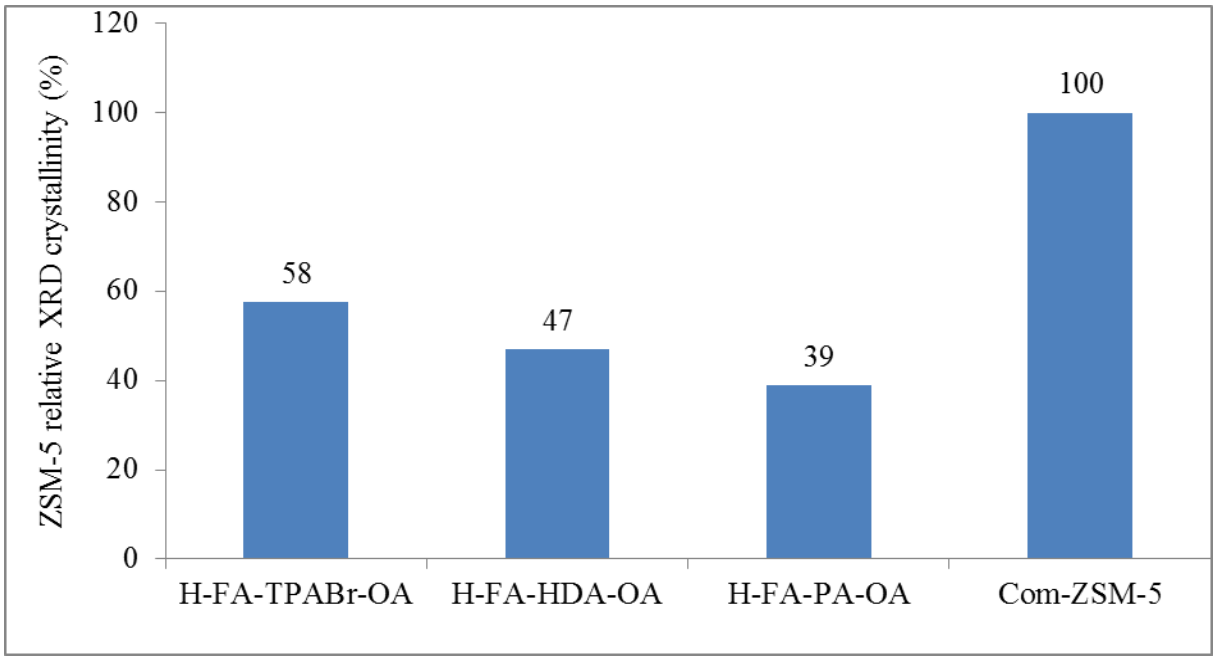

Figure 4.15: Calculated ZSM-5 relative XRD crystallinity of the oxalic acid treated zeolite ZSM-5 products H-FA-TPABr-OA, H-FA-HDA-OA and H-FA-PA-OA compared to commercial H-ZSM-5 (Com-ZSM-5).

The templating potency of TPABr, HDA and PA on the zeolite crystallinity was thus quantified and Figure 4.15 showed that the ZSM-5 relative crystallinity of H-FA-TPABr-OA, H-FA-HDA-OA and H-FA-PA-OA was 58, 47 and 39 % respectively. It was noteworthy that the use of TPABr as structure directing agent led to the highest relative crystallinity despite the small molar amount used compared to HDA and PA (see Table 3.4). According to Petrik et al., (1995), the choice of template in the synthesis of ZSM-5 zeolite plays an important role in ensuring an achievement of high percentage crystallinity. Van der Gaag, (1987) reported that the strength of the template in forming ZSM-5 zeolite decreases in an order: TPABr>HDA>PA, which in agreement with the results presented in Figure 4.15.

4.4.2. Morphological analysis of the oxalic acid treated zeolite products H-FA-TPABr-OA, H-FA-HDA-OA and H-FA-PA-OA by Scanning Electron Microscopy

Figure 4.16 compares the scanning electron microscopy (SEM) micrographs of FA, oxalic acid treated zeolite products H-FA-TPABr-OA, H-FA-HDA-OA and H-FA-PA-OA to that of a commercial H-ZSM-5. FA-TPABr, FA-HDA and FA-PA that were synthesised using the revised synthesis conditions as shown in Section 4.4.1, were transformed to their H-form through treatment with NH_4NO_3 and calcination, and treated with a saturated oxalic acid solution and calcination to obtain H-FA-TPABr-OA, H-FA-HDA-OA and H-FA-PA-OA (Section 3.3.1.1). H-FA-TPABr-OA, H-FA-HDA-OA and H-FA-PA-OA were analysed using the SEM.

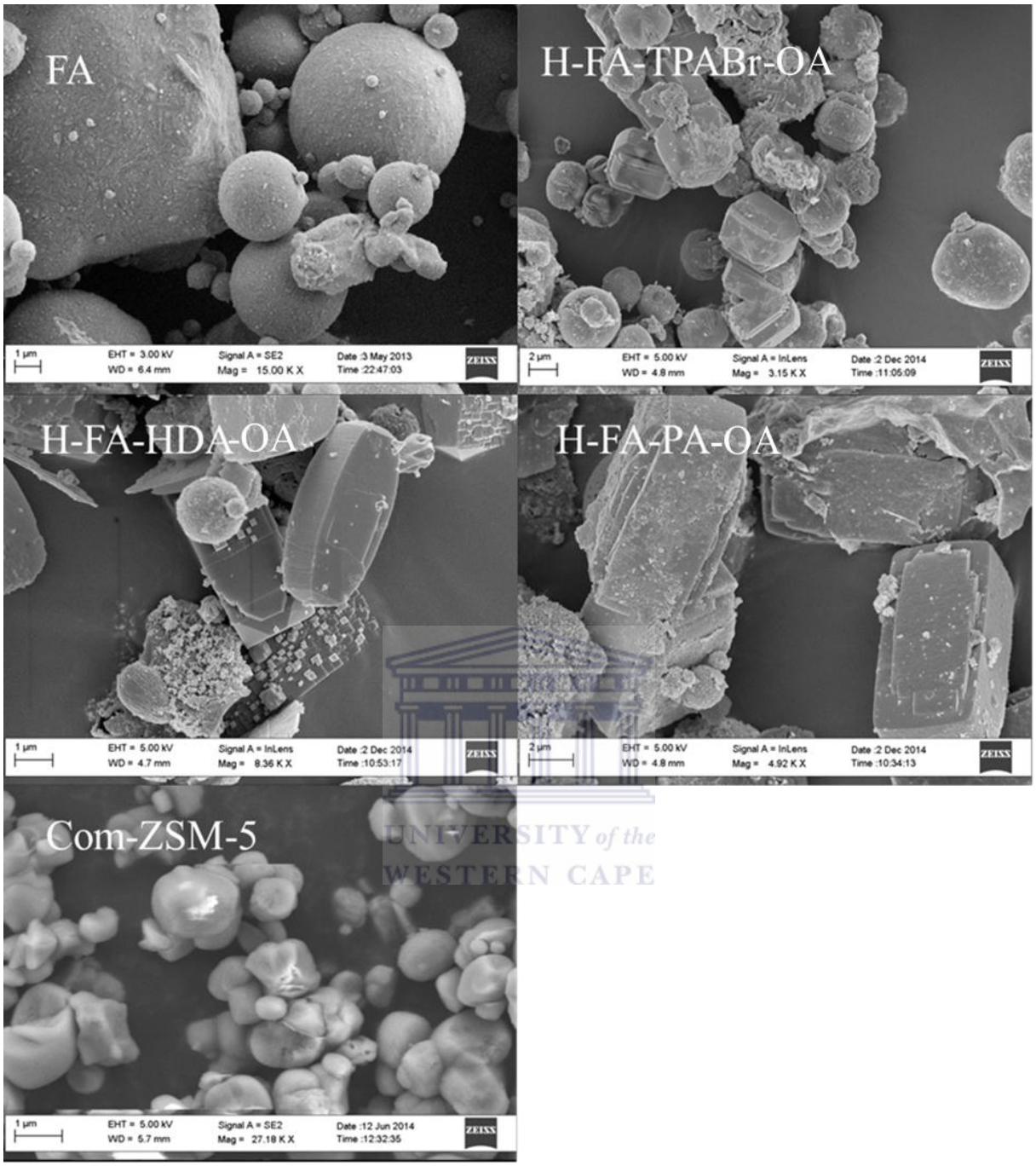

Figure 4.16: SEM micrographs of the as-received FA, H-FA-TPABr-OA, H-FA-HDA-OA and H-FA-PA-OA and commercial H-ZSM-5 (Com-ZSM-5).

The SEM image of the as-received fly ash (FA) was discussed in Section 4.2. It could be observed in Figure 4.16 that the zeolite ZSM-5 crystals in H-FA-TPABr-OA, H-FA-HDA-OA and H-FA-PA-OA samples had various morphologies different from FA particles. H-FA-TPABr-OA and commercial H-ZSM-5 crystals were spherulitic. The crystals of H-FA-HDA-OA or H-FA-PA-OA were described as lath-shaped particles by Petrik et al., (1995) or coffin-

shaped particles by Ohrman, (2005). H-FA-PA-OA and H-FA-HDA-OA particles were larger than H-FA-TPABr-OA particles. The transformation of the FA feedstock into ZSM-5 zeolite crystals was not complete as amorphous material is visible in all fly ash-based ZSM-5 zeolite images. However, this amorphous material could be more visible in the SEM micrographs if H-FA-TPABr-OA, H-FA-HDA-OA and H-FA-PA-OA were not treated subsequently with NH_4NO_3 and saturated oxalic acid solutions. Petrik et al, (1995) investigated the influence of TPABr and HDA on the morphology of ZSM-5 zeolite crystals and reported that the use of TPABr or HDA as structure directing agent led to the formation of spherulitic or lath-shaped crystals, which corroborated the results presented in Figure 4.16. Van der Gaag (1987) also reported that the morphology of ZSM-5 changed from particles without crystalline appearance to well-crystallised samples in the order: TPABr<HDA<PA, this is in agreement with the SEM images presented in Figure 4.16. Figure 4.17 gives the mean crystal size of H-FA-TPABr-OA, H-FA-HDA-OA, H-FA-PA-OA and the commercial H-ZSM-5. The size of H-FA-TPABr-OA, H-FA-HDA-OA and H-FA-PA-OA crystals was determined using the Image J software and the mean size of 20 crystals for each sample was calculated as follows:

$$M = \frac{\sum_{i=1}^{n} x_i}{n} \quad \textbf{(Equation 4.2)}$$

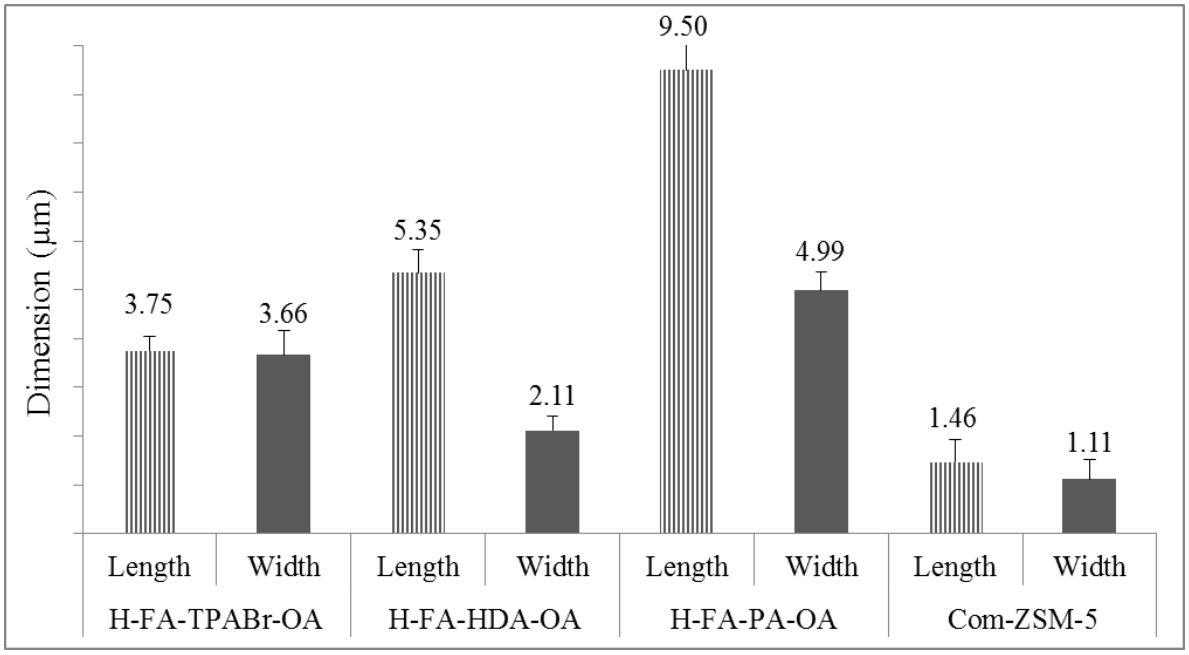

Figure 4.17: Mean ZSM-5 crystal length and width of H-FA-TPABr-OA, H-FA-HDA-OA, H-FA-PA-OA and a commercial H-ZSM-5 (Com-ZSM-5).

Figure 4.17 showed that H-FA-PA-OA crystals had the highest length and width (9.50±0.91 by 4.99±0.37 µm), followed by H-FA-HDA-OA (5.35±0.0.48 by 2.11±0.29 µm) and H-FA-TPABr-OA (3.75±0.28 by 3.66±0.49 µm). The length and width of the commercial H-ZSM-5 crystals were 1.46±0.47 by 1.11±0.42 µm. It was noteworthy that the size of the fly ash-based ZSM-5 zeolite crystals was inversely proportional to the size of the structure directing agent used.

4.4.3. Structural analysis of the oxalic acid treated H-FA-TPABr, H-FA-HDA and H-FA-PA by Fourier transform infrared

The framework vibrations of FA, the oxalic acid treated fly ash-based zeolite products H-FA-TPABr-OA, H-FA-HDA-OA and H-FA-PA-OA were compared to that of a commercial H-ZSM-5 (Com-ZSM-5) by FTIR analysis (Figure 4.18). FA-TPABr, FA-HDA and FA-PA were synthesised using the revised formulation presented in Section 4.4.1. After synthesis, FA-TPABr, FA-HDA and FA-PA were transformed in their H-form by treatment with NH_4NO_3 and calcination, then after they were treated with oxalic acid solution and calcination prior to the FTIR analysis. The as-received fly ash (FA), the oxalic acid treated fly ash-based zeolite products H-FA-TPABr-OA, H-FA-HDA-OA and H-FA-PA-OA or commercial H-ZSM-5 (Com-ZSM-5) were prepared as detailed in Section 3.4.3 and their FTIR spectra were recorded using Perkin Elmer spectrum 100 FT-IR spectrometer.

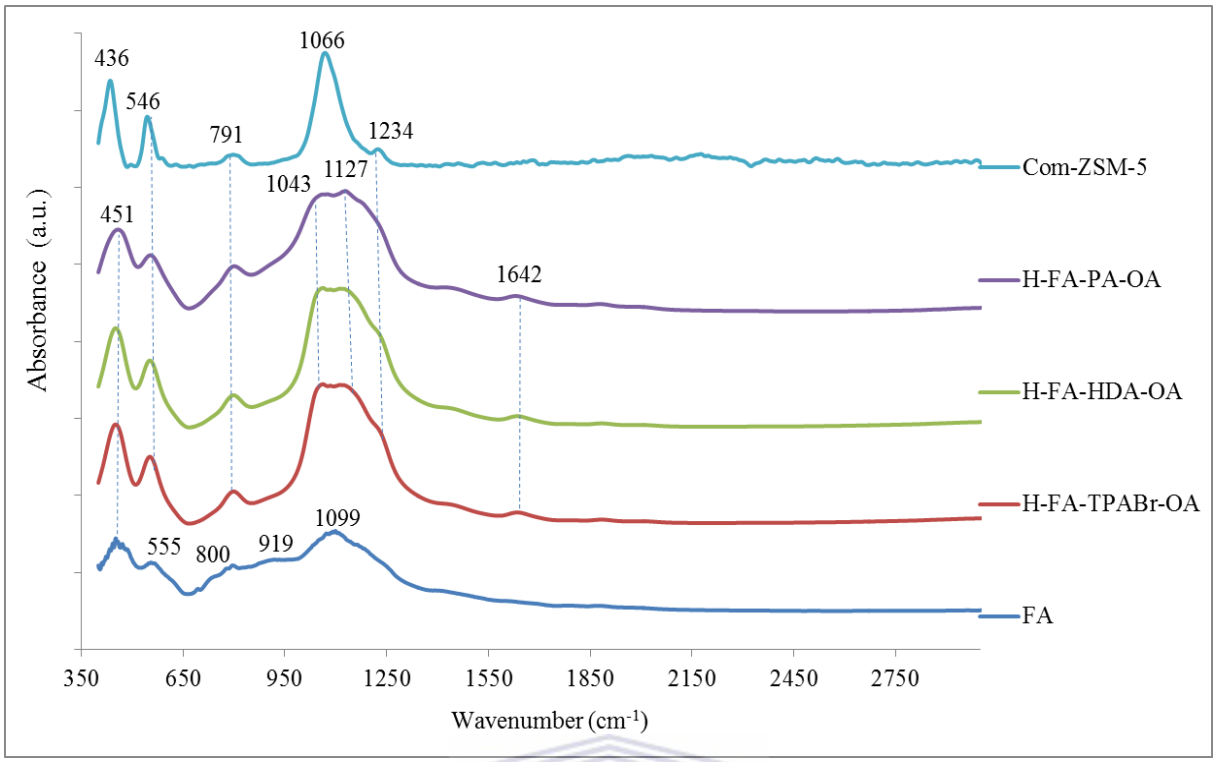

Figure 4.18: Comparison of the FTIR spectra of FA, H-FA-TPABr-OA, H-FA-HDA-OA and H-FA-PA-OA with a commercial H-ZSM-5 (Com-ZSM-5) as reference.

The FTIR spectrum of the as-received fly ash (FA) was discussed in section 4.2. The FTIR spectra of H-FA-TPABr-OA, H-FA-HDA-OA and H-FA-PA-OA in Figure 4.18 presented characteristic bands of ZSM-5 at 451, 546, 791, 1043, 1127 and 1234 cm^{-1}. The bands at 451 and 546 cm^{-1} could be attributed to a Si-O bend that characterised highly siliceous materials and double ring vibration respectively (Shirazi et al., 2008). The small band at 791 cm^{-1} could be assigned to an external symmetric stretch. The vibrational bands that overlapped at 1043 and 1127 cm^{-1} could be attributed to an internal asymmetric stretch. The shoulder that appeared at 1234 could be assigned to an external asymmetric stretch (Tao and Kanoh, 2006). There was also a small band at 1642 cm^{-1} that could be attributed to H-O-H bending of water (Saikia and Parthasarathy, 2010). The spectra of H-FA-TPABr-OA, H-FA-HDA-OA and H-FA-PA-OA had similar bands to the FTIR spectrum of the commercial H-ZSM-5 (Com-ZSM-5). However, the FTIR spectrum of Com-ZSM-5 revealed the presence of a band at 436 cm^{-1} that corresponded to a Si-O internal deformation of SiO_4 tetrahedra (Sobolev and Shah, 2015) and a band that corresponded to an internal asymmetric stretch appeared at 1066 cm^{-1} (Van der Gaag, 1987; Tao and Kanoh, 2006). Furthermore, the bands at 555, 800 and 919 cm^{-1} that were assigned to Al-O stretch for mullite, glassy-amorphous phase and Al-O stretch (AlO_4)

in-plane in the FA spectrum (section 4.2, Figure 4.3) disappeared in the spectra of H-FA-TPABr-OA, H-FA-HDA-OA and H-FA-PA-OA (Figure 4.18). Moreover, a characteristic band of double ring vibration of MFI appeared at 546 cm^{-1} in the H-FA-TPABr-OA, H-FA-HDA-OA and H-FA-PA-OA spectra. This is a further indication of the conversion of FA into zeolitic material. An estimation of the degree of crystallinity of the synthesised fly ash-based zeolites could be provided by the optical density ratio of Si-O bend and double ring vibration that appeared at 452 and 546 cm^{-1} respectively as follows:

$$Optical\_density\_ratio = \frac{Intensity\_of\_double\_ring\_vibration}{Intensity\_of\_Si-O\_bend}$$ **(Equation 4.3)** (Van der Gaag, 1987; Ali et al., 2003)

The intensity of Si-O bend and double ring vibration bands was measured using OriginPro 8 software. The optical density of H-FA-TPABr-OA, H-FA-HDA-OA, H-FA-PA-OA and the commercial H-ZSM-5 was 0.86, 0.90, 0.94 and 0.92 respectively. However, it was not excluded that the double ring vibration band that appeared at 543 cm^{-1} in H-FA-TPABr-OA, H-FA-HDA-OA and H-FA-PA-OA spectra could overlap with the Al-O stretch band for mullite that appeared in the spectrum of the as-received fly ash at 555 cm^{-1}; therefore the optical density ratio of H-FA-TPABr-OA, H-FA-HDA-OA and H-FA-PA-OA could not be conclusive in estimating their crystallinity. Ali et al., (2003) reported that the optical density ratio of ZSM-5 zeolite was between 0.73 and 0.81. Moreover, Shirazi et al., (2008) reported that a shift of the internal asymmetric stretch band towards higher wavenumbers came with an increase in Si/Al ratio. Therefore it could be concluded from Figure 4.18 that H-FA-TPABr-OA, H-FA-HDA-OA and H-FA-PA-OA were not fully crystallised and there was still a certain amount of amorphous silica in the final products as the band at 451 cm^{-1} was much more intense than that at 546 cm^{-1}. These results corroborated the XRD results that showed the presence of fly ash mineral phases (mullite and quartz) in the XRD patterns of H-FA-TPABr-OA, H-FA-HDA-OA and H-FA-PA-OA (Figure 4.14). Furthermore, the presence of two broad bands at 1043 and 1127 cm^{-1} that could be assigned to an internal asymmetric stretch indicated that H-FA-TPABr-OA, H-FA-HDA-OA and H-FA-PA-OA samples may have had more than one Si/Al ratio; therefore the crystals might not be homogenous.

4.4.4. Brønsted acidity of the oxalic acid treated H-FA-TPABr, H-FA-HDA and H-FA-PA

The protonation method of the oxalic acid treated fly ash-based ZSM-5 zeolite products H-FA-TPABr-OA, H-FA-HDA-OA and H-FA-PA-OA, and a commercial ZSM-5 was detailed in section 3.3.1.1. The synthesised FA-TPABr, FA-HDA and FA-PA samples were transformed into their H-form by ion exchanging with 0.5 M of NH_4NO_3 solution, followed by calcination, then treatment with a saturated oxalic acid solution and re-calcined as detailed in section 3.3.1.1. The number of Brønsted acid sites of the oxalic acid treated products H-FA-TPABr-OA, H-FA-HDA-OA and H-FA-PA-OA was determined through the H/D isotope exchange as done according to section 3.4.6. Hydrogen (H) on the acid sites of the zeolite was substituted by its isotope deuterium (D). Afterwards, D was back-exchanged with H and H_xOD_y composed of H_2O, D_2O and HDO was collected and analysed by ^1H NMR. Figure 4.19 presents the number of Brønsted of acid sites (mmol H^+ per gram of zeolite) of H-FA-TPABr-OA, H-FA-HDA-OA and H-FA-PA-OA, and a commercial H-ZSM-5.

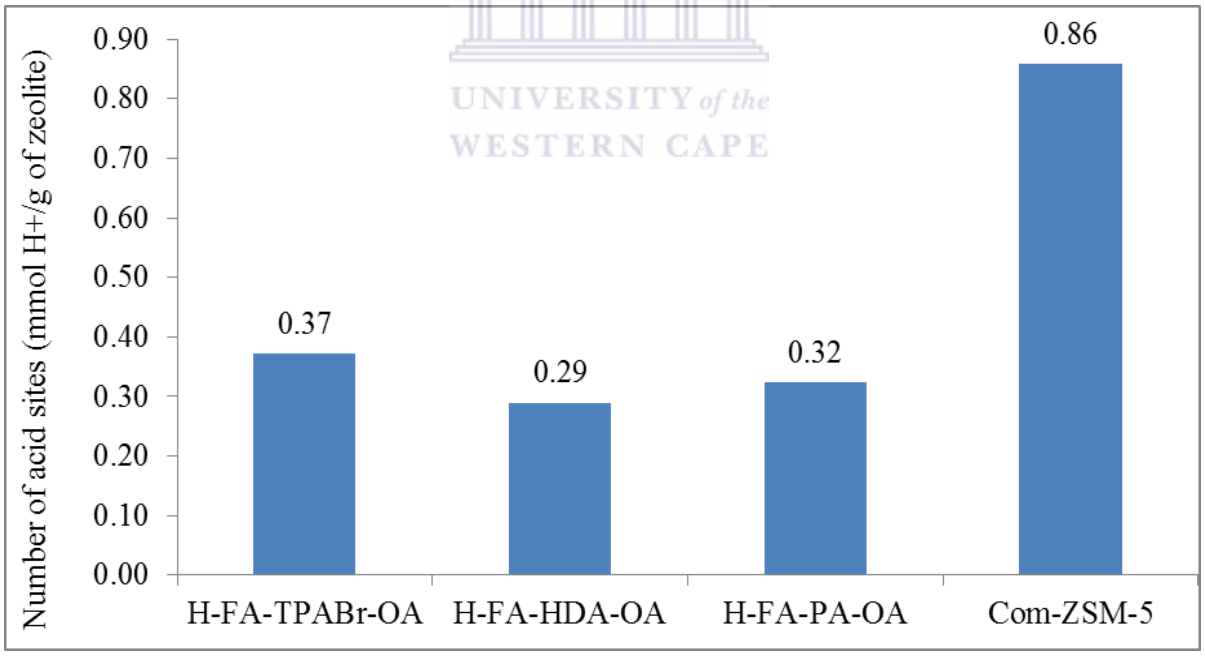

Figure 4.19: Number of Brønsted acid sites (mmol H^+/g of zeolite) of H-FA-TPABr-OA, H-FA-HDA-OA, H-FA-PA-OA and commercial H-ZSM-5 (Com-ZSM-5).

Figure 4.19 showed that the number of Brønsted acid sites of H-FA-TPABr-OA, H-FA-HDA-OA, H-FA-PA-OA and the commercial H-ZSM-5 was 0.37, 0.29, 0.32 and 0.86 mmol H^+ per

gram of zeolite, respectively. The deficiency in the number of Brønsted acid sites indicated low incorporation of Al into the framework structure during the synthesis or significant removal of Al during the treatment with oxalic acid, which could be affected by the Si/Al ratio used during the synthesis as well as the presence of unreacted mineral phases (quartz and mullite) that resulted in a mixed phase zeolite product (Figure 4.14).

4.4.5. Aluminium coordination analysis of the oxalic acid treated H-FA-TPABr, H-FA-HDA and H-FA-PA by ^{27}Al nuclear magnetic resonance

Figure 4.20 compares the ^{27}Al solid state NMR spectra of the oxalic acid treated fly ash-based zeolite products H-FA-TPABr-OA, H-FA-HDA-OA and H-FA-PA-OA with that of a commercial H-ZSM-5 and $Al(NO_3)_3$ solution (0.1 M) as references. The oxalic acid treated ZSM-5 zeolite products H-FA-TPABr-OA, H-FA-HDA-OA and H-FA-PA-OA were synthesised from the as-received coal fly as detailed in Section 3.3.1.1.

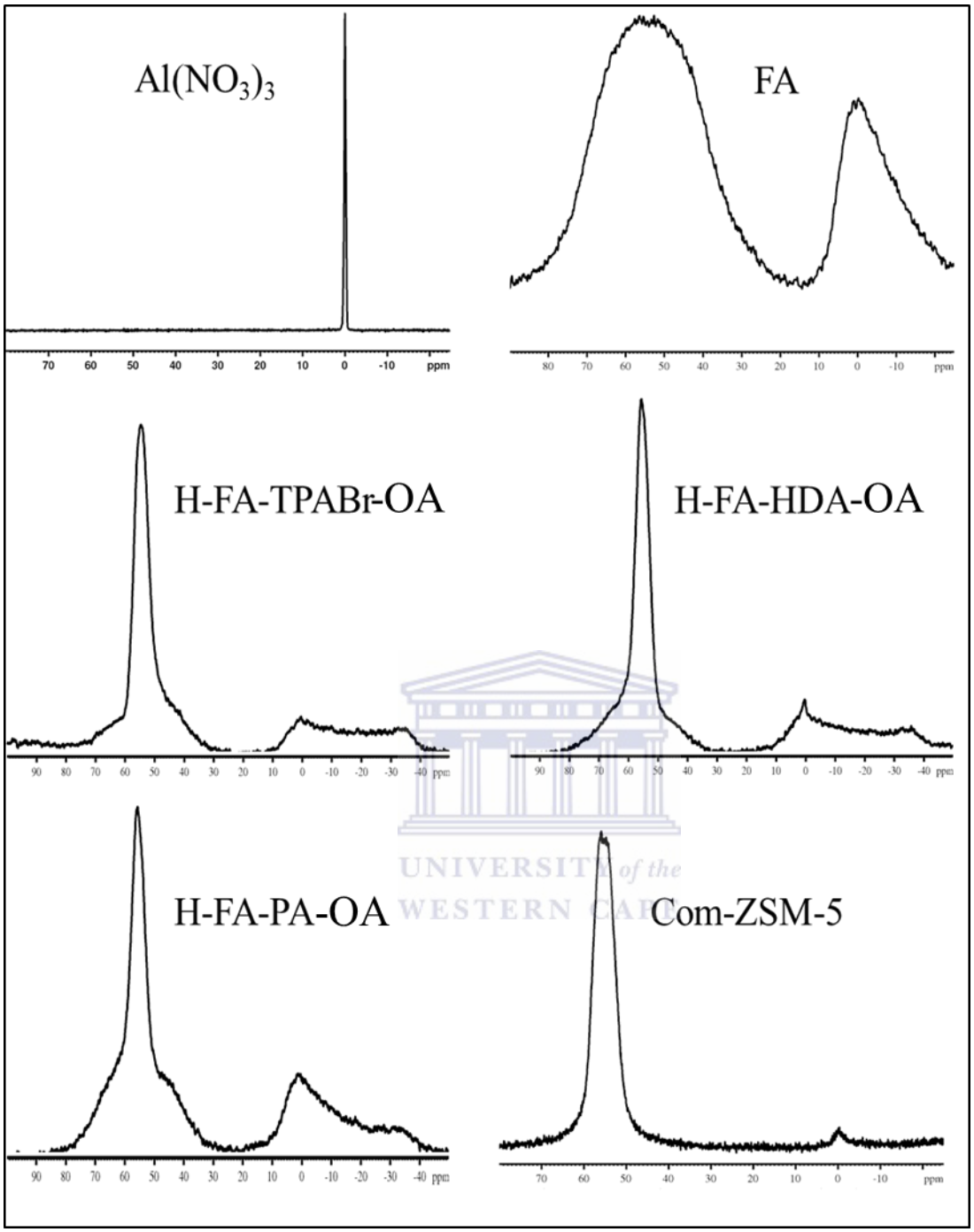

Figure 4.20: ^{27}Al NMR spectra of a reference (0.1 M $Al(NO_3)_3$), FA, H-FA-TPABr-OA, H-FA-HDA-OA and H-FA-PA-OA and a commercial H-ZSM-5 (Com-ZSM-5).

Figure 4.20 showed that the spectrum of the reference $Al(NO_3)_3$ presented a signal at 0 ppm that corresponded to extra-framework octahedrally coordinated aluminium. There was the presence of two wide characteristic signals of framework tetrahedrally coordinated aluminium and extra-framework octahedrally coordinated aluminium at about 55 ppm and 0 ppm respectively in the as-received fly ash (FA) spectrum. The ^{27}Al NMR spectra of H-FA-

TPABr-OA, H-FA-HDA-OA and H-FA-PA-OA showed an intense and narrow signal at about 55 ppm and a small and wide signal ranged between 10 ppm and – 40 ppm, indicating the partial conversion of the as-received fly ash (FA) in a crystalline structure. The signal at about 55 ppm of H-FA-TPABr-OA, H-FA-HDA-OA and H-FA-PA-OA was similar to that of a commercial ZSM-5 and that of ZSM-5 zeolite reported by Triantafyllidis et al., (2004) and Sazama et al., (2011). However, the wide signal ranged between 10 ppm and – 40 ppm in the H-FA-TPABr-OA, H-FA-HDA-OA and H-FA-PA-OA showed that not all the aluminium atoms present in FA were part of the lattice structure of the ZSM-5 framework. This corroborated the XRD results (Figure 4.14) that showed the presence of unreactive FA phases in the H-FA-TPABr-OA, H-FA-HDA-OA and H-FA-PA-OA patterns. Table 4.2 gives the percentage of framework and extra-framework aluminium in $Al(NO_3)_3$, H-FA-TPABr-OA, H-FA-HDA-OA, H-FA-PA-OA and commercial H-ZSM-5 zeolite that were determined by ^{27}Al NMR analysis. The percentage of framework and extra-framework aluminium was calculated as follows:

$$\% = \frac{Integration_i}{\sum Integration_i} * 100 \quad \textbf{(Equation 4.4)}$$

With i, framework or extra-framework aluminium.

Table 4.2: Percentage of framework and extra-framework Al in $Al(NO_3)_3$, FA, H-FA-TPABr-OA, H-FA-HDA-OA and H-FA-PA-OA, and commercial H-ZSM-5 zeolite as well as their number of their Brønsted acid sites.

Sample	Framework tetrahedrally coordinated Al (%)	Extra-framework octahedrally coordinated Al (%)	Number of Brønsted acid sites (mmol H^+/g)
Reference $Al(NO_3)_3$	0.0	100.0	/
FA	70.8	29.2	/
H-FA-TPABr-OA	88.4	11.6	0.37
H-FA-HDA-OA	84.0	16.0	0.29
H-FA-PA-OA	82.0	18.0	0.32
Commercial H-ZSM-5	98.5	1.5	0.86

It could be observed in Table 4.2 that the percentage of framework aluminium of H-FA-TPABr-OA, H-FA-HDA-OA and H-FA-PA-OA was 88.4, 84.0 and 82.0 % respectively. These results followed the same trend as their XRD relative crystallinity, which was 58, 47 and 39 % respectively (Figure 4.15). However, the percentage of framework aluminium of H-FA-TPABr-OA, H-FA-HDA-OA and H-FA-PA-OA did not follow the same trend as the numbers of their Brønsted acid sites, which were 0.37, 0.29 and 0.32 mmol H^+ per gram of zeolite respectively. Hence, H-FA-TPABr-OA, H-FA-HDA-OA and H-FA-PA-OA properties did not correspond with the statement made by Louis et al., (2004) that the number of Brønsted acid sites of ZSM-5 zeolite was equal to its framework aluminium concentration.

4.5. Chapter summary

The optimum conditions of the synthesis of fly ash-based ZSM-5 zeolite were obtained by varying chemical parameters such as the amount of the as-received fly ash, fumed silica, TPABr, water in the hydrothermal gel as well as physical parameters such as the time and temperature of the aging and hydrothermal synthesis. A suitable formulation for the synthesis of ZSM-5 zeolite from as-received South African coal fly ash (FA) was identified, which was: 0.75 g of FA, 0.75 g of fumed silica, 0.25 g of NaOH, 1.5 g of TPABr, 20 mL of deionised,

aging (12 h and 20 °C) and hydrothermal synthesis (24 h and 120 °C). It was noteworthy that the increase in TPABr, deionised water content and aging time, and decrease in the hydrothermal synthesis time and temperature improved the quality of the final product with the disappearance of the analcime phase. Moreover, tetrapropylammonium bromide (TPABr) was substituted by 1,6-hexanediame (HDA) and 1-propylamine (PA) in the hydrothermal gel in order to investigate the effect of the structure directing agent on the properties of the final product. The hydrothermal molar regime used was Si(4.8), Al(1.0), Na(1.5), H_2O(267.6), TPABr(0.7) for FA-TPABr sample ; Si(4.8), Al(1.0), Na(1.5), H_2O(267.6), HDA(2.1) for FA-HDA sample and Si(4.8), Al(1.0), Na(1.5), H_2O(267.6), PA(4.1) for FA-PA sample. The temperature and time of the hydrothermal synthesis used was 160 °C and 72 h respectively. Those conditions led to the synthesis of FA-TPABr, FA-HDA and FA-PA composed of ZSM-5, mullite and quartz phases. The effect of the structure directing agent on the characteristics of ZSM-5 zeolite synthesised from coal fly ash has not been reported in the literature. The synthesised fly ash-based ZSM-5 zeolite products (FA-TPABr, FA-HDA and FA-PA) were transformed to their H-form and treated with a saturated oxalic acid solution prior to analysis by XRD, SEM, FTIR, Brønsted acidity and ^{27}Al NMR. The XRD analysis showed that the oxalic acid treated ZSM-5 zeolite products H-FA-TPABr-OA, H-FA-HDA-OA and H-FA-PA-OA had a relative crystallinity of 58, 47 and 39 % respectively. Moreover, the use of the revised synthesis formulation of FA-TPABr, FA-HDA and FA-PA according to the most suitable chemical and physical parameters led to the disappearance of the dense analcime phase in the final ZSM-5 products and the relative XRD crystallinity of H-FA-TPABr-OA, H-FA-HDA-OA and H-FA-PA-OA had the same trend as the percentage of their NMR framework Al that was 88.4, 84.0 and 82.0 % respectively. This correlation was important in the description of the fly ash-based ZSM-5 zeolite and has not been reported yet in the literature. However, there was poor correlation between the framework tetrahedrally coordinated Al of H-FA-TPABr-OA, H-FA-HDA-OA and H-FA-PA-OA and their number of Brønsted acid sites determined by H/D isotope exchange technique, which was 0.37, 0.29 and 0.32 mmol H^+ per gram of zeolite respectively. The SEM micrographs showed that H-FA-PA-OA had the largest ZSM-5 crystals followed by H-FA-HDA-OA. The participation of the as-received fly ash in the formation of ZSM-5 zeolite framework could be demonstrated by FTIR and ^{27}Al NMR analyses. However, the presence of unreacted fly ash phases (mullite and quartz) in H-FA-TPABr-OA, H-FA-HDA-OA and H-FA-PA-OA and their small number of Brønsted acid sites could lead to the conclusion that the synthesis of ZSM-5 zeolite from

South African coal fly ash still needs to be optimised. Therefore, in the next section the as-received fly ash will be pre-treated with concentrated sulphuric acid (95-99 %) before being used in the synthesis of ZSM-5 zeolite. The acid pre-treatment could remove a certain amount of aluminium and some other undesirable elements from the fly ash feedstock that could affect the product quality.

CHAPTER 5: CHARACTERISATION OF ZSM-5 ZEOLITE SYNTHESISED FROM ACID TREATED COAL FLY ASH

5.1. Introduction

This chapter presents the effect of concentrated sulphuric acid (95-99 %) treatment on the chemical composition of the as-received fly ash. The properties of the as-received fly ash (FA) and acid treated fly ash (AL) are compared using XRD, SEM, FTIR, ^{27}Al NMR and XRF. It also highlights the characteristics of ZSM-5 zeolite samples (AL-TPABr, AL-HDA and AL-PA) that were synthesised from the acid treated fly ash (AL) with tetrapropylammonium bromide (TPABr), 1,6-hexanediamine (HDA) or 1-propylamine (PA) as organic structure directing agent using the synthesis formulations detailed in Table 3.5. The synthesised AL-TPABr, AL-HDA and AL-PA were transformed into their H-form by treatment with a NH_4NO_3 solution and calcination, thereafter they were dealuminated by treatment with a saturated oxalic acid solution and calcined as detailed in Section 3.3.1.2.

5.2. Effect of the H_2SO_4 treatment on the characteristics of fly ash

The effect of the treatment of the as-received fly ash with concentrated sulphuric acid (95-99 %) was investigated in this section by comparing the characteristics of the as-received fly ash (FA) and acid treated fly ash (AL) by XRD, SEM, FTIR, ^{27}Al NMR and XRF. The as-received FA (100 g) was mixed with 500 mL of concentrated H_2SO_4 (95-99 %) at 200 °C for 2 h. After filtration, the acid treated fly ash (AL) was washed with deionised water (Section 3.3.1.2). Figure 5.1 compares the XRD patterns of the as-received fly ash (FA) and acid treated fly ash (AL).

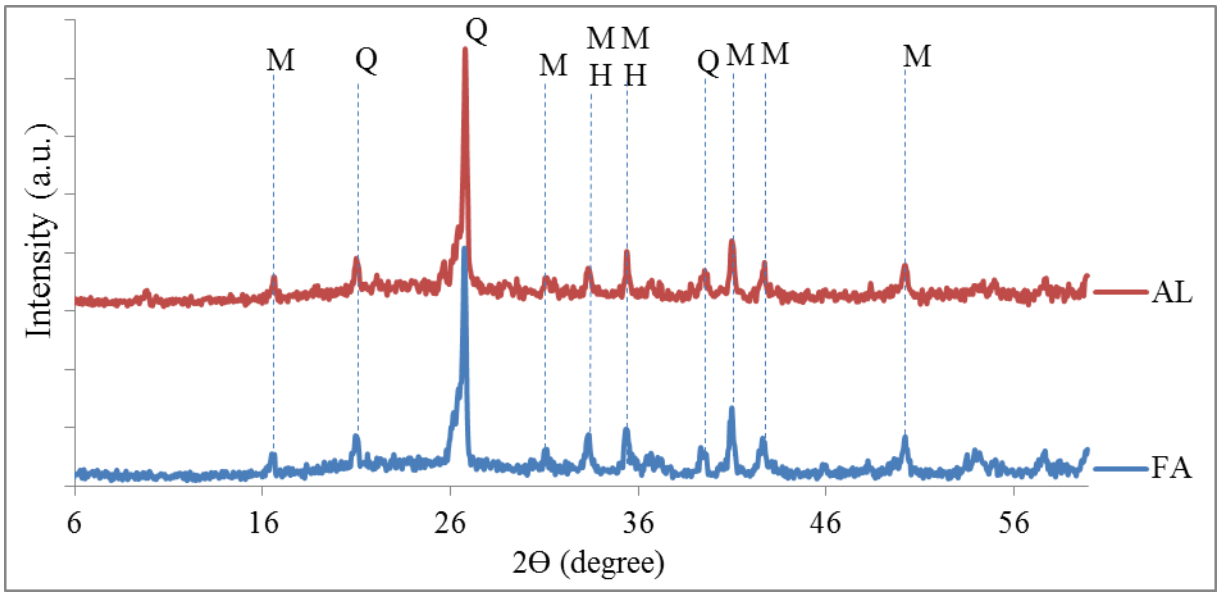

Figure 5.1: Comparison of XRD patterns of the as-received fly ash (FA) and H_2SO_4 treated fly ash (AL) (M=mullite; Q=quartz; H=hematite).

The major mineral phases found in the as-received fly ash (FA) were mullite, quartz and hematite as discussed in Section 4.2. It could be seen that FA and AL had the same mineralogical phase composition: mullite, quartz and hematite phases. Moreover, the H_2SO_4 treatment did not completely digest the amorphous phase of fly ash, which could be observed both before (FA) and after acid leaching (AL) as a hump between 18 and 33° 2Θ.

Figure 5.2 compares the SEM micrographs of the as-received fly ash (FA) and H_2SO_4 treated fly ash (AL).

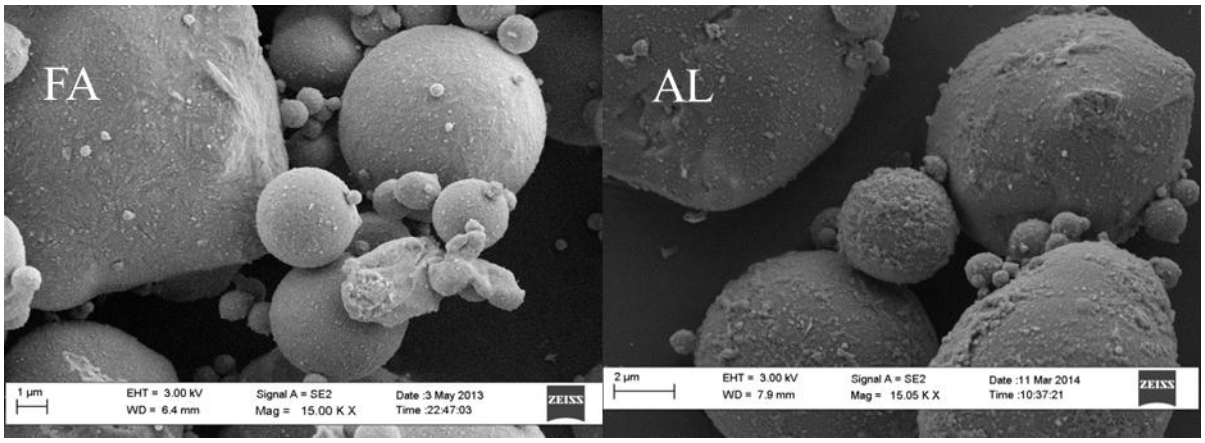

Figure 5.2: Comparison of SEM micrographs of the as-received fly ash (FA) and H_2SO_4 treated fly ash (AL).

Figure 5.2 showed that FA and AL were made of spherical particles that were characteristic of the morphology of coal fly ash. Therefore, the acid treatment conditions applied in this study were not able to digest fly ash particles. However, the fly ash particles that were smooth before (FA) acid treatment became rough thereafter (AL), which could indicate that the acid treatment removed surface impurities or etched the particles.

Figure 5.3 compares the FTIR spectra of the as-received fly ash (FA) and H_2SO_4 treated fly ash (AL).

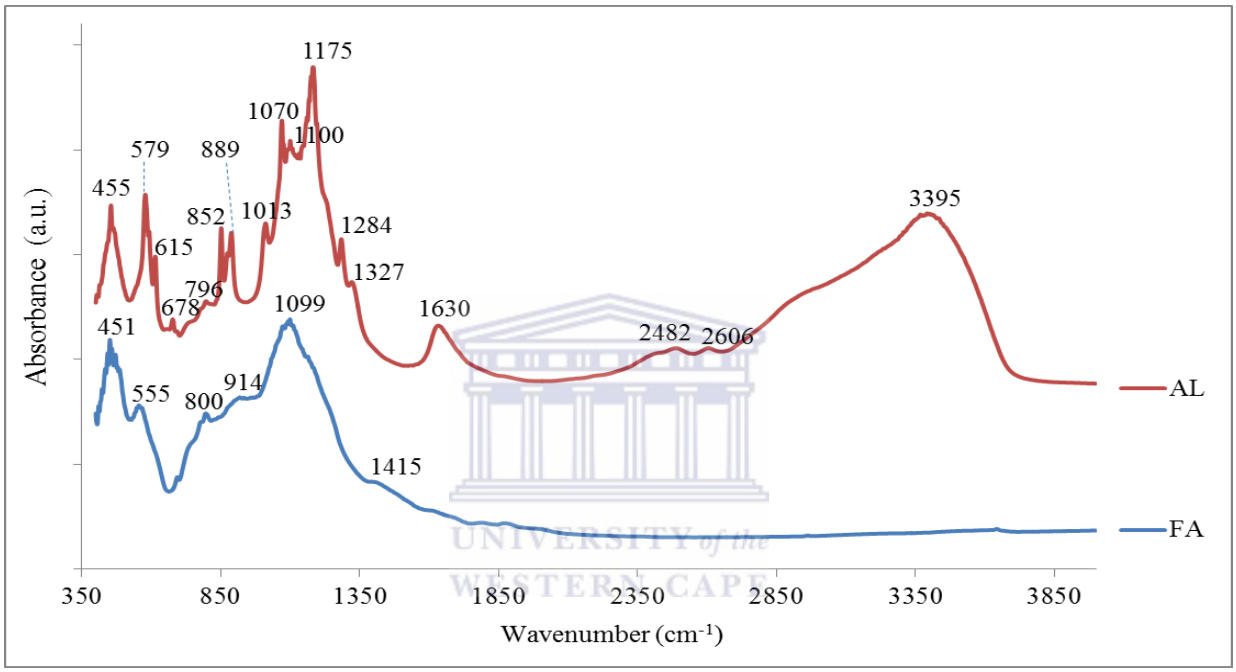

Figure 5.3: Comparison of FTIR spectra of the as-received fly ash (FA) and H_2SO_4 treated fly ash (AL).

The FTIR spectrum of FA was discussed in Section 4.2. It could be observed in Figure 5.3 that the FTIR spectrum of AL was different from that of FA. AL presented bands at 455 and 579 cm^{-1} that could correspond to Si-O-Si symmetric bend and Al-O stretch (AlO_6) (Voll et al., 2002). The bands at 615 and 678 cm^{-1} could be assigned to a symmetric stretching of Si-O-T (T=Si or Al) and Al-O stretching for condensed AlO_6 octahedral (Sobolev and Shah, 2015). A band that appeared at 796 cm^{-1} could be attributed to a glassy-amorphous and quartz phases (Abou Rida et al., 2014; Saikia and Parthasarathy, 2010). The vibrational bands that appeared at 852 and 889 cm^{-1} could be assigned to OH deformation linked to Al^{3+} and OH deformation linked to $2Al^{3+}$ respectively (Saikia and Parthasarathy, 2010). The bands at 1013, 1070, 1100 and 1175 cm^{-1} could correspond to Si-O asymmetric stretch for mullite,

glass phase and quartz (Voll et al., 2002; Abou Rida et al., 2014). These bands overlapped in FA spectrum and appeared as a broad band at 1099 cm^{-1}. The bands at 1284 and 1327 cm^{-1} could correspond to Al-O for AlO_4 and the band at 1630 cm^{-1} could be assigned to H-O-H bending of water (Saikia and Parthasarathy, 2010). The bands at 2482 and 2606 cm^{-1} could be attributed Si-OH vibrations (Efimov et al., 2003). The band that appeared at 3395 cm^{-1} could be due to H-O-H stretching of absorbed water (Saikia and Parthasarathy, 2010). Figure 5.3 showed that the treatment of the as-received fly ash with concentrated sulphuric acid modified its structure. Criado et al., (2007) also reported similar observations on the fly ash spectrum while deconvoluting the band associated with the Si-O bond asymmetric stretching vibrations in the ash activated with sodium hydroxide solution. They reported that a band at 1100 cm^{-1} could be split into three bands at 996, 1081 and 1185 cm^{-1} that were associated with the vitreous phase of fly ash, quartz and mullite respectively. However these modifications were only on the surface particles as the XRD and SEM results did not show any difference between FA and AL (Figures 5.1 and 5.2).

Figure 5.4 compares the ^{27}Al NMR spectra of the as-received fly ash (FA) and H_2SO_4 treated fly ash (AL).

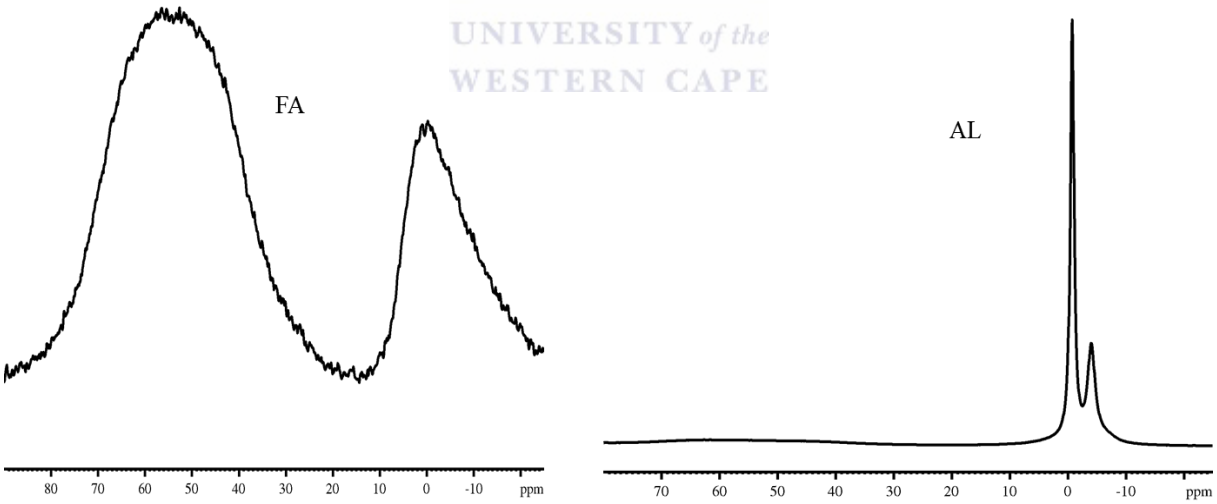

Figure 5.4: Comparison of the ^{27}Al NMR spectra of the as-received fly ash (FA) and H_2SO_4 treated fly ash (AL).

The ^{27}Al NMR spectrum in Figure 5.4 showed that FA presented two signals characteristic extra-framework and framework aluminium, which were distinguished based on the signals of two references namely $Al(NO_3)_3$ and commercial ZSM-5 as discussed in Section 4.4.5. The spectrum of AL presented two narrow peaks at 0 and -4 ppm that could correspond to the

extra-framework octahedrally coordinated aluminium. These results could explain the change in structural vibrations that was observed in Figure 5.3. However, the SEM micrographs of both FA and AL presented only few changes on the surface (Figure 5.2) and the XRD patterns of FA and AL were similar (Figure 5.1). Therefore, the difference observed by ^{27}Al NMR was only surface modification of FA by the H_2SO_4 treatment.

The H_2SO_4 treatment of the as-received FA feedstock aimed to increase its Si/Al ratio by removing Al, as well as to reduce the percentage of other elements such as Ca, Mg, K and Fe which might affect the formation rate and properties of the synthesised ZSM-5 zeolite samples. Figure 5.5 summarises the XRF results of the fly ash before (FA) and after (AL) the H_2SO_4 acid treatment. The XRF method was described in Section 3.4.4.

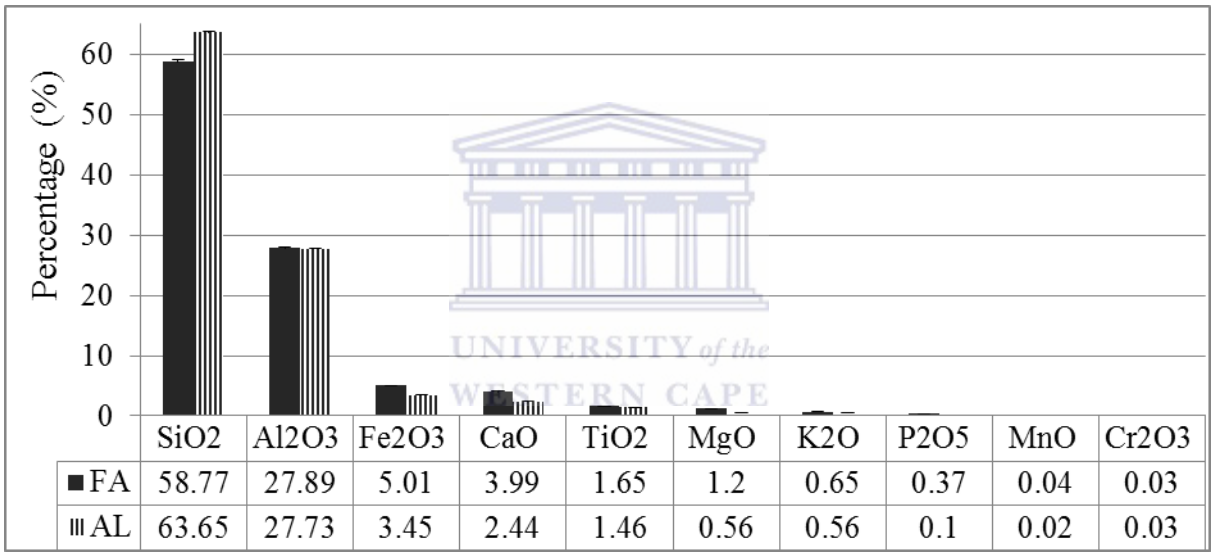

	SiO2	Al2O3	Fe2O3	CaO	TiO2	MgO	K2O	P2O5	MnO	Cr2O3
FA	58.77	27.89	5.01	3.99	1.65	1.2	0.65	0.37	0.04	0.03
AL	63.65	27.73	3.45	2.44	1.46	0.56	0.56	0.1	0.02	0.03

Figure 5.5: Elemental composition of fly ash (FA) and acid treated fly ash (AL) obtained by XRF (n=4).

Figure 5.5 showed that the percentage of SiO_2 increased from 58.77±0.34 % to 63.65±0.08 % after acid leaching; while the percentage of other FA major elements slightly decreased. The percentage of Al_2O_3 decreased only from 27.86±0.16 % (FA) to 27.73±0.06 % (AL). In effect, the percentage of SiO_2 increased mainly because of removal of Fe_2O_3, CaO, TiO_2, MgO and P_2O_5. This treatment caused the Si/Al ratio to increase from 1.86 (FA) to 2.02 (AL). These results showed that the treatment of FA with H_2SO_4 (95-99 %) was not adequate to remove sufficient aluminium for the Si/Al molar ratio to be above the required ratio (Si/Al>10) for the synthesis of ZSM-5 zeolite. However, Lai-Shi et al., (2011) reported

that 87 % of Al_2O_3 could be extracted from coal fly ash which was treated with concentrated H_2SO_4 (ratio acid to FA was 5:1) at 200~210 °C for 80 min. But many studies are in disagreement with that report as it was stated by Vassilev et al., (2003) that sintering, hydrothermal, acidic and alkaline treatments and some physical separation technologies for bulk fly ash processing are commonly ineffective, expensive or environmentally harmful. Furthermore, Liu et al., (2012) and Yao et al., (2014) reported that the sintering of ash with CaO at a temperature between 1000 to 1200 °C prior to the acid leaching was necessary to recover 70 to 90 % of Al_2O_3. On the other hand, the H_2SO_4 treatment reduced the percentage of other metal oxides such as Fe_2O_3, CaO, TiO_2, MgO, K_2O, P_2O_5 or MnO in AL. Some of these metals may affect the synthesis of ZSM-5 zeolite from fly ash. Indeed, Kirov and Filizova, (2012) investigated the influence of extra-framework cations (Na^+, K^+, Ca^{2+} and Mg^{2+}) in the zeolitization process. They concluded that Ca^{2+}, Na^+ and Mg^{2+} governed the stability of large channels thanks to their high hydration capacity and their location in large channels. In parallel, Petrik, (2009) showed that K^+ is a structure-breaking cation and hinders the zeolitization process. However, the complexity of the bulk composition of coal FA renders it difficult to relate any outcome significantly to a particular component (Vassilev et al., 2003).

5.3. Effect of the structure directing agent on the properties of ZSM-5 zeolite synthesised from H_2SO_4 treated fly ash (AL)

The H_2SO_4 treatment of the as-received fly ash (FA) did not only slightly increase the Si/Al molar ratio but also removed some undesirable metals that may affect the zeolitization process. Hence, it can be predicted that ZSM-5 zeolite samples synthesised from the H_2SO_4 treated fly ash (AL) would have better physical and chemical properties than the samples synthesised from the as-received fly ash (FA) (see section 4.4). ZSM-5 zeolite was then synthesised from AL using three different directing agents (tetrapropylammonium bromide, 1,6-hexanediamine or 1-propylamine).

A similar study to the one presented in chapter 4 regarding the effect of tetrapropylammonium bromide (TPABr), 1,6-hexanediamine (HDA) or 1-propylamine (PA) on fly ash-based ZSM-5 zeolite is reported in this section. However, in this section the as-received fly ash (FA) was substituted by the H_2SO_4 treated fly ash (AL) as source of silicon and aluminium and fumed silica was added to adjust the Si/Al ratio because it was still low (2.02) in AL for the synthesis

of ZSM-5 zeolite that requires a Si/Al ratio of above 10. The same suitable synthesis conditions reported in Section 4.3.7 were used to synthesise AL-TPABr, AL-HDA or AL-PA from AL. AL-TPABr, AL-HDA and AL-PA were transformed into their H-form and treated with oxalic acid. The effect of the fly ash H_2SO_4 treatment on the synthesis of fly ash-based ZSM-5 zeolite was investigated by characterising the oxalic acid treated ZSM-5 zeolite products H-AL-TPABr-OA, H-AL-HDA-OA and H-AL-PA-OA by XRD, SEM, FTIR, Brønsted acidity, ^{27}Al NMR and BET surface area analyses.

5.3.1. Mineralogical study of the oxalic acid treated ZSM-5 zeolite products H-AL-TPABr-OA, H-AL-HDA-OA and H-AL-PA-OA by X-ray diffraction

AL-TPABr, AL-HDA and AL-PA samples were synthesised under the following conditions: 0.75 g of H_2SO_4 treated fly ash (AL), 0.75 g of fumed silica, 0.25 g of NaOH, 1 g of the structure directing agent (TPABr, HDA or PA), 20 mL of deionised water, aging (6 h, room temperature) and hydrothermal synthesis (72 h, 160 °C). Thereafter, AL-TPABr, AL-HDA and AL-PA samples were transformed into their H-form and treated with oxalic acid as detailed in Section 3.3.1.2. Figure 5.6 gives the XRD patterns of the H_2SO_4 treated fly ash (AL), as well as the oxalic acid treated ZSM-5 zeolite products H-AL-TPABr-OA, H-AL-HDA-OA and H-AL-PA-OA, and commercial H-ZSM-5 (Com-ZSM-5). The XRD method used in this study was detailed in Section 3.4.1.

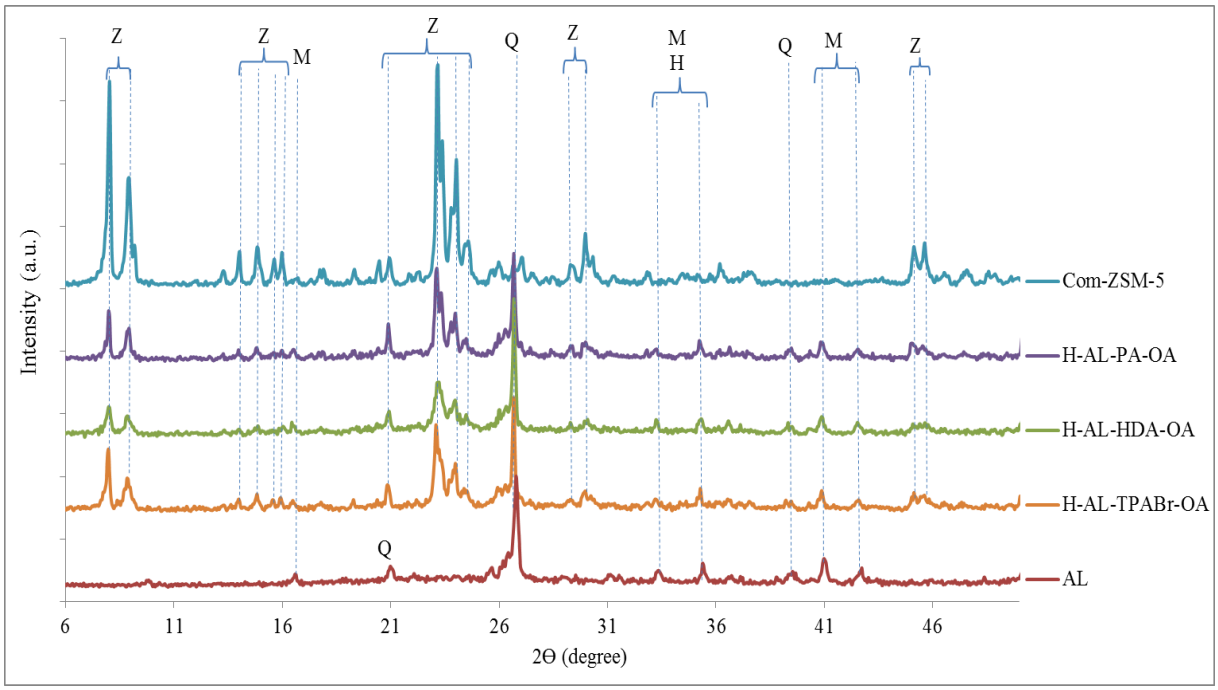

Figure 5.6: XRD patterns of the H_2SO_4 treated fly ash (AL), H-AL-TPABr-OA, H-AL-HDA-OA, H-AL-PA-OA and commercial H-ZSM-5 (Com-ZSM-5) (Z= ZSM-5 zeolite, M=mullite, Q=quartz, H=hematite).

Figure 5.6 showed that AL had the same mineralogical composition as FA (Figure 5.1): mullite, quartz and hematite phases. Moreover, the H_2SO_4 treatment did not completely digest the amorphous phase of fly ash, which could be observed before (FA) and after acid leaching (AL) between 18 and 33° 2Θ. The characteristic peaks of ZSM-5 zeolite at 7.7, 8.9, 12.5, 13.8, 14.6, 14.9, 15.8, 21.2, 23, 23.9, 24.4, 25.6, 29, 29.7, 44.9 and 45.4° 2Θ could be observed in the XRD patterns of H-AL-TPABr-OA, H-AL-HDA-OA and H-AL-PA-OA, which was confirmed by the XRD patterns of the commercial ZSM-5 zeolite and the collection of simulated XRD power patterns for zeolites (Treacy and Higgins, 2001). It was noteworthy that the revised synthesis formulation and conditions adopted from chapter 4 led to the formation of fly ash-based ZSM-5 zeolite samples without a dense analcime contaminant phase. The presence of unreacted fly ash phases (mullite and quartz) remaining in H-AL-TPABr-OA, H-AL-HDA-OA and H-AL-PA-OA patterns showed that the H_2SO_4 pre-treatment of fly ash was not able to enhance the dissolution of mullite and quartz from fly ash; neither did the oxalic acid post-synthesis treatment have an effect on mullite and quartz. Therefore, more severe conditions than that applied in this study would be required in order to dissolve mullite and quartz phases and increase the ZSM-5 relative XRD crystallinity. However, the acid leaching was accompanied with a slight decrease in the percentage of some

elements such as Fe, Ti, Ca, Mg and K (Figure 5.5), which could have an effect on the crystallinity of the synthesised zeolites. Figure 5.7 gives the calculated ZSM-5 relative XRD crystallinity of H-AL-TPABr-OA, H-AL-HDA-OA and H-AL-PA-OA with the commercial H-ZSM-5 (Com-ZSM-5) as a reference using Equation 4.1.

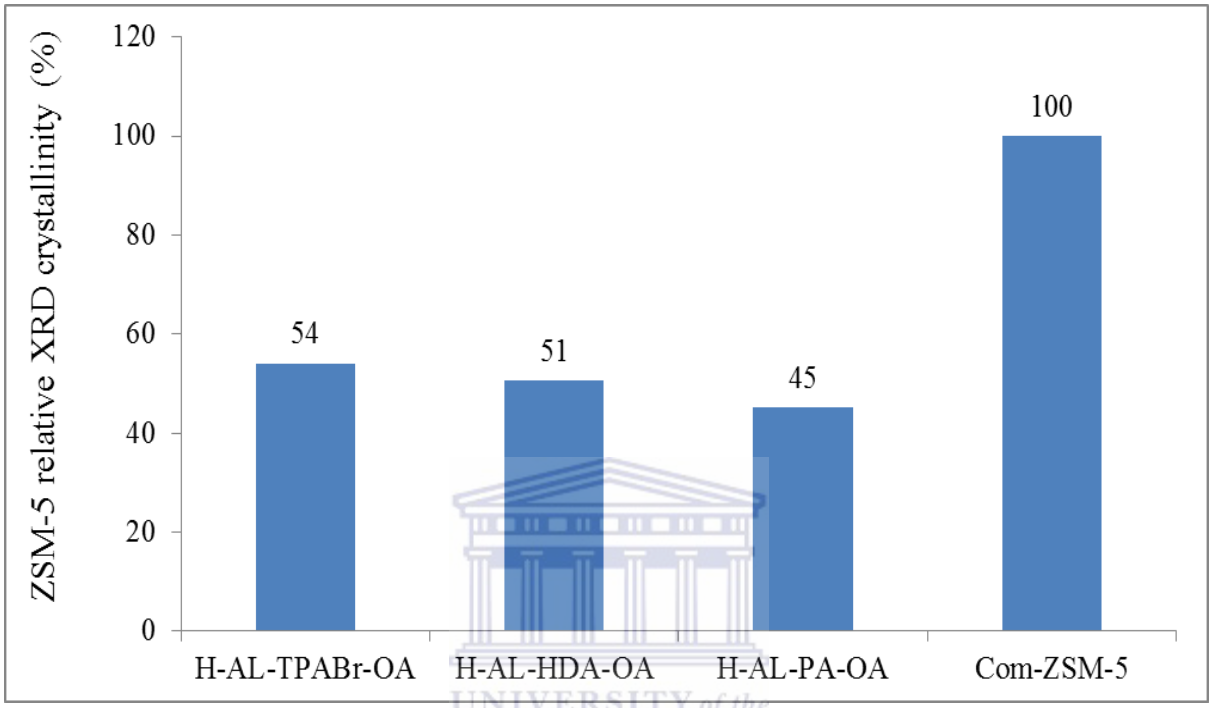

Figure 5.7: Calculated ZSM-5 relative XRD crystallinity H-AL-TPABr-OA, H-AL-HDA-OA and H-AL-PA-OA and the commercial H-ZSM-5 (Com-ZSM-5).

Figure 5.7 showed that H-AL-TPABr-OA (54 %) had the highest calculated ZSM-5 relative XRD crystallinity followed by H-AL-HDA-OA (51 %) and H-AL-PA-OA (45 %). Moreover, by comparing the relative XRD crystallinity of H-FA-TPABr-OA, H-FA-HDA-OA and H-FA-PA-OA (Figure 4.15) to that of H-AL-TPABr-OA, H-AL-HDA-OA and H-AL-PA-OA (Figure 5.7) it could be observed that the H_2SO_4 acid leaching of the FA feedstock slightly increased the ZSM-5 XRD phase purity of the zeolites synthesised with HDA and PA as templates but not of that synthesised with TPABr. In fact, the ZSM-5 relative XRD crystallinity of H-FA-TPABr-OA, H-FA-HDA-OA and H-FA-PA-OA was 58 %, 47 % and 39 % respectively as shown in Figure 4.15. The results presented in Figure 5.7 corroborated the findings reported by Van der Gaag (1987) in which the template order in forming zeolite ZSM-5 was TPABr>HDA>PA.

5.3.2. Morphological analysis and elemental composition of the oxalic acid treated ZSM-5 zeolite products H-AL-TPABr-OA, H-AL-HDA-OA and H-AL-PA-OA by scanning electron microscopy-energy dispersive spectroscopy

Figure 5.8 shows micrographs of the H_2SO_4 treated fly ash (AL), as well as the oxalic acid treated ZSM-5 zeolite products H-AL-TPABr-OA, H-AL-HDA-OA and H-AL-PA-OA, and commercial H-ZSM-5. H-AL-TPABr-OA, H-AL-HDA-OA and H-AL-PA-OA were synthesised as follows: 0.75 g of H_2SO_4 treated fly ash (AL), 0.75 g fumed silica, 0.25 g of NaOH, 1 g of the structure directing agent (TPABr, HDA or PA), 20 mL of de-ionised water, aging (6 h, room temperature) and hydrothermal synthesis (72 h, 160 °C). After the synthesis, AL-TPABr, AL-HDA and AL-PA samples were transformed into their H-form and treated with a saturated oxalic acid solution to obtain H-AL-TPABr-OA, H-AL-HDA-OA and H-AL-PA-OA as was detailed in Section 3.3.1.2.

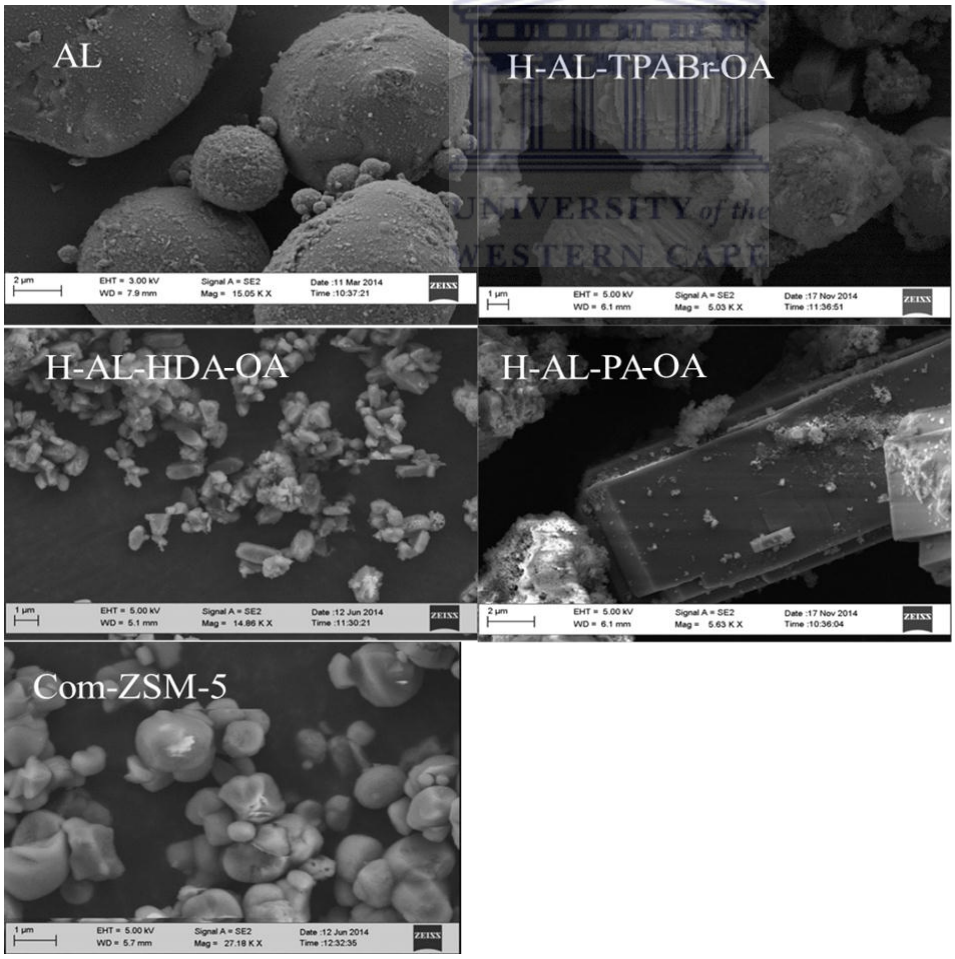

Figure 5.8: SEM micrographs of the H_2SO_4 treated fly ash (AL), H-AL-TPABr-OA, H-AL-HDA-OA, H-AL-PA-OA and commercial H-ZSM-5 (Com-ZSM-5).

The micrograph of the H_2SO_4 treated fly ash (AL) was discussed in Section 5.2. The commercial H-ZSM-5 crystals were spherulitic as described in Section 4.4.2. Figure 5.8 showed that H-AL-TPABr-OA, H-AL-HDA-OA and H-AL-PA-OA resulted in ZSM-5 crystals with different morphologies, varying in size and shape depending on the structure directing agent used. H-AL-TPABr-OA was composed of polycrystalline structures with a spherulitic habit, while H-AL-HDA-OA and H-AL-PA-OA were composed of small rod-shaped particles and large lath-shaped crystals respectively. However, the micrographs showed that ZSM-5 crystals were mixed with an amorphous phase. The micrographs of different fly ash-based ZSM-5 zeolite samples that were synthesised in this study showed that the shape of ZSM-5 crystals could be tailored either by pre-treating fly ash with concentrated sulphuric acid or changing the structure directing agent. These results corroborated the findings of Petrik, (2009), who reported that the shape of ZSM-5 zeolite could be modified by changing some synthesis parameters such as the template type, and sodium, potassium or aluminium source. According to Sang et al., (2004), the difference in ZSM-5 crystal morphology is caused by the difference in size and geometric shape of the structure directing agents used, which orient the crystal growth differently. The synthesis of ZSM-5 zeolite made of polycrystalline structures with a spherullic habit was also reported by Chu et al., (2009) who synthesised ZSM-5 using SBA-15 and tetrapropylammonium hydroxide (TPAOH) as silica source and structure directing agent respectively. Figure 5.9 gives the mean crystal length and width of H-AL-TPABr-OA, H-AL-HDA-OA and H-AL-PA-OA. The length and width of ZSM-5 crystals were measured using Image J software and the mean crystal length and width for each sample was calculated using Equation 4.2.

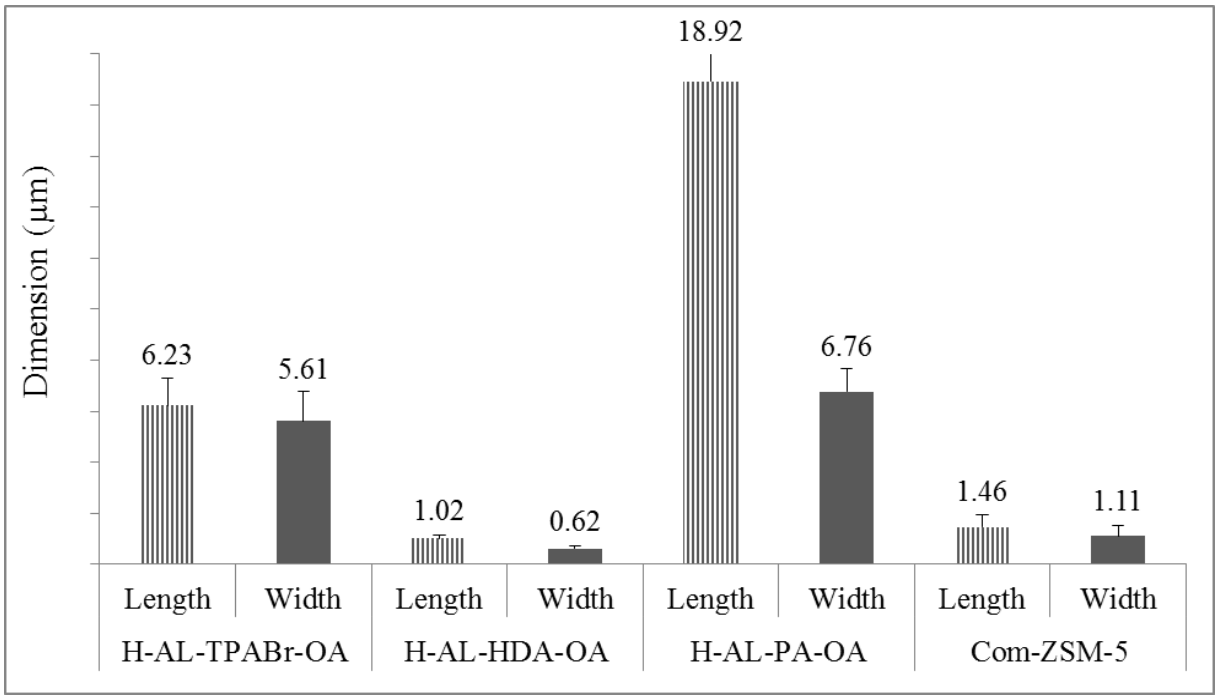

Figure 5.9: Mean crystal length and width of H-AL-TPABr-OA, H-AL-HDA-OA, H-AL-PA and the commercial H-ZSM-5 (Com-ZSM-5).

Figure 5.9 showed that the ZSM-5 crystals of H-AL-PA-OA (length=18.92±2.01 µm; width=6.76±0.91 µm) were bigger than those of H-AL-TPABr-OA (length=6.23±1.05 µm; width=5.61±1.18 µm) and H-AL-HDA-OA (length=1.02±0.14 µm; width=0.62±0.09 µm). On the other hand, Figure 4.17 showed the length and width crystals of H-FA-TPABr-OA, H-FA-HDA-OA and H-FA-PA-OA were 3.75±0.28 by 3.66±0.49 µm; 5.35±0.48 by 2.11±0.29 µm; 9.50±0.91 by 4.99±0.37 µm respectively, and those of the commercial H-ZSM-5 crystals were 1.46±0.47 by 1.11±0.42 µm. The treatment of fly ash with sulphuric acid prior to the hydrothermal synthesis led to the variation of the size of fly ash-based ZSM-5 zeolites crystals. The crystal size of fly ash-based ZSM-5 zeolite products synthesised with TPABr and PA increased with the acid treatment of fly ash prior to the synthesis, while the crystal size of fly ash-based zeolite ZSM-5 synthesised with HDA decreased with the acid treatment prior to the synthesis. However, Sang et al., (2004), reported that the structure directing agents affected the morphology and had little effect on the crystal size of ZSM-5 zeolite. Therefore, the change in size observed in this study could mainly be due to the acid pre-treatment of the starting material (fly ash), which affected the composition of the hydrothermal gel, due to the removal of impurities that could affect the crystal habit.

The effect of the post synthesis treatment with oxalic acid on the synthesised H-AL-TPABr, H-AL-HDA and H-AL-PA was investigated by comparing the elemental composition of H-AL-TPABr, H-AL-HDA and H-AL-PA to that of H-AL-TPABr-OA, H-AL-HDA-OA and H-AL-PA-OA that was determined via energy dispersive spectroscopy (EDS) (Table 5.1). Ten different spots of each sample were analysed, and their average and standard deviation were determined. H-AL-TPABr-OA, H-AL-HDA-OA and H-AL-PA-OA were obtained as detailed in section 3.3.1.2. The synthesised AL-TPABr, AL-HDA and AL-PA were first transformed in their H-form by treatment with NH_4NO_3 solution followed by calcination. Thereafter, H-AL-TPABr, H-AL-HDA and H-AL-PA were treated with an aqueous saturated solution of oxalic acid at ratio of 1:10, at 80 °C for 6 h under reflux conditions to obtain H-AL-TPABr-OA, H-AL-HDA-OA and H-AL-PA-OA. Afterwards, they were calcined at 550 °C for 3 h in air in order to burn off the remaining oxalic acid.

Table 5.1: Elemental composition of H-AL-TPABr, H-AL-HDA and H-AL-PA compared to that of H-AL-TPABr-OA, H-AL-HDA-OA and H-AL-PA-OA (n=10).

Element	H-AL-TPABr (%)	H-AL-TPABr-OA (%)	H-AL-HDA (%)	H-AL-HDA-OA (%)	H-AL-PA (%)	H-AL-PA-OA (%)
O	64.6±0.3	65.1±0.2	64.7±0.5	65.8±0.2	64.9±0.3	65.1±0.3
Si	25.7±0.5	27.2±0.5	26.5±0.5	27.0±0.3	26.5±0.5	27.7±0.6
Al	7.8±0.5	6.7±0.6	6.8±0.3	5.7±0.3	7.0±0.5	5.7±0.4
Na	0.4±0.3	0.3±0.3	1.0±0.8	0.9±0.4	0.5±0.5	0.6±0.3
Mg	0.5±0.4	0.1±0.1	0.1±0.4	0.0±0.0	0.3±0.3	0.3±0.3
Fe	0.4±0.2	0.2±0.1	0.3±0.2	0.3±0.2	0.4±0.2	0.2±0.2
Ca	0.4±0.1	0.3±0.2	0.5±0.2	0.2±0.2	0.2±0.1	0.1±0.1
K	0.2±0.2	0.1±0.1	0.1±0.1	0.1±0.1	0.1±0.1	0.1±0.1
Si/Al	3.3	4.1	3.9	4.7	3.8	4.9

It could be observed in Table 5.1 that the Si/Al of H-AL-TPABr, H-AL-HDA and H-AL-PA increased after treatment with oxalic acid in H-AL-TPABr-OA, H-AL-HDA-OA and H-AL-PA-OA, which showed that oxalic acid solution was able to dealuminate H-AL-TPABr, H-AL-HDA and H-AL-PA. The aim of the oxalic acid treatment was to remove as much aluminium as possible in order to get rid of the mullite phase from the final products while keeping the ZSM-5 structure undestroyed. However, none of the Si/Al ratios was above 10 characteristic for ZSM-5 zeolite. This could be due to the presence of unreacted fly ash mullite phase in the final products as was shown in Figure 5.6. The low percentage of Na in H-AL-TPABr, H-AL-HDA and H-AL-PA was an indication that the transformation of AL-TPABr, AL-HDA and AL-PA into their H-form ion-exchanged most of the Na. Furthermore, the post synthesis treatment of H-AL-TPABr, H-AL-HDA and H-AL-PA with oxalic acid also removed some other elements such as Mg, Fe, Ca and K. The results support the findings of Yan et al., (2003) who also observed a higher Si/Al ratio after oxalic acid treatment. Thus post-treatment with oxalic acid provides a further route to tailor product properties and remove impurities.

5.3.3. Structural analysis of the oxalic acid treated ZSM-5 zeolite products H-AL-TPABr-OA, H-AL-HDA-OA and H-AL-PA-OA by Fourier transform infrared

Figure 5.10 presents the FTIR spectra of the H_2SO_4 treated fly ash (AL), as well as oxalic acid treated, dealuminated ZSM-5 zeolite products H-AL-TPABr-OA, H-AL-HDA-OA and H-AL-PA-OA, and the commercial H-ZSM-5 zeolite (Com-ZSM-5). H-AL-TPABr-OA, H-AL-HDA-OA and H-AL-PA-OA were synthesised by mixing 0.75 g of AL, 0.75 g of fumed silica, 0.25 g of NaOH, 1 g of the structure directing agent (TPABr, HDA or PA), 20 mL of deionised water. The mixture was aged in room temperature for 6 h, and underwent hydrothermal synthesis at 160 °C for 72 h. After synthesis, AL-TPABr, AL-HDA and AL-PA samples were detemplated, ion exchanged with NH_4NO_3 and transformed into their H-form by calcination, and then dealuminated with oxalic acid to obtain H-AL-TPABr-OA, H-AL-HDA-OA and H-AL-PA-OA as detailed in Section 3.3.1.2.

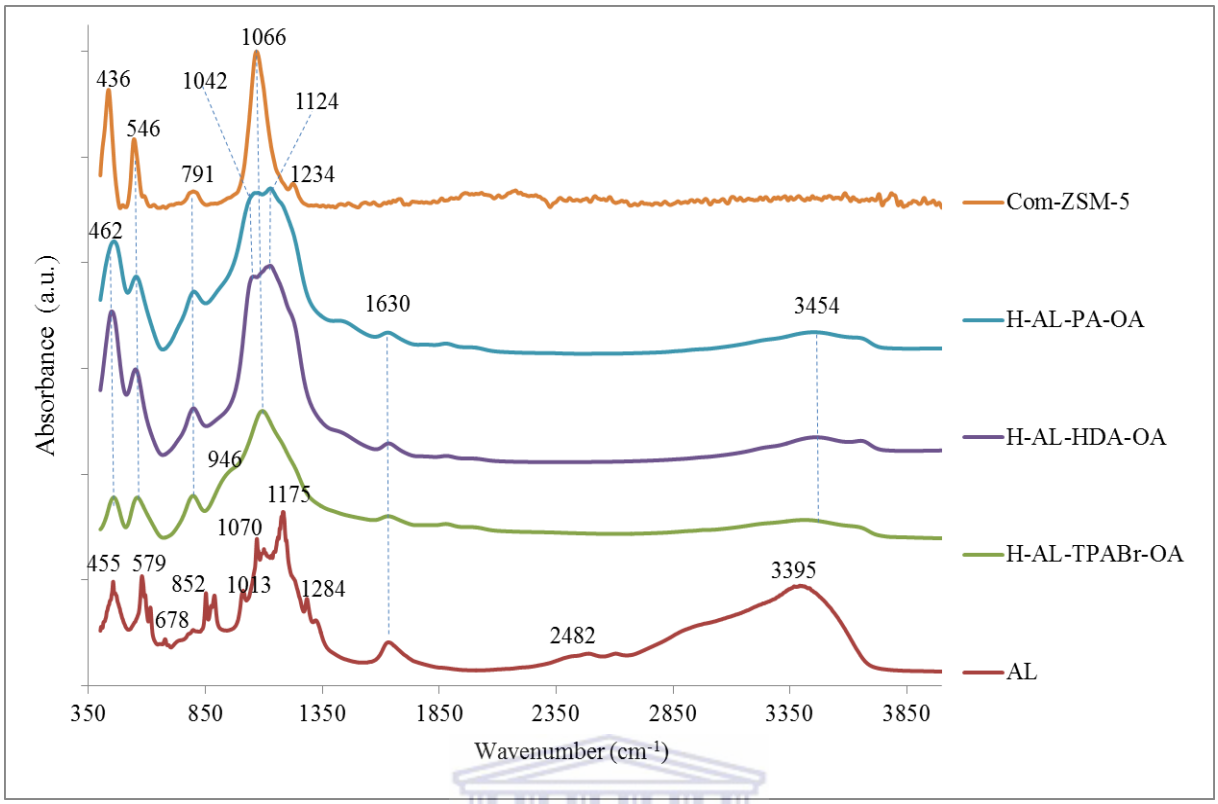

Figure 5.10: FTIR spectra of the H_2SO_4 treated fly ash (AL), H-AL-TPABr-OA, H-AL-HDA-OA and H-AL-PA-OA compared to commercial H-ZSM-5 (Com-ZSM-5).

The FTIR spectra of Com-ZSM-5 and AL were discussed in sections 4.4.3 and 5.2 respectively. The FTIR spectrum of H-AL-TPABr-OA had vibrational bands at 462 and 546 cm^{-1} that could be assigned to a Si-O bend and double ring respectively, while the band at 791 cm^{-1} could be assigned to an external symmetric stretch (Shirazi et al., 2008). The band that appeared at 946 cm^{-1} could be assigned to Si-O-Al stretch out of plane of mullite (Voll et al., 2002). The vibrational band at 1066 cm^{-1} could be attributed to a Si-O internal asymmetric stretch (Ali et al., 2003). The vibrational bands at 1630 and 3454 cm^{-1} could be assigned to H-O-H bending of water and H-OH stretching of absorbed water respectively (Saikia and Parthasarathy, 2010). The FTIR spectra of H-AL-HDA-OA and H-AL-PA-OA presented similar vibrational bands as the FTIR spectrum of H-AL-TPABr-OA except that they did not have a band at 946 cm^{-1}. Moreover, they had two vibrational bands that overlapped at 1042 and 1124 cm^{-1} that could correspond to an internal asymmetric stretch (Ali et al., 2003). It was noteworthy that the FTIR spectra of H-AL-TPABr-OA, H-AL-HDA-OA and H-AL-PA-OA did not reveal C-H bands in the region between 2852 and 2988 cm^{-1} that would be due to the presence of the structure directing agent in the final products (Shirazi et

al., 2008) showing that the detemplation was complete. Furthermore, the presence of two characteristic bands of an internal asymmetric stretch vibrations at 1042 and 1124 cm^{-1} in the FTIR spectra of H-AL-HDA-OA and H-AL-PA-OA could be an indication that they had more than one Si/Al ratio, Ali et al., (2003) reported that the presence of two or more different vibrational bands of an internal asymmetric stretch in the spectra of aluminosilicates was due to different Si/Al ratios in the samples, hence it could be concluded that they were not homogeneous. Moreover, the degree of crystallinity of H-AL-TPABr-OA, H-AL-HDA-OA and H-AL-PA-OA could be estimated via their optical density ratio (Equation 4.3 in section 4.4.3) that was found to be 0.99, 0.86 and 0.93 respectively. Therefore, it could be concluded that H-AL-TPABr-OA would be more crystalline than H-AL-HDA-OA and H-AL-PA-OA. This was in agreement with ZSM-5 relative XRD crystallinity that was 54, 51 and 45 % for H-AL-TPABr-OA, H-AL-HDA-OA and H-AL-PA-OA respectively. However, even if the optical density ratio values showed an important degree of double ring vibration in the H-AL-TPABr-OA, H-AL-HDA-OA and H-AL-PA-OA spectra, indicating a high crystallinity, these values could not be conclusive because the Al-O stretch (AlO_6) vibrational band at 579 cm^{-1} from AL spectrum could affect the intensity of double ring band of the synthesised fly ash-based zeolites spectra at 543 cm^{-1}. This made it difficult to compare the degrees of crystallinity of H-FA-TPABr-OA, H-FA-HDA-OA and H-FA-PA-OA to that of H-AL-TPABr-OA, H-AL-HDA-OA and H-AL-PA-OA using their optical density ratio.

5.3.4. Brønsted acidity of the oxalic acid treated ZSM-5 zeolite products H-AL-TPABr-OA, H-AL-HDA-OA and H-AL-PA-OA

AL-TPABr, AL-HDA or AL-PA were ion-exchanged to the NH_4^+ form using 0.5 M of NH_4NO_3 solution four times at 80 °C for 1 h each time. Afterwards, the ion-exchanged fly ash-based ZSM-5 zeolite samples were transformed into their H-form by calcination at 550 °C for 3 h. The obtained H-AL-TPABr, H-AL-HDA and H-AL-PA were then treated with a saturated oxalic acid solution and calcined to obtain H-AL-TPABr-OA, H-AL-HDA-OA and H-AL-PA-OA as detailed in section 3.3.1.2. The treatment with oxalic acid solution was motivated by the fact that Yan et al., (2003) reported that Y zeolite was dealuminated using an oxalic acid solution. Applying this method to the current study would mainly remove extra-framework aluminium in the fly ash-based ZSM-5 zeolite samples. Figure 5.11 presents the number of Brønsted acid sites (mmol H^+ per gram of zeolite) of H-AL-TPABr-OA, H-AL-HDA-OA and H-AL-PA-OA. The number of Brønsted acid sites was determined through the

H/D isotope exchange as detailed in section 3.4.6. Hydrogen (H) on the acid sites of the zeolite was substituted by its isotope deuterium (D). Afterwards, D was back-exchanged with H and H_xOD_y composed of H_2O, D_2O and HDO was collected and analysed by ^1H NMR.

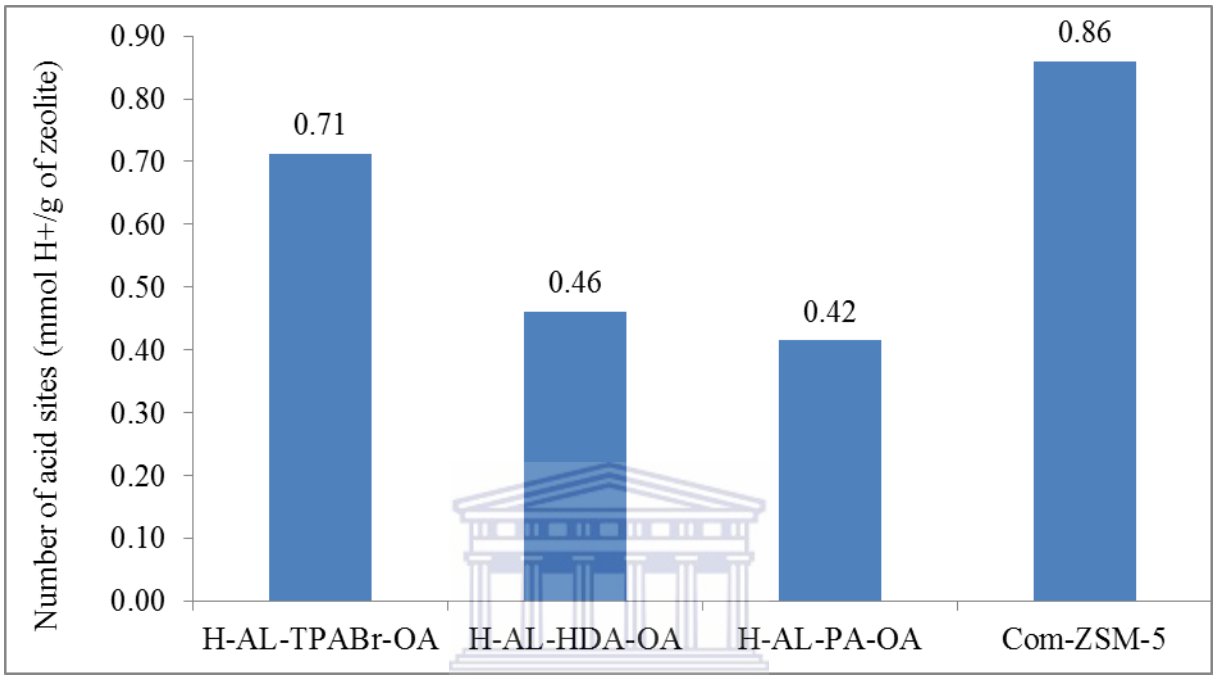

Figure 5.11: Number of Brønsted acid sites (mmol H+/g of zeolite) of H-AL-TPABr-OA, H-AL-HDA-OA and H-AL-PA-OA compared to the commercial H-ZSM-5 (Com-ZSM-5).

Figure 5.11 showed that the number of Brønsted acid sites of H-AL-TPABr-OA, H-AL-HDA-OA, H-AL-PA-OA and commercial H-ZSM-5 (Com-ZSM-5) was 0.71, 0.46, 0.42 and 0.86 mmol H^+ per gram of zeolite, respectively. It was important to remember that the number of Brønsted acid sites of H-FA-TPABr-OA, H-FA-HDA-OA and H-FA-PA-OA was 0.37, 0.29 and 0.32 mmol H^+ per gram of zeolite, respectively (Figure 4.19). Hence, it could be seen that the H_2SO_4 leaching of the fly ash prior to the synthesis process led to a considerable increase in the number of Brønsted acid sites of H-AL-TPABr-OA, H-AL-HDA-OA and H-AL-PA-OA.

5.3.5. Aluminium coordination analysis of the oxalic acid treated ZSM-5 zeolite products H-AL-TPABr-OA, H-AL-HDA-OA and H-AL-PA-OA by ^{27}Al nuclear magnetic resonance

The percentage of framework or extra-framework aluminium of H-AL-TPABr-OA, H-AL-HDA-OA and H-AL-PA-OA was investigated by comparing their ^{27}Al solid state NMR spectra with that of a commercial ZSM-5 as shown in Figure 5.12. An $Al(NO_3)_3$ solution (0.1 M) was used as reference. H-AL-TPABr-OA, H-AL-HDA-OA and H-AL-PA-OA were synthesised from H_2SO_4 treated fly ash (AL) and fumed silica with TPABr, HDA or PA as structure directing agent. After synthesis, AL-TPABr, AL-HDA and AL-PA were transformed into their H-form by treatment with NH_4NO_3 solution and calcination followed by dealumination with a saturated oxalic acid solution to obtain H-AL-TPABr-OA, H-AL-HDA-OA and H-AL-PA-OA.

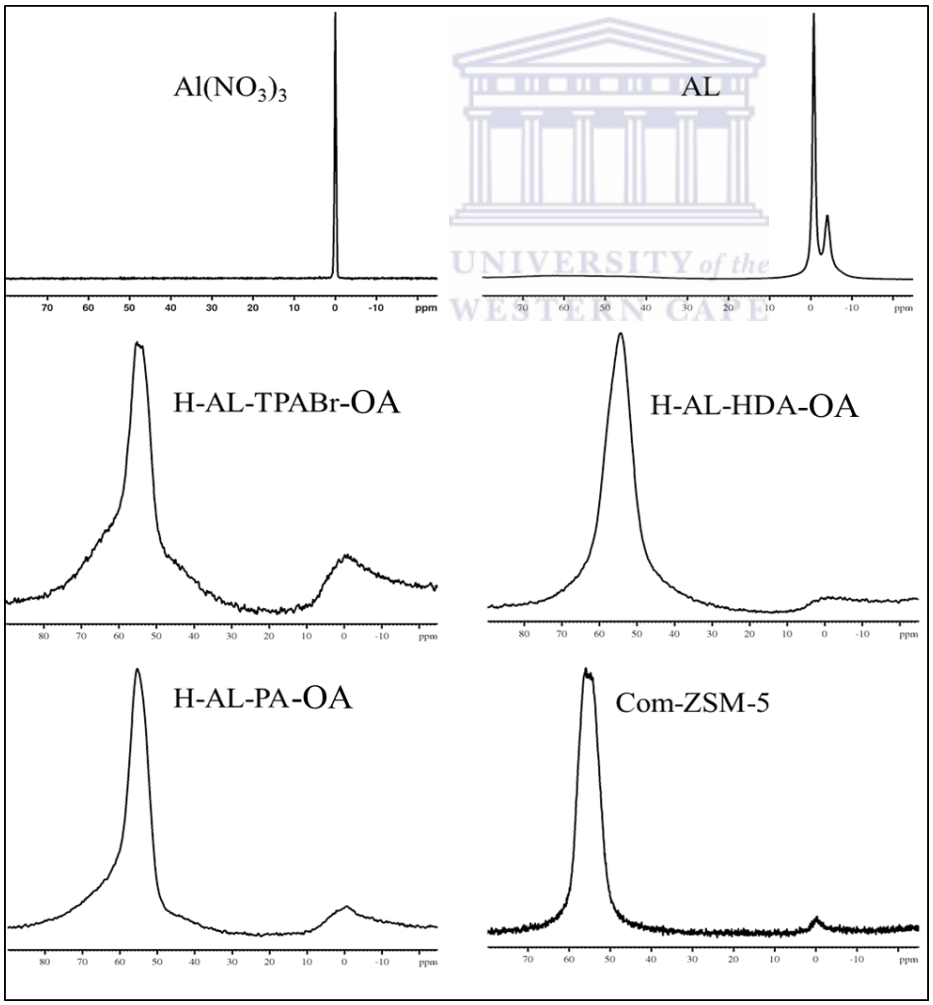

Figure 5.12: ^{27}Al NMR spectra of a reference (0.1 M $Al(NO_3)_3$), H_2SO_4 treated fly ash (AL), H-AL-TAPBr-OA, H-AL-HDA-OA, H-AL-PA-OA and the commercial H-ZSM-5 (Com-ZSM-5).

The ^{27}Al NMR spectra of $Al(NO_3)_3$ and commercial ZSM-5 were discussed in Sections 4.4.5 while that of AL was discussed in Section 5.2. The spectrum of AL presented an intense signal at about 0 ppm that corresponded to extra-framework octahedrally coordinated aluminium, which was a surface signal as the XRD and SEM did not reveal any change between FA and AL (Figures 5.1 and 5.2). Figure 5.12 showed that the ^{27}Al NMR spectra of H-AL-TPABr-OA, H-AL-HDA-OA and H-AL-PA-OA presented a small signal at about 0 ppm that corresponded to extra-framework octahedrally coordinated aluminium and an intense signal at about 55 ppm that corresponded to framework tetrahedrally coordinated aluminium, and they were similar to the spectrum of commercial ZSM-5.

Table 5.2 gives the percentage of framework and extra-framework aluminium in $Al(NO_3)_3$, H_2SO_4 treated fly ash (AL), H-AL-TPABr-OA, H-AL-HDA-OA, H-AL-PA-OA and commercial H-ZSM-5 zeolite that were determined by ^{27}Al NMR analysis.

Table 5.2: Percentage of framework aluminium in $Al(NO_3)_3$, AL, H-AL-TPABr-OA, H-AL-HDA-OA, H-AL-PA-OA and commercial H-ZSM-5 zeolite.

Sample	Framework tetrahedrally coordinated Al (%)	Extra-framework octahedrally coordinated Al (%)	Number of Brønsted acid sites (mmol H^+/g)
Reference $Al(NO_3)_3$	0.0	100.0	/
AL	0.0	100.0	/
H-AL-TPABr-OA	79.9	20.1	0.71
H-AL-HDA-OA	98.9	1.1	0.46
H-AL-PA-OA	88.1	11.9	0.42
Commercial H-ZSM-5	98.5	1.5	0.86

Among the synthesised fly ash-based ZSM-5 zeolite samples, H-AL-HDA-OA had the highest framework aluminium percentage (98.9 %), followed by H-AL-PA-OA (88.1 %) (Table 5.2). These results did not follow the same trend as the ZSM-5 XRD relative crystallinity of H-AL-TPABr-OA, H-AL-HDA-OA and H-AL-PA-OA that was 54, 51

and 45 % respectively. It was also not possible to relate the percentage of framework aluminium of H-AL-TPABr-OA, H-AL-HDA-OA and H-AL-PA-PA to the number of their Brønsted acid sites that was 0.71, 0.46, 0.42 mmol H^+ per gram of zeolite respectively. Therefore, the rule suggested by Louis et al., (2004) that the number of Brønsted acid sites of ZSM-5 zeolite was equal to its framework aluminium content is not supported by these data. This is ascribed to the complexity of the feedstock that was a heterogeneous waste (fly ash); hence it was difficult to predict the product quality.

5.3.6. Surface area analysis of the oxalic acid treated ZSM-5 zeolite products H-AL-TPABr-AO, H-AL-HDA-OA and H-AL-PA-OA by N_2 Brunauer-Emmett-Teller

The BET surface area of H-AL-TPABr-OA, H-AL-HDA-OA, H-AL-PA-OA and the commercial H-ZSM-5 were compared by N_2 adsorption-desorption measurements performed at 77.41 K as described in Section 3.4.7. H-AL-TPABr-OA, H-AL-HDA-OA and H-AL-PA-OA were prepared as follows: 0.75 g of H_2SO_4 treated fly ash (AL) was mixed with 0.75 g of fumed silica, 0.25 g of NaOH, 1 g of the structure directing agent (TPABr, HDA or PA) and 20 mL of deionised water. The mixture was aged at room temperature for 6 h before it underwent hydrothermal synthesis at 160 °C for 72 h. The synthesised AL-TPABr, AL-HDA and AL-PA were transformed into their H-form and dealuminated to obtain H-AL-TPABr-OA, H-AL-HDA-OA and H-AL-PA-OA as detailed in Section 3.3.1.2. Prior to the N_2 adsorption, the samples were degassed at 90 °C for 2 h and 400 °C for 4 h in order to remove moisture adsorbed inside the porous network. Figure 5.13 gives the adsorption/desorption isotherms of N_2 and BET surface area of H-AL-TPABr-OA, H-AL-HDA-OA, H-AL-PA-OA and the commercial H-ZSM-5.

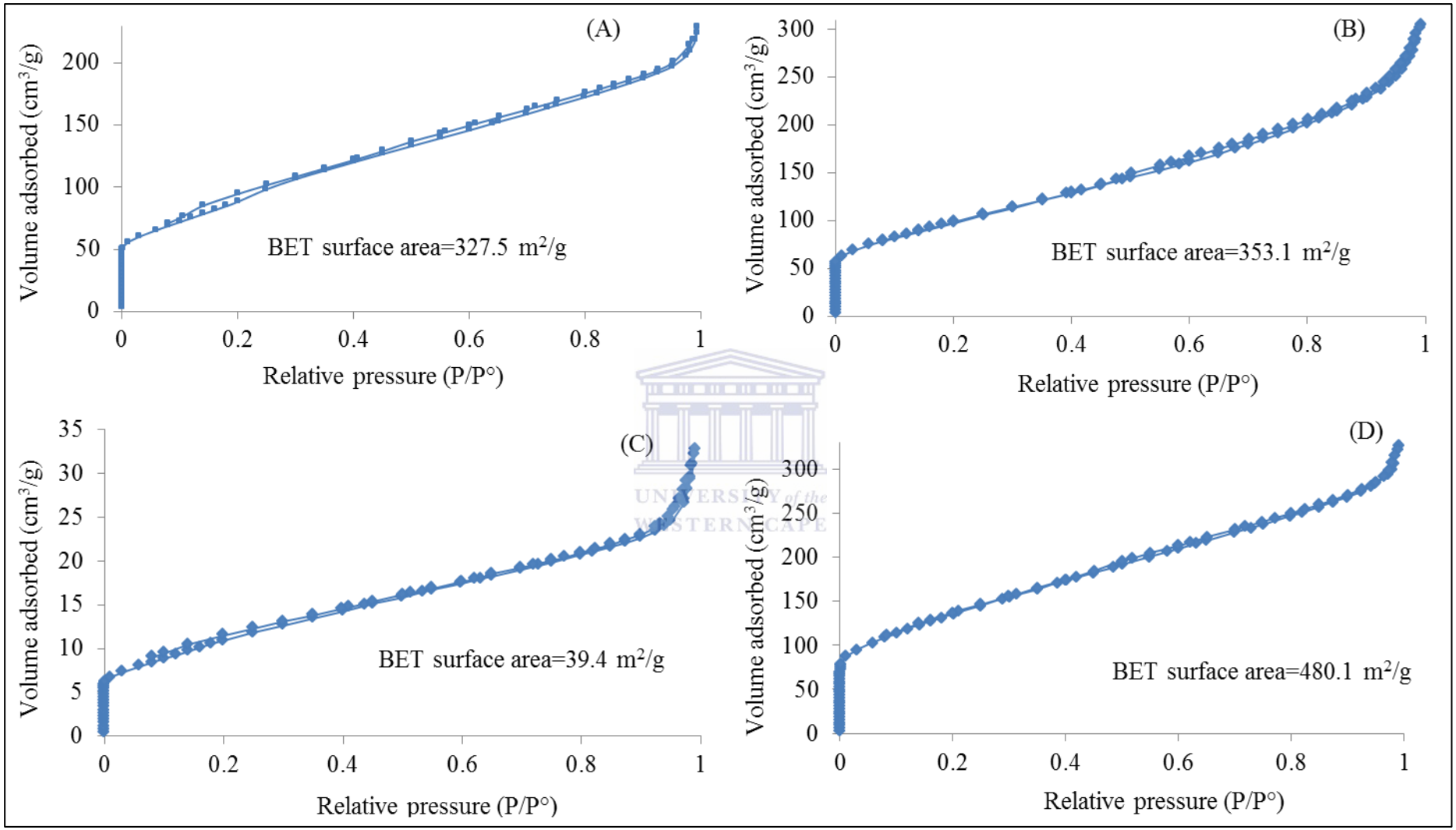

Figure 5.13: Adsorption/desorption isotherms of N_2 at 77.41 K and BET surface area of (A) H-AL-TPABr-OA, (B) H-AL-HDA-OA and (C) H-AL-PA-OA, and (D) commercial H-ZSM-5.

Figure 5.13 showed that the N_2 adsorption-desorption isotherms of H-AL-TPABr-OA (A), H-AL-HDA-OA (B), H-AL-PA-OA (C) and commercial ZSM-5 (D) were that of type IV with the presence of a small hysteresis loop, which is characteristic of mesoporous materials (Lowell et al., 2004). Among the fly ash-based ZSM-5 zeolite samples, H-AL-HDA-OA had the highest BET surface area (353.1 m^2/g), followed by H-AL-TPABr-OA (327.5 m^2/g). H-AL-PA-OA had the lowest BET surface area of 39.4 m^2/g. This could not be due the presence of the structure directing agent in the framework because the FTIR spectra of H-AL-TPABr-OA, H-AL-HDA-OA and H-AL-PA-OA did not reveal the characteristic bands of the structure directing agents (Figure 5.10). However, it was not excluded that the amorphous species could cause pore blockage in H-AL-PA-OA structure. Moreover, the BET surface areas of H-AL-TPABr-OA, H-AL-HDA-OA and H-AL-PA-OA were inversely proportional to their crystal size as H-AL-PA-OA had the biggest ZSM-5 crystals followed by H-AL-TPABr-OA (Figure 5.4). Garcia-Martinez and Li, (2015) reported that a reference nano-crystalline ZSM-5 exhibited a BET surface area of 459 m^2/g, which was not far from that of the commercial H-ZSM-5 (480.1 m^2/g) used in this study.

Table 5.3 compares the surface area distribution, Si/Al ratio, number of Brønsted acid sites, relative XRD crystallinity, percentage of framework tetrahedrally coordinated aluminium and crystal size of H-AL-TPABr-OA, H-AL-HDA-OA and H-AL-PA-OA to that of the commercial H-ZSM-5 (Com-ZSM-5).

Table 5.3: Surface area distribution, Si/Al ratio, number of Brønsted acid sites, relative XRD crystallinity, percentage of framework aluminium and crystal size of H-AL-TPABr-OA, H-AL-HDA-OA and H-AL-PA-OA compared to the commercial H-ZSM-5 (Com-ZSM-5).

Properties		H-AL-TPABr-OA	H-AL-HDA-OA	H-AL-PA-OA	Com-ZSM-5
Surface area (m^2/g)	Micropores	61.15	56.01	9.04	85.06
	Mesopores	259.70	259.81	27.37	308.77
	Macropores	9.67	37.26	2.98	86.32
BET surface area (m^2/g)		327.53	353.08	39.40	480.15
Si/Al		4.1	4.7	4.9	29
Number of Brønsted acid site (mmol H^+/g)		0.71	0.46	0.42	0.86
Relative XRD crystallinity (%)		54	51	45	100
Framework aluminium (%)		79.9	98.9	88.1	98.5
Crystal size (µm)	Length	6.23±1.05	1.02±0.14	18.92±2.01	1.46±0.47
	Width	5.61±1.18	0.62±0.09	6.76±0.91	1.11±0.42

Table 5.3 showed that H-AL-TPABr-OA, H-AL-HDA-OA and H-AL-PA-OA were mainly mesoporous, which could explain the presence of the hysteresis loop in their N_2 adsorption-desorption isotherms (Figure 5.13). However, the micropore surface area of H-AL-TPABr-OA, H-AL-HDA-OA, H-AL-PA-OA and the commercial H-ZSM-5 could be higher that presented in Table 5.3 if an adsorptive with a higher resolution adsorption than N_2 was used. It could be seen that the BET surface area of H-AL-TPABr-OA, H-AL-HDA-OA and H-AL-PA-OA was inversely proportional to their crystal size. However, the mesopores surface areas of H-AL-TPABr-OA and H-AL-HDA-OA were close to one another. Moreover, it was not possible to relate all the properties of H-AL-TPABr-OA, H-AL-HDA-OA and H-AL-PA-OA to one another. However, their Si/Al ratio was inversely proportional to their relative XRD crystallinity and number of Brønsted acid sites. Even if the BET surface area of H-AL-PA-

OA (39.40 m^2/g) was too low for it to compete with commercial ZSM-5 catalysts, H-AL-TPABr-OA and H-AL-HDA-OA presented an acceptable BET surface area value for a catalytic application such as Methanol-to-Olefin (MTO) conversion even with only 54 % and 51 % of relative crystallinity respectively. The adsorptive (nitrogen) used in this study does not give high-resolution adsorption isotherms for ZSM-5; therefore it does not reveal significant details of the low-pressure region where micropore filling occurs (Cejka et al., 2007). The difference in BET surface area of H-AL-TPABr-OA, H-AL-HDA-OA and H-AL-PA-OA may affect their catalytic activity, as was reported by Cejka et al., (2007) that the surface area and porosity are important properties in the field of catalysis design and heterogeneous catalysis.

5.4. Chapter summary

In conclusion, the H_2SO_4 treatment of the as-received fly ash did not have a significant effect on the properties of the ZSM-5 precursor as there was no significant difference in the mineralogical phase composition between the as-received fly ash (FA) and the H_2SO_4 treated fly ash (AL). Furthermore, the SEM micrographs showed that the FA and AL particles were different only on their surface. However, the structural study of FA and AL by ^{27}Al NMR and FTIR revealed several vibrational transformations that occurred on their surface. Moreover, the investigation that was carried on the NMR aluminium coordination revealed that most of the mullite was trapped in the glassy phase of the as-received fly ash because the ^{27}Al NMR of AL only showed the presence of extra-framework aluminium while there were not changes in mineralogical phase composition and particle shape and size between FA and AL. These results were corroborated by the elemental composition of FA and AL that showed only minor changes. It could then be concluded that the main aim of the H_2SO_4 treatment of the as-received fly ash, which was to remove a significant amount of aluminium, was not achieved because the Si/Al ratio in FA and AL was 1.86 and 2.02 respectively. Therefore, extra fumed silica was still needed in order to adjust the Si/Al ratio in the hydrothermal gel. However, it could be observed by using the synthesis formulation that was optimised in Chapter 4 and by substituting FA by AL the product quality was improved. The mineralogical phase composition did not reveal the presence of the dense analcime phase that was observed during the variation of synthesis parameters in Section 4.3. Moreover, the ZSM-5 relative XRD crystallinity increased from 47 and 39 % in H-FA-HDA-OA and H-FA-PA-OA (Figure 4.15) to 51 and 45 % in H-AL-HDA-OA and H-AL-PA-OA (Figure 5.7) respectively. While the

ZSM-5 relative XRD crystallinity decreased from 58 % in H-FA-TPABr-OA to 54 % in H-AL-TPABr-OA. The H_2SO_4 pre-treatment also modified the ZSM-5 crystal size and shape in the fly ash-based ZSM-5 zeolite samples depending on the structure directing agent used. The ZSM-5 crystals were transformed from spherulitic in H-FA-TPABr-OA (Figure 4.16) to polycrystalline structures with a spherulitic habit in H-AL-TPABr-OA (Figure 5.8). The size of ZSM-5 changed from 3.75±0.28 by 3.66±0.49 µm in H-FA-TPABr-OA to 6.23±1.05 by 5.61±1.18 µm in H-AL-TPABr-OA; from 5.35±0.0.48 by 2.11±0.29 µm in H-FA-HDA-OA to 1.02±0.14 by 0.62±0.09 µm in H-AL-HDA-OA, and from 9.50±0.91 by 4.99±0.37 µm in H-FA-PA-OA to 18.92±2.01 by 6.76±0.91 µm in H-AL-PA-OA. The Brønsted acidity was the only property that showed clearly the effect of the H_2SO_4 pre-treatment on the product quality. The number of Brønsted acid sites changed from 0.37, 0.29 and 0.32 mmol H^+ per gram of zeolite in H-FA-TPABr-OA, H-FA-HDA-OA and H-FA-PA-OA (Figure 4.19) to 0.71, 0.46 and 0.42 mmol H^+ per gram of zeolite in H-AL-TPABr-OA, H-AL-HDA-OA and H-AL-PA-OA (Figure 5.11). H-AL-TPABr-OA and H-AL-HDA-OA had an acceptable BET surface area of 327. 5 and 353.1 m^2/g respectively compared to that of the commercial H-ZSM-5 (480.1 m^2/g) while the BET surface area of H-AL-PA-OA was only 39.4 m^2/g. The difference in BET surface area could be affected by the difference in ZSM-5 crystal size. Even if the H_2SO_4 pre-treatment of the as-received fly ash prior to the synthesis ameliorated some qualities of the final products, it was difficult to establish a correlation between the H_2SO_4 treatment and properties of the final ZSM-5 products. This could be due to the complexity of the feedstock (fly ash) even after being treated with concentrated sulphuric acid prior to the hydrothermal synthesis. Therefore the process still needed to be ameliorated in order to synthesise a competitive fly ash-based ZSM-5 zeolite. Thus extracting silicon and aluminium from fly ash and using the extracts in the synthesis of ZSM-5 zeolite was deemed to be a solution to avoid the presence of fly ash quartz and mullite impurities that affected the quality of the products, and that is investigated in Chapter 6. Moreover, even though this chapter only presented the characteristic of H-AL-TPABr-OA, H-AL-HDA-OA and H-AL-PA-OA, the characteristic of the catalytic products over H-AL-TPABr, H-AL-HDA and H-AL-PA are also investigated in Chapter 7.

CHAPTER 6: CHARACTERISATION OF ZSM-5 ZEOLITE SYNTHESISED FROM FUSED FLY ASH EXTRACT WITHOUT AN ADDITIONAL SOURCE OF SILICA

6.1. Introduction

In Chapter 4 and Chapter 5 unfused fly ash was used as starting material for the synthesis of ZSM-5 zeolite and an additional Si source (fumed silica) was added to adjust the Si/Al ratio. This chapter focuses on using a fusion step linked with oxalic acid treatment of the fused feedstock to avoid the addition of fumed silica to adjust the Si/Al ratio. The first part of this chapter presents the characteristics of different fused fly ash extracts before and after the treatment with oxalic acid. The second part focuses on the characteristics of ZSM-5 zeolite synthesised from fused fly ash extracts with tetrapropylammonium bromide (TPABr), 1,6-hexanediamine (HDA) and 1-propylamine (PA) as organic structure directing agents using XRD, SEM, FTIR, Brønsted acidity analysis, ^{27}Al NMR and N_2 BET .

6.2. Characteristics of fused fly ash extracts

Fused fly ash extracts (FFAE, FFAE1 and FFAE2) were characterised using XRD, SEM, FTIR and ICP. FFAE, FFAE1 and FFAE2 were obtained as follows: fused fly ash was mixed with deionised water. After filtration, concentrated sulphuric acid (95-99 %) was added dropwise to the filtrate to lower the pH to 10. A white precipitate called fused fly ash extract (FFAE) was formed, filtered and dried. FFAE powder was treated with a saturated oxalic acid solution (ratio 1:10) at 80 °C for 6 h. The treated fused fly ash extract called FFAE1 was washed and dried. Then, FFAE1 was treated for the second time with a fresh oxalic solution to obtain a new fused fly ash extract called FFAE2 as described in Section 3.3.1.3.

Figure 6.1 compares the XRD pattern of FFAE, FFAE1 and FFAE2.

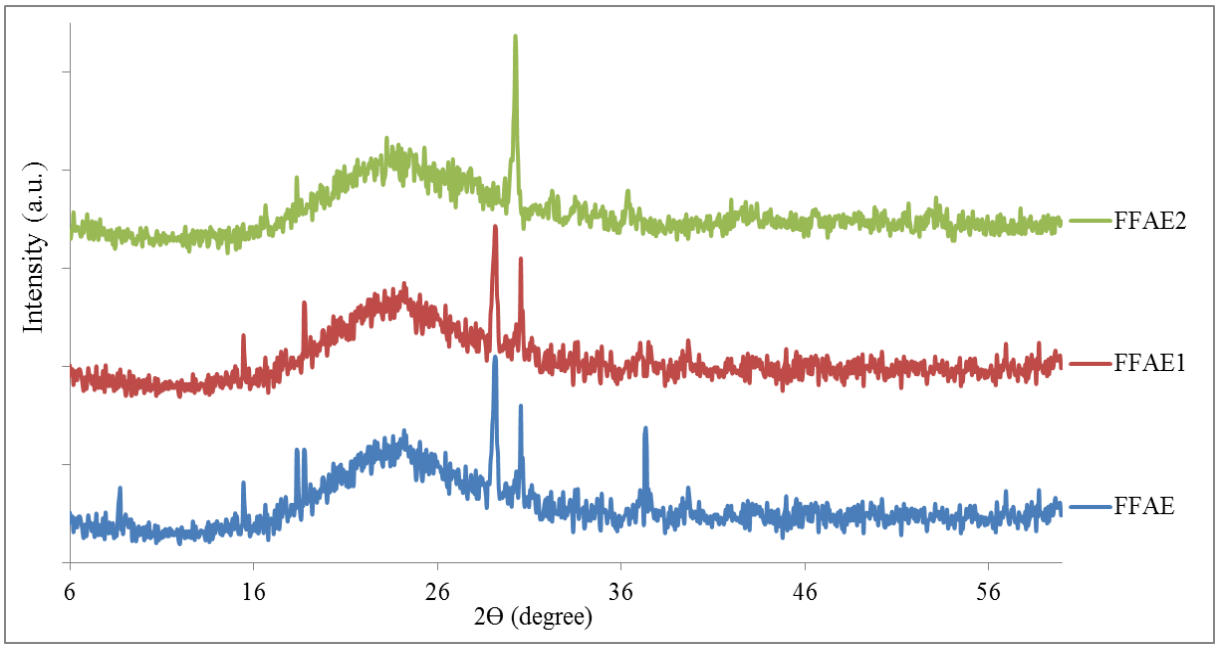

Figure 6.1: Comparison of XRD patterns of fused fly ash extracts (FFAE, FFAE1 and FFAE2).

Figure 6.1 showed that the fused fly ash extracts (FFAE, FFAE1 and FFAE2) were mainly amorphous that was characterised by the presence of a hump between 18 and 36° 2Θ. Furthermore, these XRD patterns of FFAE, FFAE1 and FFAE2 and that of the as-received fly ash (Section 4.2, Figure 4.1) had in common only the hump that characterises amorphous silica. The fusion process digested the refractory quartz and mullite phases completely as the results showed in Figure 6.1 were in agreement with the XRD pattern of amorphous silica reported by Abou Rida and Harb, (2014).

Figure 6.2 presents the SEM micrographs of FFAE, FFAE1 and FFAE2.

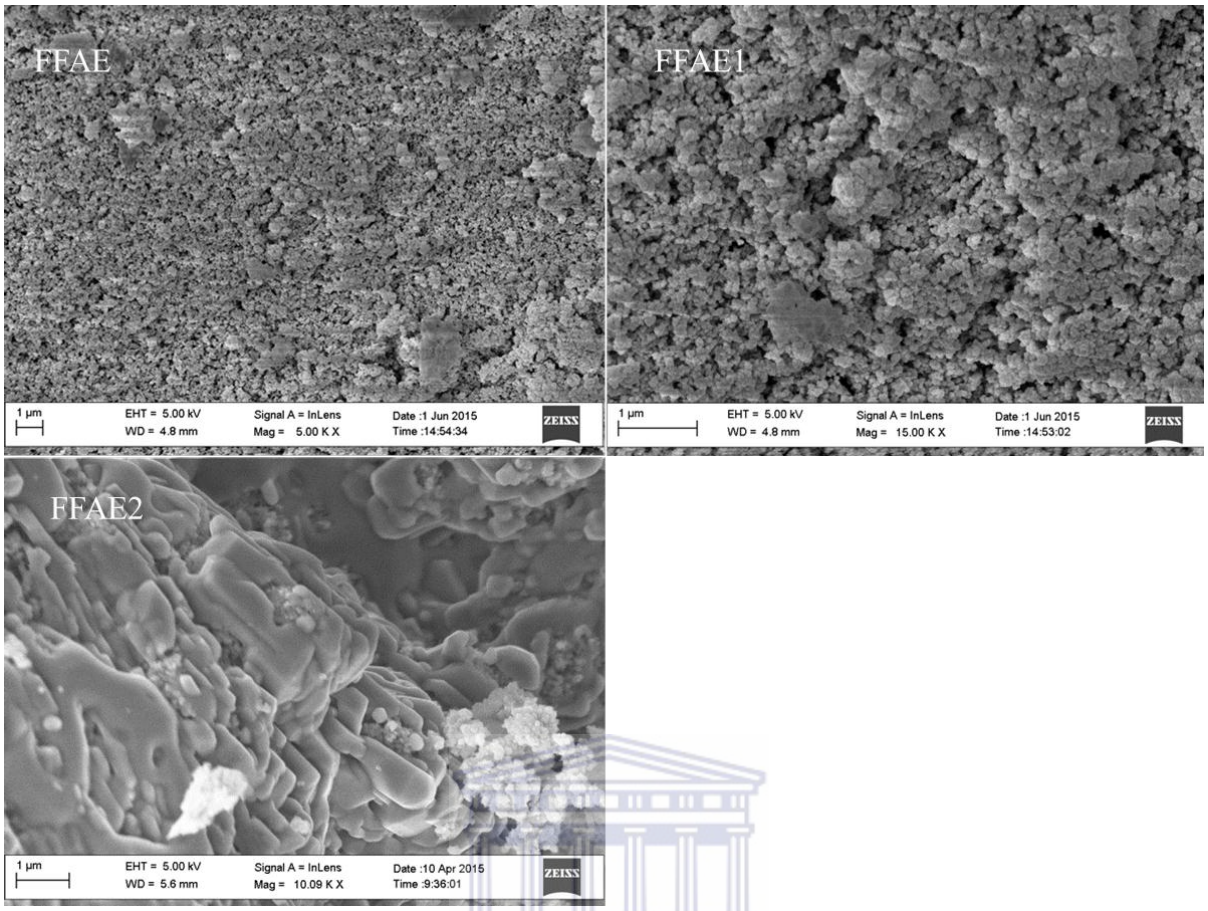

Figure 6.2: Comparison of SEM micrographs of fused fly ash extracts (FFAE, FFAE1 and FFAE2).

Figure 6.2 showed that the morphology depicted in the SEM micrographs of FFAE, FFAE1 and FFAE2 were different to that of the as-received fly ash which was composed of spherical particles (Figure 4.2). However, the SEM micrographs of fused fly ash extracts (FFAE, FFAE1 and FFAE2) were similar to that of the amorphous silica that was synthesised by Abou Rida and Harb, (2014).

Figure 6.3 compares the FTIR spectra of FFAE, FFAE1 and FFAE2.

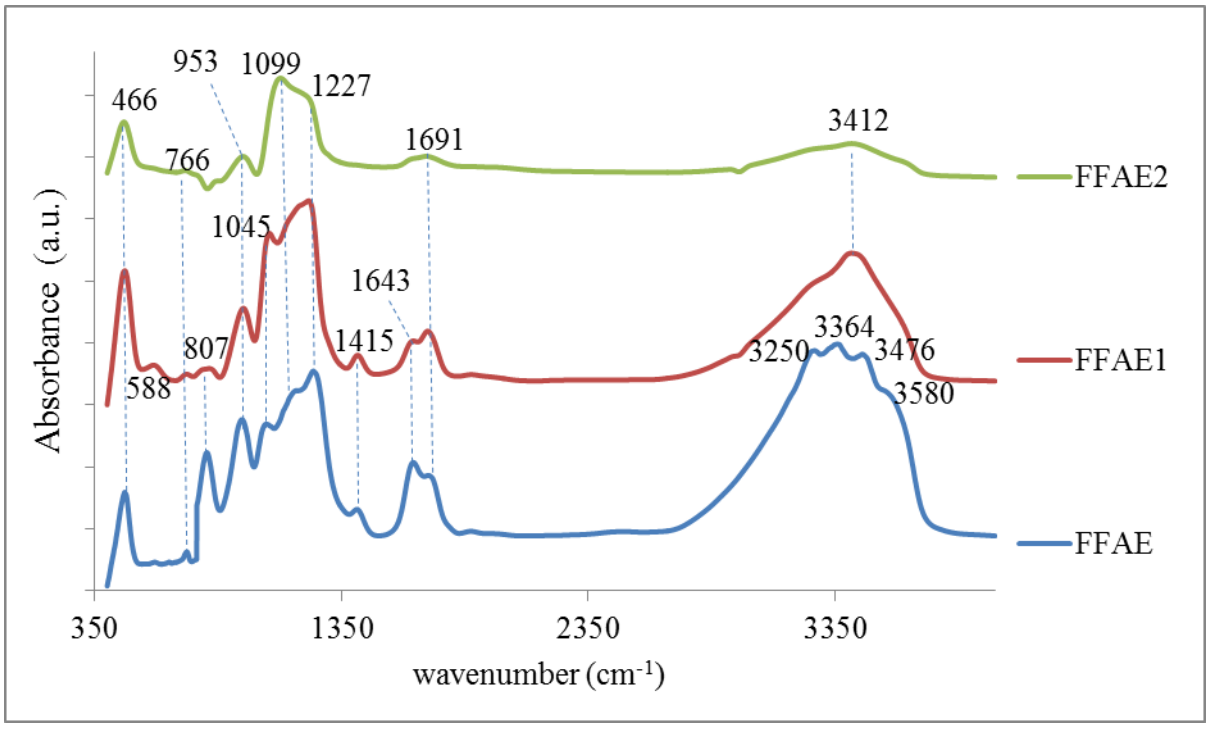

Figure 6.3: Comparison of FTIR spectra of fused fly ash extracts (FFAE, FFAE1 and FFAE2).

It could be seen in Figure 6.3 that the FTIR spectra of FFAE, FFAE1 and FFAE2 had four common bands. The vibrational bands that appeared at 466 and 766 cm^{-1} could be assigned to a bending vibration of the Si-O-Si bond and stretching vibration of Si-O-Si bond respectively, this indicated a condensation of SiO^- anoins (Abou Rida and Harb, 2014). The band at 953 cm^{-1} could be assigned to Si-O stretch of monomeric or dimeric SiO^- species (Bass and Turner, 1997). The vibrational band at 1691 could be assigned to H-O-H bending of water (Saikia and Parthasarathy, 2010). Besides those common bands, the FTIR spectrum of FFAE had a band at 807 cm^{-1} that corresponded to a stretching vibration of Si-O-Si bond (Abou Rida and Harb, 2014). The bands at 1045, 1099 and 1227 cm^{-1} could be assigned to asymmetric stretching vibrations (Tao and Kanoh, 2006; Ali et al., 2003). It was noteworthy that the bands at 953, 1045, 1099 and 1227 cm^{-1} indicated the degree of condensation of SiO^- species (Bass, 1997), with the band at 953 cm^{-1} corresponding to the monomeric or dimeric SiO^-, the band at 1045 cm^{-1} corresponding to a ring formed by condensation of SiO^- species and the bands at 1099 and 1227 cm^{-1} corresponding to a polymer of SiO^- species. The bands that appeared at 1415 and 1643 cm^{-1} could be attributed to the carbonate and H-O-H bending of water respectively (Miller and Wilkins, 1952; Saikia and Parthasarathy, 2010). The bands at 3250, 3364, 3476 and 3580 cm^{-1} could be due to H-OH stretching of absorbed water (Saikia

and Parthasarathy, 2010). The FTIR spectrum of FFAE1 also had the bands 807, 1045, 1227, 1415 and 1643 cm^{-1} that could correspond to the same vibrations of the FTIR spectrum of FFAE. However, it also had bands at 588 and 3412 cm^{-1} that could be attributed to Al-O stretch and H-OH stretching of absorbed water (Voll et al., 2002; Saikia and Parthasarathy, 2010). The FFAE2 spectrum had similar vibrational bands to FFAE and FFAE1 (Figure 6.3). However, it was noteworthy that the intensity of the band at 953 cm^{-1} decreased from the FFAE spectrum to that of FFAE2, moreover FFAE2 spectrum did not reveal a band at 1045 cm^{-1}, the band at 1099 cm^{-1} was more intense in the FFAE2 spectrum than in that of FFAE and FFAE1. These observations could lead to the conclusion that the treatment with oxalic acid removed a certain amount of monomeric and dimeric SiO^- species in FFAE1 and FFAE2, and the degree of condensed SiO^- species was high in FFAE2. This could affect the zeolitization process when using FFAE, FFAE1 or FFAE2 as source of Si and Al. Moreover, it could be observed that the spectra of FFAE, FFAE1 and FFAE2 were different to that of the commercial H-ZSM-5 presented in Figure 5.10, which corroborated the fact that these precursors did not show any ZSM-5 phase as also seen in the XRD patterns.

The XRD and FTIR results showed that FFAE, FFAE1 and FFAE2 powders were mainly amorphous silica with a mixture of monomeric, dimeric and polymeric SiO^- species. However, their elemental composition needed to be determined in order to know if they could be used as feedstocks for the synthesis of ZSM-5 zeolite. Therefore, they were digested following the method used by Missengue et al., (2015) as described in section 3.3.2. The digestates of FFAE, FFAE1 and FFAE2 were diluted in 2 % HNO_3 aqueous solution as detailed in section 3.4.5 prior to be analysed by ICP-OES. The elemental composition of FFAE, FFAE1 and FFAE2 was then determined (Figure 6.4).

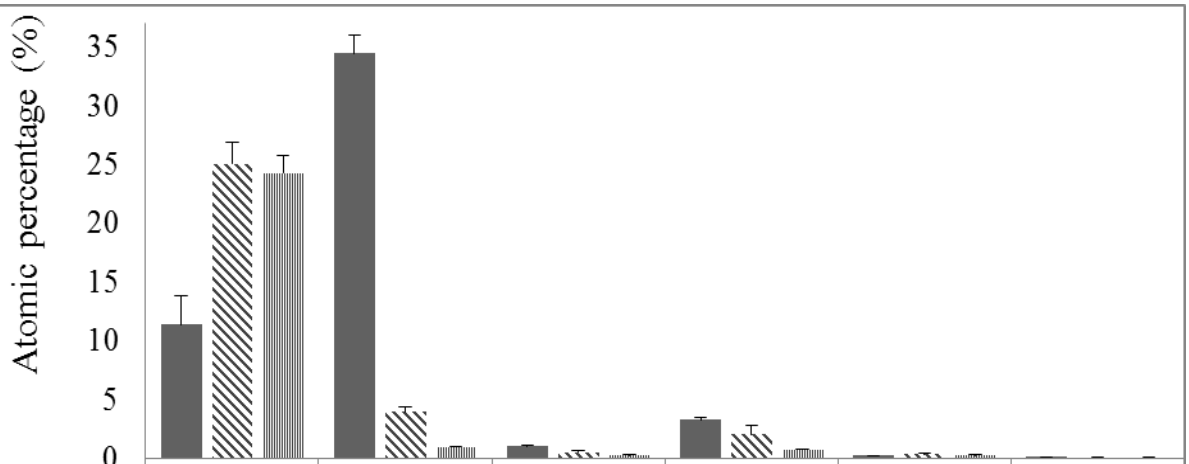

	Si	Na	Al	Ca	P	Mg
FFAE	11.4	34.5	1.1	3.3	0.3	0.2
FFAE1	25.1	4	0.6	2.1	0.4	0.1
FFAE2	24.3	1	0.3	0.8	0.3	0.1

Figure 6.4: Elemental composition in of FFAE, FFAE1 and FFAE2 (n=3).

The elemental composition of FFAE, FFAE1 and FFAE2 presented in Figure 6.4 was given in percentage of each element in the sample. Besides minor cations in the extracts, Figure 6.4 did not present the percentage of oxygen that formed silica with silicon because ICP-OES analyser only detects and quantifies cations. It could be seen that sodium (34.5±1.5 %) was the most abundant element in the fused fly ash extract (FFAE) that precipitated after treating the fused fly ash filtrate with concentrated sulphuric acid, followed by silicon (11.4±2.5 %), calcium (3.3±0.2 %) and aluminium (1.1±0.1 %). Moreover, the Si/Al molar ratio of FFAE was found to be 10. The first treatment of FFAE with a saturated oxalic solution removed most of the sodium as well as a certain percentage of aluminium and calcium. This resulted in silicon (25.1±1.8 %) being the most abundant element in FFAE1, followed by sodium (4.0±0.4 %), calcium (2.1±0.7 %) and aluminium (0.6±0.1 %). The Si/Al molar ratio of FFAE1 was 42. The second treatment with a saturated oxalic solution removed more sodium, aluminium and calcium. Hence silicon (24.3±1.5 %) was still the most abundant element in FFAE2, followed by sodium (1.0±0.0 %), calcium (0.8±0.0 %) and aluminium (0.3±0.1 %). The Si/Al molar ratio was 81. From these findings, it was predictable that FFAE, FFAE1 and FFAE2 with a Si/Al molar ratio of 10, 42 and 81 respectively, could be used to synthesise ZSM-5 zeolite. Moreover, the yield of FFAE, FFAE1 and FFAE2 from the starting mass of

the as-received fly ash (FA) was 31, 20 and 16 % respectively. This yield was calculated as follows: $Yield = \frac{mass(extract)}{mass(FA)} * 100$ **(Equation 6.1)**

It was reported by Van der Gaag, (1987) that ZSM-5 zeolite is a high silica zeolite with Si/Al≥11. Shcherban et al., (1995) reported a similar chemical composition (160-220 g/dm^{-3} of Na_2O, 100-250 g/dm^{-3} of SiO_2, 2-7 g/dm^{-3} of Al_2O_3 and 0.1-0.9 g/dm^{-3} of Fe_2O_3) with a high Si/Al ratio in an alkaline fly ash filtrate. Awizar et al., (2013) reported the equations of formation of silica by subsequently treating rice husk ash with NaOH and H_2SO_4 as follows:

$SiO_2(Ash) + 2NaOH \rightarrow Na_2SiO_3 + H_2O$ (**Equation 2.2**)

$Na_2SiO_3 + H_2SO_4 \rightarrow SiO_2 + Na_2SO_4 + H_2O$ (**Equation 2.3**)

However, the synthesis of high silica ZSM-5 zeolite from coal fly ash without an additional source of silica has not yet been reported.

6.3. Effect of the elemental composition of fused fly extracts on the properties of the synthesised ZSM-5 zeolite

FFAE, FFAE1 and FFAE2 powders obtained as discussed in Section 6.2 were used as starting materials for the synthesis of ZSM-5 zeolite without an additional source of silica. The powdered extract (FFAE, FFAE1 or FFAE2) (2 g) was mixed with 0.4 g of NaOH, 1.5 g of tetrapropylammonium bromide (TPABr) and 50 mL of deionised water (Table 3.6). The mixture was aged at room temperature for 30 min before undergoing a hydrothermal crystallisation at 160 °C for 72 h. The variation of the percentage of Si, Na, Al and Ca in FFAE, FFAE1 and FFAE2 (Figure 6.4) affected the number of moles of these elements in the gel and that of water and TPABr in the molar regime, hence the number of moles of water in FFAE, FFAE1 and FFAE2 was 3473, 5556 and 13890 mol and that of TPABr was 4, 7 and 14 mol respectively (Table 3.6). The synthesised products FFAE-TPABr, FFAE1-TPABr and FFAE2-TPABr were transformed into their H-form using 0.5 M NH_4NO_3 solution four times followed by calcination at 550 °C for 3 h (Section 3.3.1.3).

It was noteworthy that no solid product was formed when FFAE was used to synthesise FFAE-TPABr even if its Si/Al molar ratio of 10 was within the range required for the synthesis of ZSM-5 zeolite. Hattori and Yashina, (1994) investigated the effect of Na/Si ratio on the synthesis of ZSM-5 zeolite. They reported that below a Na/Si ratio of 0.016, the synthesised ZSM-5 zeolite was mixed with an amorphous phase; a pure phase of ZSM-5 zeolite was formed when the Na/Si ratio was between 0.016 and 0.4 and the increase in Na/Si ratio from 0.4 was accompanied by formation of ZSM-5 zeolite and α-SiO_2. Similar observations were reported by Singh and Dutta, (2003) in organic-free ZSM-5 zeolite synthesis. Moreover, they stated that the instability of the ZSM-5 zeolite was attributed to excess sodium. Whereas in the present study, the hydrothermal gel of FFAE-TPABr had a Na/Si ratio of 5 as shown in Table 3.6, which was much higher than the ratio reported by Hattori and Yashina, (1994) or Singh and Dutta, (2003). Therefore, it could be concluded that the high sodium content in FFAE prevented the crystallisation of ZSM-5 zeolite to occur. Hence, only H-FFAE1-TPABr and H-FFAE2-TPABr were further analysed using XRD, SEM, FTIR, and for their Brønsted acidity, ^{27}Al NMR and N_2 BET.

6.3.1. Mineralogical study of H-FFAE1-TPABr and H-FFAE2-TPABr by X-ray diffraction

Figure 6.5 compares the XRD patterns of the Si and Al precursors FFAE1 and FFAE2 to those of the synthesised H-FFA1-TPABr and H-FFAE2-TPABr with a commercial H-ZSM-5 (Com-ZSM-5) as reference.

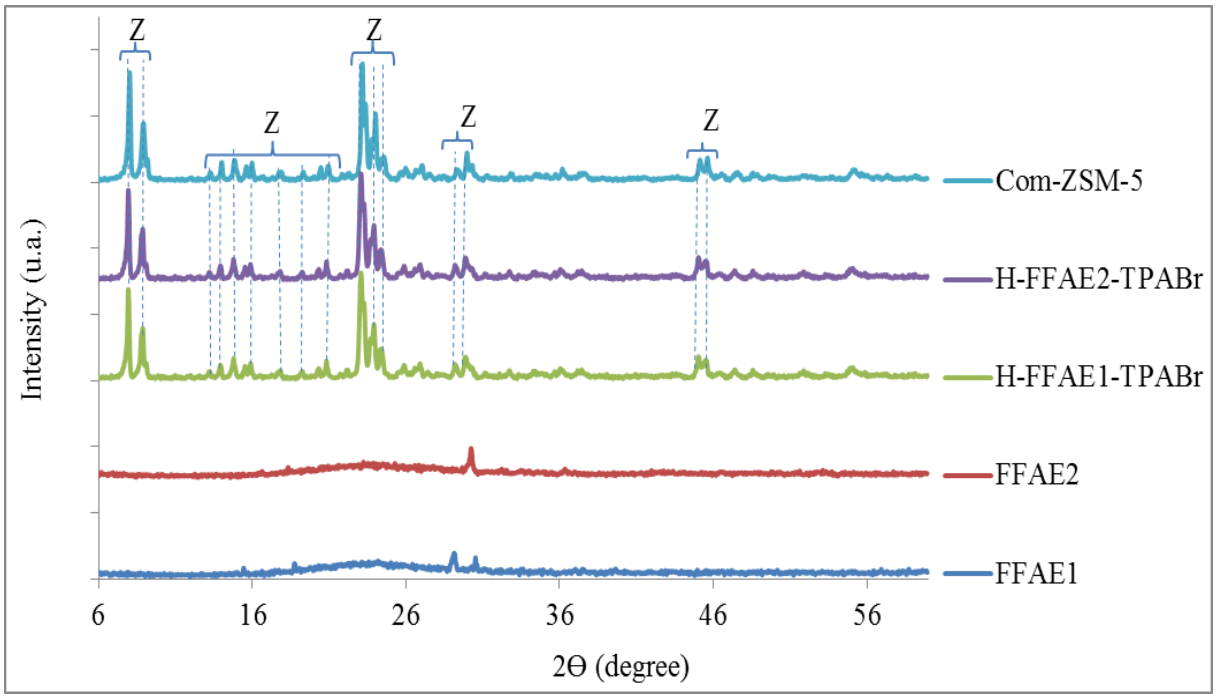

Figure 6.5: XRD patterns of Si and Al precursors (FFAE1 and FFAE2), H-FFAE1-TPABr, H-FFAE2-TPABr and commercial H-ZSM-5 (Com-ZSM-5) (Z=ZSM-5 zeolite).

FFAE1 and FFAE2 precursors consisted mainly of amorphous phase as discussed in Section 6.2. It could be observed in Figure 6.5 that the XRD patterns of H-FFAE1-TPABr and H-FFAE2-TPABr were identical to that of the commercial zeolite H-ZSM-5 (Com-ZSM-5). This was confirmed by comparison with the collection of simulated XRD power patterns for zeolites (Treacy and Higgins, 2001). The synthesis of ZSM-5 from fly ash normally required an addition of an important amount of silica source to adjust the Si/Al ratio as shown in earlier chapters. Kalyankar et al., (2011) synthesised ZSM-5 zeolite from Indian fly ash with a SiO_2/A_2O_3 ratio of 3. Silica sol was added to get a SiO_2/A_2O_3 ratio of 37.2 in the hydrothermal gel. Reanvattana, (2005) synthesised high purity ZSM-5 zeolite from a mixture of fused fly ash filtrate and added silica extracted from rice husk ash. Chareonpanich et al., (2004) synthesised ZSM-5 zeolite from Thailand fly ash with SiO_2/Al_2O_3 ratio of 1.6. SiO_2 extracted from rice husk ash was added to adjust the Si/Al molar ratio to 20, 40, 60, 80, 100 or 200. However, The results that were presented in this chapter showed that the use of fusion linked with oxalic acid treatment led to the synthesis of a pure ZSM-5 without the addition of an extra silica source unlike when using the as-received fly ash for the synthesis of H-FA-TPABr-OA or H_2SO_4 treated fly ash for the synthesis of H-AL-TPABr-OA or that presented in the literature that required an addition of silica source to adjust the Si/Al ratio in the

hydrothermal gel. The final products (H-FA-TPABr-OA and H-AL-TPABr-OA) still contained the unreacted feedstock phases (mullite and quartz) (Figures 4.14 and 5.6). Figure 6.6 presents the calculated ZSM-5 relative XRD crystallinity of H-FFAE1-TPABr and H-FFAE2-TPABr with a commercial H-ZSM-5 (Com-ZSM-5) as a reference. The ZSM-5 relative XRD crystallinity was determined according to the formulation suggested by Nicolaides, (1999) (Equation 4.1).

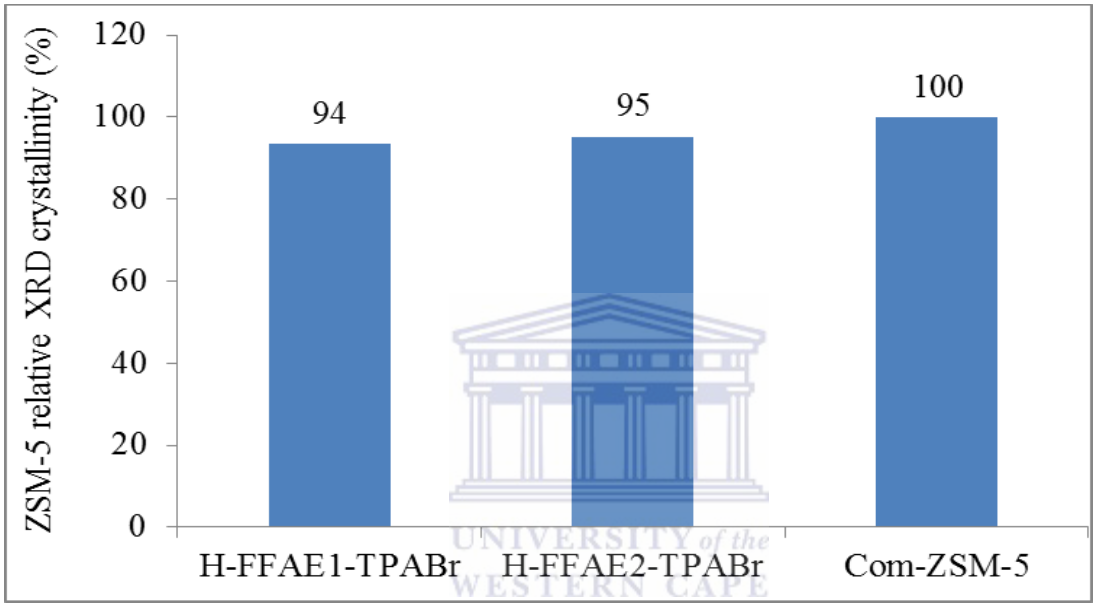

Figure 6.6: Calculated ZSM-5 relative XRD crystallinity of H-FFAE1-TPABr and H-FFAE2-TPABr compared to a commercial H-ZSM-5 zeolite (Com-ZSM-5).

Figure 6.6 showed that the calculated ZSM-5 relative XRD crystallinity of H-FFAE1-TPABr and H-FFAE2-TPABr was 94 and 95 % respectively relative to the commercial H-ZSM-5 zeolite, which was much higher than what was achieved when using additional silica. A second treatment of silica extract (FFAE1) with a saturated oxalic acid solution (FFAE2) led to only a slight increase in the ZSM-5 relative crystallinity. FFAE was not converted into ZSM-5, which was ascribed to its high Na content that came from NaOH used to fuse the as-received fly ash. Indeed, Hattori and Yashina, (1994) reported that a high Na content in a synthesis gel of ZSM-5 zeolite led to formation of α-SiO_2.

Furthermore, the ZSM-5 relative XRD crystallinity of H-FFAE1-TPABr and H-FFAE2-TPABr was much higher than that of H-FA-TPABr-OA (58 %) or H-AL-TPABr-OA (54 %) (Figures 4.15 and 5.7).

It should be noted that only the characteristics of H-FFAE1-TPABr and H-FFAE2-TPABr will be discussed in the sub-sections below because no product crystals of FFAE-TPABr were formed when FFAE was used as starting material.

6.3.2. Morphological study and elemental composition of H-FFAE1-TPABr and H-FFAE2-TPABr by scanning electron microscopy-energy dispersive spectroscopy

The influence of the elemental composition of the feedstocks FFAE1 and FFAE2 on the morphology of the synthesised H-FFAE1-TPABr and H-FFAE2-TPABr with TPABr as structure directing agent was investigated by scanning electron microscopy. FFAE1 was obtained by precipitating silica extract from the filtrate of fused fly ash using a concentrated sulphuric acid (FFAE), then treating FFAE with a saturated solution of oxalic acid. FFAE2 was prepared by treating FFAE1 with a fresh saturated oxalic acid solution as was explained in Section 3.3.1.3. FFAE1-TPABr or FFAE2-TPABr was obtained as follows: 2 g of FFAE1 or FFAE2; 0.4 g of NaOH; 1.5 g of TPABr and 50 mL of deionised water, to obtain a molar regime of Si(36), Al(1), Na(27), H_2O(5556), TPABr(7) or Si(81), Al(1), Na(56), H_2O(13890), TPABr(14) respectively (Table 3.6). The obtained hydrothermal gel underwent aging at room temperature for 30 min followed by hydrothermal synthesis at 160 °C for 72 h. The synthesised FFAE1-TPABr and FFAE2-TPABr were transformed into their H-form through treatment with 0.5 M of NH_4NO_3 solution at 80 °C for 1 h (repeated four times) followed by calcination at 550 °C for 3 h to obtain H-FFAE1-TPABr and H-FFAE2-TPABr (Section 3.3.1.3). Figure 6.7 presents the SEM micrographs of Si and Al precursors FFAE1 and FFAE2, H-FFAE1-TPABr, H-FFAE2-TPABr and the commercial H-ZSM-5.

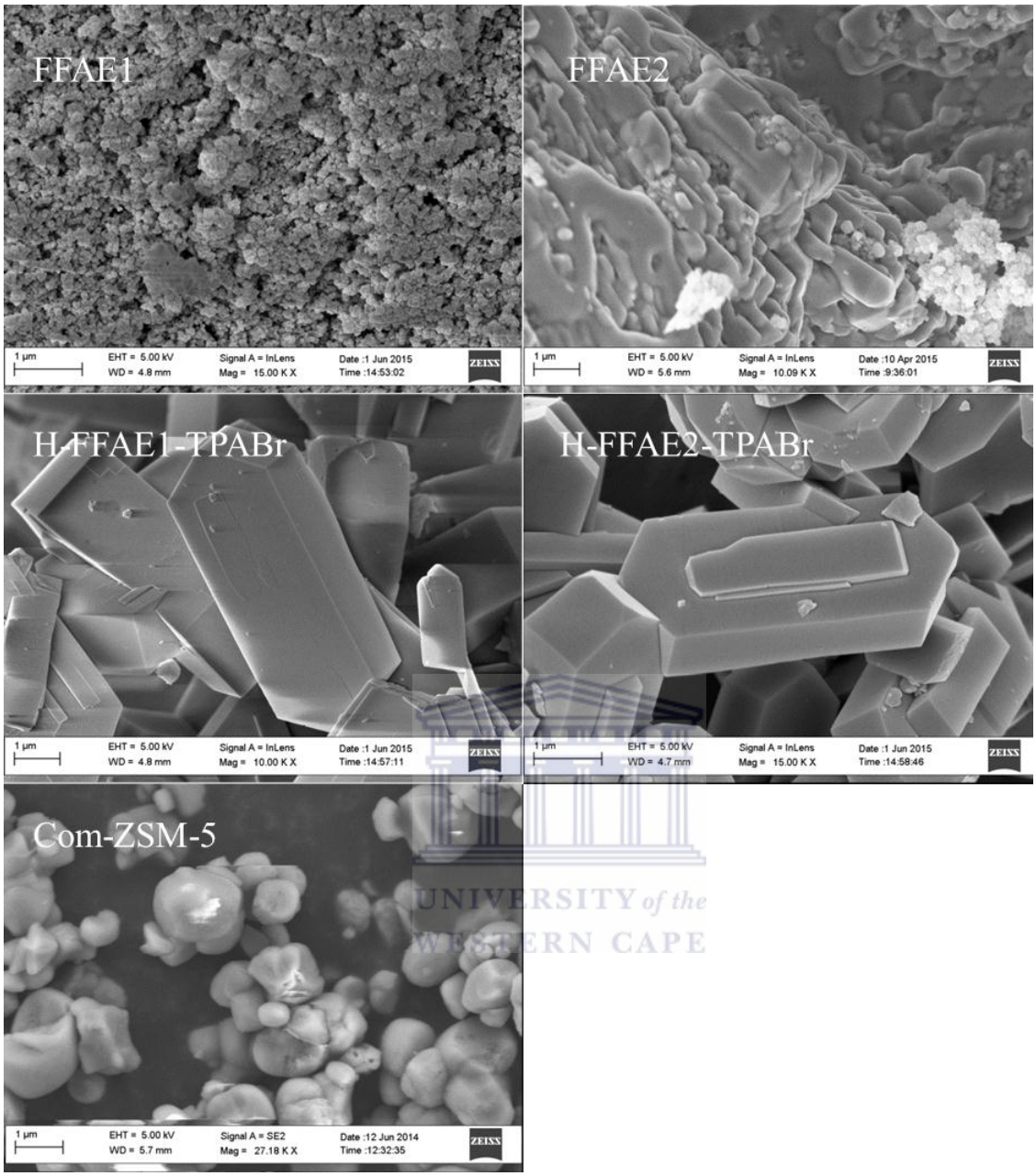

Figure 6.7: SEM micrographs of Si and Al precursors FFAE1 and FFAE2, H-FFAE1-TPABr, H-FFAE2-TPABr and commercial H-ZSM-5 (Com-ZSM-5).

The SEM micrographs showed that FFAE1 and FFAE2 were amorphous materials as discussed in Section 6.2. Figure 6.7 showed that the amorphous FFAE1 or FFAE2 was transformed into lath-shaped (or coffin-shaped) crystals characteristic of ZSM-5 after hydrothermal synthesis (H-FFAE1-TPABr or H-FFAE2-TPABr). The crystal shape of H-FFAE1-TPABr or H-FFAE2-TPABr was different from the spherulitic shape obtained from the two first sources of silicon and aluminium: fly ash (H-FA-TPABr-OA) and H_2SO_4 treated fly ash (H-AL-TPABr-OA) described in Chapter 4 (Section 4.4.2) and Chapter 5

(Section 5.3.2) respectively, or that reported by Petrik et al., (1995). This indicated that the composition of the hydrothermal gel was an important factor influencing the particle shape of ZSM-5zeolite. It was noteworthy that no amorphous phase was visible in the micrographs of the final products (H-FFAE1-TPABr and H-FFAE2-TPABr).

Figure 6.8 presents the mean crystal length and width of the H-FFAE1-TPABr or H-FFAE2-TPABr, using Equation 4.2.

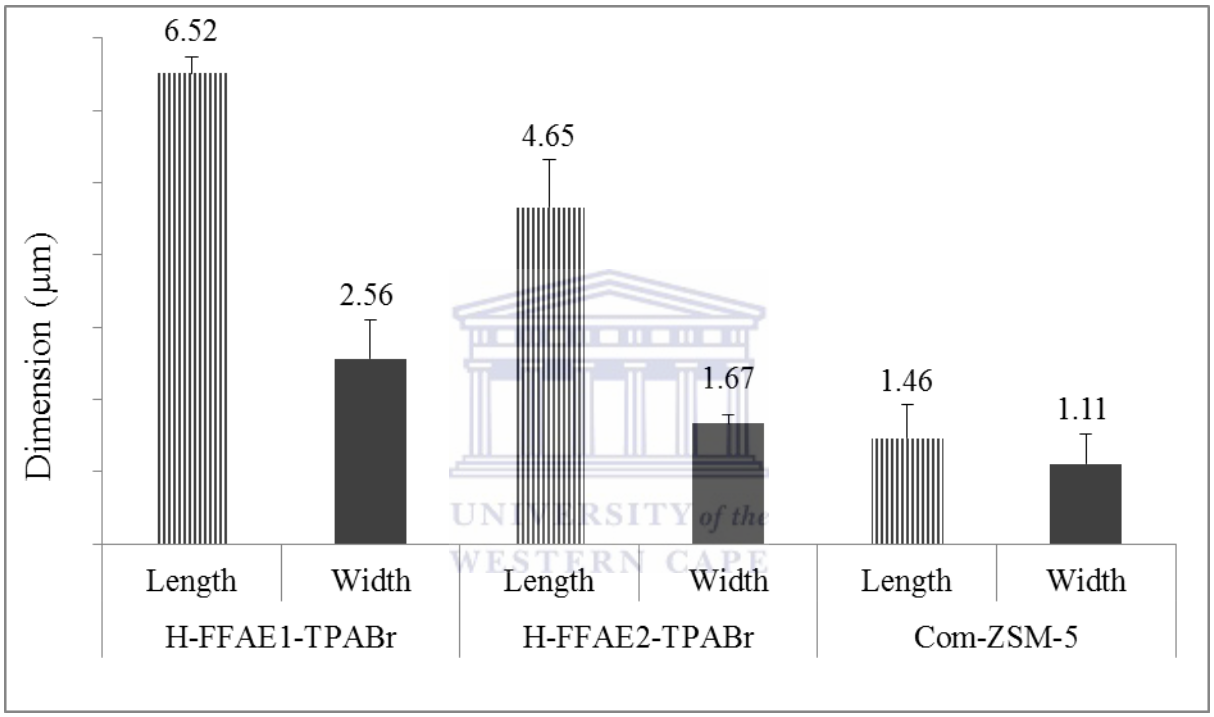

Figure 6.8: Mean crystal length and width of the H-FFAE1-TPABr, H-FFAE2-TPABr and a commercial H-ZSM-5 (Com-ZSM-5).

It could be seen from Figure 6.8 that the ZSM-5 crystal length and width decreased from H-FFAE1-TPABr (6.52±0.22 by 2.56±0.53 µm) to H-FFAE2-TPABr (4.65±0.67 by 1.67±0.12 µm), while the Si/Al ratio of their precursor feedstocks FFAE1 and FFAE2 was 42 and 81 respectively. However, these findings were in disagreement with the results reported by Shirazi et al., (2008), who stated that the ZSM-5 crystal size increased from 1 to 9 µm when the Si/Al molar ratio in the hydrothermal gel increased from 10 to 50. Furthermore, in the present study it was difficult to relate the decrease in ZSM-5 crystal size to the increase in Si/Al molar ratio as other chemical parameters such as the number of moles of sodium, TPABr or water also varied from the hydrothermal gel of FFAE1-TPABr to that of FFAE2-

TPABr (Table 3.6). Table 6.1 compares the semi quantitative elemental composition of the H-FFAE1-TPABr and H-FFAE2-TPABr to that of a commercial H-ZSM-5. The elemental composition was determined by analysing 10 spots of each sample by EDS.

Table 6.1: Elemental composition of the H-FFA1-TPABr, H-FFAE2-TPABr, and commercial H-ZSM-5 (Com-ZSM-5) (n=10).

Element	H-FFAE1-TPABr (%)	H-FFAE2-TPABr (%)	Com-ZSM-5 (%)
O	66.1±0.3	65.7±0.7	66.2±0.2
Si	32.1±0.4	31.8±0.7	32.0±0.2
Al	0.9±0.4	0.5±0.5	1.1±0.3
Na	0.7±0.7	1.3±1.5	0.4±0.4
Mg	0.0±0.0	0.3±0.4	0.1±0.2
Fe	0.1±0.1	0.1±0.2	0.0±0.0
Ca	0.0±0.0	0.1±0.1	0.1±0.1
K	0.1±0.1	0.1±0.2	0.1±0.1
Si/Al	36	60	29

Table 6.1 showed that the Si/Al ratio of the H-FFAE1-TPABr, H-FFAE2-TPABr and the commercial H-ZSM-5 (Com-ZSM-5) was 36, 60 and 29 respectively. There was a correlation between the Si/Al ratio of the H-FFAE1-TPABr and H-FFAE2-TPABr, and that of their precursor FFAE1 and FFAE2 that was 42 and 81 respectively. There was only a tiny amount of exchangeable cations remaining in the final products after ion exchange and calcination showing that the ion exchange procedure was adequate to overcome diffusional constraints in the large lath-shaped crystals of the fly ash-based H-ZSM-5.

6.3.3. Structural analysis of H-FFAE1-TPABr and H-FFAE2-TPABr by Fourier transform infrared

H-FFAE1-TPABr and H-FFAE2-TPABr samples were synthesised from the fused fly ash extracts FFAE1 and FFAE2 without an addition of fumed silica in the conditions that were detailed in Section 3.3.1.3 with the molar regime of Si(36), Al(1), Na(27), H_2O(5556), TPABr(7) and Si(81), Al(1), Na(56), H_2O(13890), TPABr(14) respectively. The synthesised FFAE1-TPABr and FFAE2-TPABr were transformed into their H-form by treatment with NH_4NO_3 solution followed by calcination as was detailed in Section 3.3.1.3. Figure 6.9 presents the FTIR spectra of the Si and Al precursors FFAE1 and FFAE2, H-FFAE1-TPABr, H-FFAE2-TPABr and commercial H-ZSM-5 (Com-ZSM-5).

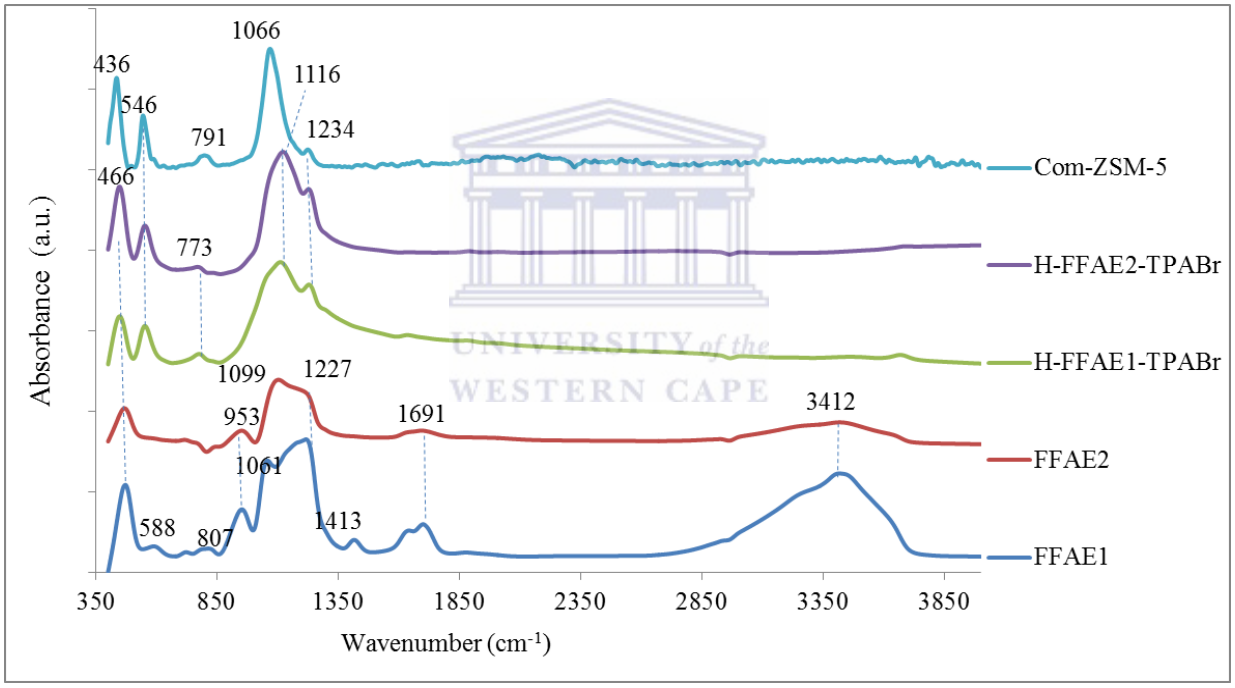

Figure 6.9: FTIR spectra of the Si and Al precursors FFAE1 and FFAE2, H-FFAE1-TPABr, H-FFAE2-TPABr and commercial H-ZSM-5 (Com-ZSM-5).

The FTIR spectra of the feedstocks FFAE1 and FFAE2 were presented in Section 6.2 and that of the commercial ZSM-5 was discussed in section 4.4.3. Figure 6.9 showed that H-FFAE1-TPABr and H-FFAE2-TPABr spectra had a band at 466 cm^{-1} that could be assigned to a Si-O-Si bend. A band at 546 cm^{-1} could correspond to a double ring (Shirazi et al., 2008). It was noteworthy that the double ring band characteristic of the zeolite framework appeared after synthesising H-FFAE1-TPABr and H-FFAE2-TPABr from FFAE1 and FFAE2 respectively.

This was further confirmation of the successful synthesis of ZSM-5 zeolite from fused fly ash extracts (FFAE1 and FFAE2) without any additional source of silica, which was indicated by XRD patterns (Figure 6.5). The FTIR spectra of H-FFAE1-TPABr and H-FFAE2-TPABr also presented bands at 773, 1116 and 1234 cm^{-1} that corresponded to external symmetric stretch, internal and external asymmetric stretch respectively (Shirazi et al., 2008; Van der Gaag, 1987). It could also be observed that there was no appearance of a C-H band in the region between 2852 and 2988 cm^{-1} that could indicate the presence of the structure directing agent TPABr in H-FFAE1-TPABr and H-FFAE2-TPABr (Shirazi et al., 2008) showing that the detemplation was complete. Although, the spectra of H-FFAE1-TPABr and H-FFAE2-TPABr were similar to that of commercial H-ZSM-5 (Com-ZSM-5), it could be noticed that a band shift was observed from 773 cm^{-1} in H-FFAE1-TPABr and H-FFAE2-TPABr compared to 791 cm^{-1} in commercial H-ZSM-5 (ZSM-5) and from 1116 cm^{-1} in H-FFAE1-TPABr and H-FFAE2-TPABr to 1066 cm^{-1} in commercial H-ZSM-5 (ZSM-5). According to Shirazi et al., (2008), a shift of the internal asymmetric stretch band towards higher wavenumbers was due to an increase in Si/Al ratio and Ali et al., (2003) reported that the shift was because of the slightly lower mass of aluminium compared to that of silicon. It could then be concluded that the shift of the internal asymmetric stretch observed in Figure 6.9 was due to the difference in Si/Al ratio of the H-FFAE1-TPABr and H-FFAE2-TPABr, and the commercial H-ZSM-5 that was 36, 60 and 29 respectively (Table 6.1). Moreover, the optical density ratio of H-FFAE1-TPABr and H-FFAE2-TPABr, determined using the Si-O-Si bend and double ring vibration bands at 466 and 546 cm^{-1} (Equation 4.3 in Section 4.4.3), was 0.96 and 0.90 respectively, which was an indication that the degree of crystallinity was higher in H-FFAE1-TPABr than in H-FFAE2-TPABr. This could be in relation to the degree of polymerisation of SiO^- species in the precursors FFAE1 and FFAE2 as it was concluded in Section 6.2 (Figure 6.3) that the degree of monomeric and dimeric SiO^- species was high in FFAE1 compared to FFAE2. Therefore, the high degree of SiO^- polymerisation in FFAE2 was a handicap to the zeolitization process of H-FFAE2-TPABr.

Moreover, the comparison of the FTIR spectra of FA and AL (Figure 5.3), FFAE1, FFAE2 and H-FFAE1-TPABr (Figure 6.9) would help to distinguish between the bands characteristic of the amorphous phase of fly ash, quartz, mullite and ZSM-5. Table 6.2 summarises different bands in FA, AL, FFAE1, FFAE2 and H-FFAE1-TPABr spectra and their attribution.

Table 6.2: Comparison of FA, AL, FFAE1, FFAE2 and H-FFAE1-TPABr FTIR data.

FA		AL		H-FFAE1-TPABr	
cm^{-1}	Attribution	cm^{-1}	Attribution	cm^{-1}	Attribution
451	Si-O-Si bend	455	Si-O-Si bend	466	Si-O-Si bend
555	Al-O stretch	579	Al-O stretch	546	Double ring
800	Amorphous phase	615	Si-O-T stretch	773	Si-O stretch
919	Al-O stretch (AlO_4)	678	Al-O stretch (AlO_6)	1116	Si-O stretch
1099	Si-O stretch	796	Amorphous phase	1234	Si-O stretch
1415	Carbonate	852	OH deformation (Al^{3+})		
1876	Potassium phosphate	889	OH deformation ($2Al^{3+}$)		
		1013	Si-O stretch		
FFAE1		1070	Si-O stretch	FFAE2	
cm^{-1}	Attribution	1100	Si-O stretch	cm^{-1}	Attribution
466	Si-O-Si bend	1175	Si-O stretch	466	Si-O-Si bend
766	Si-O-Si stretch	1284	Al-O for AlO_4	766	Si-O-Si stretch
953	Si-O stretch	1327	Al-O for AlO_4	953	Si-O stretch
1045	Si-O stretch	1630	H-O-H bend (water)	1045	Si-O stretch
1227	Si-O stretch	2482	Si-OH vibration	1099	Si-O stretch
1415	Carbonate	2606	Si-OH vibration	1227	Si-O stretch
1643	H-O-H bend (water)	3395	H-O-H stretch (water)	1415	Carbonate
1691	H-O-H bend (water)			1691	H-O-H bend (water)
3412	H-O-H stretch (water)			3412	H-O-H stretch (water)

Table 6.2 revealed that FA was composed of several overlapped bands that could only be observed after treatment with concentrated H_2SO_4 (AL) or silica extraction (FFAE1). It could be seen that the Si-O-Si bend characteristic of siliceous materials was present in FA, AL and FFAE1. However, it appeared at 451 cm^{-1} in FA (Si/Al=1.86) and shifted to higher wavelength with the increase in Si/Al ratio, 455 cm^{-1} in AL (Si/Al=2.02) and 466 cm^{-1} in FFAE1 (Si/Al=42), which was an amorphous material. The Al-O stretch band that appeared between 555 and 579 cm^{-1} was present only in FA and AL spectra due to the low aluminium content in FFAE1; however the band also shifted to a higher wavelength with an increase in Si/Al ratio. The bands at 555, 800, 919 and 1099 cm^{-1} in the FA spectrum hid several bands that appeared in AL by using a concentrated H_2SO_4 treatment. The treatment of FA with

concentrated H_2SO_4 revealed the presence of Al-O bands related to the presence of mullite at 579, 615, 678, 852, 889, 1284 and 1327 cm^{-1}, which did not appeared in FFAE1 spectrum because of the absence of mullite in the sample as shown by its XRD pattern (Figure 6.1). The Si-O stretch bands that appeared between 953 and 1227 cm^{-1} in FA, AL and FFAE1 spectra were related to the presence of the amorphous phase of fly ash, quartz and mullite. Furthermore, their shifting towards low or high wavelengths could be related to the aluminium content and distribution (AL) or the condensation of SiO^- species. However, the degree of SiO^- condensation in FFAE1 could be revealed by treating FFAE1 with a saturated oxalic acid solution as detailed in Section 3.3.1.3. And it could be observed in Figure 6.9 that the intensity of the SiO^- monomeric or dimeric band at 953 cm^{-1} decreased and a SiO^- polymeric band appeared at 1099 cm^{-1}. The difference between the bands related to the amorphous silica and ZSM-5 could be observed by comparing the FFAE1 and FFAE1-TPABr spectra. The appearance of a double ring band at 546 cm^{-1} in FFAE1-TPABr was an indication of the transformation of FFAE1 into zeolitic material. Moreover, the disappearance of the SiO^- monomeric or dimeric band at 953 cm^{-1} and an appearance of a band at 1116 cm^{-1} also indicated the condensation of SiO^- in FFAE1-TPABr into the zeolite framework structure.

6.3.4. Brønsted acidity of H-FFAE1-TPABr and H-FFAE2-TPABr

H-FFAE1-TPABr and H-FFAE2-TPABr were synthesised from FFAE1 (Si/Al=42) and FFAE2 (Si/Al=81). Thereafter they were detemplated before being transformed to their H-form using 0.5 M NH_4NO_3 followed by calcination at 550 °C for 3 h as detailed in Section 3.3.1.3. Figure 6.10 compares the number of Brønsted acid sites of H-FFAE1-TPABr, H-FFAE2-TPABr with the commercial H-ZSM-5 (Com-ZSM-5) using the H/D exchange isotope technique (Section 3.4.6).

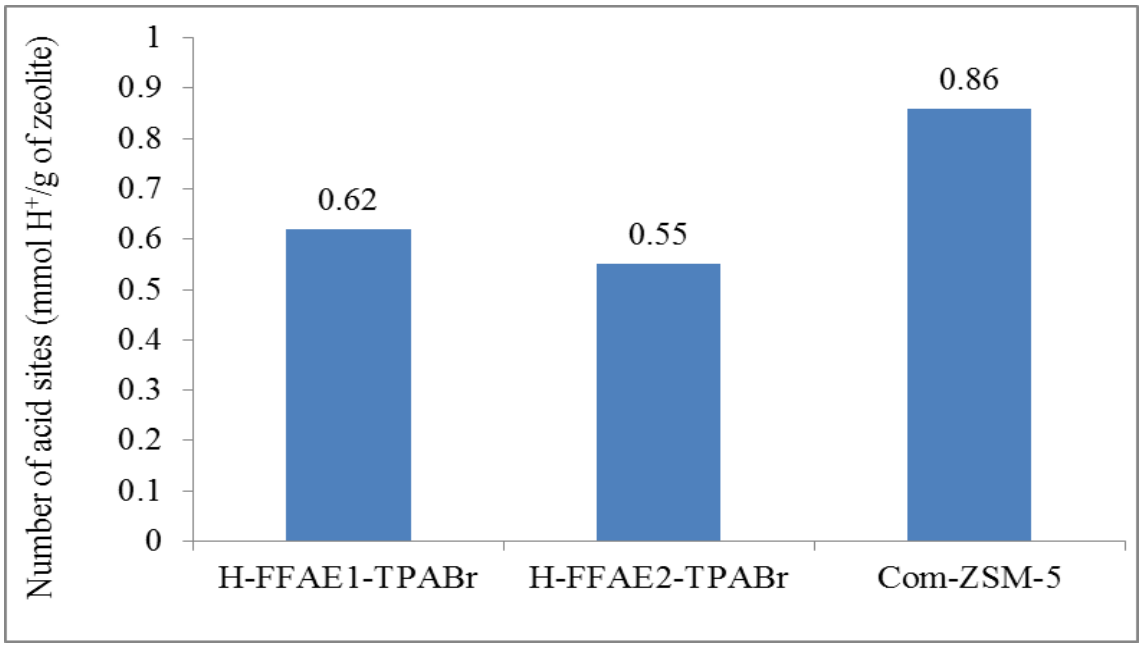

Figure 6.10: Number of Brønsted acid sites (mmol H+/g of zeolite) of the H-FFAE1-TPABr, H-FFAE2-TPABr and the commercial H-ZSM-5 (Com-ZSM-5).

Figure 6.10 showed that the number of Brønsted acid sites of H-FFAE1-TPABr, H-FFAE2-TPABr and commercial H-ZSM-5 (Com-ZSM-5) was 0.62, 0.55 and 0.86 mmol H^+ per gram of zeolite, respectively. It could be observed that the number of Brønsted acid sites of the synthesised zeolites H-FFAE1-TPABr, H-FFAE2-TPABr decreased with an increase in their Si/Al ratio that was 36 and 60 respectively (Table 6.1). This indicated that the number of Brønsted acid sites was related to their aluminium content.

6.3.5. Aluminium coordination analysis of H-FFAE1-TPABr and H-FFAE2-TPABr by ^{27}Al nuclear magnetic resonance

The influence of the elemental composition of the precursors FFAE1 and FFAE2 on the aluminium coordination in fly ash-based ZSM-5 zeolite products (H-FFAE1-TPABr and H-FFAE2-TPABr) was investigated by comparing the ^{27}Al solid state NMR spectra of FFAE1, FFAE2, H-FFAE1-TPABr and H-FFAE2-TPABr with that of a commercial H-ZSM-5 as shown in Figure 6.11. $Al(NO_3)_3$ solution (0.1 M) was used as reference. H-FFAE1-TPABr and H-FFAE2-TPABr were obtained as follows: FFAE1 or FFAE2 (2 g), 0.4 g of NaOH, 1.5 g of TPABr and 50 mL of deionised water (Table 3.6). The hydrothermal crystallisation was performed at 160 °C for 72 h. The synthesised products FFAE1-TPABr

and FFAE2-TPABr were transformed in their H-form through ion exchange with NH_4NO_3 solution followed by calcination (Section 3.3.1.3).

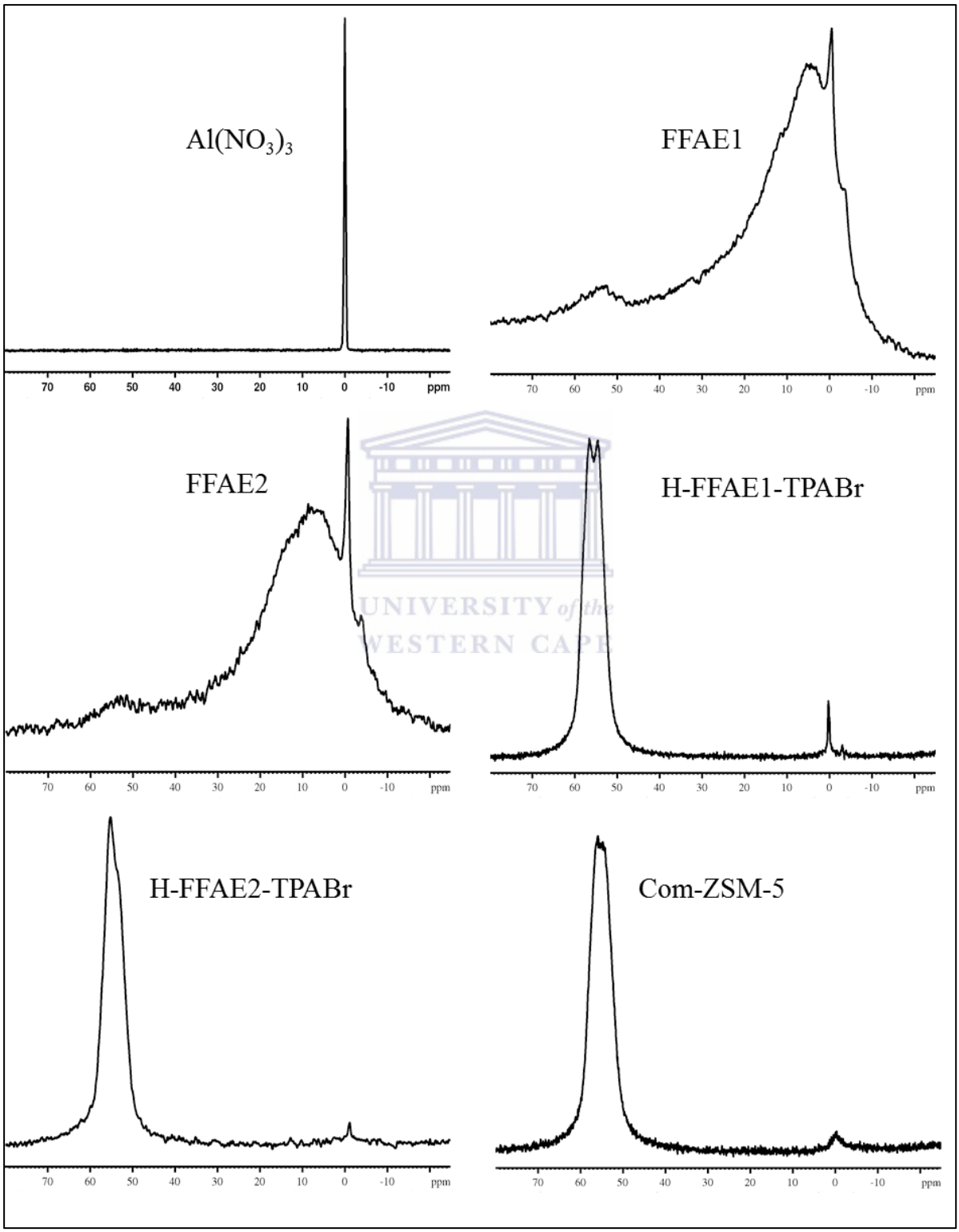

Figure 6.11: ^{27}Al NMR spectra of a reference (0.1 M $Al(NO_3)_3$), FFAE1, FFAE2, H-FFAE1-TPABr, H-FFAE2-TPABr and commercial H-ZSM-5.

A commercial zeolite ZSM-5 and $Al(NO_3)_3$ were used as references to differentiate between the types of ^{27}Al NMR signals. It could be observed in Figure 6.11 that the presence of an intense signal appeared in FFAE1 and FFAE2 spectra at 0 ppm. These samples also had an intense but broad signal at 10 ppm and a small, broad signal at about 52 ppm. The signals at 0, 10 and 52 ppm disappeared after synthesis in H-FFAE1-TPABr and H-FFAE2-TPABr, with the appearance of an intense and narrow signal at 55 ppm. It was stated in the literature that the signal at about 0 ppm corresponded to extra-framework octahedrally coordinated Al and an intense signal at about 55 ppm corresponded to framework tetrahedrally coordinated Al (Triantafyllidis et al., 2004; Sazama et al., 2011). Byrappa and Yoshimura, (2001) stated that when the extra-framework aluminium species are in the form of polymeric aluminium oxide, broad signals of tetrahedral coordination ($Al^{IV'}$) or penta-coordinated species may appeared in the region between 30-50 ppm due to the distortions of the octahedral symmetry of the AlO_6 units. Therefore, it could be concluded that FFAE1 and FFAE2 had aluminium in several coordinations, and the zeolite products H-FFAE1-TPABr and FFAE2-TPABr had mainly framework tetrahedrally coordinated aluminium.

Table 6.3 gives the percentage of framework and extra-framework aluminium in $Al(NO_3)_3$, FFAE1, FFAE2, H-FFAE1-TPABr, H-FFAE2-TPABr and the commercial ZSM-5 zeolite.

Table 6.3: Percentage of framework and extra-framework aluminium in 0.1 M $Al(NO_3)_3$, FFAE1, FFAE2, H-FFAE1-TPABr, H-FFAE2-TPABr and the commercial H-ZSM-5 and the number of the Brønsted acid sites of the zeolites.

Sample	Framework tetrahedrally coordinated Al (%)	Extra-framework octahedrally coordinated Al (%)	Number of Brønsted acid sites (mmol H^+/g)
Reference $Al(NO_3)_3$	0.0	100.0	/
FFAE1	15.0	85.0	/
FFAE2	11.5	88.5	/
H-FFAE1-TPABr	98.6	1.4	0.62
H-FFAE2-TPABr	97.8	2.2	0.55
Commercial H-ZSM-5	98.5	1.5	0.86

It could be seen from Table 6.3 that FFAE1 and FFAE2 contained 85 and 88.5 % of extra-framework octahedrally coordinated Al respectively. It was noteworthy that the ^{27}Al NMR spectra of FA and AL had 29.2 and 100 % of extra-framework aluminium (Tables 4.2 and 5.2). However, they were trapped in a glassy phase of fly ash, which was the cause of their poor conversion into framework tetrahedrally coordinated aluminium. Indeed, the percentage of framework aluminium in H-FA-TPABr-OA and H-AL-TPABr-OA spectra was only 88.4 and 79.9 % respectively. While H-FFAE1-TPABr and H-FFAE2-TPABr contained 98.6 and 97.8 % of framework tetrahedrally coordinated aluminium. Moreover, there was a correlation between the percentage of framework aluminium in H-FFAE1-TPABr and H-FFAE2-TPABr spectra and the number of their Brønsted acid sites that was 0.62 and 0.55 mmol H^+ per gram of zeolite. This was in agreement with the statement made by Louis et al., (2004) that the number of Brønsted acid sites of ZSM-5 zeolite was equal to its framework aluminium content.

6.3.6. Surface area analysis of H-FFAE1-TPABr and H-FFAE2-TPABr by N_2 Brunauer-Emmett-Teller

Figure 6.12 shows the adsorption/desorption isotherms of N_2 and BET surface area of H-FFAE1-TPABr, H-FFAE2-TPABr and the commercial H-ZSM-5, which were determined by N_2 adsorption-desorption measurements performed at 77.41 K. H-FFAE1-TPABr and H-FFAE2-TPABr were degassed at 90 °C for 2 h and 400 °C for 4 h prior to the BET analysis as shown in Section 3.4.7. H-FFAE1-TPABr and H-FFAE2-TPABr were synthesised from fused fly ash extracts (FFAE1 and FFAE2) in the following synthesis conditions: FFAE1 or FFAE2 (2 g), 0.4 g of NaOH, 1.5 g of TPABr and 50 mL of deionised water. The gel underwent aging at room temperature for 30 min followed by hydrothermal crystallisation at 160 °C for 72 h. FFAE1-TPABr and FFAE2-TPABr products were transformed in their H-form through ion exchange with NH_4NO_3 solution followed by calcination (Section 3.3.1.3).

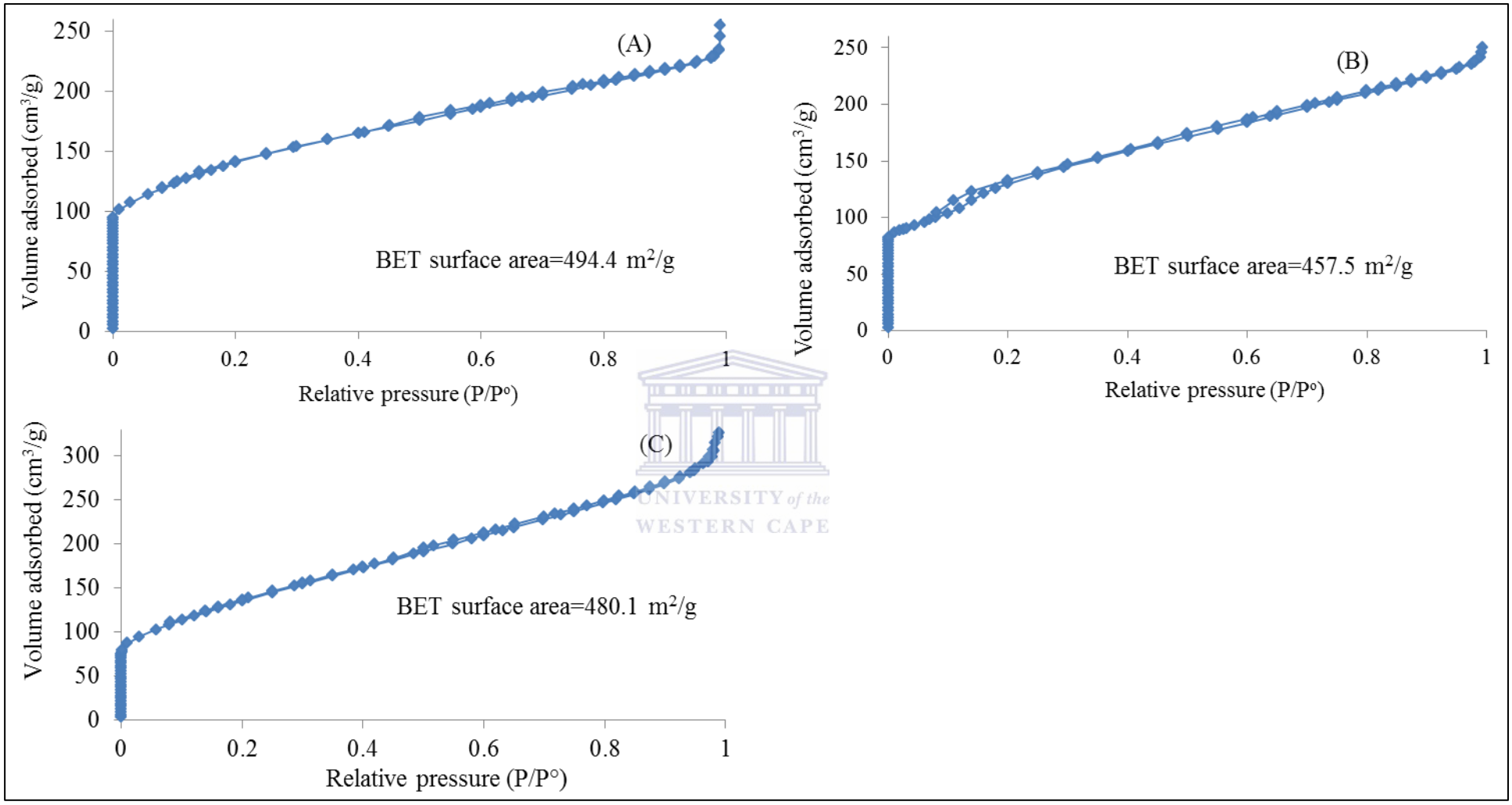

Figure 6.12: Adsorption/desorption isotherms of N_2 at 77.41 K and BET surface area of (A) H-FFAE1-TPABr, (B) H-FFAE2-TPABr and (C) commercial H-ZSM-5.

It could be seen from Figure 6.12 that the adsorption-desorption isotherms of H-FFAE1-TPABr, H-FFAE2-TPABr and the commercial ZSM-5 were that of type IV with the presence of a small hysteresis loop characteristic of the presence of mesopores in their structure (Lowell et al., 2004). The BET surface area of H-FFAE1-TPABr, H-FFAE2-TPABr and the commercial H-ZSM-5 was 494.4, 457.5 and 480.1 m^2/g respectively, showing that a pure phase of ZSM-5 could be synthesised from fly ash extracts without an additional silica source and had textural properties that were similar to that of a commercial ZSM-5 zeolite. It was also noteworthy that the BET surface area of the synthesised fly ash-based ZSM-5 zeolite products decreased with an increase in their Si/Al ratio that was 36 and 60 respectively (Table 6.1). This could indicate that the presence of more aluminium in the ZSM-5 framework would lead to an increase in the BET surface area. However, these results were in disagreement with Shirazi et al., (2008) who reported that the BET surface area of ZSM-5 zeolite synthesised from aluminium sulphate, sodium silicate and TPABr increased with an increase in molar ratios of Si/Al (10, 25, 40 and 50) in the hydrothermal gel. They synthesised their zeolites under agitation speed of 700 rpm at 180 °C for 24 h. However, it would be difficult to compare their results to that of the present study as the source of starting materials and the synthesis conditions applied were different. Moreover, in the present study only two Si/Al ratios (42 and 81) of the precursors FFAE1 and FFAE2 were compared; which does not give a conclusive trend or optimum. Table 6.4 compares the textural properties of the synthesised ZSM-5 zeolite products H-FFAE1-TPABr and H-FFAE2-TPABr to that of a commercial H-ZSM-5.

Table 6.4: Properties of the synthesised ZSM-5 zeolite products H-FFAE1-TPABr and H-FFAE2-TPABr compared to a commercial H-ZSM-5 (Com-ZSM-5).

Properties		H-FFAE1-TPABr	H-FFAE2-TPABr	Com-ZSM-5
Surface area (m^2/g)	Micropores	80.90	158.23	85.06
	Mesopores	161.23	231.01	308.77
	Macropores	252.26	68.41	86.32
BET surface area (m^2/g)		494.40	457.50	480.15
Si/Al		36	60	29
Number of Brønsted acid site (mmol H^+/g)		0.62	0.55	0.86
Relative XRD crystallinity (%)		94	95	100
Optical density ratio		0.96	0.90	0.92
Framework aluminium (%)		98.6	97.8	98.5
Crystal size (µm)	Length	6.52±0.22	4.65±0.67	1.46±0.47
	Width	2.56±0.53	1.67±0.12	1.11±0.42

It could be seen in Table 6.4 that the surface area distribution of the synthesised zeolites H-FFAE1-TPABr and H-FFAE2-TPABr differed depending on the Si/Al ratio of their precursors FFAE1 (Si/Al=42) and FFAE2 (Si/Al=81). The micropores and mesopores surface area of H-FFAE1-TPABr was lower than that of H-FFAE2-TPABr, while its macroporous surface area was higher than that of H-FFAE2-TPABr. The micropores and mesopores surface area of the fly ash-based ZSM-5 zeolite (H-FFAE1-TPABr and H-FFAE2-TPABr) was proportional to their Si/Al ratio but inversely proportional to the number of their Brønsted acid site, optical density ratio, percentage of framework tetrahedrally coordinated aluminium and crystal size.

This section showed that a pure ZSM-5 phase could be synthesised for the first from fly ash without the addition of extra silica and Si/Al ratio could be varied by treating a powder fly ash extract with an oxalic acid solution.

6.4. Effect of the structure directing agent on the properties of ZSM-5 zeolite synthesised from a fused fly ash extract (FFAE1)

FFAE1 powder was used as starting material for the synthesis of ZSM-5 zeolite without an additional source of silica. FFAE1 was chosen as ZSM-5 instead of FFAE2 because a second treatment of the fly ash extract was not necessary to synthesise ZSM-5 zeolite. Tetrapropylammonium bromide (TPABr), 1,6-hexane diamine (HDA) or 1-propylamine (PA) was used as structure directing agent in the conditions summarised in Table 3.6: FFAE1 (2 g), 0.4 g of NaOH, 1.5 g of a structure directing agent (TPABr, HDA or PA) and 50 mL of deionised water were mixed at room temperature for 30 min. The obtained mixture underwent hydrothermal crystallisation at 160 °C for 72 h. It was noteworthy that 1.5 g of TPABr, HDA or PA corresponded to different number of moles as shown in Table 3.6. The synthesised FFAE1-TPABr, FFAE1-HDA and FFAE1-PA products were transformed to their H-form using 0.5 M of NH_4NO_3 solution followed by calcination to get H-FFAE1-TPABr, H-FFAE1-HDA and H-FFAE1-PA (Section 3.3.1.3).

6.4.1. Mineralogical study of H-FFA1-TPABr, H-FFAE1-HDA and H-FFAE1-PA by X-ray diffraction

The effect of the structure directing agent on the mineralogy of zeolites synthesised from FFAE1 was investigated by substituting TPABr by HDA or PA. Figure 6.13 compares the XRD patterns of the precursor FFAE1, H-FFAE1-TPABr, H-FFAE1-HDA and H-FFAE1-PA with that of a commercial H-ZSM-5 zeolite (Com-ZSM-5).

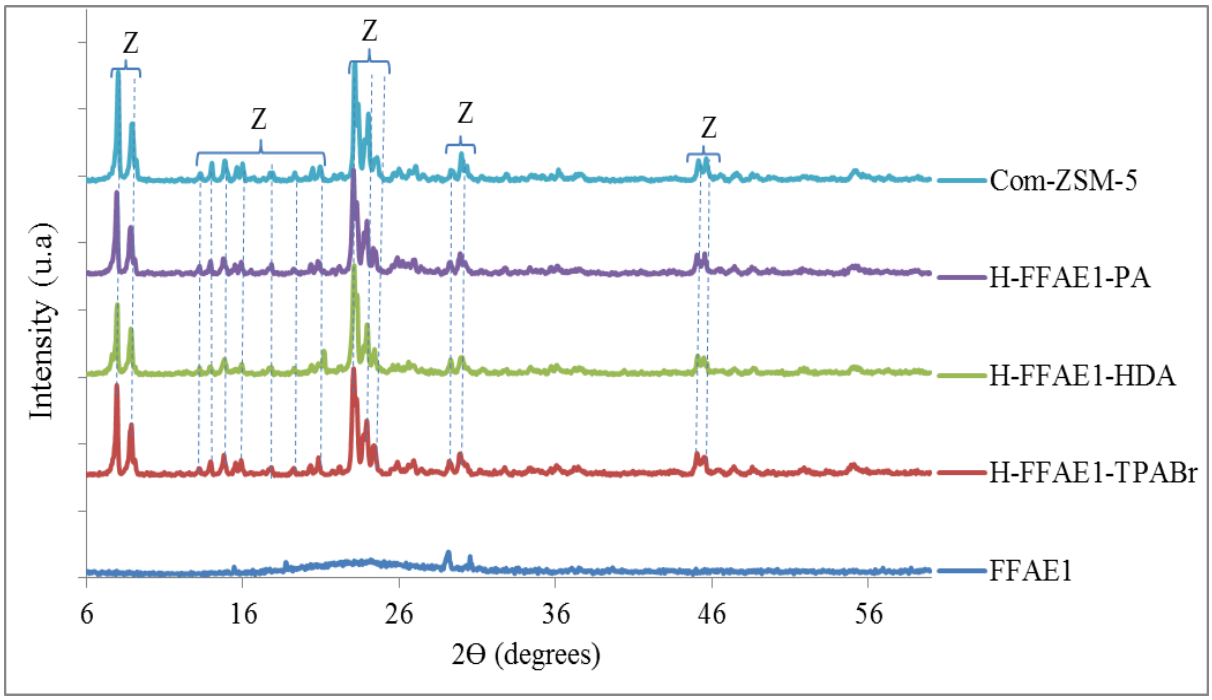

Figure 6.13: XRD patterns of Si and Al precursors (FFAE1), H-FFAE1-TPABr, H-FFAE1-HDA, H-FFAE1-PA and the commercial H-ZSM-5 (Com-ZSM-5) (Z= ZSM-5 zeolite).

Figure 6.13 showed that high purity ZSM-5 zeolite (H-FFAE1-TPABr, H-FFAE1-HDA or H-FFAE1-PA) was synthesised from an amorphous fused fly ash extract (FFAE1) using three different structure directing agents (TPABr, HDA and PA), as confirmed by comparison with the XRD pattern of the commercial H-ZSM-5 zeolite (Com-ZSM-5) and the collection of simulated XRD powder patterns for zeolites (Treacy and Higgins, 2001). The XRD showed that the synthesised zeolites were without any residual fly ash mineral phases thus fusion of fly ash followed by acid precipitation and oxalic acid extraction (see Section 3.3.1.3) provided a suitable mullite and quartz free feedstock for ZSM-5 synthesis. While the zeolite ZSM-5 products synthesised from the as-received fly ash (H-FA-TPABr-OA, H-FA-HDA-OA and H-FA-PA-OA) (Figure 4.14) or acid treated fly ash (H-AL-TPABr-OA, H-AL-HDA-OA and H-AL-PA-OA) (Figure 5.6) still contained fly ash mineral phases namely mullite and quartz. Moreover, the use of cheap structure directing agents such as HDA and PA in the synthesis of pure phase of ZSM-5 zeolite from a fused fly ash extract made the process more feasible economically and offset the cost of the fusion process.

Figure 6.14 compares the calculated ZSM-5 relative XRD crystallinity (Equation 4.1) of H-FFAE1-TPABr, H-FFAE1-HDA and H-FFAE1-PA with the commercial H-ZSM-5 zeolite (Com-ZSM-5) as reference.

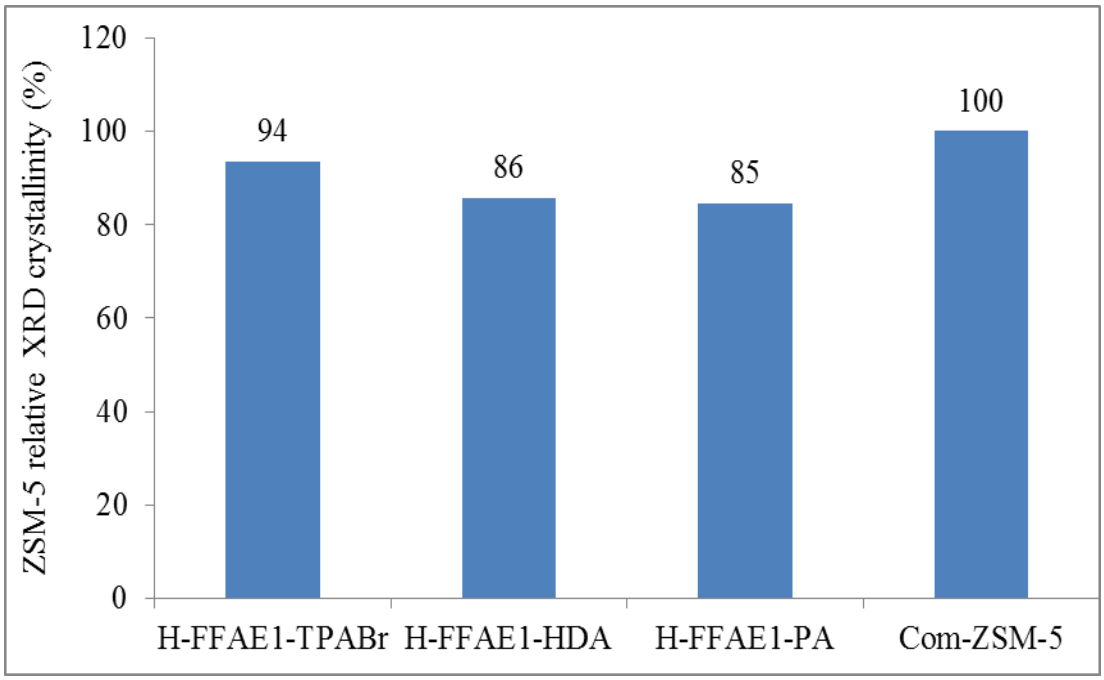

Figure 6.14: Calculated ZSM-5 relative XRD crystallinity of H-FFAE1-TPABr, H-FFAE1-HDA and H-FFAE1-PA compared to the commercial H-ZSM-5 zeolite (Com-ZSM-5).

Figure 6.14 showed that the calculated ZSM-5 relative XRD crystallinity of H-FFAE1-TPABr, H-FFAE1-HDA and H-FFAE1-PA was 94 %, 86 % and 85 % respectively. It could then be concluded that the type of structure directing agent used had a more significant impact on crystallinity than the elemental composition of the fused fly ash feedstock (FFAE1 and FFAE2) (Figure 6.6). It was also noteworthy that the ZSM-5 relative XRD crystallinity of ZSM-5 zeolite products synthesised from the as-received fly ash (H-FA-TPABr-OA, H-FA-HDA-OA and H-FA-PA-OA) (Figure 4.15) or acid treated fly ash (H-AL-TPABr-OA, H-AL-HDA-OA and H-AL-PA-OA) (Figure 5.7) was much lower than that of the ZSM-5 zeolite products synthesised from the fused fly ash extract (H-FFAE1-TPABr, H-FFAE1-HDA and H-FFAE1-PA) (Figure 6.14), hence the oxalic acid treatment of the fused fly ash extract prior to synthesis was a more suitable route than dealumination of the synthesised zeolite products (Chapter 4 and Chapter 5) for high quality ZSM-5.

6.4.2. Morphological analysis and elemental composition of H-FFAE1-TPABr, H-FFAE1-HDA and H-FFAE1-PA by scanning electron microscopy-energy dispersive spectroscopy

The influence of the structure directing agent (TPABr, HDA and PA) on the morphology of ZSM-5 zeolite products synthesised from FFAE1 was investigated. FFAE1 (2 g) was mixed

with 0.4 g of NaOH, 1.5 g of TPABr, HDA or PA and 50 mL of deionised water. The obtained hydrothermal gel was aged at room temperature for 30 min followed by a crystallisation at 160 °C for 72 h. The final FFAE1-TPABr, FFAE1-HDA and FFAE1-PA products were transformed to their H-form using 0.5 M of NH_4NO_3 solution followed by calcination at 550 °C for 3 h (Section 3.3.1.3). Figure 6.15 presents the SEM micrographs of FFAE1, H-FFAE1-TPABr, H-FFAE1-HDA, H-FFAE1-PA and the commercial H-ZSM-5.

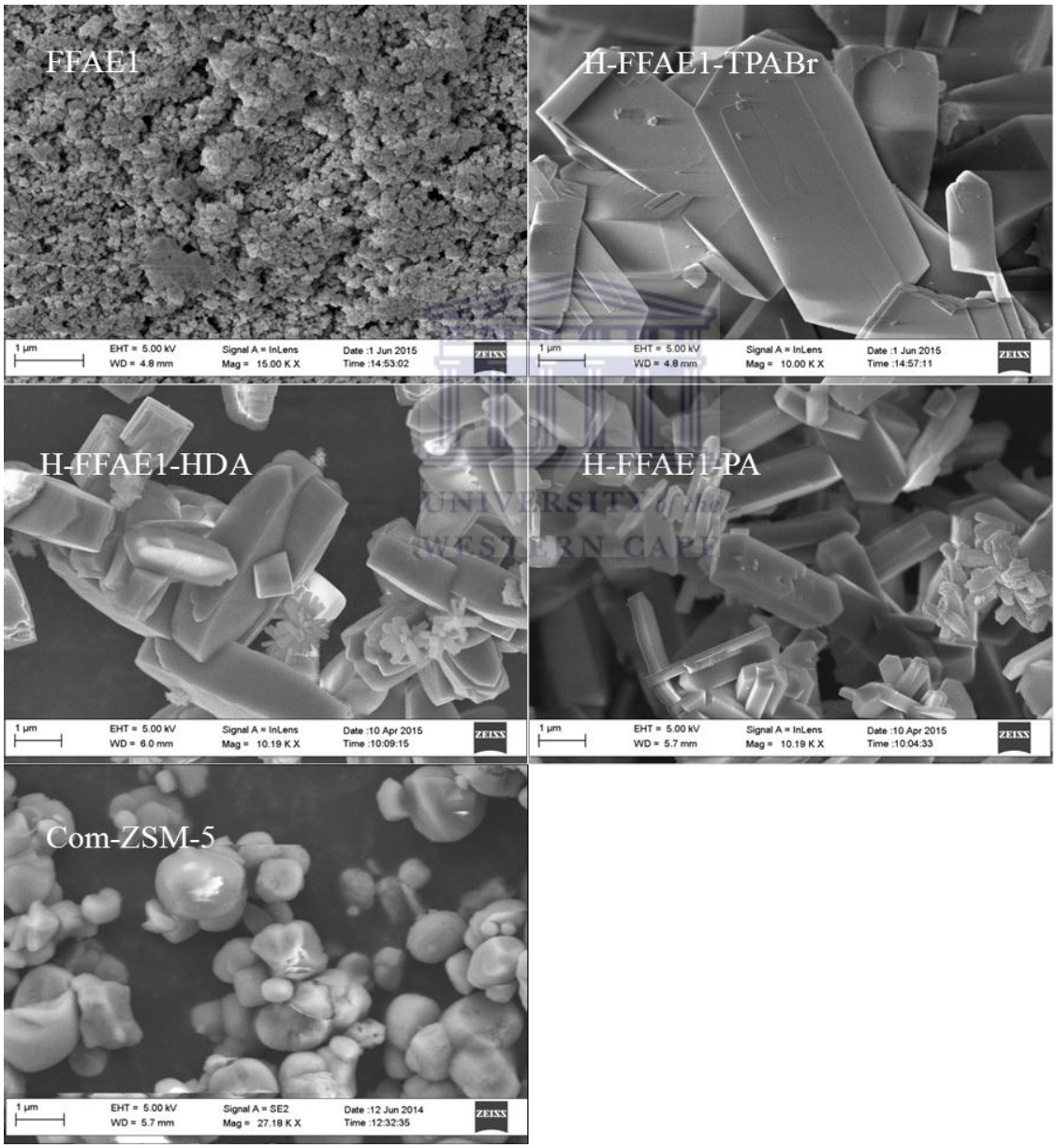

Figure 6.15: SEM micrographs of FFAE1, H-FFAE1-TPABr, H-FFAE1-HDA, H-FFAE1-PA and the commercial H-ZSM-5 (Com-ZSM-5).

The commercial ZSM-5 crystals were spherulitic as presented in Section 4.4.2. Figure 6.15 showed the transformation of the amorphous fused fly ash extract (FFAE1) to the characteristic lath-shaped particles of ZSM-5 zeolite (H-FFAE1-TPABr, H-FFAE1-HDA and H-FFAE1-PA) with morphologies that differed somewhat from one another depending on the structure directing agent used (TPABr, HDA or PA). It was also noteworthy that no amorphous material was visible in the micrographs of the final products. Furthermore, similar lath-shaped particles to H-FFAE1-HDA and H-FFAE1-PA were observed when as-received fly ash (FA) and fumed silica had been used as source of silicon and aluminium (see Section 4.4.2). Petrik et al., (1995) reported the formation of lath-shaped particles when HDA or PA was used as structure directing agent with a similar molar regime but using fumed silica as feedstock. However, only the PA template induced the same shape of ZSM-5 zeolite regardless of the source of silicon and aluminium (FA, AL or FFAE1) as shown by comparing Figure 4.16, Figure 5.8 and Figure 6.15. It could also be observed that the ZSM-5 crystals of H-FFAE1-TPABr, H-FFAE1-HDA and H-FFAE1-PA were relatively homogeneous (Figure 6.15) compared to those of H-FA-TPABr-OA, H-FA-HDA-OA and H-FA-PA-OA (Figure 4.16) or H-AL-TPABr-OA, H-AL-HDA-OA and H-AL-PA-OA (Figure 5.8), which were mixed with some amorphous material. Figure 6.16 presents the mean crystal length and width of H-FFAE1-TPABr, H-FFAE1-HDA and H-FFAE1-PA crystals.

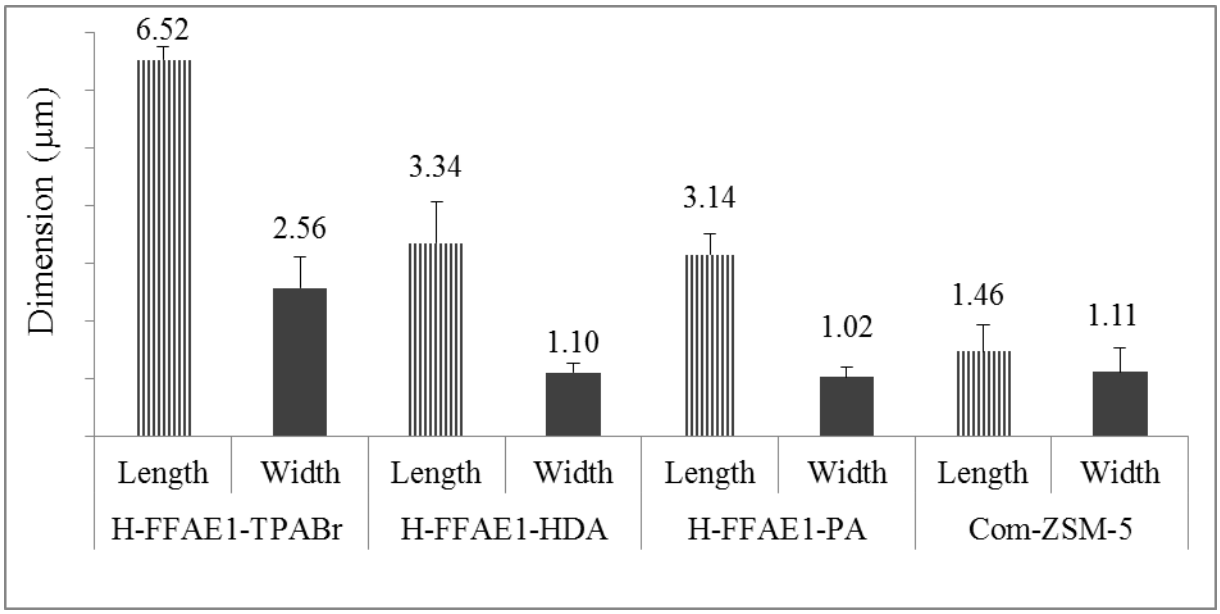

Figure 6.16: Mean crystal length and width of H-FFAE1-TPABr, H-FFAE1-HDA, H-FFAE1-PA and the commercial H-ZSM-5 (Com-ZSM-5).

It could be observed in Figure 6.16 that H-FFAE1-TPABr had the highest mean crystal length and width of 6.52±0.22 by 2.56±0.53 µm followed by H-FFAE1-HDA (3.34±0.72 by 1.10±0.15 µm) and H-FFAE1-PA (3.14±0.37 by 1.02±0.16 µm). It could be observed that the mean crystal size of the synthesised fly ash-based ZSM-5 zeolite products decreased with the size of the structure directing agent used. And this contrary to the findings presented in Figure 4.17 and Figure 5.9 as well as what was reported by Petrik et al., (1995) who stated that longer chain amines and TPABr led to the formation of small ZSM-5 crystals while shorter chain length amines led to the formation of larger particles. However, the current study presented different ways of changing the morphology and homogeneity of ZSM-5 particles by varying the template, source and composition of silicon and aluminium precursors. And this is in agreement with Petrik et al., (1995), Petrik, (2009), Bleken et al., (2012) and Wang et al., (2008) who reported that parameters such as the degree of polymerization of the silica, nature of the cations present, type of template could influence the crystallisation and morphology of ZSM-5 zeolite.

The elemental composition of H-FFAE1-TPABr, H-FFAE1-HDA and H-FFAE1-PA and the commercial H-ZSM-5 was determined by analysing 10 spots of each sample by EDS. Table 6.5 summarises the results of the EDS analysis.

Table 6.5: Elemental composition H-FFA1-TPABr, H-FFAE1-HDA, H-FFAE1-PA and commercial H-ZSM-5 (Com-ZSM-5) (n=10).

Element	H-FFAE1-TPABr (%)	H-FFAE1-HDA (%)	H-FFAE1-PA (%)	Com-ZSM-5 (%)
O	66.1±0.3	66.3±0.7	65.8±0.7	66.2±0.2
Si	32.1±0.4	32.5±0.5	31.8±1.1	32.0±0.2
Al	0.9±0.4	0.6±0.5	0.8±0.8	1.1±0.3
Na	0.7±0.7	0.4±0.7	1.1±0.1	0.4±0.4
Mg	0.0±0.0	0.1±0.1	0.3±0.4	0.1±0.2
Fe	0.1±0.1	0.1±0.1	0.1±0.1	0.0±0.0
Ca	0.0±0.0	0.1±0.1	0.1±0.1	0.1±0.1
K	0.1±0.1	0.0±0.0	0.1±0.2	0.1±0.1
Si/Al	36	55	42	29

It could be observed in Table 6.5 that the Si/Al ratio of H-FFAE1-TPABr, H-FFAE1-HDA and H-FFAE1-PA was 36, 55 and 42 respectively. These results showed the type of structure directing agent used affected the Si/Al ratio of the final products, while they were all synthesised from the same precursor FFAE1 (Si/Al=41). H-FFAE1-PA was the only sample with a Si/Al ratio close to that of the precursor FFAE1. Therefore, TPABr, HDA and PA influenced the degree of Al incorporated into the zeolite crystal lattice while directing the formation ZSM-5 zeolite, with HDA being the structure directing agent mainly excluding Al incorporation. This could also explain the difference in shape of the synthesised H-FFAE1-TPABr, H-FFAE1-HDA and H-FFAE1-PA.

6.4.3. Structural analysis of H-FFA1-TPABr, H-FFAE1-HDA and H-FFAE1-PA by Fourier transform infrared

Figure 6.17 presents the FTIR spectra of FFAE1, H-FFAE1-TPABr, H-FFAE1-HDA, H-FFAE1-PA and the commercial H-ZSM-5. FFAE1, FFAE1-TPABr, FFAE1-HDA and FFAE1-PA were obtained through the method detailed in Section 3.3.1.3.

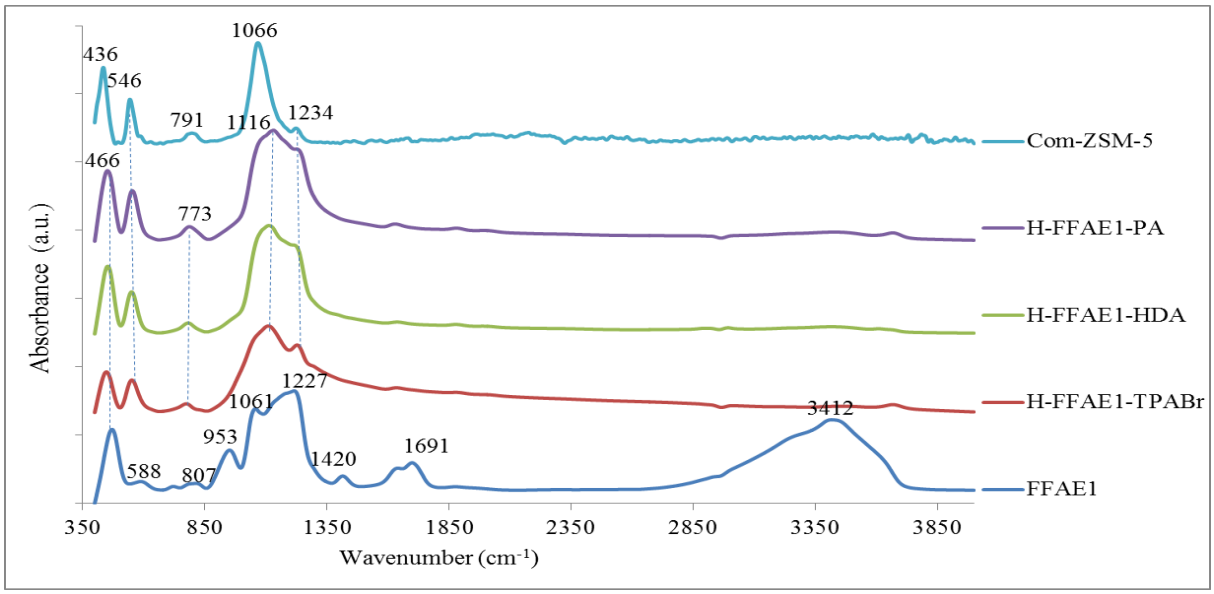

Figure 6.17: FTIR spectra of the Si and Al precursor FFAE1, H-FFAE1-TPABr, H-FFAE1-HDA, H-FFAE1-PA and commercial H-ZSM-5 (Com-ZSM-5).

The FTIR spectra of FFAE1 and the commercial ZSM-5 were analysed and discussed in Section 6.2 and Section 4.4.3 respectively. FFAE1 was used as feedstock in the synthesis of ZSM-5 zeolite without an additional source of silica, using TPABr, HDA or PA as structure directing agent. It was noteworthy that the spectra of synthesised fly ash-based zeolites (H-FFAE1-TPABr, H-FFAE1-HDA and H-FFAE1-PA) showed the characteristic reflection of ZSM-5 zeolite (Figure 6.17). The bands appearing at 464, 546, 773, 1116 and 1234 cm^{-1} were assigned and discussed in section 6.3.3. In conclusion, the shift of the internal asymmetric stretch band from 1064 cm^{-1} in commercial H-ZSM-5 (Com-ZSM-5) spectrum to 1116 cm^{-1} in H-FFAE1-TPABr, H-FFAE1-HDA and H-FFAE1-PA could be due to the Si/Al ratio in H-FFAE1-TPABr, H-FFAE1-HDA and H-FFAE1-PA that was higher than in commercial H-ZSM-5 (Com-ZSM-5) (Table 6.5). The optical density ratio of H-FFAE1-TPABr, H-FFAE1-HDA and H-FFAE1-PA was 0.96, 0.89 and 0.94 respectively, showing that H-FFAE1-TPABr was the most crystalline sample; however this crystallinity estimation did not follow the same trend as the relative XRD crystallinity (Figure 6.14), of 94, 86 and 85 % for H-FFAE1-TPABr, H-FFAE1-HDA and H-FFAE1-PA respectively. Moreover, the optical density ratio of H-FFAE1-TPABr, H-FFAE1-HDA and H-FFAE1-PA could not be compared to that of H-FA-TPABr-OA, H-FA-HDA-OA and H-FA-PA-OA (Section 4.4.3) or H-AL-TPABr-OA, H-AL-HDA-OA and H-AL-PA-OA (Section 5.3.3) because the FTIR spectrum of their precursors FA an AL had a Al-O stretch band between 555 and 579 cm^{-1} that could interfere

with the intensity of the double ring band that appeared at 546 cm^{-1} in the spectra of the synthesised zeolite products (Figure 4.18 and Figure 5.10), while there was no band that could interfere the intensity of the double ring band in H-FFAE1-TPABr, H-FFAE1-HDA and H-FFAE1-PA. Therefore the band that appeared at 546 cm^{-1} in H-FFAE1-TPABr, H-FFAE1-HDA and H-FFAE1-PA spectra was only the result of the zeolitization process of FFAE1. These results showed that fly ash could be used as cheap feedstock after fusion extraction and acid precipitation followed by oxalic acid treatment in the synthesis of ZSM-5 zeolite without any additional silica source, using cheap and readily available structure directing agents, which could be considered as breakthrough in the synthesis of high silica zeolites and zeolite-like materials from fly ash as this has not yet been reported.

6.4.4. Brønsted acidity of H-FFA1-TPABr, H-FFAE1-HDA and H-FFAE1-PA

The number of Brønsted acid sites of H-FFA1-TPABr, H-FFAE1-HDA and H-FFAE1-PA was determined through the H/D isotope exchange as detailed in Section 3.4.6. This section investigated the influence of the structure directing agent on the number of Brønsted acid sites of the synthesised ZSM-5 zeolite products. H-FFA1-TPABr, H-FFAE1-HDA and H-FFAE1-PA were synthesised from FFAE1 as follows: FFAE1 (2 g), 0.4 g of NaOH, 1.5 g of the structure directing agent (TPABr, HDA or PA) and 50 mL of deionised water were mixed at room temperature for 3 h. The obtained hydrothermal gel underwent crystallisation at 160 °C for 72 h. The synthesised FFAE1-TPABr, FFAE1-HDA and FFAE1-PA were transformed in their H-form using NH_4NO_3 solution followed by calcination at 550 °C for 3 h to obtain H-FFA1-TPABr, H-FFAE1-HDA and H-FFAE1-PA (Section 3.3.1.3). Figure 6.18 compares the number of Brønsted acid sites of H-FFAE1-TPABr, H-FFAE1-HDA and H-FFAE1-PA to that of the commercial H-ZSM-5 (Com-ZSM-5).

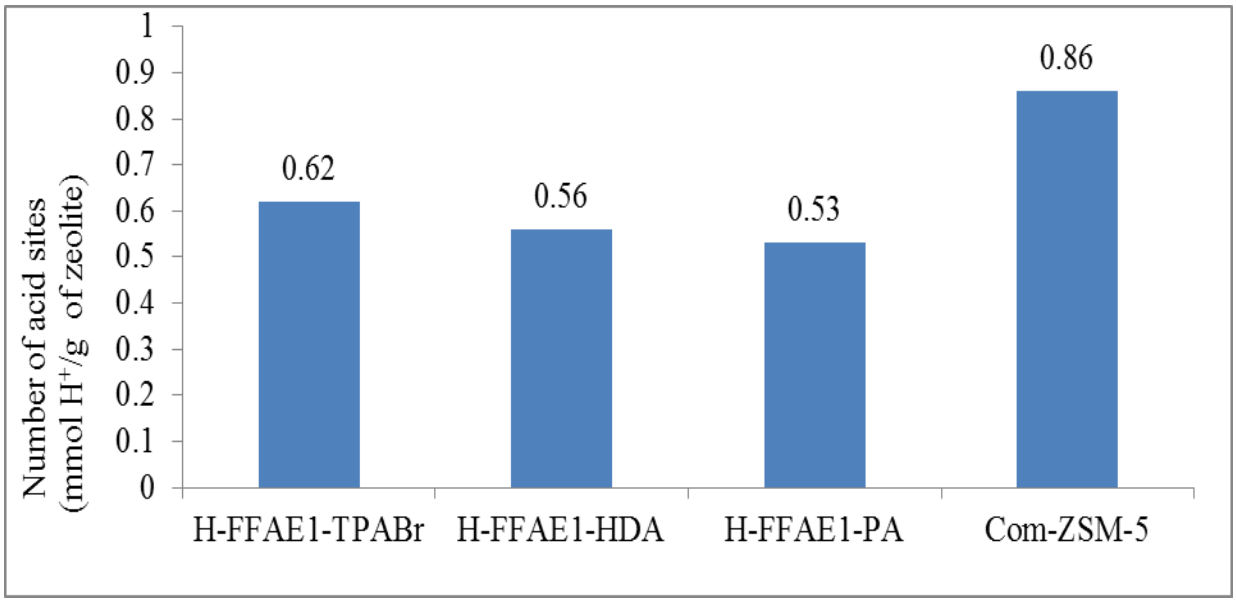

Figure 6.18: Number of Brønsted acid sites (mmol H+/g of zeolite) of H-FFAE1-TPABr, H-FFAE1-HDA, H-FFAE1-PA and the commercial H-ZSM-5 (Com-ZSM-5).

Figure 6.18 showed that the number of Brønsted acid sites of H-FFAE1-TPABr, H-FFAE1-HDA and H-FFAE1-PA was 0.62, 0.56, 0.53 mmol H^+ per gram of zeolite respectively, which was lower, compared to that of the commercial H-ZSM-5 zeolite (ComZSM-5) of 0.86 mmol H^+ per gram of zeolite. It could be observed that the type of structure directing agent had an effect on the number of Brønsted acid sites of the final products. And the same trend was observed for the number of Brønsted acid site of the dealuminated H-AL-TPABr-OA, H-AL-HDA-OA and H-AL-PA-OA that was 0.71, 0.46 and 0.42 mmol H^+ per gram of zeolite (Figure 5.11). Furthermore, the number of Brønsted acid sites of H-FFAE1-TPABr, H-FFAE1-HDA and H-FFAE1-PA followed the same trend as their relative XRD crystallinity that was 94, 86 and 85 % respectively. However, there was no correlation between the number of Brønsted acid sites of H-FFAE1-TPABr, H-FFAE1-HDA and H-FFAE1-PA and their Si/Al ratio that was 36, 55 and 42 (Section 6.4.2) nor their optical density ratio that was 0.96, 0.89 and 0.94 respectively (Section 6.4.3). By comparing the number of Brønsted acid sites of H-FFAE1-TPABr, H-FFAE1-HDA and H-FFAE1-PA, it could be predicted that H-FFAE1-TPABr had the highest framework aluminium content followed by H-FFAE1-HDA.

6.4.5. Aluminium coordination analysis of H-FFA1-TPABr, H-FFAE1-HDA and H-FFAE1-PA by ^{27}Al nuclear magnetic resonance

Figure 6.19 shows the influence the structure directing agent on aluminium coordination in the zeolite framework. The ^{27}Al solid state NMR spectra of FFAE1, H-FFAE1-TPABr, H-FFAE1-HDA, H-FFAE1-PA are compared with those of a commercial H-ZSM-5 zeolite and 0.1 M $Al(NO_3)_3$. H-FFAE1-TPABr, H-FFAE1-HDA and H-FFAE1-PA were synthesised from FFAE1, detemplated and transformed into H-form as detailed in Section 3.3.1.3.

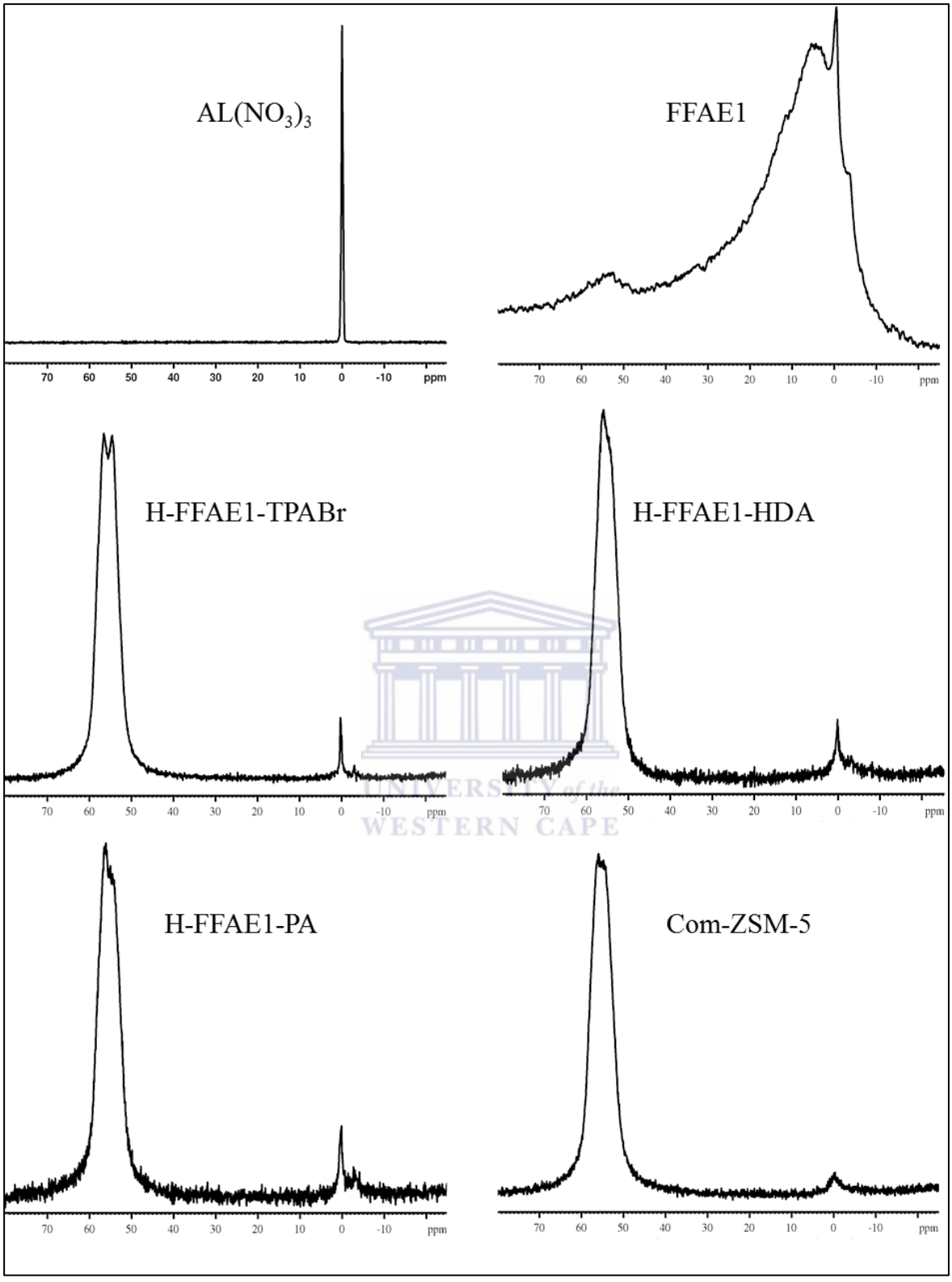

Figure 6.19: ^{27}Al NMR spectra of a reference (0.1 M $Al(NO_3)_3$), FFAE1, H-FFAE1-TPABr, H-FFAE1-HDA, H-FFAE1-PA and the commercial H-ZSM-5.

Figure 6.19 showed that the signal of the extra-framework octahedrally coordinated Al present at about 0 ppm in FFAE1 almost completely disappeared after hydrothermal synthesis and the Al in the feedstock was transformed into framework tetrahedrally coordinated Al (at about 55 ppm) in H-FFAE1-TPABr, H-FFAE1-HDA or H-FFAE1-PA. These results corroborated the findings obtained by Triantafyllidis et al., (2004) and Sazama et al., (2011) who reported similar signals of framework tetrahedrally coordinated Al around 55 ppm.

Table 6.6 gives the percentage of framework and extra-framework aluminium of FFAE1, H-FFAE1-TPABr, H-FFAE1-HDA, H-FFAE1-PA and the commercial H-ZSM-5 zeolite.

Table 6.6: percentage of framework and extra-framework Al of 0.1 M $Al(NO_3)_3$, FFAE1, H-FFAE1-TPABr, H-FFAE1-HDA, H-FFAE1-PA and commercial H-ZSM-5 zeolite and the number of their Brønsted acid sites.

Sample	Framework tetrahedrally coordinated Al (%)	Extra-framework octahedrally coordinated Al (%)	Number of Brønsted acid sites (mmol H^+/g)
Reference $Al(NO_3)_3$	0.0	100.0	/
FFAE1	15.0	85.0	/
H-FFAE1-TPABr	98.6	1.4	0.62
H-FFAE1-HDA	96.5	3.5	0.56
H-FFAE1-PA	95.8	4.2	0.53
Commercial H-ZSM-5	98.5	1.5	0.86

Table 6.6 showed that the percentage of framework aluminium of H-FFAE1-TPABr, H-FFAE1-HDA and H-FFAE1-PA was 98.6, 96.5 and 95.8 % respectively. these results could not be related to the Si/Al ratio of H-FFAE1-TPABr, H-FFAE1-HDA and H-FFAE1-PA that was 36, 55 and 42 respectively; however, there was a correlation between the percentage of framework aluminium of H-FFAE1-TPABr, H-FFAE1-HDA and H-FFAE1-PA and their calculated ZSM-5 relative XRD crystallinity that was 94, 86 and 85 % respectively (Figure 6.14) as well as the number of their Brønsted acid sites that was 0.62, 0.56

and 0.53 mmol H^+ per gram of zeolite respectively (Figure 6.18). And this was obtained even though the number of moles of TPABr (7 mol) used in the hydrothermal gel was lower than those of HDA (20 mol) or PA (38 mol) (Table 3.6). These results were in agreement with Van der Gaag, (1987) who reported that the crystallinity of ZSM-5 zeolite synthesised from a small template such as 1-propylamine or a large one such as tetrapropylammonium bromide could be similar only if the amount of smaller template was double that of the amount the larger template. The high purity of H-FFAE1-TPABr, H-FFAE1-HDA and H-FFAE1-PA (Figure 6.13) led to more correlation between their properties unlike H-AL-TPABr-OA, H-AL-HDA-OA and H-AL-PA-OA that had a relative XRD crystallinity of 54, 51 and 45 % respectively with only a few correlations between their properties (Table 5.3).

6.4.6. Surface area analysis of H-FFA1-TPABr, H-FFAE1-HDA and H-FFAE1-PA by N_2 Brunauer-Emmett-Teller

H-FFAE1-TPABr, H-FFAE1-HDA and H-FFAE1-PA were synthesised as follows: FFAE1 (2 g), 0.4 g of NaOH, 1.5 g of TPABr, HDA or PA and 50 mL of deionised water were aged at room temperature for 30 min. The obtained hydrothermal gel underwent a crystallisation at 160 °C for 72 h. The synthesised fly ash-based zeolites FFAE1-TPABr, FFAE1-HDA and FFAE1-PA were transformed into their H-form using NH_4NO_3 solution followed by calcination (Section 3.3.1.3). Figure 6.20 gives the adsorption/desorption isotherms of N_2 and BET surface area of H-FFAE1-TPABr, H-FFAE1-HDA, H-FFAE1-PA and the commercial H-ZSM-5. The conditions used for N_2 BET analysis were detailed in Section 3.4.7.

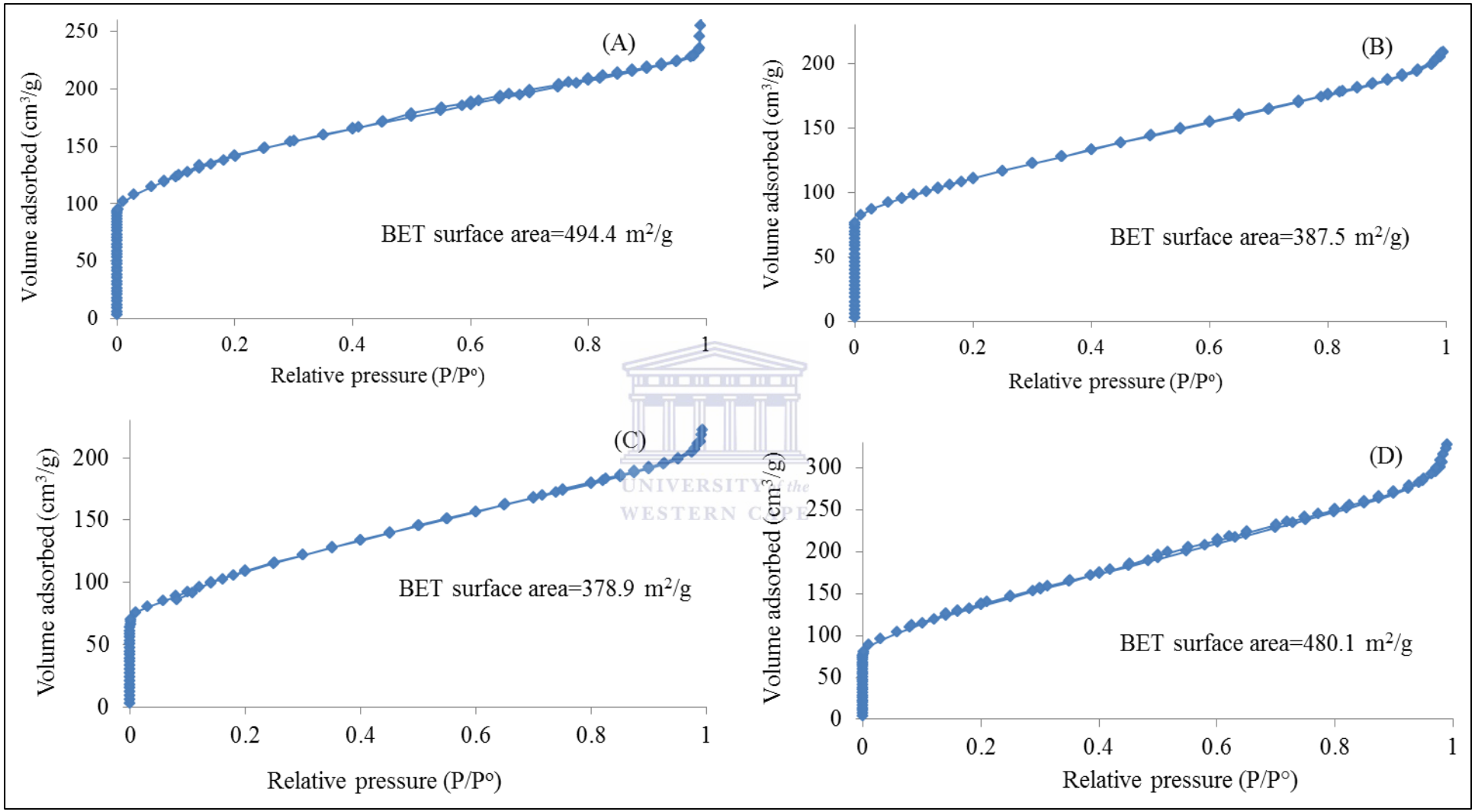

Figure 6.20: Adsorption/desorption isotherms of N_2 at 77.41 K and BET surface area of (A) H-FFAE1-TPABr, (B) H-FFAE1-HDA, (C) H-FFAE1-PA and (D) commercial H-ZSM-5.

As for H-FFAE1-TPABr and H-FFAE2-TPABr, and the commercial H-ZSM-5 in Figure 6.12, the adsorption-desorption isotherms of H-FFAE1-HDA and H-FFAE1-PA were also that of type IV (Figure 6.20) (Lowell et al., 2004). The BET surface area of H-FFAE1-TPABr, H-FFAE1-HDA and H-FFAE1-PA was 494.4, 387.5 and 378.9 m^2/g respectively. H-FFAE1-TPABr presented a better N_2 adsorption than H-FFAE1-HDA and H-FFAE1-PA, despite its big ZSM-5 crystals of 6.52±0.22 by 2.56±0.53 µm compared to those of H-FFAE1-HDA (3.34±0.72 by 1.10±0.15 µm) and H-FFAE1-PA (3.14±0.37 by 1.02±0.16 µm) (Figure 6.16). Moreover, the BET surface area of H-FFAE1-TPABr, H-FFAE1-HDA and H-FFAE1-PA could be related to the type and size of the structure directing agent that was used in their synthesis. It could be observed in Figure 6.20 that the BET surface area of the synthesised zeolites was proportional to the molecular size of their structure directing agent. Table 6.7 compares the properties of the synthesised ZSM-5 zeolite products H-FFAE1-TPABr, H-FFAE1-HDA and H-FFAE1-PA to that of the commercial H-ZSM-5.

Table 6.7: Properties of the synthesised ZSM-5 zeolite products H-FFAE1-TPABr, H-FFAE1-HDA and H-FFAE1-PA compared to a commercial H-ZSM-5 (Com-ZSM-5).

Properties		H-FFAE1-TPABr	H-FFAE1-HDA	H-FFAE1-PA	Com-ZSM-5
Surface area (m^2/g)	Micropores	80.90	50.00	69.52	85.06
	Mesopores	161.23	181.42	205.38	308.77
	Macropores	252.26	156.09	104.01	86.32
BET surface area (m^2/g)		494.40	387.50	378.90	480.15
Si/Al		36	55	42	29
Number of Brønsted acid site (mmol H^+/g)		0.62	0.56	0.53	0.86
Relative XRD crystallinity (%)		94	86	85	100
Optical density ratio		0.96	0.89	0.94	0.92
Framework aluminium (%)		98.6	96.5	95.8	98.5
Crystal size (µm)	Length	6.52±0.22	3.34±0.72	3.14±0.37	1.46±0.47
	Width	2.56±0.53	1.10±0.15	1.02±0.16	1.11±0.42

Table 6.7 showed that H-FFAE1-TPABr, H-FFAE1-HDA and H-FFAE1-PA had an important macropores surface area compared to the commercial H-ZSM-5. This might influence their catalytic efficiency as the external surface area has less effect on the selectivity of a zeolite. Their large ZSM-5 crystals would also affect their catalytic efficiency as all their micropores and mesopores might not be easily accessible. While the surface area of H-AL-TPABr-OA, H-AL-HDA-OA and H-AL-PA-OA was mainly composed of mesopores (Table 5.3). This might cause H-AL-TPABr-OA, H-AL-HDA-OA and H-AL-PA-OA to have a catalytic efficiency as good as that of H-FFAE1-TPABr, H-FFAE1-HDA and H-FFAE1-PA even with the presence of unreacted fly ash mineral phases in their structures, especially the H-AL-HDA-OA that had a small crystal size of 1.02±0.14 by 0.62±0.09 µm. Moreover, the BET surface area of H-FFAE1-TPABr, H-FFAE1-HDA and H-FFAE1 could not be related to their Si/Al ratio nor to their optical density ratio; however there was a correlation between their BET surface area, number of Brønsted acid sites, relative XRD crystallinity, framework tetrahedrally coordinated aluminium and crystal size.

6.5. Chapter summary

ZSM-5 crystals were formed only when FFAE1 or FFAE2 was used as a starting material. No crystalline product was formed during the synthesis of FFAE-TPABr even if its precursor FFAE had a Si/Al ratio of 10 that was within the range for the synthesis of ZSM-5 zeolite. This could be due to the high sodium content in FFAE. Hence, it was important to reduce the amount of sodium as well as aluminium through a treatment of FFAE with a saturated oxalic acid prior to the hydrothermal synthesis. FFAE1 and FFAE2 were obtained after the first and second treatment of FFAE with oxalic acid solution respectively. It was important to mention that H-FFAE1-TPABr and H-FFAE2-TPABr were synthesised without any additional source of silica, and the synthesis of high purity ZSM-5 zeolite from fly ash without any additional silica source has not yet been reported. Therefore, the findings of this study offered a progress in the use of fly ash which is considered by many as being only a waste. Up to now, the use of fly ash in the synthesis of high silica content zeolites such as ZSM-5 is subject to much criticism because of its low Si/Al ratio (~ 2). Therefore, previously an addition of an important amount of silica source was required to increase the Si/Al ratio to more than 10. The addition of an important amount of silica source in the hydrothermal gel and the presence of unreacted fly ash in the final product after synthesis do not promote the synthesis of high silica zeolites as a way to valorise fly ash, and limit the commercialisation and applications of

fly ash-based ZSM-5 zeolite. Therefore, the synthesis of high purity ZSM-5 zeolite (H-FFAE1-TPABr and H-FFAE2-TPABr) from the fused fly ash extract without addition of silica constitutes a breakthrough in the use of fly ash for the synthesis of high purity ZSM-5 zeolite. Moreover, TPABr was substituted by 1,6-hyexanediamne (HDA) and 1-propylamine (PA) in the hydrothermal gel that was used to synthesise a high purity zeolite ZSM-5 from the fused fly ash extract (FFAE1), which gave more options in the synthesis conditions depending on the availability and cost of the structure directing agents, and the desired properties of the synthesised fly ash-based ZSM-5 zeolite. This study showed that different grades of ZSM-5 zeolite could be synthesised from the as-received fly ash (FA) (Chapter 4), acid treated fly ash (AL) (Chapter 5) or fused fly ash extracts (FFAEs) (Chapter 6). If the synthesis of ZSM-5 zeolite from FA and AL required an addition of fumed silica to adjust the Si/Al ratio and their final products contained unreacted fly ash mineral phases, high purity ZSM-5 zeolite was synthesised from FFAEs without addition of fumed silica. Moreover, the use of FA or AL in the synthesis of ZSM-5 zeolite also led to final zeolite products with less predictable correlations between their chemical and physical properties. And because the composition of the fly ash changes from one source to another, the synthesis conditions of ZSM-5 zeolite from FA or AL might require to be optimised whenever the source of fly ash will be changed. While the use of fusion of fly ash followed by treatment with oxalic acid prior to the synthesis would lead to a much more pure precursor powder for which the source of fly ash would not affect the ZSM-5 qualities synthesis conditions and properties. However, the catalytic reactions still need to be performed over the ZSM-5 zeolite products that were synthesised from FA, AL or FFAEs in order to evaluate the contribution of each treatment in the catalytic efficiency of the synthesised fly ash-based ZSM-5 zeolite products.

CHAPTER 7: APPLICATION OF FLY ASH-BASED ZSM-5 ZEOLITE AS SOLID ACID CATALYST

7.1. Introduction

The catalytic efficiency of some of the fly ash-based ZSM-5 zeolite products in the Methanol-to-Olefins (MTO) and Nazarov reactions was compared to that of the commercial ZSM-5. The first part of this chapter (Section 7.2) highlights the Methanol-to-Olefins (MTO) conversion and selectivity toward ethylene and propylene over fly ash-based zeolites that were synthesised from the acid treated fly ash before (H-AL-TPABr, H-AL-HDA and H-AL-PA) and after (H-AL-TPABr-OA, H-AL-HDA-OA and H-AL-PA-OA) treatment with oxalic acid as well as H-FFAE2-TPABr, H-FFAE1-TPABr, H-FFAE1-HDA and H-FFAE1-PA that were synthesised from oxalic acid treated fused fly ash extracts FFAE1 and FFAE2. The second part (Section 7.3) presents the Nazarov cyclisation of 1-phenyl-2-ethylpropenone H-TPABr-OA, H-AL-HDA-OA and H-AL-PA-OA. The use of H-TPABr-OA, H-AL-HDA-OA and H-AL-PA-OA in the Nazarov cyclisation was motivated by the fact that their MTO effectiveness was easily related to their properties; thus the Nazarov cyclisation was used to investigate if the same effectiveness trend could be obtained with other reaction.

7.2. Methanol-to-Olefins (MTO) conversion

The MTO conversion was performed over the ZSM-5 samples synthesised from the acid treated fly ash (H-AL-TPABr, H-AL-HDA, H-AL-PA, H-AL-TPABr-OA, H-AL-HDA-OA and H-AL-PA-OA) as well as those from the fused fly ash extracts (H-FFAE1-TPABr, H-FFAE2-TPABr, H-FFAE1-HDA and H-FFAE1-PA). The commercial ZSM-5 zeolite characterised as detailed in Chapter 4, Chapter 5 and Chapter 6 was used as reference. The calculations of MTO conversion and selectivity toward ethylene and propylene were presented in Equation 3.2 and Equation 3.3 (Section 3.3.3.1). On the one hand, H-AL-TPABr, H-AL-HDA and H-AL-PA were prepared as follows: 0.75 g of AL, 0.75 g fumed silica, 0.25 g of NaOH, 1 g of a structure directing agent (TPABr, HDA or PA) and 20 mL of deionised water were aged at room temperature for 2 h. The obtained gel was used to synthesise ZSM-5 zeolite products at 160 °C for 72 h as detailed in Section 3.3.1.2. The synthesised zeolites AL-TPABr, AL-HDA and AL-PA were transformed into their H-form

through treatment with a NH_4NO_3 solution and calcination. Afterwards, H-AL-TPABr, H-AL-HDA and H-AL-PA were treated with a saturated oxalic acid solution at 80 °C for 6 h followed by calcination at 550 °C for 3 h to obtain H-AL-TPABr-OA, H-AL-HDA-OA and H-AL-PA-OA. On the other hand, H-FFAE1-TPABr, H-FFAE2-TPABr, H-FFAE1-HDA and H-FFAE1-PA were prepared as follows: 2 g of FFAE1 (Si/Al=42) or FFAE2 (Si/Al=81) was mixed with 0.4 g of NaOH, 1.5 g of structure directing agent (TPABr, HDA or PA) and 50 mL of deionised water (Table 3.6). The obtained mixture was aged at room temperature for 30 min before hydrothermal crystallisation at 160 °C for 72 h as shown in Section 3.3.1.3. The obtained FFAE1-TPABr, FFAE2-TPABr, FFAE1-HDA and FFAE1-PA products were transformed into their H-form via the conditions detailed above.

7.2.1. Methanol-to-Olefins (MTO) conversion over H-AL-TPABr, H-AL-HDA and H-AL-PA

Figure 7.1 compares the percentage of MTO conversion and selectivity toward ethylene (C_2) and propylene (C_3) over H-AL-TPABr, H-AL-HDA and H-AL-PA with that of a commercial H-ZSM-5 zeolite.

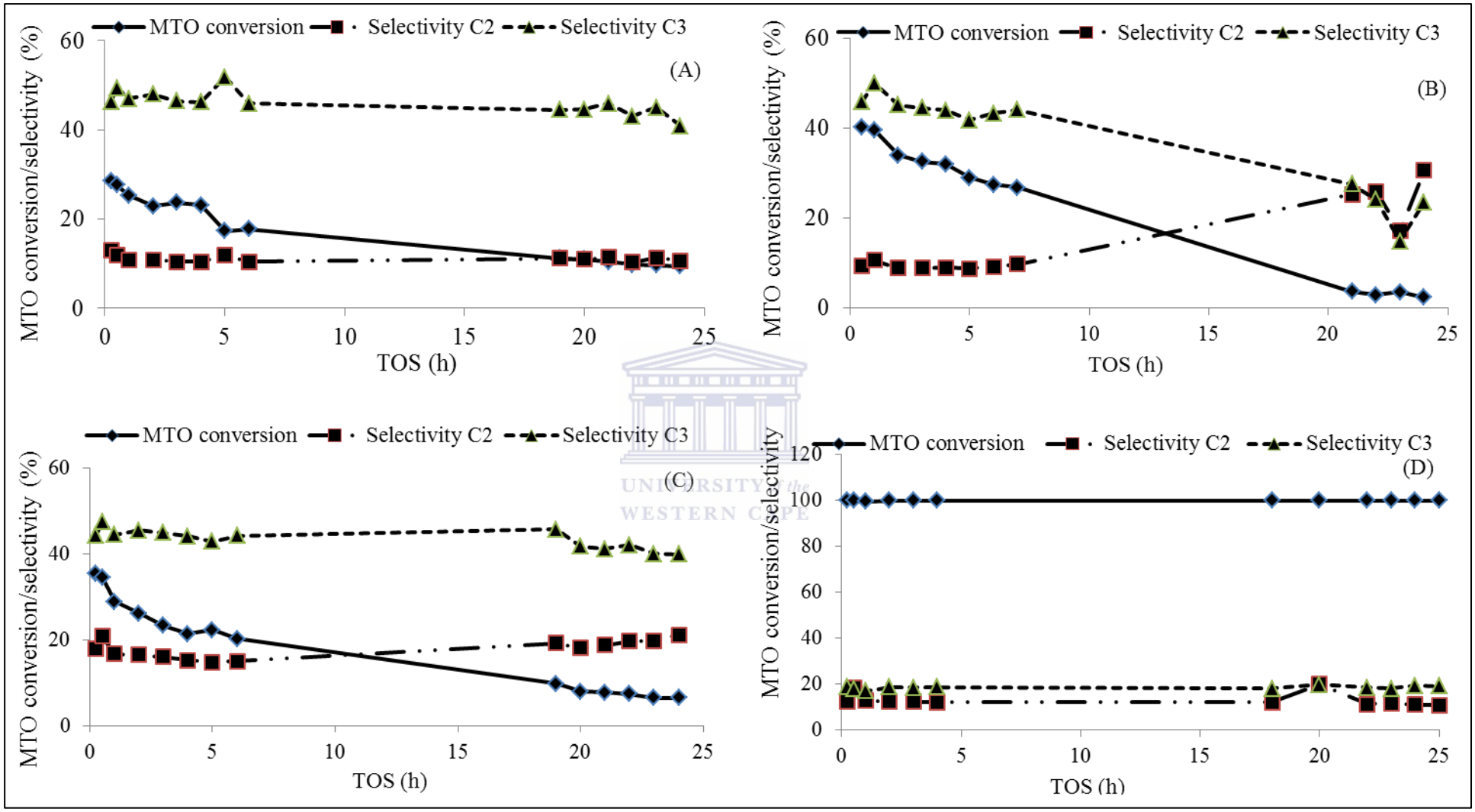

Figure 7.1: MTO conversion and selectivity toward C_2 and C_3 over (A) H-AL-TPABr, (B) H-AL-HDA and (C) H-AL-PA compared with (D) commercial H-ZSM-5 (TOS=time on stream).

Figure 7.1 showed that the MTO conversion over H-AL-TPBAr, H-AL-HDA and H-AL-PA was 25 %, 40 % and 29 % after 1 h of time on stream (TOS), which was insignificant compared to 100 % MTO conversion over the commercial H-ZSM-5 zeolite. Moreover, H-AL-TPBAr, H-AL-HDA and H-AL-PA deactivated quickly, while the commercial zeolite H-ZSM-5 was still stable after 24 h of TOS. It was also noteworthy that H-AL-TPABr and H-AL-PA had a C_3/C_2 ratio of 4.2 and 2.7, while the C_3/C_2 of a commercial H-ZSM-5 zeolite was 1.3. However, the synthesis conditions of H-AL-TPABr, H-AL-HDA and H-AL-PA still needed to be optimised in order to enhance their MTO catalytic effiency.

7.2.2. Methanol-to-Olefins (MTO) conversion over H-AL-TPABr-OA, H-AL-HDA-OA and H-AL-PA-OA

The post-synthesis treatment of H-AL-TPABr, H-AL-HDA and H-AL-PA with oxalic acid was performed to remove Al and some other elements such as Mg, Fe, Ca and K as shown in Table 5.1 to obtain H-AL-TPABr-OA, H-AL-HDA-OA and H-AL-PA-OA. Figure 7.2 presents the MTO conversion and selectivity toward ethylene (C_2) and propylene (C_3) over H-AL-TPABr-OA, H-AL-HDA-OA and H-AL-PA-OA with the commercial H-ZSM-5 zeolite as reference. The method that was used for the MTO conversion was detailed in Section 3.3.3.1.

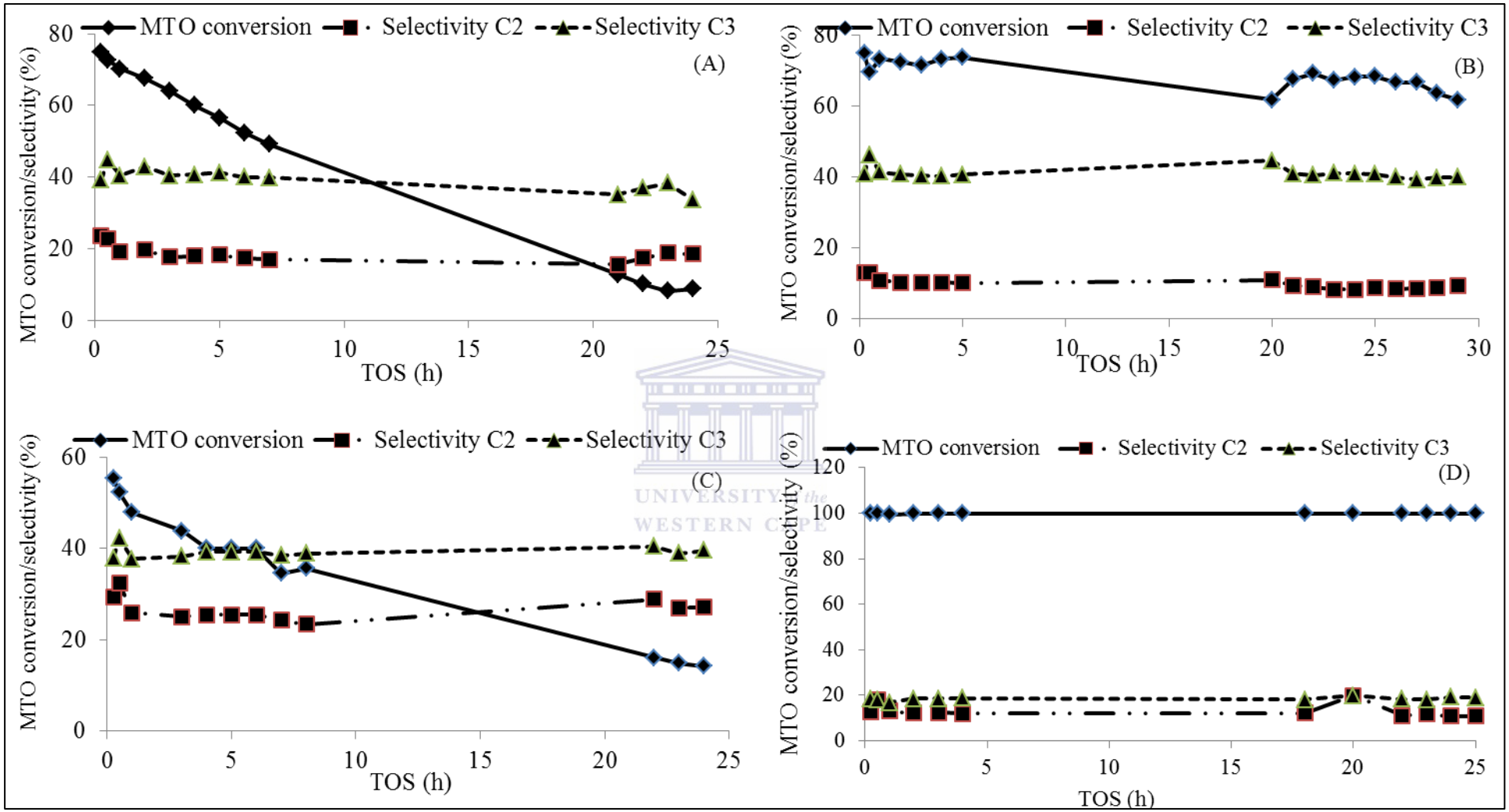

Figure 7.2: MTO conversion and selectivity toward C_2 and C_3 over (A) H-AL-TPABr-OA, (B) H-AL-HDA-OA and (C) H-AL-PA-OA compared with (D) the commercial H-ZSM-5.

Figure 7.2 showed that the MTO conversion over H-AL-TPBAr-OA, H-AL-HDA-OA and H-AL-PA-OA was 70, 73 and 48 % after 1 h of time on stream (TOS). Moreover, the H-AL-TPBAr-OA and H-AL-PA-OA deactivated quickly, but H-AL-HDA-OA was amost stable with a MTO conversion of 62 % after 29 h of TOS. Moreover, the C_3/C_2 ratio of H-AL-TPBAr-OA, H-AL-HDA-OA and H-AL-PA-OA was 2.1, 3.7 and 1.5 respectively after 1 h of TOS. These results showed that oxalic acid could be used to enhance the MTO efficiency of fly ash-based ZSM-5 zeolite products in some cases but caused rapid deactivation in others.

There were two parameters of the synthesised zeolites that were directly related to their MTO catalytic activity, which were the crystal size and the BET surface area. Indeed, H-AL-PA-OA (length=18.92±2.01 µm; width=6.76±0.91 µm) had the biggest ZSM-5 crystals followed by H-AL-TPABr-OA (length=6.23±1.05 µm; width=5.61±1.18 µm) and H-AL-HDA-OA (length=1.02±0.14 µm; width=0.62±0.09 µm) (Figure 5.9), which showed that the ZSM-5 crystal size of H-AL-TPABr-OA, H-AL-HDA-OA and H-AL-PA-OA was inversely proportional to their MTO conversion efficiency. Moreover the BET surface area of the H-AL-TPABr-OA, H-AL-HDA-OA and H-AL-PA-OA was 327.53, 353.08 and 39.40 m^2/g respectively, which was directly proportionel to their MTO conversion efficiency. It could be concluded that the small size of ZSM-5 crystal and high surface area of H-AL-HDA-OA led to a high MTO conversion efficiency and slow deactivation compared to H-AL-TPABr-OA and H-AL-PA-OA. Indeed, it was reported by Wan et al., (2013) that a decrease in ZSM-5 crystal size improved the methanol conversion and reduced coking on the catalyst. Chen et al., (2012) reported that ZSM-5 zeolite with small crystals has a long life. Liu et al., (2015) investigated the effect of the BET surface area on the MTO conversion by loading different amounts of MoO_3 onto zeolite H-ZSM-5 and reported that the increase in MoO_3 loading was accompanied by a decrease in BET surface area, which led to a decrease in MTO conversion.

On the other hand, it was not easy to relate the MTO conversion efficiency of the H-AL-TPABr-OA, H-AL-HDA-OA and H-AL-PA-OA to the number of their Brønsted sites that was 0.71, 0.42 and 0.46 mmol H^+ per gram of zeolite (Figure 5.11), even though it is well known that zeolite acidity plays an important role in their catalytic applications (Louis et al., 2010; Dai et al., 2011, Chen et al., 2012), hence diffisional constraints and coking of catalysts pores (of large crystal sizes) was more likely the cause of the catalyst deactivation.

7.2.3. Methanol-to-Olefins (MTO) conversion over H-FFAE1-PA, H-FFAE1-HDA, H-FFAE1-TPABr and H-FFAE2-TPABr

H-FFAE1-TPABr, H-FFAE1-HDA, H-FFAE1-PA and H-FFAE2-TAPBr synthesised without an additional source of silica (see Table 3.6) were used as MTO catalysts (Section 3.3.3.1). This section was divided into two parts: the first part investigated the effect of Si/Al ratio on the MTO efficiency over H-FFAE1-TPABr and H-FFAE2-TPABr that were synthesised from FFAE1 (Si/Al=42) and FFAE2 (Si/Al=81) respectively, while the second part investigated the effect of the structure directing agent (TPABr, HDA and PA) on the MTO efficiency over H-FFAE1-TPABr, H-FFAE1-HDA and H-FFAE1-PA.

7.2.3.1. Influence of Si/Al ratio on the Methanol-to-Olefins efficiency over H-FFAE1-TPABr and H-FFAE2-TPABr

Figure 7.3 compares the MTO conversion and selectivity toward ethylene (C_2) and propylene (C_3) over H-FFAE1-TPABr (Si/Al=36) and H-FFAE2-TPABr (Si/Al=60) with that of a commercial H-ZSM-5 zeolite (Si/Al=29).

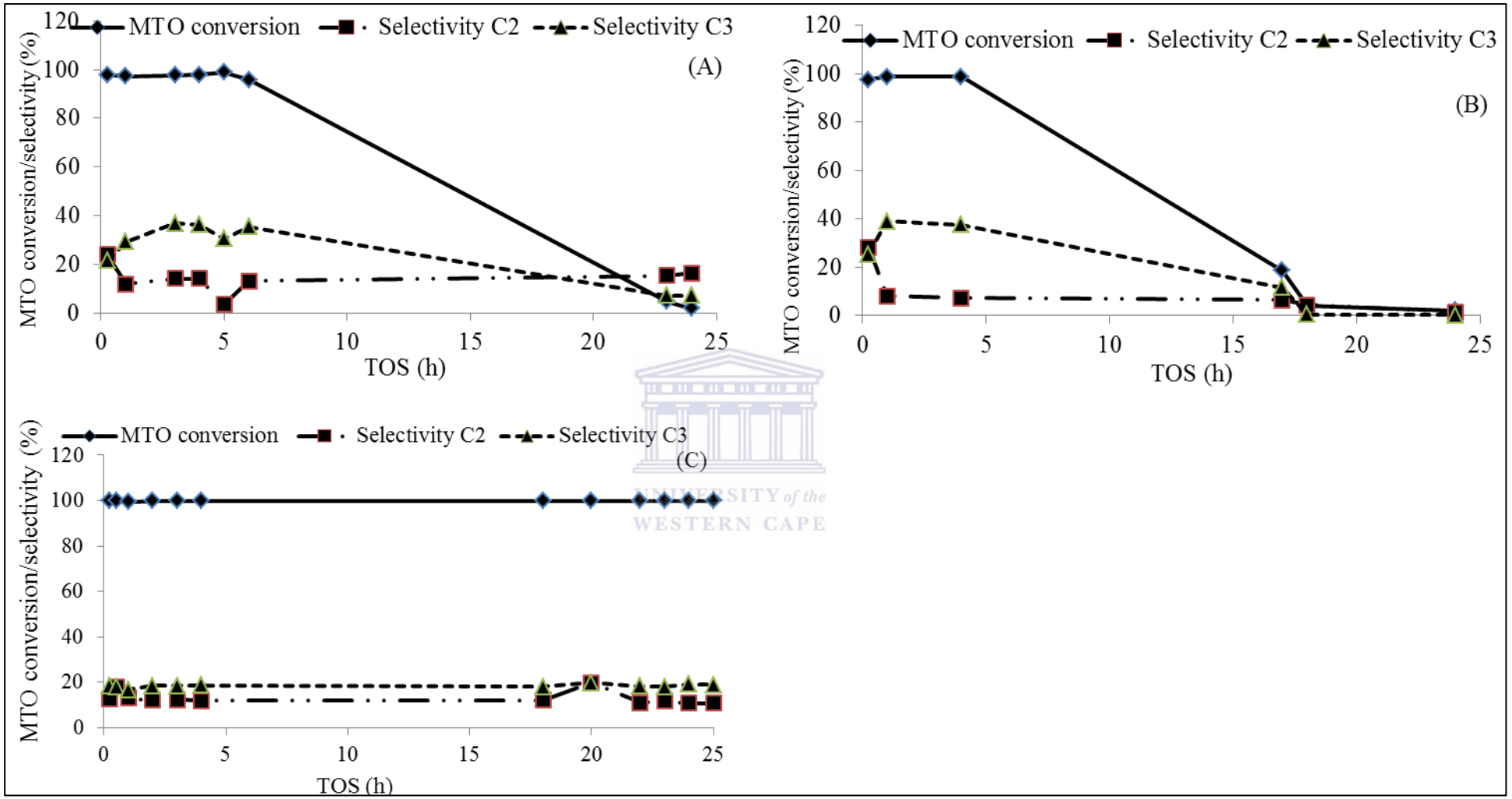

Figure 7.3: MTO conversion and selectivity toward C_2 and C_3 over (A) H-FFAE1-TPABr, (B) H-FFAE2-TPABr and (C) the commercial H-ZSM-5.

The MTO conversion over H-FFAE1-TPABr (Si/Al=36), H-FFAE2-TPABr (Si/Al=60) and the commercial H-ZSM-5 (Si/Al=29) were 99, 99 and 100 % respectively after 5 h of TOS. Thereafter, the MTO conversion over H-FFAE1-TPABr and H-FFAE2-TPABr drastically dropped to 2 % after 24 h of TOS, despite their high BET surface area of 494.4 and 457.5 m^2/g respectively. These results showed that increasing the Si/Al ratio from H-FFAE1-TPABr to H-FFAE2-TPABr did not enhance the MTO efficiency of the synthesised fly ash-based catalysts, therefore a second treatment of the fused fly ash extract with oxalic acid solution was not necessary in the process. Table 7.1 compares the properties and MTO effeciency of H-FFAE1-TPABr, H-FFAE2-TPABr and a commercial ZSM-5 zeolite.

Table 7.1: Properties of H-FFAE1-TPABr, H-FFAE2-TPABr and the commercial H-ZSM-5 (Com-ZSM-5), and their MTO conversion and selectivity.

			H-FFAE1-TPABr	H-FFAE2-TPABr	Com-ZSM-5
Brønsted acid sites (mmol H^+/g)			0.62	0.55	0.86
Crystal size (µm)		Length	6.52	4.65	1.46
		Width	2.56	1.67	1.11
Relative XRD crystallinity (%)			94	95	100
BET surface area (m^2/g)			494.4	457.5	480.2
MTO reaction	1 h	X(%)	99	97	100
		C_3/C_2	4.9	2.5	1.3
	5 h	X(%)	99	99	100
		C_3/C_2	5.2	8.7	1.6
	24 h	X(%)	2	2	100
		C_3/C_2	0.16	0.5	1.8

X(%)=conversion, C_3=selectivity toward propylene and C_2=selectivity toward ethylene.

It could be observed in Table 7.1 that H-FFAE1-TPABr and H-FFA2-TPABr had similar behaviour as MTO catalysts. They were both active until 5 h of TOS with a good propylene selectivity over ethylene. Thereafter, they deactivated with a conversion of 2 % after 24 h of TOS. Howerver, the similarity in the catalytic behaviour of H-FFAE1-TPABr and H-FFAE2-TPABr did not allow a correlation to be established between their properties and their MTO efficetiveness. It was noteworthy that H-FFAE1-TPABr and H-FFAE2-TPABr were synthesised from oxalic acid treated FFAE1 and FFAE2 as detailed in Section 3.3.1.3. FFAE1 was obtained after the first treatment of FFAE with oxalic acid while FFAE2 after the second treatment. And the MTO results of H-FFAE1-TPABr and H-FFAE2-TPABr presented in Figure 7.3 and Table 7.1 could lead to the conclusion that the second treatment of FFAE with oxalic acid was not necessary since it did not improve the catalytic effectiveness of the synthesised zeolite ZSM-5 products. Moreover, although this study presented an innovative way of synthesising ZSM-5 zeolite from fly ash without adding any silica source, the synthesised fly ash-based ZSM-5 zeolites still would need to be tailored in order to stabilise their MTO conversion and it was most likely that the large crystal sizes promoted rapid deactivation.

7.2.3.2. Influence of the structure directing agent on Methanol-to-Olefins conversion over H-FFAE1-TPABr, H-FFAE1-HDA and H-FFAE1-PA

Figure 7.4 summarises the effect of the structure directing agent TPABr, HDA and PA on the catalytic performance of the fly ash-based ZSM-5 zeolite products by comparing the percentage of MTO conversion and selectivity toward ethylene (C_2) and propylene (C_3) over H-FFAE1-TPABr, H-FFAE1-HDA and H-FFAE1-PA with that over the commercial H-ZSM-5 zeolite.

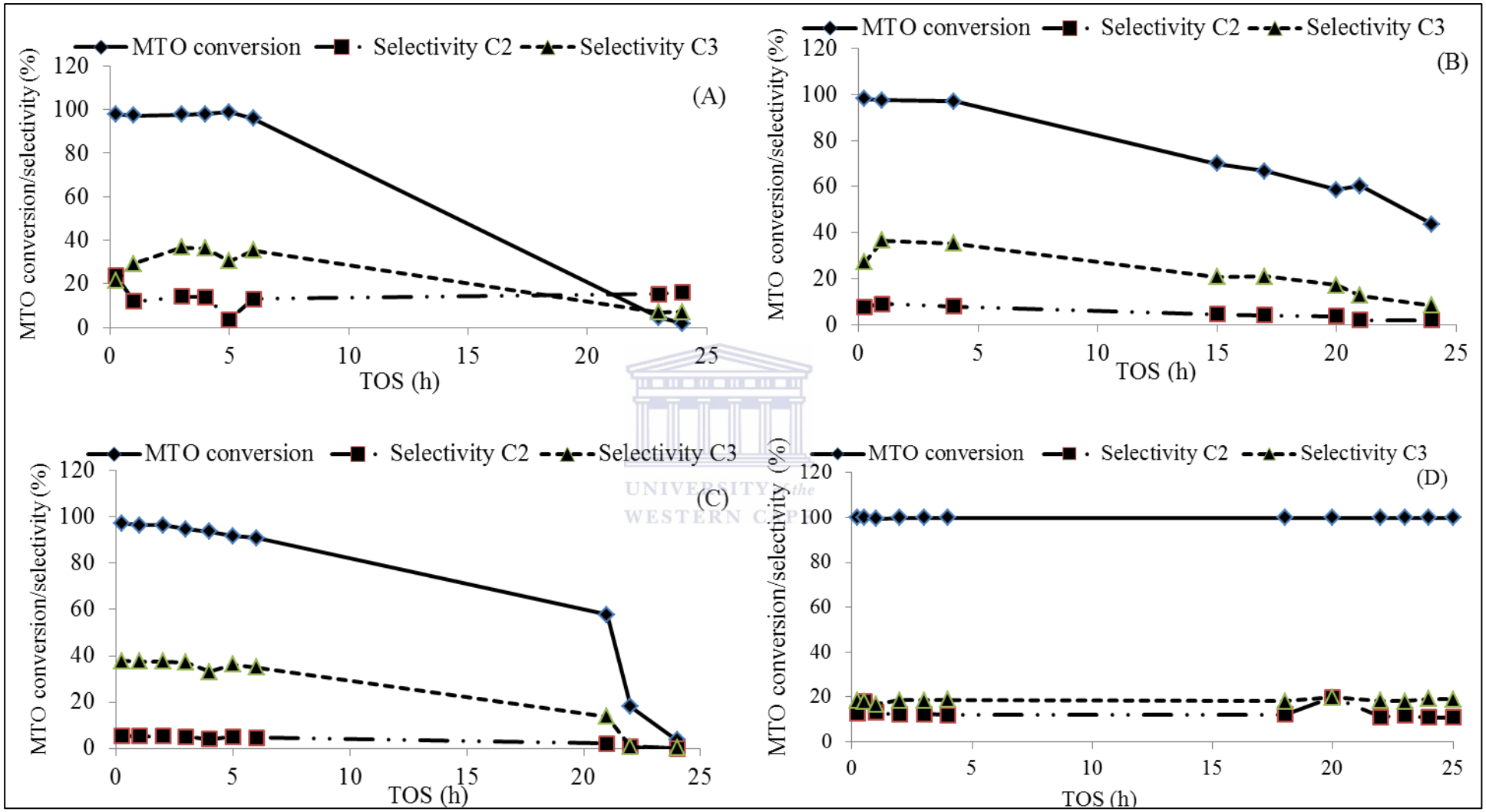

Figure 7.4: MTO conversion and selectivity toward C_2 and C_3 over (A) H-FFAE1-TPABr, (B) H-FFAE1-HDA, (C) H-FFAE1-PA and (D) the commercial H-ZSM-5.

Figure 7.4 showed that the MTO conversion over H-FFAE1-TPABr, H-FFAE1-HDA and H-FFAE1-PA was 99, 97 and 92 % respectively after 5 h of TOS. Moreover, H-FFAE1-HDA was more stable than H-FFAE1-TPABr and H-FFAE1-PA with a MTO conversion 44 % after 24 h of TOS, while that of H-FFAE1-TPABr and H-FFAE1-PA fell to 2 and 4 % respectively after 24 h of TOS. It was noteworthy that ZSM-5 zeolite product synthesised using HDA as structure directing agent had better catalytic activity than those synthesised using TPABr and PA regardless of the source of silica and alumina (Figure 7.2 and Figure 7.4). Table 7.2 compares the properties and MTO effeciency of H-FFAE1-TPABr, H-FFAE1-HDA, H-FFAE1-PA and the commercial H-ZSM-5 zeolite.

Table 7.2: Properties of H-FFAE1-TPABr, H-FFAE1-HDA, H-FFAE1-PA and a commercial H-ZSM-5, and their MTO conversion and selectivity.

			H-FFAE1-TPABr	H-FFAE1-HDA	H-FFAE1-PA	Com-ZSM-5
Brønsted acid sites (mmol H^+/g)			0.62	0.56	0.53	0.86
Crystal size (μm)	Length		6.52	3.34	3.14	1.46
	Width		2.56	1.10	1.02	1.11
Relative XRD crystallinity (%)			94	86	85	100
BET surface area (m^2/g)			494.4	387.5	378.9	480.2
MTO reaction	1 h	X(%)	99	98	97	100
		C_3/C_2	4.9	4.1	7.0	1.3
	5 h	X(%)	99	97	92	100
		C_3/C_2	5.2	4.5	7.1	1.6
	24 h	X(%)	2	44	4	100
		C_3/C_2	0.2	4.3	2.3	1.8

X(%)=conversion, C_3=selectivity toward propylene and C_2=selectivity toward ethylene.

Unlike in the case of H-AL-TPABr-OA, H-AL-HDA-OA and H-AL-PA-OA in which their MTO effectiveness could be related to their BET surface area and crystal size, it was difficult to relate the MTO effectiveness of H-FFAE1-TPABr, H-FFAE1-HDA, and H-FFAE1-PA to their properties. However, HDA was still the structure directing agent that led to a ZSM-5 zeolite product with the best catalytic effectiveness. Therefore, it was not excluded that the size, shape or number of positive charges in solution (1 for TPABr, 2 for HDA and 1 for PA) of the structure directing agents used for the synthesis of ZSM-5 zeolite influenced the catalytic effectiveness of the zeolite products. However, the synthesis conditions still need to be improved in order for H-FFAE1-HDA to be competitive.

7.3. Nazarov cyclisation of 1-phenyl-2-ethylpropenone over H-AL-TPABr-OA, H-AL-HDA-OA and H-AL-PA-OA

The Nazarov cyclisation was the second probe reaction used to investigate the efficiency of fly ash-based ZSM-5 zeolite products. Only H-AL-TPABr-OA, H-AL-HDA-OA and H-AL-PA-OA were used as acid catalysts in the Nazarov reaction because their efficiency in the MTO reaction was easily related to their properties such as BET surface area and crystal size (Section 7.2.2). Therefore the aim of the Nazarov cyclisation was to investigate if the same efficiency trend of the fly ash-based ZSM-5 zeolite products could be observed using another reaction. H-AL-TPABr, H-AL-HDA and H-AL-PA were dealuminated with a saturated solution of oxalic acid as detailed in Section 3.3.1.2, before being used as solid catalysts in the synthesis of 2-ethylindan-1-one through Nazarov cyclisation of 1-phenyl-2-ethylpropenone, with hexamethyl benzene as internal standard (Equation 3.5). Their catalytic efficiency was compared to that of the commercial H-ZSM-5 and a blank reaction was performed without any zeolite (Section 3.3.3.2(b)). The precursor 1-phenyl-2-ethylpropenone was synthesised from 1-phenylbutan-1-one and formaldehyde through Manich condensation (Section 3.3.3.2(a)). Figure 7.5 presents the ^{1}H NMR spectra of the precursor 1-phenyl-2-ethylpropenone and final products after Nazarov cyclisation over H-AL-TPABr-OA, H-AL-HDA-OA, H-AL-PA-PA and the commercial H-ZSM-5.

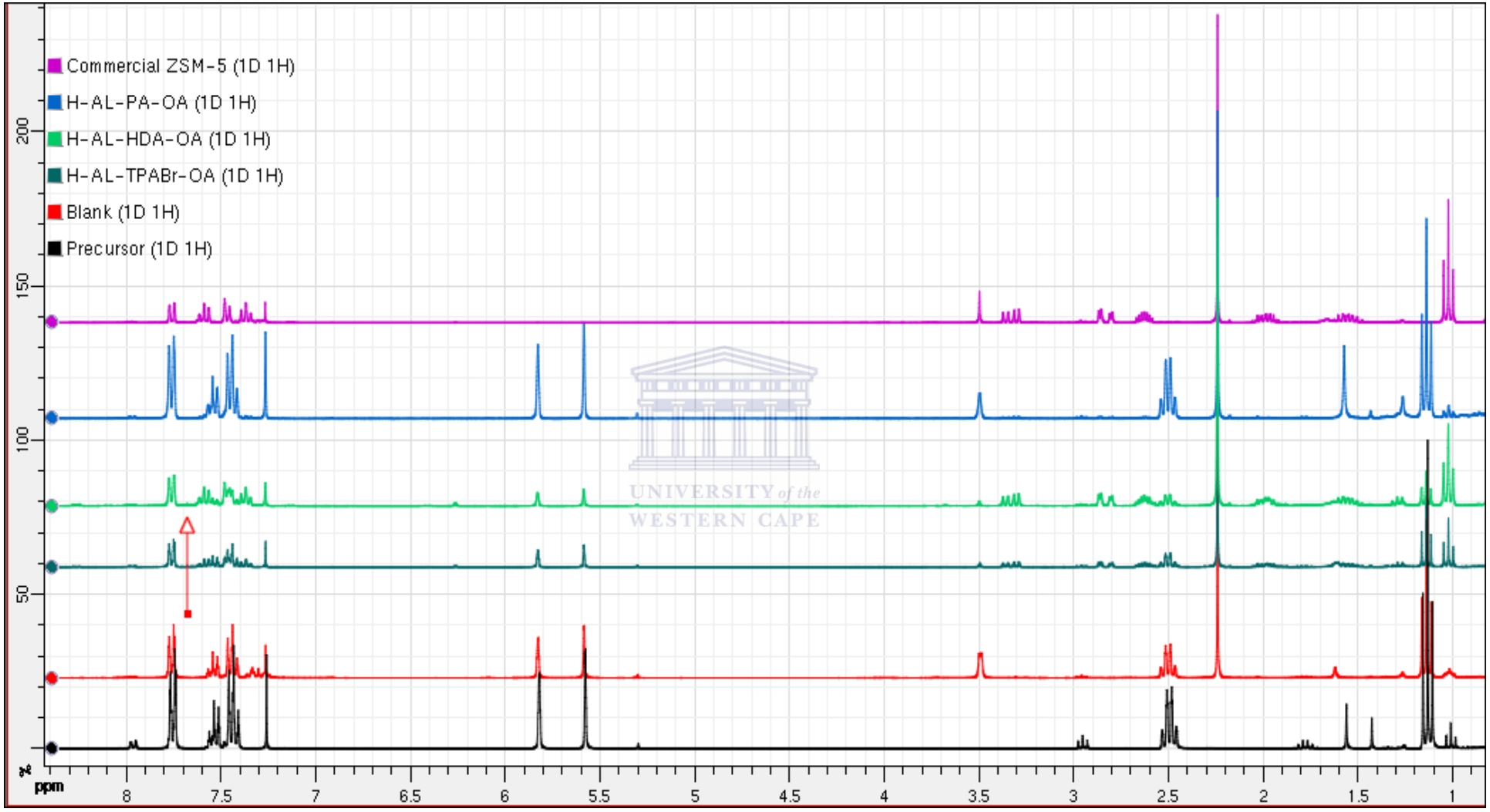

Figure 7.5: ^{1}H NMR spectra of the precursor (1-phenyl-2-ethylpropenone), product of blank Nazarov cyclisation without zeolite and products of Nazarov cyclisation over H-AL-TPABr-OA, H-AL-HDA-OA, H-AL-PA-OA and the commercial H-ZSM-5 zeolite.

The ^{1}H NMR spectrum of the precursor showed that 1-phenyl-2-ethylpropenone was successfully synthesised from 1-phenylbutan-1-one and formaldehyde as confirmed by ChemNMR^{1}H estimation. Besides the characteristic signals of 1-phenyl-2-ethylpropenone at 1.1, 2.5, 5.6 and 5.8 ppm; the synthesised precursor also presented signals of 1-phenylbutan-1-one at 1.0, 1.75 and 2.95 ppm. This showed that the purification of the precursor using a column chromatography (cyclohexane/ethyl acetate 90:10) was not complete. However, this study was a proof of concept showing that fly ash-based ZSM-5 zeolite samples could be used as heterogeneous catalysts in Nazarov cyclisation of 1-phenyl-2-ethylpropenone regardless of its purity. The signals that ranged between 7.0 and 8.0 ppm characterised the aromatic rings of all the products present within each sample, hence they were not used to distinguish the targeted product (2-ethylindan-1-one), or reagent (1-phenyl-2-ethylpropenone) or by-products.

The spectrum of the product of the blank reaction showed characteristic signals of the precursor 1-phenyl-2-ethylpropenone at 1.1, 2.5, 5.6 and 5.8 ppm with signals of some impurities at 1.0, 1.2, 1.6, 3.5 and 5.3 ppm. A singlet at 2.24 ppm corresponded to the 18 equivalent protons of the internal standard hexamethyl benzene. Furthermore it was noteworthy that in an equimolar reaction, the integration ratio of protons of the 1-phenyl-2-ethylpropenone alkene bond (5.6 or 5.8 ppm) and hexamethyl benzene protons was 1:18, which would lead to the 1-phenyl-2-ethylpropenone alkene signals with very low integration compared to hexamethyl benzene, and would not be detected. Therefore, the number of moles of hexamethyl benzene was divided by 6 to get an integration ratio of 1:3. Moreover, the decrease in that ratio was used to monitor the conversion of 1-phenyl-2-ethylpropenone as hexamethyl benzene was not involved in the reaction and its integration remained constant.

The spectra of the final products obtained over H-AL-TPABr-OA and H-AL-HDA-OA showed that the signal integration of the 1-phenyl-2-ethylpropenone alkene bond at 5.6 or 5.8 ppm decreased compared to that of the blank reaction, reducing the integration ratio between 1-phenyl-2-ethylpropenone alkene protons and hexamethyl benzene protons to 0.49:3 and 0.23:3 respectively. Furthermore, besides the characteristic signals of 1-phenyl-2-ethylpropenone at 1.1, 2.5, 5.6 and 5.8 ppm, the final products of H-AL-TPABr-OA and H-AL-HDA-OA also contained characteristic signals of 2-ethylindan-1-one at 1.0, 1.6, 2.6, 2.8 and 3.3 ppm. The spectrum of the product of H-AL-PA-OA was similar to that of the blank reaction with an integration ratio between 1-phenyl-2-ethylpropenone alkene protons and hexamethyl benzene protons of 1:3, indicating 1-phenyl-2-ethylpropenone could not be

converted into 2-ethylindan-1-one over H-AL-PA-OA. The spectrum of the commercial ZSM-5 product showed a total conversion of 1-phenyl-2-ethylpropenone to 2-ethylindan-1-one. The 1-phenyl-2-ethylpropenone conversion (X) and selectivity (S) toward 2-ethylindan-1-one of the Nazarov cyclisation products were determined following the formulae below:

From the integration ratio 1:3

$$\frac{yield}{3} = \frac{1-x}{3} \Rightarrow X(\%) = yield * 100 \quad \textbf{(Equation 7.1)}$$

With x the average of integrations of 1-phenyl-2-ethylpropenone alkene protons (5.6 and 5.8 ppm) and X(%) the conversion.

$$S(\%) = \frac{\sum_{i=1}^{3} (\text{int}\,egration)_i}{\frac{3}{Rdt}} * 100 \quad \textbf{(Equation 7.2)}$$

With S (%) the selectivity and i the signal of the final product proton at 2.6, 2.8 or 3.3 ppm. Table 7.3 summarises the properties of H-AL-TPABr-OA, H-AL-HDA-OA, H-AL-PA-OA and the commercial H-ZSM-5 together with their Nazarov cyclisation conversion (X) and selectivity (S).

Table 7.3: Properties of H-AL-TPABr-OA, H-AL-HDA-OA, H-AL-PA-OA and the commercial H-ZSM-5, and their Nazarov and MTO conversion and selectivity.

			H-AL-TPABr-OA	H-AL-HDA-OA	H-AL-PA-OA	Com-ZSM-5
Brønsted acid sites (mmol H^+/g)			0.71	0.46	0.42	0.86
Crystal size (µm)		Length	6.23	1.02	18.92	1.46
		Width	5.61	0.62	6.76	1.11
Relative XRD crystallinity (%)			54	51	45	100
BET surface area (m^2/g)			327.5	353.1	39.4	480.2
Nazarov cyclisation		X(%)	51	77	0	100
		S(%)	74	72	0	100
MTO reaction	1 h	X(%)	70	73	48	100
		C_3/C_2	2.1	3.8	1.5	1.3
	5 h	X(%)	57	74	40	100
		C_3/C_2	2.3	4.0	1.5	1.6
	24 h	X(%)	9	68	14	100
		C_3/C_2	1.8	4.9	1.5	1.8

X(%)=conversion, S(%)=selectivity toward 2-ethylindan-1-one, C_3=selectivity toward propylene and C_2=selectivity toward ethylene.

Table 7.3 showed that the Nazarov cyclisation conversion over H-AL-TPABr-OA, H-AL-HDA-OA and H-AL-PA-OA and the commercial H-ZSM-5 was 51, 77, 0 and 100 % respectively. Furthermore, only the commercial H-ZSM-5 had 100 % selectivity toward the targeted product 2-ethylindan-1-one; however, the spectra of H-AL-TPABr-OA and H-AL-HDA-OA did not reveal the presence of the expected by-product chloro(2-ethyl-3-phenylbut-3-en-1-yl)benzene or any other by-product despite their relatively lower selectivity of 74 and 72 % respectively toward the final product 2-ethylindan-1-one. Moreover, there was a correlation between the Nazarov and MTO effectiveness of H-AL-TPABr-OA, H-AL-HDA-OA and H-AL-PA-OA and their BET surface area and crystal size, with H-AL-HDA-OA being the best catalyst of the three fly ash-based ZSM-5 zeolite products. Indeed H-AL-HDA-OA had the smallest ZSM-5 crystals and highest BET surface area. Therefore its acceptable Nazarov and MTO effectiveness could be related to an easy diffusion of reagents, intermediate or final products throughout its pores unlike H-AL-TPABr-OA or H-AL-PA-OA that had bigger ZSM-5 crystals and lower BET surface area. Moreover, Song et al., (2000) reported that zeolites are well known for their selectivity allowing discrimination between molecules based on their size and/or shape. Indeed, in a homogeneous medium, Nazarov cyclisation is a reaction that requires the presence of a Lewis acid (Aggarwal and Belfield, 2003); however zeolites allow acid-mediated reactions to be performed in a more eco-friendly way (Corma, 1995). Sani-Souna-Sido et al., (2008) reported the use of ZSM-5 zeolite purchased from Zeolyst in the synthesis of 2-ethylindan-1-one from 1-phenyl-2-ethylpropenone with a conversion and selectivity of 94 and 100 % respectively. However, H-AL-HDA-OA with a conversion and selectivity of 77 and 72 % respectively was a promising fly ash-based solid acid catalyst, which could retain scientific attention in the valorisation of coal fly ash.

7.4. Chapter summary

In summary, it was proven in this chapter that ZSM-5 zeolite products that were synthesised from South African coal fly ash could be used as heterogeneous catalysts in Methanol-to-Olefins (MTO) and Nazarov reactions. The screening study of the synthesised fly ash-based ZSM-5 zeolite products that was performed in Chapter 4, Chapter 5 and Chapter 6 with variation of their synthesis conditions allowed the selection of some fly ash-based catalysts that would be effective in the two reactions mentioned above. H-AL-TPABr, H-AL-HDA, H-AL-PA, H-AL-TPABr-OA, H-AL-HDA-OA and H-AL-PA-OA were used as solid catalysts

in the MTO reaction. It could be seen that the transformation of H-AL-HDA into H-AL-HDA-OA through treatment with oxalic acid increased and stabilised its MTO effectiveness. This would be due to its high surface area and small crystal size reducing diffusional constraints. The dealumination of H-AL-TPABr and H-AL-PA only increased their MTO effectiveness in the first 60 minutes where after they rapidly deactivated. The MTO reaction was also performed over the H-form of the ZSM-5 zeolite products that were synthesised from fused fly ash extracts (FFAE1 and FFAE2) without an addition of fumed silica. It could be observed that an increase in Si/Al ratio from 36 in H-FFAE1-TPABr to 60 in H-FFAE2-TPABr did not ameliorate the MTO effectiveness of the final products. It was observed that both catalysts converted 99 % of methanol after 5 h of TOS, but afterwards, they rapidly deactivated. Therefore, it was not necessary to treat the fused fly ash extract more than once with oxalic acid prior to the synthesis of ZSM-5 zeolite. However, substituting TPABr by HDA and using FFAE1 as Si and Al precursor led to the synthesis of H-FFAE1-HDA with an acceptable MTO effectiveness and stability, even though the synthesis conditions still need to be ameliorated. As in the case of MTO conversion, the ZSM-5 crystal size of H-AL-TPABr-OA, H-AL-HDA-OA and H-AL-PA-OA was also inversely proportional to their Nazarov cyclisation efficiency, while their BET surface area was directly proportional to their conversion efficiency. The similarity in behaviour of H-AL-TPABr-OA, H-AL-HDA-OA and H-AL-PA-OA toward both reactions could confirm the diffusion of molecules throughout the catalysts was crucial for their catalytic efficiency, and H-AL-PA-OA showed significant pore occlusion which caused diffusional constraints preventing cyclisation.

CHAPTER 8: GENERAL CONCLUSION AND RECOMMENDATIONS

8.1. Introduction

This chapter reassesses the aims and objectives that had been set out in Chapter 1. It also draws a summary of major findings of this thesis by highlighting an overview of the accomplishments and contributions of the results from a scientific and industrial point of view and outlines recommendations for future work.

8.2. General conclusions

The gaps related to the synthesis of ZSM-5 zeolite from coal fly ash found in the literature are summarised in this section as well as the different findings of the study.

8.2.1. Gaps from the literature related to the current study

The aim and objectives (Section 1.7) of this study were set out based on the gaps found in the literature. This study focused on the synthesis of ZSM-5 zeolite from South African coal fly ash that is generated during the combustion of coal. South African power stations generate about 36.22 million tonnes of coal fly ash per year, which causes huge economic and environmental problems due its costly disposal and contamination of soil, surface and ground water by the toxic elements that leach from it. Several studies, including the synthesis of zeolites, have been conducted in order to reuse coal fly ash. The literature reported that different grades of low and intermediate silica zeolites such as zeolites, types A, X, Y, P and sodalite had been successfully synthesised from South African coal fly ash at the laboratory scale. However, the synthesis of high silica zeolites such as ZSM-5 zeolite had not been yet synthesised from South African coal fly ash despite its important applications as solid acid catalysts. This could be due to the presence of coal fly ash elements in the synthesised fly ash-based catalysts that could affect the accuracy and precision of a reaction and the excessive amount of additional silica that had to be added to adjust the Si/Al ratio. This does not promote the synthesis of ZSM-5 zeolite from South African coal fly ash, as the synthesis of high purity ZSM-5 zeolite from fly ash without an addition of silica source has not been yet reported. Moreover, among the organic structure directing agents that are used in the synthesis of ZSM-5 zeolite only TPA^+ cation had been used to synthesise ZSM-5 zeolite from fly ash. Hence, this current study aimed to synthesise different grades of ZSM-5 zeolite from

South African coal fly ash with and without an addition silica source and using three different organic structure directing agents namely tetrapropylammonium bromide (TPABr); 1,6-hexanediamine (HDA) and 1-propylamine (PA). The synthesised South African coal fly ash-based ZSM-5 zeolite products were used as solid catalyst in the Nazarov and Methanol-to-Olefin (MTO) reactions. All the questions that were asked in chapter 1 in order to meet the study objectives have been answered and are summarised in the findings section below.

8.2.2. Findings of this study

Several studies reported the synthesis of ZSM-5 zeolite from various sources of coal fly ash and additional silica. Hence, the first part of this current study was to find a suitable synthesis formulation of ZSM-5 zeolite from South African coal fly ash (FA) obtained at Arnot power station. Chemical parameters such as fly ash, fumed silica, NaOH, the structure directing agent and water content as well as physical parameters such as time and temperature of the aging and hydrothermal synthesis significantly influenced the final product quality. The most suitable hydrothermal gel was prepared by mixing 0.75 g of the as-received FA with 0.75 g of fumed silica, 0.25 g of NaOH, 1.5 g of structure directing agent (TAPBr, HDA or PA) and 20 mL of deionised water. After aging at room temperature for 2 h, the gel underwent hydrothermal synthesis at 160 °C and 72 h. The synthesised fly ash-based ZSM-5 zeolite products were detemplated, transformed in their H-form with NH_4NO_3 followed by calcination and then treated with oxalic acid. The obtained ZSM-5 zeolite products namely H-FA-TPABr-OA, H-FA-HDA-OA and H-FA-PA-OA were characterised by XRD, SEM, FTIR and ^{27}Al NMR. Their number of Brønsted acid sites was also determined using the H/D isotope exchange technique. The XRD showed that ZSM-5 zeolite was successfully synthesised from the mixture of the as-received FA and fumed silica. However, H-FA-TPABr-OA, H-FA-HDA-OA and H-FA-PA-OA only contained 58, 47 and 39 % of ZSM-5 phase that was mixed with some fly ash phases such as mullite and quartz. The SEM analysis revealed the transformation of spherical fly ash particles into crystals characteristic of ZSM-5 in H-FA-TPABr-OA, H-FA-HDA-OA and H-FA-PA-OA, with different size depending on the structure directing agent used. The FTIR analysis did not give conclusive results of the implication of fly ash in the zeolitization process as the double ring band of zeolitic materials in H-FA-TPABr-OA, H-FA-HDA-OA and H-FA-PA-OA overlapped with the Al-O stretch band for the glassy-amorphous phase, mullite and quartz. Hence, it was not possible to

estimate the crystallinity of H-FA-TPABr-OA, H-FA-HDA-OA and H-FA-PA-OA based on their optical density ratio. The number of Brønsted acid sites of H-FA-TPABr-OA, H-FA-HDA-OA and H-FA-PA-OA was 0.37, 0.29 and 0.32 mmol H^+ per gram of zeolite, which was very low compared to that of the commercial H-ZSM-5 of 0.86 mmol H^+ per gram of zeolite. The ^{27}Al NMR analysis showed that the percentage of extra-framework octahedrally coordinated aluminium was reduced from 29.2 % in the as-received FA to 11.6, 16.0 and 18.0 in H-FA-TPABr-OA, H-FA-HDA-OA and H-FA-PA-OA. The rest was transformed into framework tetrahedrally coordinated aluminium, which was an indication of the participation of fly ash in the formation ZSM-5 in H-FA-TPABr-OA, H-FA-HDA-OA and H-FA-PA-OA. The results presented in Chapter 4 proved that a high silica zeolite such as ZSM-5 could be synthesised from South African coal fly ash with other structure directing agents than TPA^+, which was not reported yet in the literature. However, the addition of a significant amount of fumed silica to adjust the Si/Al ratio, as well as the presence of fly ash mineral phases in the final zeolite products and their poor chemical and physical properties compared to that of the commercial ZSM-5 obtained from Zeolyst could not promote the use H-FA-TPABr-OA, H-FA-HDA-OA and H-FA-PA-OA as solid catalysts. Moreover, the synthesis conditions would need to be optimised from one source of coal fly ash to another one as the composition of South African coal fly ash varies from one source to another one. Hence, it was deemed necessary to improve the synthesis conditions by pre-treating the as-received fly ash prior to the hydrothermal synthesis.

The first innovative approach to improve the quality of the fly ash-based ZSM-5 zeolite products was to pre-treat the as-received South African coal fly ash with a concentrated H_2SO_4 (95-99 %) prior to the zeolitization process in order to remove a certain amount of aluminium so as to minimise the amount of additional fumed silica needed in the hydrothermal gel. Moreover, the acid treatment would remove other elements that could have unknown and/or undesirable effects in the synthesis process. However, the pre-treatment with a concentrated H_2SO_4 (95-99 %) solution was able to increase the Si/Al ratio only from 1.86 in the as-received fly ash (FA) to 2.02 in the acid treated fly ash (AL). Other elements such as Fe, Ca, Ti, Mg and P were also removed from the fly ash feedstock during the H_2SO_4 treatment. The acid treated fly ash (AL) underwent the same synthesis conditions as the as-received fly ash (FA) with TPABr, HDA or PA as structure directing agent. The synthesised AL-TPABr, AL-HDA and AL-PA were detemplated, transformed into their H-form and further dealuminated using an oxalic acid solution. The Si/Al ratio was increased from 3.3,

3.9 and 3.8 in H-AL-TPABr, H-AL-HDA and H-AL-PA to 4.1, 4.7 and 4.9 in H-AL-TPABr-OA, H-AL-HDA-OA and H-AL-PA-OA. The H_2SO_4 treatment of the as-received fly ash prior to the synthesis process and the dealumination of the final products with oxalic acid solution were not able to increase the Si/Al ratio above 10 which is a ratio characteristic of ZSM-5 zeolite. The XRD patterns of H-AL-TPABr-OA, H-AL-HDA-OA and H-AL-PA-OA products still showed the presence of fly ash mineral phases (mullite and quartz) and their ZSM-5 relative crystallinity was 54, 51 and 45 % respectively. However, the pre-treatment of fly ash with H_2SO_4 prior to the synthesis significantly increased the number of Brønsted acid sites of the final products to 0.71, 0.46 and 0.42 mmol H^+ per gram of zeolite for H-AL-TPABr-OA, H-AL-HDA-OA and H-AL-PA-OA respectively, showing the effect of the structure directing agent on the acidity of the synthesised zeolites. Moreover, the effect of the structure directing agent could also be observed for the BET surface area of H-AL-TPABr-OA, H-AL-HDA-OA and H-AL-PA-OA that was 327.5, 353.1 and 39.4 m^2/g respectively, and was inversely proportional to their crystal size. Despite a slight amelioration of some properties of the fly ash-based ZSM-5 zeolite products by pre-treating the as-received fly ash by concentrated H_2SO_4 prior to the hydrothermal synthesis, the quality of the synthesised fly ash-based zeolite ZSM-5 products (H-AL-TPABr-OA, H-AL-HDA-OA and H-AL-PA-OA) was still not competitive with the commercial ZSM-5 zeolite products.

The synthesis of ZSM-5 zeolite from South African coal fly ash using the conditions detailed above did not show any improvement in the reuse of coal fly ash for the synthesis of ZSM-5 zeolite but gave optimised synthesis conditions. Hence, there was need for a second innovative approach in the synthesis of coal fly ash-based ZSM-5 zeolite, which consisted of extracting a powder form fused fly ash extract (FFAE) with a Si/Al ratio of 10. FFAE was amorphous and its XRD did not reveal the presence of other fly ash mineral phases such as mullite and quartz. FFAE was thus an adequate precursor for the synthesis of ZSM-5 without an additional silica source. However, no solid product was formed when 2 g of FFAE was mixed with 0.42 g of NaOH, 1.5 g of TPABr and 50 mL of deionised water. The mixture was aged at room temperature for 30 min before undergoing hydrothermal synthesis at 160 °C for 72 h. ZSM-5 could not crystallised because of an important Na content in FFAE. Thus, the further treatment of FFAE with oxalic acid proved to be an innovative route to remove most of the Na that was contained in FFAE prior to the zeolitization process. Moreover, the Si/Al in the extract could be increased by a second treatment of FFAE with oxalic acid solution. ZSM-5 zeolite could be synthesised from the oxalic acid treated FFAE namely FFAE1 and

FFAE2 with TPABr as structure directing agent and this offered a route to factor Si/Al ratio. The synthesised zeolite H-FFAE1-TPABr and H-FFAE2-TPABr had ZSM-5 relative crystallinity of 94 and 95 % respectively, showing their high purity compared to the ZSM-5 zeolite products that were synthesised from the as-received fly ash or the acid treated fly ash. The BET surface area and number of Brønsted acid sites of H-FFAE1-TPABr and H-FFAE2-TPABr were 494.4 and 457.5 m^2/g and 0.62 and 0.55 mmol H^+ per gram of zeolite respectively. The ZSM-5 relative crystallinity, BET surface area and number of Brønsted acid sites of H-FFAE1-TPABr and H-FFAE2-TPABr were close to that of the commercial ZSM-5 zeolite, which were 100 %, 480.2 m^2/g and 0.86 mmol H^+ per gram of zeolite respectively. The success of the synthesis of ZSM-5 zeolite products (H-FFAE1-TPABr and H-FFAE2-TPABr) from FFAE1 and FFAE2 constituted a breakthrough in the synthesis of ZSM-5 zeolite from fly ash that was subject to criticism because of the important amount of silica source that needed to be added in the hydrothermal gel in order to adjust the Si/Al ratio. The new route also minimised the presence of fly ash mineral phases and other impurities in the final products. The synthesis of high purity ZSM-5 zeolite from fly ash has not previously been reported in the literature. Several treatments of FFAE with oxalic acid also offered a possibility of varying the Si/Al ratio of fly ash-based ZSM-5 zeolite products as the Si/Al ratio of H-FFAE1-TPABr and H-FFAE2-TPABr was 36 and 60 respectively. Moreover, ZSM-5 zeolite could also be synthesised from FFAE1 with TPABr being substituted by HDA and PA, which constituted another novelty of this study as no one has reported the synthesis of ZSM-5 from fly ash or fly ash extract with structure directing agents other than the TPA^+ cation. Furthermore, the availability and lower cost of the HDA and PA structure directing agents as well as the difference in properties of the synthesised fly ash-based ZSM-5 zeolite products (H-FFAE1-TPABr, H-FFAE1-HDA and H-FFAE1-PA) offered more options in the synthesis and use of fly ash-based ZSM-5 zeolite products.

Methanol-to-Olefin (MTO) and Nazarov reactions were two probe reactions that were used to distinguish between the efficiency of ZSM-5 zeolite products synthesised from the acid treated fly ash (AL) and those synthesised from fused fly ash extracts (FFAE1 and FFAE2). The effect of dealumination of H-AL-TPABr, H-AL-HDA and H-AL-PA with a saturated oxalic acid solution was investigated by comparing the MTO conversion and selectivity toward ethylene and propylene over H-AL-TPABr, H-AL-HDA, H-AL-PA, H-AL-TPABr-OA, H-AL-HDA-OA and H-AL-PA-OA. The MTO conversion over H-AL-TPABr, H-AL-HDA and H-AL-PA was less than 40 % after 1 h of TOS and the catalysts rapidly deactivated.

However, H-AL-HDA had the highest MTO conversion. H-AL-TPABr-OA, H-AL-HDA-OA and H-AL-PA-OA presented better MTO conversion than H-AL-TPABr, H-AL-HDA and H-AL-PA of 70, 73 and 48 % respectively. However, only H-AL-HDA-OA was still stable after 29 h of TOS with a MTO conversion of 62 %. Moreover, it could be observed that the MTO conversion over H-AL-TPABr-OA, H-AL-HDA-OA and H-AL-PA-OA was related to their BET surface area and ZSM-5 crystal size. The use of HDA as structure directing agent led to a ZSM-5 zeolite product that had the smallest ZSM-5 crystal size and the highest BET surface area; which gave the highest and most stable MTO conversion.

The Nazarov cyclisation of 1-phenyl-2-ethylpropenone over H-AL-TPABr-OA, H-AL-HDA-OA and H-AL-PA-OA was carried out in order to confirm that their catalytic efficiency was related to their ZSM-5 crystal size and BET surface area. A similar trend to that of MTO reaction was observed when H-AL-TPABr-OA, H-AL-HDA-OA and H-AL-PA-OA were used as catalysts in the Nazarov cyclisation, with H-AL-HDA-OA having the highest conversion and selectivity toward the final product 2-ethylindan-1-one, followed by H-AL-TPABr-OA. It was then concluded that the relative effectiveness of H-AL-TPABr-OA, H-AL-HDA-OA and H-AL-PA-OA might be related to diffusional constraints of large ZSM-5 crystals.

On the other hand, the ZSM-5 zeolite products that were synthesised from the fused fly ash extracts (H-FFAE1-TPABr, H-FFAE2-TPABr, H-FFAE1-HDA and H-FFAE1-PA) were also used as MTO catalysts. The effect of the number of oxalic acid treatments of FFAE was investigated by comparing the MTO conversion over H-FFAE1-TPABr with H-FFAE2-TPABr. And it was observed that H-FFAE1-TPABr and H-FFAE2-TPABr had the same MTO conversion of 99 % leading to the conclusion that the second treatment of FFAE was not necessary. However, H-FFAE1-TPABr and H-FFAE2-TPABr rapidly deactivated. Moreover, in the case where HDA or PA was substituted for TPABr in the synthesis of H-FFAE1-HDA and H-FFAE1-PA, the three catalysts were still active after 5 h of TOS, but only H-FFAE1-HDA showed 44 % MTO conversion after 24 h of TOS. These results showed that the synthesis conditions of H-FFAE1-TPABr, H-FFAE2-TPABr, H-FFAE1-HDA and H-FFAE1-PA should still be improved in order to stabilise their MTO effectiveness.

8.3. Recommendations

This study had shown that a pre-treatment of fly ash with a concentrated H_2SO_4 (95-99 %) solution or fusion of fly ash with NaOH followed by treatment of the extract with oxalic acid improved the qualities of the final fly ash-based ZSM-5 zeolite products. However, the H_2SO_4 conditions used to leach fly ash, that were used to increase the Si/Al ratio of the starting fly ash material did not work effectively, as the Si/Al ratio only increased from 1.86 in FA to 2.02 in AL. Therefore the same amount of fumed silica used with FA was also used with AL but the final products, H-AL-TPABr-OA, H-AL-HDA-OA and H-AL-PA-OA still contained fly ash mineral phases. This route of fly ash-based ZSM-5 zeolite synthesis did not resolve the problem that was pointed out in Chapter 1. It has been reported that power-consuming processes such as roasting or sintering of fly ash were used prior to the acid leaching in order to enhance the aluminium extraction. This could be adopted in future in order to remove as much aluminium as possible from fly ash and use less fumed silica in the synthesis process. Moreover, the synthesised H-AL-TPABr-OA, H-AL-HDA-OA and H-AL-PA-OA could not compete with the commercial catalyst in the Methanol-to-Olefin (MTO) and Nazarov reactions due to diffusional constraints. The creation of a secondary pore system consisting of mesopores as well as micropores in zeolite crystals could be a sufficient route to minimize the diffusional limitation of molecules and improve the catalyst efficiency. Therefore, mesopore directing agents could be added during the zeolitization process to synthesise a hierarchical fly ash-based ZSM-5 zeolite, to enhance its catalyst efficiency.

The fusion of fly ash followed by the treatment with a saturated oxalic acid solution led to the synthesis of a high purity fly ash-based ZSM-5 zeolite without the addition of fumed silica. The synthesised fly ash-based ZSM-5 zeolite products had a high MTO efficiency. However, they rapidly deactivated after 5 h of TOS. This could not promote their application as catalysts. Therefore a post-synthesis treatment of these fly ash-based ZSM-5 zeolite products is required in order to stabilise their catalytic efficiency. It was reported in the literature that the desilication of a very high silica content ZSM-5 zeolite with NaOH solution created a hierarchical pore system, thus enhanced the catalytic efficiency of ZSM-5 zeolite. This process could be adopted in future in order to stabilise the catalytic activity of ZSM-5 products that were synthesised from fused fly ash extracts. Furthermore, metals such as Pt, Mg could be loaded onto the synthesised ZSM-5 in order to prevent quick deactivation of the catalyst.

The findings of this study showed that the MTO deactivation of ZSM-5 that was synthesised from the fused fly ash extract was related to its large crystal size; therefore the synthesis route that would lead to the formation of nanocrystalline ZSM-5 could be investigated.

It was also observed that the catalysts that were synthesised using HDA as structure directing agent were more active than those synthesised using TPABr or PA. This current study showed that other organic structure directing agents could lead to the synthesis of high quality fly ash-based ZSM-5 zeolite with a better catalytic efficiency. Therefore, a screening of ZSM-5 structure directing agents could lead to other suitable ZSM-5 templates.

REFERENCES

Abou Rida, M., Harb, F. (2014), "Synthesis and characterization of amorphous silica nanoparitcles from aqueous silicates using cationic surfactants", *Journal of Metals, Materials and Minerals*, Vol. 24, Issue 1. pp. 37-42.

Adamczyk, Z., Bialecka, B. (2005), "Hydrothermal synthesis of zeolites from Polish coal fly ash", *Polish Journal of Environmental Studies*, Vol. 14, Issue 6, 713-719.

Adriano, D.C., Page, A.L., Elseewi, A.A., Chang, A.C., Straughan, I. (1980), "Utilization and disposal of fly ash and other coal residues in terrestrial ecosystems", *A review Journal of Environmental Quality*, Vol. 9, pp. 333-344.

Aggarwal, V.K., Belfield, A.J. (2003), "Catalytic asymmetric Nazarov reactions promoted by chiral Lewis acid complexes", *Organic Letters*, Vol. 5, Issue 26, pp. 5075-5078.

Ahmaruzzaman, M. (2010) "A review on the utilization of fly ash", *Process in Energy and Combustion Science*, Vol. 36, pp. 327-363.

Akinyemi, S.A., Akinlua, A., Gitari, W.M., Akinyeye, R.O., Petrik, L.F. (2011), "The leachability of major elements at different stages of weathering in dry disposal coal fly ash, *Coal Combustion and Gasification Products*, Vol. 3, pp. 28-40.

Ali, M.A., Brisdon,B. J., Thomas, W.J. (2003), "Synthesis, Characterization and Catalytic Activity of ZSM-5 Zeolites Having Variable Silicon-to-Aluminum Ratios", *Applied Catalysis, A: General*, Vol. 252, pp. 149-162.

Al-Shawabkeh, A., Matsuda, H., Hasatani, M. (1995), "Comparative reactivity of treated FBC- and PCC-fly ash for SO2 removal", *Canadian Journal* of *Chemical Engineering*, Vol. 73, pp. 678–685.

Amber, I., Folayan, C., Suleiman, R., Atta, A.Y. (2013), "Application of synthesised zeolite A from Kankara kaolin for solar adsorption refrigeration", *Journal of Mechanical Engineering and Technology*, Vol. 5, No 1, 33-44.

Ashbrook, S.E., Dawson, D.M., Seymour, V.R. (2014), "Recent Developments in Solid-State NMR Spectroscopy of Microporous Materials", *Physical Chemistry Chemical Physics*, Vol. 16, pp. 8223-8242.

Atta, A.Y., Ajayi, O.A., Adefila, S.S. (2007) "Synthesis of faujasite zeolites from Kankara kaolin clay", *Journal of Applied Sciences Research*, Vol. 3, Issue 10, pp. 1017-1021.

Auerbach, S.M., Carrado, K.A., Dutta, P. (2003), "*Handbook of zeolite science and technology*", Marcel Dekker, Inc., New York.

Awizar, D.A., Othman, N.K., Jalar, A., Daud, A.R., Rahman, I.A., Al-hardan N.H. (2013), "Nanosilicate extraction from rice husk ash as green corrosion inhibitor", *International Journal of Electrochemical Science*, Vol. 8, pp. 1759-1769.

Babajide, O., Petrik, L., Musyoka, N., Ameer, F. (2012), "Novel zeolite Na-X synthesized from fly ash as a heterogeneous catalyst in biodiesel production", *Catalysis Today*, Vol. 190, pp. 54-60.

Baerlocher, C., Meier, W.M., Olson, D.H. (2007), "*Atlas of Zeolite Structure Types"*, 7th Edition, Elsevier, Amsterdam.

Bagguley, D. M. S. (1992)." *Pulsed Magnetic Resonance: NMR, ESR, and Optics (A Recognition of E. L. Hahn)*", Oxford University Press.

Baldyga, J., Jasinska, M., Jodko, K., Petelski, P. (2012), "Precipitation of amorphous colloidal silica from aqueous solutions-aggregation problem", *Chemical Engineering Science*, Vol. 77, pp. 207–216.

Barrer, R.M. (1945), "Separation of mixtures using zeolites as molecular sieves. I. Three classes of molecular – sieve zeolite", *Journal of the Society of Chemical Industry*, Vol. 64, p. 130.

Barrer, R.M., Baynham, J.W., Bultitude, F.W., Meier, W.M. (1959), "Hydrothermal chemistry of the silicates. Part VIII. Low-temperature crystal growth of aluminosilicates, and of some gallium and germanium analogues", .*Journal of the Chemical Society*, pp. 195-208.

Barzetti, T., Selli, E., Moscotti, D., Forni, L. (1996), "Pyridine and ammonia as probes for FTIR analysis of solid acid catalysts", *Journal of the Chemical Society, Faraday Transactions*, Vol. 92, Issue 8, pp. 1401-1407.

Bass, J.L., Turner, G.L. (1997), "Anion distribution in sodium silicate solutions. Characterization by ^{29}Si NMR and infrared spectroscopies, and vapor phase osmometry", *Journal of Physical Chemistry B*, Vol. 101, pp. 10638-10644.

Bayense, C.R., Van Hooff., J.H.C., de Haan, J.W., Van de Ven, L.J.M., Kentgens, A.P.M. (1993), "Introduction of gallium in HZSM5 and HY zeolites by post-synthesis treatment with trimethylgallium", *Catalysis Letters*, Vol. 17, pp. 349-361.

Bekkum, V.H., Flanigen, E.M., Jansen, J.C. (1991), "*Introduction to zeolite science and practice*", Elsevier Science, Amsterdam, Netherlands.

Belviso, C., Cavalcante, F., Lettino, A., Fiore, S. (2009), "Zeolite synthesised from fused coal fly ash at low temperature using seawater for crystallization", *Coal Combustion and Gasification Products*, Vol. 1, Issue 1, pp. 7-13.

Bibby, D.M., Dale, M.P. (1985), "Synthesis of silica-sodalite from nonaqueous systems", *Nature*, Vol. 317, pp. 157-158.

Bjørgen, M., Joensen, F., Holm, M.S., Olsbye, U.,Lillerud, K.P., Svelle, S. (2008), "Methanol to gasoline over zeolite H-ZSM-5: Improved catalyst performance by treatment with NaOH", *Applied Catalysis A: General*, Vol. 345, pp. 43–50.

Bleken, F.L., Chavan, S., Olsbye, U., Boltz, M., Ocampo, F., Louis, B. (2012), "Conversion of methanol into light olefins over ZSM-5 zeolite: Strategy to enhance propene selectivity", *Applied Catalysis A: General*, Vol. 447-448, pp. 178-185.

Boltz, M., de Mattos, M.C.S, Esteves, P.M, Pale, P., Louis, B. (2012), "Green route for the chlorination of nitrobenzene", *Applied Catalysis A: General*, Vol. 449, pp. 1– 8.

Boltz, M., Louis, B. (2013), "*Design microscopique de zeolithes ZSM-5 pour la conversion du methanol en olefines legeres*", Groupe d'Etude en Catalyse, Cap d'Agde, France.

Boltz, M., Losch, P., Louis, B., Rioland, G., Tzanis, L., Daou, T.J. (2014), "MFI-type zeolite nanosheets for gas-phase aromatics chlorination: a strategy to overcome mass transfer limitations", *RSC Advances*, Vol.4, pp. 27242-27249

Bonilla, G., Diaz, I., Tsapatsis, M., Jeong, H.K., Lee, Y., Vlachos, D.G. (2004), "Zeolite (MFI) crystal morphology control using organic structure-directing agents", *Chemistry of Materials*, Vol. 16, pp. 5697-5705.

Braunbarth, C.M., Behrens, P., Felsche, J., van de Goor, G., Wildermuth, G., Engelhardt, G. (1996), "Synthesis and characterization of two new silica sodalities containing ethanolamine or ethylenediamine as guest species: $[C_2H_7NO]_2[Si_6O_{12}]_2$ and $[C_2H_8N_2]_2[Si_6O_{12}]_2$", *Zeolites*, Vol. 16, p. 207.

Braunbarth, C.M., Behrens, P., Felsche, J., van de Goor, G. (1997), "Phase transitions and thermal behaviour of silica sodalites", *Solid State Ionics*, Vol. 101-103, pp. 1273-1277.

Breck, D.W. (1974), "*Zeolite Molecular Sieves"*, John Wiley & Sons, Ltd, New York.

Byrappa, K., Yoshimura, M. (2001), "*Handbook of Hydrothermal Technology*", Noyes Publications / William Andrew Publishing, LLC, New York.

Cejka, J., van Bekkum, H., Corma, A., Schuth, F. (2007), "*Introduction to zeolite science and practice*". 3rd Edition Elsevier, Oxford.

Chal, R., Gerardin, C., Bulut, M., Van Donk, S. (2011), "Overview and industrial assessment of synthesis strategies towards zeolites with mesopores", *ChemCatChem*, Vol. 3, pp. 67-81.

Chareonpanich, M., Namto, T., Kongkachuichay, P., Limtrakul, J. (2004), "Synthesis of ZSM-5 zeolite from lignite fly ash and rice husk ash", *Fuel Processing Technology*, Vol. 85, pp. 1623–1634.

Chassaing, S., Kumarraja, M., Sido, A.S.S., Pale, P., Sommer, J. (2007), "Click chemistry in Cu^{I}-zeolites: The Huisgen (3+2)-cycloaddition", *Organic Letters*, Vol. 9, Issue 5, pp. 883-886.

Chen, D., Moljord, K., Holmen, A. (2012), "A methanol to olefins review: diffusion, coke formation and deactivation on SAPO type catalysts", *Microporous and Macroporous Materials*, Vol. 164, pp. 239-250.

Cheng-You, W., Hong-Fa, Y., Hui-Fang, Z. (2012), "Extraction of aluminium by pressure acid-leaching method from coal fly ash", *Transactions of Nonferrous Metals Society of China*, Vol. 22, pp. 2282-2288.

Chester, A.W., Derouane, E.G. (2009) "*Zeolite characterization and catalyst: A tutorial*", Springer, London.

Chigondo, M., Guyo, U., Shumba, M., Chigondo, F., Nyamunda, B., Moyo, M., Nharingo, T. (2013), "Synthesis and characterisation of zeolites from coal fly ash (CFA)", *IRACST – Engineering Science and Technology: an International Journal*, Vol. 3, Issue 4, pp. 714-718.

Chu, N., Yang, J., Li, C., Cui, J., Zhao, Q., Yiu, X., Lu, J., Wang, J. (2009), "An unusual hierarchical ZSM-5 microsphere with good catalytic performance in methane dehydroaromatization", *Microporous and Mesoporous Materials*, Vol. 118, Issue 1-3, pp. 169-175.

Chunfeng, W., Jiansheng, L.I., Xia, S., Lianjun, W., Xiuyun, S. (2009), "Evaluation of zeolites synthesized from fly ash as potential adsorbents for wastewater containing heavy metals", *Journal of Environmental Sciences*, Vol. 21, pp. 127-136.

Chung, F.H., Smith, D.K. (2000), "*Industrial applications of X-ray diffraction*", Marcel Dekker, Inc. New York.

Corma, A. (1995), "Inorganic solid acids and their use in acid-catalysed hydrocarbon reactions", *Chemical Reviews*, Vol. 95, Issue 3, pp. 559-614.

Cooper, E.R., Andrews, C.D., Wheatley, P.S., Webb, P.B., Wormald, P., Morris, R.E. (2004), "Ionic liquids and eutectic mixtures as solvent and template in synthesis of zeolite analogues", *Nature*, Vol. 430, p. 1012.

Crelling, J.C., Hagemann, H.W., Sauter, D.H., Ramani, R.V., Vogt, W., Leininger, D., Krzack, S., Meyer, B., Orywal, F., Reimert, R., Bonn, B., Bertmann, U., Klose, W., Dach, G. (2010), "*Coal*", Ullmann's Encyclopedia of Industrial Chemistry, Wiley Online Library.

Criado, M., Fernandez-Jimenez, A., Palomo, A. (2007), "Alkali activation of fly ash: Effect of the SiO_2/Na_2O ratio part 1: FTIR study", *Microporous and Mesoporous Materials*, Vol. 106, pp. 180-191.

Csencsits, R., Gronsky, R. (1988), "*Preparation of zeolites for TEM using microtomy*", In: Bravman JC, Anderson RM, McDonald ML (eds) Specimen Preparation for transmission electron microscopy of materials. Proceedings of Materials Research Society, Vol. 115, Boston, MA, 1987, p 103.

Cubillas, P., Anderson, M. W. (2010), "*Synthesis mechanism: crystal growth and nucleation, in zeolites and catalysis: synthesis, reactions and applications*" (eds) J. Čejka, A. Corma and S. Zones), Wiley-VCH Verlag GmbH & Co. KGaA, Weinheim, Germany.

Cundy, C.S., Cox, P.A. (2005), "The hydrothermal synthesis of zeolites: Precursors, intermediates and reaction mechanism", *Microporous and Mesoporous Materials*, Vol. 82, pp. 1-78.

Dai, W., Wang, X., Wu, G., Guan, N., Hunger, M., Li, L. (2011), "Methanol-to-Olefin conversion on silicoaluminophosphate catalysts: Effect of Brønsted acid sites and framework structures*", ACS Catalysis*, Vol. 1, Issue 4, pp. 292-299.

Davini, P. (1996), "Investigation of the SO_2 adsorption properties of $Ca(OH)_2$- fly ash systems", *Fuel*, Vol. 75, pp. 713–716.

Davis, M.E. (2002), "Ordered porous materials for emerging applications", *Nature*, Vol. 417, pp. 813-821.

Derouane, E.G., Lemos, F., Naccache, C., Ribeiro, F.R. (1991), "*Zeolite microporous soilids: synthesis, structure and reactivity*", Springer Science & Business Media, Sintra-Estoril, Protugal.

Devadas, M. (2006), "*Selective catalytic reduction (SCR) of nitrogen oxides with ammonium over Fe-ZSM-5*", PhD thesis, Swiss Federal Institute of Technology, Zurich.

Dong, J., Xu, Z., Kuznicki, S.M. (2009), "Magnetic multi-functional nano-composites for environmental applications", *Advanced Functional Materials*, Vol. 19, pp. 1268-1275.

Drzaj, B., Hocevar, S., Pejovink, S. (2011), "*Zeolites: synthesis, structure, technology and application*", Technology & Engineering, Elsevier, Oxford.

Eary, L.E., Rai, D., Mattigold, S.V, Ainsworth, (1990), "Geochemical factors controlling the mobilization of inorganic constituents from fossil fuel combustion residues: II. Review of the minor elements", *Journal of Environmental Quality*, Vol. 19, pp. 202 – 214.

Efimov, A.M., Pogareva, V.G., Shashkin, A.M. (2003), "Water-related bands in the IR absorption spectra of silicate glasses", *Journal of Non-Crystalline Solids*, Vol. 332, Issue 1-3, pp: 93-114.

Eisler, R. (2012), "*The Fukushima 2011 disaster*", CRC Press Taylor & Francis Group, London.

Elmas, E., Yildiz, K., Toplan, N., Toplan, H.O. (2013), "Effect of mechanical activation on mullite formation in an alumina-quartz ceramics system", *Materials and Technology*, Vol. 47, Issue 4, pp. 413-416.

Eskom, (2011). "*Electricity Supply Commission, South Africa*", Annual Report, www.eskom.co.za, [accessed on January 31, 2012].

Farneth, W.E., Gorte, R.J. (1995), "Methods for characterizing zeolite acidity", *Chemical Reviews*, Vol. 95, pp. 615-635.

Flanigen, E.M. (1976), "*Structural analysis by infrared spectroscopy*", In: Rabo JA (ed) Zeolite chemistry and catalysis, ACS Monograph 171, American Chemical Society, Washington, DC, pp. 80–117.

Flanigen, M., Broach, R.W., Wilson, S.T. (2010), "Zeolites in industrial separation and catalysis", WILEY-VCH Verlag GmbH & Co. KGaA, Weinheim, Germany.

Flanigen, E., Patton, R. L. (1978), "*Silica polymorph*", US Patent 4,073,865.

Fansuri, H., Pritchard, D., Zhang Dong-ke. (2008), "*Manufacture of low-grade zeolites from fly ash for fertilizer applications*", Research Report 91 for Cooperative research Centre for coal in sustainable development, Australia.

Foner, H.A., Robl, T.L., Hower, J.C., Graham, U.M. (1999), "Characterization of fly ash from Israel with reference to its possible utilization", *Fuel*, Vol. 78, pp. 215–223.

Friedel, G. (1896), "New experiments on zeolites", *Bulletin de la Société Française de Minéralogie et de Cristallographie*, Vol. 19, pp. 363-390.

Garcia-Martinez, J., Li, K. (2015), "*Mesoporous zeolites: preparation, characterization and application*", 1st Edition Wiley-VCH Verlag GmbH & Co. KGaA, Germany.

Georgiev, D., Bogdanov, B., Angelova, K., Markovska, I., Hristov, Y. (2009), "*Synthetic zeolites: structure, classification, current trends in zeolite synthesis review*", International Science Conference, Stara Zagora, Bulgaria.

Gilson, J.P., Marie, O., Mintova, S., Valtchev, V. (2011), "*Emerging applications of zeolites*", 5th International FEZA Conference, 3rd FEZA School on Zeolites, Valence, Spain, pp. 245-299.

Gitari, W.M., Somerset, V.S., Petrik, L.F., Key, D., Iwuoha, E., Okujeni, C. (2003), "*Treatment of acid mine drainage with fly ash: Removal of major, minor, elements, SO_4 and utilization of the solid residues for wastewater treatment*", International Ash Utilization Symposium, Center for Applied Energy Research, University of Kentucky, pp. 1 – 23.

Goodhew, P.L. (1972), "*Specimen preparation in materials science*", Practical Methods in Electron Microscopy, North-Holland, Amsterdam, p. 198.

Gottlieb, B., Gilbert, S.G., Evans, L.G. (2010), "*Coal ash: The toxic threat to our health and environment*", Report from Physicians for Social responsibility and Earth Justice, USA.

Grandjean, F. (1910) Optical study of the absorption of the heavy vapors by certain zeolites", *Comptes Rendus de l'Académie des Sciences*, Vol. 149, pp. 866 – 868.

Grob, R.L., Barry, E.F. (2004), "*Modern practice of gas chromatography*", 4th Edition John Wiley & Sons, New Jersey, USA.

Groppo, J., Honaker, R. (2009) "Economical recovery of fly ash-derived magnetics and evaluation for coal cleaning", *Energeia*, Vol. 20, Issue 6.

Guth, J.L., Kessler, H. (1999), "*Catalysis and zeolites: Fundamentals and Applications",* eds J. Weitkam, & L. Puppe. Springer-Verlag.Berlin, Chapter 1, pp. 1.

Guang-Hui, B., Wei, T., Xiang-Gang, W., Jin-Guo, Q., Peng, X., Peng-Cheng, L. (2010), "Alkali desilicated coal fly ash as substitute of bauxite in lime-soda sintering process for aluminium production", *Transactions of Nonferrous Metals Society of China*, Vol. 20, pp. 169-175.

Gupta, A.K., Singh, R.P., Ibrahim, M.H., Lee, B.K. (2012) "Fly ash for agriculture: Implications for soil properties, nutrients, heavy metals, plants growth and pest control", *Agroecology and Strategies for Climate Change*, Vol 8, pp. 266-286.

Harris, R.K. (1986), "*Nuclear magnetic resonance spectroscopy*", Longman, Essex.

Hattori, T., Yashima, T. (1994), "*Zeolites and microporous crystals*", Technology & Engineering, Elsevier, Amsterdam, Netherlands.

Hay, R.L., Sheppard, R.A. (2001), "Occurrence of zeolites in sedimentary rocks: An overview", *Mineralogical Society of America, Reviews in Mineralogy*, Vol. 45, pp. 217-234.

Herrmann, R., Schwieger, W., Scharf, O., Stenzel, C., Toufar, H., Schmachtl, M., Ziberi, B., Grill, W. (2005), "In-situ diagnostics of zeolite crystallization by ultrasonic monitoring", *Microporous and Mesoporous Materials*, Vol. 80, pp. 1-9.

Hoffmann, F., Cornelius, M., Morell, J., Froba, M. (2006), "Silica-based mesoporous organic-inorganic hybrid materials", *Angewandte Chemie International Edition*, Vol. 45, Issue 20, pp. 3216-3251.

Holler, H., Wirsching, G.U. (1985), "Zeolite formation from fly ash", *Fortschritte Minerals*, Vol. 63, pp. 21-43.

Hollman G.G., Steenbruggen, G., JanssenJurkovicova, M. (1999), "A two-step process for the synthesis of zeolites from coal fly ash", *Fuel*, Vol. 78, pp 1225–1230.

Hou, X., Jones, B.T. (2000), "*Inductively coupled plasma/optical emission spectrometry*", Encyclopedia of Analytical Chemistry, John Wiley & Sons Ltd, Chichester, pp. 9468-9485.

Htun, M.M.H., Htay, M.M., Lwin, M.Z. (2012), "*Preparation of zeolite (NaX, faujasite) from pure silica and alumina sources*", International Conference on Chemical Processes and Environmental Issues, Singapore.

Huang, J., Jiang, Y., Reddy Marthala, V.R., Wang, W., Sulikowski, B., Hunger, M. (2007), "In situ 1H MAS NMR investigations of the H/D exchange of alkylaromatic hydrocarbons on zeolites H-Y, La, Na-Y, and H-ZSM-5", *Microporous and Mesoporous Materials*, Vol. 99, pp. 86–90.

Hudec, P. (2011), "*FCC catalyst – key element in refinery technology*", 45th International Petroleum Conference, Brastilava, Slovak Republic.

Hunger, M. (1997), "Brønsted acid sites in zeolites characterized by multi-nuclear solid-state NMR spectroscopy", *Catalysis Reviews: Science and Engineering*, Vol. 39, pp. 345–393.

Inaba, M., Murata, K., Saito, M., Takahara, I. (2006), "Ethanol conversion to aromatic hydrocarbons over several zeolite catalysts", *Reaction Kinetics and Catalysis Letters*, Vol. 88, Issue 1, pp. 135-142.

Inada, M., Tsujimoto, H., Eguchi, Y., Enomoto, N., Hojo, J. (2005), "Microwave assisted zeolite synthesis from fly ash in hydrothermal process", *Fuel*, Vol. 84, pp. 1482-1486.

Inglesi, R. (2010), "Aggregate electricity demand in South Africa: conditional forecasts to 2030", *Applied Energy*, Vol. 87, pp. 197-204.

Ismail, M.A., Eltayeb, M.A.Z., Abdel Maged, S.A. (2013), "Elimination of heavy metals from aqueous solutions using zeolite LTA synthesized from Sudanese clay", *Research Journal of Chemistry Sciences*, Vol. 3, Issue 5, pp. 93-98.

Jacob, B. (1998), "*A comparative study of medium and large pore zeolites in alkylation reactions*", PhD thesis, Cochin University of Science and Technology, India.

Jacobsen, N.E. (2007), "*NMR spectroscopy explained: simplified theory, applications and examples for organic chemistry and structural biology*", 4th Edition John Wiley & Sons, New Jersey, USA.

Jacobson, B., Anderson, W.A., Arnold, J.T. (1954), "A proton magnetic resonance study of hydration of deoxyribonuclease acid", *Nature,* Vol. 173, pp. 772-773.

Jha, B., Singh, D.N. (2011), "A review on the synthesis, characterization and industrial applications of fly ash zeolites", *Journal of Materials Education*, Vol. 33, Issue 1-2, pp. 65-132.

Jennings, W. (2012), "*Analytical gas chromatography*", Academic Press Inc., London, UK.

Jiao, J., Wang, W., Sulikowski, B., Weitkamp, J., Hunger, M. (2006), "^{29}Si and ^{27}Al MAS NMR characterization of non-hydrated zeolites Y upon adsorption of ammonia", *Microporous and Mesoporous Materials*, Vol. 90, pp. 246–250.

Joshi, R.C., Lohtia, R.P. (1997), "*Fly ash in concrete production, properties and uses*", Gordon and Breach Science Publishers, Amsterdam, p 128.

Kalyankar, A.N., Choudhari, A.L., Joshi, A.A. (2011), "Low frequency dielectric properties of fly ash based zeolite ZSM-5", *International Journal of Basic and Applied Research*, Vol. 1, pp. 59-63.

Kalyoncu, R.S. (2001), "*Coal Combustion Products (U.S. GEOLOGICAL SURVEY MINERALS YEARBOOK—2001)"* http://minerals.usgs.gov/minerals, [accessed on March 5, 2012].

Keeler, J. (2010), "*Understanding NMR spectroscopy*", 2nd Edition John Wiley & Sons, Oxford, UK.

Kirov, G., Filizova, L. (2012), "Cationic hydration impact on zeolite formation and properties: A review and discussion", *Bulgarian Academy of Sciences, Bulgarian Mineralogical Society*, Vol. 49, pp. 65-82.

Kitaev, L.E., Kolesnikova, E.E., Biryukova, E.N., Kolesnichenko, N.V., Khadzhiev, S.N. (2013), "Formation of superacid centers in the structure of zeolite ZSM-5", *Russian Journal of Physical Chemistry A*, Vol. 87, Issue 4, pp. 668-673.

Klamrassamee, T., Pavasant, P., Laosiripojana, N. (2010), "Synthesis of zeolite from coal fly ash: Its application as water sorbent", *Engineering Journal*, Vol. 14, Issue 1, pp. 37-44.

Kollander, B. (2011), "*Inductively coupled plasma-atomic emission spectrometry: Exploring the limits of different sample preparation strategies*", Acta Universitatis Upsaliensis Uppsala, p. 60.

Koukouzas, N., Hämäläinen, J., Papanikolaou, D., Tourunen, A., Jäntti, T. (2007), "Mineralogical and elemental composition of fly ash from pilot scale fluidised bed combustion of lignite, bituminous coal, wood chips and their blends", *Fuel*, Vol. 86, pp. 2186–2193.

Kuwahara, Y., Ohmichi, T., Kameqawa, T., Mori, K., Yamashita, H. (2010), "A novel conversion process for waste slag: synthesis of a hydrotalcite-like compound and zeolite from blast furnace slag and evaluation of adsorption capacities", *Journal of Materials Chemistry*, Vol. 20, pp. 5052-5062.

Krüger, J. E. (2003), "*South African fly ash: a cement extender South African Coal Ash Association*" Monograph publication on behalf of South African Coal Ash Association (SACAA), Silverton, RSA.

Lercher, J., Jentys, A. (2011), "*Basic concepts in zeolite acid-base catalysis*", 5th International FEZA Conference, 3rd FEZA School on Zeolites, Valence, Spain, pp. 181-210.

Lewis A., Pascual, M.R., Andreassen, J.P. (2014), "*Understanding crystallization and precipitation processes*", Workshop, Department of Chemical Engineering, University of Cape Town, Isisango Conference Centre, Midrand, South Africa.

Lai-Shi, L., Yu-Sheng, W., Ying-Ying, L., Yu-Chun, Z., (2011) "Extraction of alumina from coal fly ash with sulphuric acid leaching method". *The Chinese Journal of Process Engineering*, Vol. 11, Issue 2, pp. 254-258.

Langmuir, I. (1918), "The adsorption of gases on plane surfaces of glass, mica and platinum", *Journal of the American Chemical Society*, Vol. 40, Issue 9, pp. 1361-1403.

Liu, B., France, L., Wu, C., Jiang, Z., Kuznetsov, V.L., Al-Megren, H.A., Al-Kinany, M., Aldrees, S.A., Xiao, T., Edwards, P.P. (2015), "Methanol-to-Hydrocarbons conversion over MoO_3/H-ZSM-5 catalysts prepared via lower temperature calcination: a route to tailor the distribution and evolution of promoter Mo species, and their corresponding catalytic properties", *Chemical Science*, Vol. 6, pp. 5152-5163.

Liu, K. Xue, J., Zhu, J. (2012) "Extracting alumina from coal fly ash using acid sintering-leaching process", *Light Metals*, pp. 201-206.

Losch, P., Boltz, M., Bernardon, C., Louis, B., Palcic, A., Valtchev, V. (2016), "Impact of external surface passivation of nano-ZSM-5 zeolites in the methanol-to-olefins reaction", *Applied Catalysis A: General*, Vol. 509, pp: 30-37.

Louis, B., Walspurger, S., Sommer, J. (2004), "Quantitative determination of Brønsted acid sites on zeolites: a new approach towards the chemical composition of zeolites", *Catalysis Letters*, Vol. 93, Issue 1-2, pp. 81-84.

Louis, B., Ocampo, F., Tressonnier, J.P., Maciel Pereira, M. (2010), "Hierarchical pore ZSM-5 zeolite structures: From micro- to macro-engineering of structured catalysts", *Chemical Engineering Journal*, Vol. 161, pp. 397-402.

Louis, B., Pereira, M.M., Santos, F.M., Esteves, P.M., Sommer, J. (2010), "Alkane activation over acidic zeolites: the first step", *Chemistry: A European Journal*, Vol. 16, pp. 573-576.

Lowell, S., Shields, J.E., Thomas, M.A., Thommes, M. (2004), "*Characterization of porous solids and powders: surface area, pore size and density*", Springer, New York, USA.

Lu, G.Q., Do, D.D. (1991), "Adsorption properties of fly ash particles for NO*x* removal from flue gases", *Fuel Processing Technology*, Vol. 27, pp. 95–107.

Lu, R., Tangbo, H., Wang, Q., Xiang, S. (2003), "Properties and characterization of modified H-ZSM-5 zeolites", *Journal of Natural Gas Chemistry*, Vol. 12, pp. 56-62.

Mackiewicz, S.M., Ferguson, E.G. (2005), "*Stabilization of soil with self-cementing coal ashes*", World of Coal Ash (WOCA), Lexington, Kentucly, pp: 1-7.

Madzivire, G., (2009) "*Chemistry and speciation of potentially toxic and radioactive elements during mine water treatment*" MSc thesis, Chemistry Department, University of the Western Cape, Cape Town.

Madzivire, G., Gitari, W.M., Vadapalli V.R.K, Ojumu, T.V., Petrik, L.F. (2011) "Fate of sulphate removed during the treatment of circumneutral mine water and acid mine drainage with coal fly ash: Modelling and experimental approach", *Minerals Engineering*, Vol. 24, pp. 1467-1477.

Maier, S.M., Jentys, A., Lercher, J.A. (2011), "Steaming of zeolite BEA and its effects on acidity: a comparative NMR and IR spectroscopic study", *Journal of Physical Chemistry C*, Vol. 115, Issue 16, pp. 8005-8013.

Mainganye, D., Ojumu, T.V., Petrik, L., (2013), "Synthesis of Zeolites Na-P1 from South African Coal Fly Ash: Effect of Impeller Design and Agitation", *Materials*, Vol. *6, Issue* 5, pp. 2074-2089.

Marcilly, C. (1986) "Les zéolithes: structures, synthèse et modifications", *Pétrole et Techniques*, Vol. 328, pp. 12-18.

Masoudian, S.K., Sadighi, S., Abbasi, A. (2013), "Synthesis and characterization of high aluminium zeolite X from technical grade materials", *Bulletin of Chemistry Reaction Engineering & Catalysis*, Vol. 8, Issue 1, pp. 54-60.

Meier, W.M., Baerlocher, C. (1999), "*Zeolite type frameworks: Connectivities, configurations and conformations. Molecular Sieves*", Springer-Verlag Berlin Heidelberg, Vol. 2, pp. 141-161.

Meier, W.M., Olson D.H., Baerlocher, C. (1996), "*Atlas of Zeolite Structure Types*", 4th revised Edition, Structure Commission of the International Zeolite Association, Elsevier, Boston, USA.

Miller, B.G., Tillman, D. (2008). "*Combustion engineering issues for solid fuel systems*". Elsevier, Burlington, USA.

Miller, F.A., Wilkins, C.H. (1952), "Infrared spectra and characteristic frequencies of inorganic ions", *Analytical Chemistry*, Vol. 24, Issue 8, pp. 1253-1294.

Millini, R. (2011), "*Zeolites in refining and petrochemistry*", 5th International FEZA Conference, 3rd FEZA School on Zeolites, Valence, Spain, pp. 211-243

Milton, R.M. (1959), "*Molecular sieve adsorbents*", US Patent 2,882,243.

Missengue, R.N.M., Musyoka, N.M., Madzivire, G., Babajide, O., Fatoba, O.O., Tuffin, M., Petrik, L.F. (2015), "Leaching and antimicrobial properties of silver nanoparticles loaded onto natural zeolite clinoptilolite by ion exchange and wet impregnation", *Journal of Environmental Science and Health, Part A*, Vol.0, Issue 0, pp: 1-8.

Molina, A., Poole, C. (2004), "A comparative study using two methods to produce zeolites from fly ash", *Minerals Engineering*, Vol. 17, pp. 167-173.

Moliner, M., (2011) "*Zeolites and ordered porous solids: Fundamentals and applications – Basic principles of zeolite synthesis*", 5th International FEZA Conference, 3rd FEZA School on Zeolites, Valence, Spain, pp. 37-65.

Moliner, M. (2012), "Review article: Direct synthesis of functional zeolitic materials", *ISRN Materials Science*, pp. 1-24.

Moreno, N., Querol, X., Plana, F., Andres, J.M., Janssen, M., Nugteren, H. (2002), "Pure zeolite synthesis from silica extracted from coal fly ashes", Journal of Chemical Technology and Biotechnology, Vol. 77, pp: 274-279.

Moutsatsou, A., Karakasi, O.K., Koukouzas, N., Itskos, G.S., Vasilatos, C. (2008), "*Synthesis of zeolitic materials utilizing CFB-derived coal fly ash as a raw material*", WasteEng – 2nd International Conference on Engineering for Waste Valorisation, Patras, Greece.

Muriithi, G.N. (2013), "*Re-use of South African fly ash for CO_2 capture and brine remediation*", PhD thesis, University of the Western Cape, Cape Town.

Musyoka, N. M. (2012), "*Zeolite A, X and cancrinite from South African coal fly ash: mechanism of crystallization, routes to rapid synthesis and new morphology*", PhD thesis, University of the Western Cape, Cape Town.

Musyoka, N.M., Petrik, L.F., Gitari, W.M., Balfour, G., Hums, E. (2012), "Optimization of hydrothermal synthesis of pure phase zeolite Na-P1 from South African coal fly ashes", *Journal of Environmental Science and Health, Part A*, Vol. 47, pp. 337–350.

Musyoka, N.M., Missengue, R., Kusisakana, M., Petrik L.F. (2014), "Conversion of South African clays into high quality zeolites", Applied Clay Science, Vol. 0, pp:1-5.

Nagy, J.B., Bodart, P., Hannus, I., Kiricsi, I. (1998), "*Synthesis, characterization and use of zeolitic microporous materials*", Deca Gen Ltd, Szeged, Hungary.

Narayanan, S., Sultana, A., Krishna, K., Meriaudeau, P., Naccache, C. (1995), "Synthesis of ZSM-5 type zeolites with and without template and evaluation of physicochemical properties and aniline alkylation activity", *Catalysis Letters*, Vol. 34, Issue 1-2, pp. 129-138.

Nicolaides, C.P. (1999), "A novel family of solid acid catalysts: substantially amorphous or partially crystalline zeolitic materials", *Applied Catalysis A: General*, Vol. 185, pp. 211-217.

Nyale, S.M., Babajide, O.O., Birch, G.D., Boke, N., Petrik, L.F. (2013) "Synthesis and characterization of coal fly ash-based foamed geopolymer". *Procedia Environmental Sciences*, Vol. 18, pp. 722-730.

Ohman, L.O., Ganemi, B., Bjornbom, E., Rahkamaa, K., Keiski, R.L., Paul, J. (2002), "Catalyst preparation through ion-exchange of zeolite Cu-, Ni-, Pd-, CuNi- and CuPd-ZSM-5", *Materials Chemistry and Physics*, Vol. 73, pp. 263-267.

Ohrman, O.G.W. (2005), "*Structured MFI film catalysts and adsorbents*", PhD thesis, Lulea University of Technology, Sweden.

Ojha, K., Pradhan, N.C., Samanta, A.N. (2004), "Zeolite from fly ash: synthesis and characterization", *Bulletin of Materials Science*, Vol. 27, Issue 6, pp. 555-564.

Oliverio, M., Nardi, M., Costanzo, P., Cariati, L., Cravotto, G., Giofre, S.V., Procopio, A. (2014), "Non-conventional methodologies in the synthesis of 1-indanones", *Molecules*, Vol. 19, pp. 5599-5610.

Panagiotopoulou, C., Kontori, R., Perraki, T., Kakali, G. (2007), "Dissolution of aluminosilicate minerals and by-products in alkaline media", *Journal of Materials Science*, Vol. 42, pp. 2967-2973.

Pecharsky, V.K., Zavali, P.Y. (2005), "*Fundamentals of powder diffraction and structural characterization of materials*", Springer, USA.

Petrik, L. (2009), "The influence of cation, anion and water content on the rate of formation and pore size distribution of zeolite ZSM-5", *South African Journal of Science,* Vol. 105, pp. 251-257.

Petrik, L.F., O'Connor, C.T., Schwarz, S. (1995), "The influence of various parameters on the morphology and crystal size of ZSM-5 and the relationship between morphology and crystal and propene oligomerization activity", *Catalysis by Microporous Materials: Studies in Surface Science and Catalysis,* Vol. 94, pp. 517–524.

Petrik, L.F., White, R.A., Klink, M.J., Somerset, V.S., Burgers, C.L., Fey, M.V. (2003). "*Utilization of South African fly ash to treat acid coal mine drainage and production of high quality zeolites from the residual solids*", International Ash Utilization Symposium, Lexington, Kentucky, USA.

Pfiefer, H., Freude, D., Karger, J. (1991), "*Catalysis and adsorption by zeolites*", Ohlmann et al., Eds., Elsevier: Amsterdam.

Pieterse, J.A.Z., Pirngruber, G.D., Van Bokhoven, J.A., Booneveld, S. (2007), "Hydrothermal stability of Fe-ZSM-5 and Fe-BEA prepared by wet ion-exchange for N_2O decomposition", *Applied Catalysis,* Vol. 71, pp. 16-22.

Potts, P.J., Webb, P.C. (1992), "X-ray fluorescence spectrometry", *Journal of Geochemical Exploration,* Vol. 44, Issues 1-3, pp. 251-293.

Querol, X., Moreno, N., Umaña, J.C., Alastuey, A., Hernández, E., López-Soler, A., Plana, F. (2002), "Synthesis of zeolites from fly ash: an overview", *International Journal of Coal Geology,* Vol. 50, pp. 413-423.

Ramasamy, K.K., Wang, Y. (2013), "Catalyst activity comparison of alcohols over zeolites", *Journal of Energy Chemistry,* Vol. 22, pp. 65-71.

Ramesh, K., Reddy, D.D., Biswas, A.K., Rao, A.S. (2011), "Advances in agronomy: zeolites and their potential uses in agriculture", *Academic Press,* Vol. 113, pp. 215-236.

Reanvattana, N. (2005), "*Two-stage synthesis of high purity ZSM-5 zeolite from coal fly ash and rice husk ash*", Master thesis, Chemical Engineering, Kasetsart University, Thailand.

Robson, H. (2001), "*Verified syntheses of zeolitic materials*", 2nd Edition Elsevier, Amsterdam.

Rodrigues, J.A.R., Siqueira-Filho, E.P., de Mancilha, M., Moran, P.J.S. (2003), "Preparation of a-methylene ketones by direct methylene transfer", *Synthetic Communications*, Vol. 33, Issue 2, pp. 331–340.

Roland, E., Kleinschmit, P. (2005), "*Zeolites*", Ullmann's Encyclopedia of Industrial Chemistry. John Wiley & Sons.

Ruen-ngam, D., Rungsuk, D. (2009), "Zeolite formation from coal fly ash and its adsorption potential", *Journal of the Air & Waste Management Association*, Vol. 59, pp. 1140-1147.

Saikia, B., Parthasarathy, G. (2010), "Fourier transform infrared spectroscopic characterization of kaolinite from Assam and Meghalaya, Northeastern India", *Journal of Modern Physics*, Vol. 1, pp: 206-210.

Sani-Souna-Sido, A., Chassaing, S., Pale, P., Sommer, J. (2008), "Behavior of arylvinylketones in zeolites: A systematic study", *Applied Catalysis*, Vol. 336, pp. 101-108.

Sang, S., Chang, F., Liu, Z., He, C., He, Y., Xu, L. (2004), "Difference of ZSM-5 zeolites synthesized with various templates", *Catalysis Today*, Vol. 93-95, pp. 729-734.

Sazama, P., Wichterlova, B., Dedecek, J., Tvaruskova, Z., Musilova, Z., Palumbo, L., Sklenak, S., Gonsiorova, O. (2011), "FTIR and ^{27}Al MAS NMR analysis of the effect of framework Al- and Si-defects in micro- and micro-mesoporous H-ZSM-5 on conversion of methanol to hydrocarbons", *Microporous and Mesoporous Materials*, Vol. 143, pp. 87-96.

Scheetz, B.E., Earle, R. (1998). "Utilisation of fly ash", *Current Opinion in Solid State and Material science*, Vol. 3, pp. 510-520.

Scott, J., Guang, D., Naeramitmarnsuk, K., Thabuot, M., Amal, R. (2001), "Zeolite synthesis from coal fly ash for the removal of lead ions from aqueous solution", *Journal of Chemical Technology and Biotechnology*, Vol. 77, Issue 1, pp. 63-69.

Shao, J., Z. Wang, H., Li, H. and Shao, X. (1997), "*Fly ash as an adsorbent for wastewater treatment*", 14th International Pittsburgh Coal Conference, Taiyan, Shanxi, China.

Shcherban, S., Raizman, V., Pevzner, I. (1995), "*Technologies of coal fly ash processing into metallurgical and silicate chemical products*". Int. Assn. of Science, Inc. Assn. of Engineers & Science, New York.

Shigemoto, N., Hayashi, H., Miyaura, K. (1993), "Selective formation of Na-X zeolite from coal fly ash by fusion with sodium hydroxide prior to hydrothermal reaction", *Journal of Materials Science*, Vol. 28, Issue 17, pp. 4781-4786.

Shirazi, L., Jamshidi, E., Ghasemi, M.R. (2008) "The effect of Si/Al ratio of ZSM-5 zeolite on its morphology, acidity and crystal size", *Crystal Research and Technology*, Vol 43, Issue 12, pp. 1300-1306.

Singh, R., Dutta, P.K. (2003) "*MFI: A case study of zeolite synthesis*", Marcel Dekker, Inc. The Ohio State University, Columbus, Ohio, USA.

Skousen, J.G., Sexstone, A., Ziemkiewicz, P.F. (2000) "*Acid mine drainage control and treatment*", American Society of Agronomy and American Society for Surface Mining and Reclamation Agronomy. No 41.

Skvara, F., Jilek, T., Kopecky, L. (2005) "Geopolymer materials based on fly ash", *Ceramics*, Vol. 49, Issue 3, pp. 195-204.

Speight, J.G. (2005), "*Handbook of coal analysis*", John Wiley & Sons, NJ, USA.

Sobolev, K., Shah, S.P. (2015), "*Nanotechnology in construction: proceedings of NICOM5*", Springer, Technology & Engineering, pp: 164-165.

Somerset, V., Petrik, L., Iwuoha, E. (2007), "Alkaline hydrothermal conversion of fly ash precipitates into zeolites 3: the removal of mercury and lead ions from wastewater", *Journal of Environmental Management*, pp: 1-7.

Somerset, V., Petrik, L., White, R., Klink, M., Key, D., Iwuoha, E. (2004), "The use of X-ray fluorescence (XRF) analysis in predicting the alkaline hydrothermal conversion of fly ash precipitates into zeolites", *Talanta,* Vol. 64, pp. 109–114.

Song, C., Garc's, J.M., Sugi, Y. (2000), "*Shape-selective catalysis: chemicals synthesis and hydrocarbon processing*", American Chemical Society, Vol. 738, p. 226.

Styszko-Grochowiak, K., Golas, J., Jankowski, H., Kozinski, S. (2004), "Characterization of the coal fly ash for the purpose of improvement of industrial on-line measurement of unburned carbon content", *Fuel*, Vol. 83, pp. 1847-1853.

Szostak, R., Stepto, R.F.T. (1998), "*Molecular sieves: principles of synthesis and identification*", Springer Science & Business Media,.

Takahashi, G. (2015), "Sample preparation for X-ray fluorescence analysis III. Pressed and loose powder methods", *Rigaku Journal*, Vol. 31, Issue 1, pp. 26-30.

Takeuchi, Y., Mazzi, F., Haga, N., and Galli, E. (1979), "The crystal structure of wairakite", *American Mineralogist*, Vol. 64, pp. 993-1001.

Tao, Y., Kanoh, H. (2006), "Developments and structures of mesopores in alkaline-treated ZSM-5 zeolites", *Adsorption*, Vol. 12, pp. 309-316.

Taylor, W.H. (1930), "The crystal structure of analcite ($NaAlSi_2O_6 \bullet H_2O$)", *Zeitschrift für Kristallographie*, Vol. 74, pp. 1-19.

Terasaki, O., Ohuna, T. (1995), "What can we observe in zeolite related materials by HRTEM?", *Catalysis Today*, Vol. 23, pp. 201-218.

Treacy, M.M.J., Higgins, J.B. (2001) "*Collection of simulated XRD power patterns for zeolites*", 4th Edition ELSEVIER, p.586.

Triantafillidis, C.S., Evmiridis, N., Nalbandian, L., Vasalos, I.A. (1999), "Performance of ZSM-5 as a fluid catalytic cracking catalyst additive: Effect of the total number of acid sites and particles size", *Industrial & Engineering Chemistry Research*, Vol. 38, pp. 916-927.

Triantafyllidis, K.S., Nalbandian, L., Trikalitis, P.N., Ladavos, A.K., Mavromoustakos, T., Nicolaides, C.P. (2004), "Structural, compositional and acidic characteristics of nanosized amorphous or partially crystalline ZSM-5 zeolite-based materials", *Microporous and Mesoporous Materials*, Vol. 75, pp. 89-100.

Vadapalli, V.R.K., Gitari, W.M., Ellendt, A., Petrik, L.F., Balfour G. (2010), "Synthesis of zeolite P from coal fly ash derivative and its utilisation in mine water remediation", *South African Journal of Science*, Vol. 106, Issue 5/6, pp. 1-7.

Van der Gaag, F.J. (1987), "*ZSM-5 type zeolites: Synthesis and use in gasphase reactions with ammonia*", Delft University of Technology, the Netherlands.

Van Dijk, C.P., Solbakken, A., Rovner, J.M. (1983), "*Methanol from coal and natural gas*", US Patent 4407973 A.

Varvarin, A.V., Khomenko, K.M., Brei, V.V. (2013), "Conversion of n-butanol to hydrocarbons over H-ZSM-5, H-ZSM-11, H-L and H-Y zeolites", *Fuel*, Vol. 106, pp. 617-620.

Valtchev, V. Majano, G., Mintova, S., Perez-Ramirez, J. (2013), "Tailored crystalline microporous materials by post-synthesis modification", *Chemical Society Reviews*, Vol. 42, Issue 1, pp. 263-290.

Vassilev, S.V., Menendes, R., Alvarez, D., Diaz-Somoano, M., Martinez-Tarazona, M.R. (2003), "Phase-mineral and chemical composition of coal fly ashes as a basis for their

multicomponent utilization. 1. Characterization of feed coals and fly ashes", *Fuel*, Vol. 82, pp. 1793-1811

Vassilev, S.V., Vassileva, C.G. (2007) "A new approach for the classification of coal fly ashes based on their origin, composition, properties, and behaviour", *Fuel*, Vol. 86, pp. 1490-1512.

Vassileva, C.G., Vassilev, S.V. (2002). "General observations on the phase-mineral transformations in inorganic matter of some Bulgarian coals during heating", *Completes Rendus de l'Academie Bulgare des Sciences*, Vol. 4, pp. 7-47.

Viraraghavan, T. (1993), "*Ash utilization in water quality management*", Faculty of Engineering, University of Regina, Canada, pp. 939-944.

Voll, D., Angerer, P., Beran, A., Schneider, H. (2002), "A new assignment of IR vibrational modes in mullite", *Vibrational Spectroscopy*, Vol. 30, pp. 237-243.

Wan, Z., Wang, C., Yang, H., Zhang, D. (2013), "Effect of crystal size of ZSM-5 on its catalytic activity for Methanol-to-Gasoline conversion", *Engineers Australia*, pp. 885-889.

Wang, J., Groen, J.C., Yue, W., Zhou, W., Coppens, M.O. (2008), "Facile synthesis of ZSM-5 composites with hierarchical porosity", *Journal of Materials Chemistry*, Vol. 18, pp. 468-474.

Wang, S., Wu, H. (2006). "Environmental-benign utilisation of fly ash as low-cost adsorbents", *Journal of Hazardous Materials*, Vol. 136, pp. 482-501.

Weigel, O., Steinhoff, E. (1925) "Adsorption of organic liquid vapors by chabazite", *Zeitschrift für Kristallographie*, Vol. 61, pp. 125-154.

Welna, M., Szymczycha-Madeja, A. Pohl, P. (2011), "*Quality of the trace element analysis: sample preparation steps*", Wroclaw University of Technology, Wroclaw, Poland.

Williams, D.B., Carter, C.B. (1996), "*Transmission electron microscopy – A textbook for materials science*", Plenum, New York

Wilson, S.T., Lok, B.M., Messina, C.A., Cannan, T.R., Flanigen, E.M.J. (1982), "Aluminophosphate molecular-sieves: A new class of microporous crystalline inorganic solids", *Journal of the American Chemical Society*, Vol. 104, pp. 1146-1147.

Wright, P.A., Lozinska, M. (2011), "*Structural chemistry and properties of zeolites*", 5th International FEZA Conference, 3rd FEZA School on zeolites, Valencia, Spain.

Yan, Z., Ma, D., Zhuang, J., Liu, X., Liu, X., Han, X., Chang, F., Xu, L., Liu, Z. (2003), "On the acid-dealumination of USY zeolite: a solid state NMR investigation", *Journal of Molecular Catalysis A: Chemical*, Vol. 194, pp. 153-167.

Yao, Z.T., Xia, M.S., Sarker, P.K., Chen, T. (2014), "A review of the alumina recovery from coal fly ash, with a focus in China", *Fuel*, Vol. 120, pp. 74-85.

Ye, Y., Zeng, X., Qian, W., Mingwen, (2008), "Synthesis of pure zeolites from supersaturated silicon and aluminium alkali extracts from fused fly ash", *Fuel,* Vol. 87, pp. 1800 – 1886.

Yilmaz, B., Muller, U. (2009), "Catalytic applications of zeolites in chemical industry", *Topics in Catalysis*, Vol. 52, pp. 888-895.

Zhang, W., Xin, H., Yu, Y., He, H. (2014), "Oxalic acid treatment of ZSM-5 zeolite for the enhanced photocatalytic activity of TiO_2/H-ZSM-5", *Journal of Advanced Oxidation Technologies*, Vol. 17, Issue 2, pp: 359-364.

Zhao, X. S., Lu, G. Q., Zhu, H. Y. (1997) "Effects of ageing and seeding on the formation of zeolite Y from coal fly ash", *Journal of Porous Materials,* Vol. 4, pp. 245-251.

Zhu, G., Tan, W., Sun, J., Gong, Y., Zhang, S., Zhang, Z., Liu, L. (2013), "Effects and mechanism research of the desilicationpre-treatment for high-aluminum fly ash", *Energy Fuels*, Vol. 27, pp. 6948-6954.